

# SOLID MECHANICS AND ITS APPLICATIONS

## Volume 61

---

*Series Editor:* G.M.L. GLADWELL

*Solid Mechanics Division, Faculty of Engineering  
University of Waterloo  
Waterloo, Ontario, Canada N2L 3G1*

### *Aims and Scope of the Series*

The fundamental questions arising in mechanics are: *Why?*, *How?*, and *How much?* The aim of this series is to provide lucid accounts written by authoritative researchers giving vision and insight in answering these questions on the subject of mechanics as it relates to solids.

The scope of the series covers the entire spectrum of solid mechanics. Thus it includes the foundation of mechanics; variational formulations; computational mechanics; statics, kinematics and dynamics of rigid and elastic bodies; vibrations of solids and structures; dynamical systems and chaos; the theories of elasticity, plasticity and viscoelasticity; composite materials; rods, beams, shells and membranes; structural control and stability; soils, rocks and geomechanics; fracture; tribology; experimental mechanics; biomechanics and machine design.

The median level of presentation is the first year graduate student. Some texts are monographs defining the current state of the field; others are accessible to final year undergraduates; but essentially the emphasis is on readability and clarity.

# Contact Mechanics in Tribology

by

I. G. GORYACHEVA

*Institute for Problems in Mechanics,  
Russian Academy of Sciences,  
Moscow, Russia*



**KLUWER ACADEMIC PUBLISHERS**  
DORDRECHT / BOSTON / LONDON

A C.I.P. Catalogue record for this book is available from the Library of Congress.

ISBN 0-7923-5257-2

---

Published by Kluwer Academic Publishers,  
P.O. Box 17, 3300 AA Dordrecht, The Netherlands.

Sold and distributed in the North, Central and South America  
by Kluwer Academic Publishers,  
101 Philip Drive, Norwell, MA 02061, U.S.A.

In all other countries, sold and distributed  
by Kluwer Academic Publishers,  
P.O. Box 322, 3300 AH Dordrecht, The Netherlands.

*Printed on acid-free paper*

All Rights Reserved

©1998 Kluwer Academic Publishers

No part of the material protected by this copyright notice may be reproduced or  
utilized in any form or by any means, electronic or mechanical,  
including photocopying, recording or by any information storage and  
retrieval system, without written permission from the copyright owner

Printed in the Netherlands.

In memory of my teacher  
Professor L.A. Galin

# Preface

Tribology is the science of friction, lubrication and wear of moving components. Results obtained from tribology are used to reduce energy losses in friction processes, to reduce material losses due to wear, and to increase the service life of components.

Contact Mechanics plays an important role in Tribology. Contact Mechanics studies the stress and strain states of bodies in contact; it is contact that leads to friction interaction and wear. This book investigates a variety of contact problems: discrete contact of rough surfaces, the effect of imperfect elasticity and mechanical inhomogeneity of contacting bodies, models of friction and wear, changes in contact characteristics during the wear process, etc.

The results presented in this book were obtained during my work at the Institute for Problems in Mechanics of the Russian Academy of Sciences. The first steps of this research were carried out under the supervision of Professor L.A.Galin who taught me and showed me the beauty of scientific research and solutions. Some of the problems included in the book were investigated together with my colleagues Dr.M.N.Dobychin, Dr.O.G.Chekina, Dr.I.A.Soldatenkov, and Dr.E.V.Torskaya from the Laboratory of Friction and Wear (IPM RAS) and Prof. F.Sadeghi from Purdue University (West Lafayette, USA). I would like to express my thanks to them. I am very grateful to Professor G.M.L.Gladwell who edited my book, helped me to improve the text and inspired me to this very interesting and hard work. Finally, I would like to thank Ekaterina and Alexandre Goryachev for their help in preparation of this manuscript.

I hope that this book will be useful for specialists in both contact mechanics and tribology and will stimulate new research in this field.

Irina Goryacheva  
Moscow, Russia  
December 1997

# Chapter 1

## Introduction

Tribology deals with the processes and phenomena which occur in friction interaction of solids.

The subject of tribology is *the friction contact* that is the region of interaction of bodies in contact.

Various processes of physical (including mechanical, electrical, magnetic and heat), chemical and biological nature occur at the friction contact. *Friction force*, i.e. resistance to the relative displacement of bodies, is one of the main manifestations of these processes. It is well-known that one third of the world energy resources is now spent on overcoming friction forces.

*Lubrication* of surfaces is the most efficient method for reducing friction. Various greases, liquid and solid lubricants are used for friction components, depending on the environmental conditions, materials of surfaces and types of motion.

*Wear* of contacting surfaces is the other manifestation of the processes occurring in contact interaction. Wear is a progressive loss of material from surfaces due to its fracture in friction interaction showing up in gradual change of the dimensions and shape of the contacting bodies. The precision of machines is impaired by wear, sometimes the wear leads to the machine failure. Thus the study of wear and its reasons, and elaboration of methods for improvement of wear resistance are important problems of tribology.

These discussions point to the other definition of tribology as *the science of friction, lubrication and wear of materials*. The history of tribology is presented in the monograph by Dowson (1978). The monographs by Bowden and Tabor (1950, 1964), Kragelsky (1965), Rabinowicz (1965), Kostetsky (1970), Moore (1975), Kragelsky, Dobychin and Kombalov (1982), Hutchings (1992), Singer and Pollock (1992), Chichinadze (1995), etc., the handbooks by Peterson and Winer (1980), Bhushan and Gupta (1991), etc. are devoted to fundamental and applied investigations in tribology.

Tribology can be considered as an applied science since the diminishing of the energy losses and deleterious effects of friction and wear on the environment, and the increase of machine life are the main purposes of tribological investigation.

However, deep understanding of the nature of friction and wear is the only reliable way to the successful solution of these problems. The increasing interest in fundamental problems of tribology confirms this conclusion.

Tribology has evolved on the basis of mechanics, physics, chemistry and other sciences. However, the results obtained in these fields cannot be applied directly. Tribological processes are complicated and interconnected involving multiple scales and hierarchical levels, and must be considered using results of different scientific disciplines simultaneously.

One of the main roles in the study of friction interaction belongs to mechanics.

## 1.1 Friction contact from the standpoint of mechanics

Stress concentrations near contact regions affect all processes occurring in friction interaction. High contact pressures and sliding velocities cause heating at contact zones, and substantial changes of properties of the surface layer; they also stimulate chemical reactions, resulting in the formation of secondary compounds and structures, and accelerate the mutual diffusion. The subsurface layer is subjected to high strains due to mechanical and thermal action that lead to crack initiation and growth, and finally to surface or subsurface fracture.

Mechanics of solids, in particular contact mechanics and fracture mechanics, is a powerful tool for the investigation of basic tribological problems. Contact mechanics investigates the stress-strain state near the contact region of bodies as a function of their shapes, material properties and loading conditions. Fracture mechanics is used to evaluate specific conditions which lead to the junction failure.

The first investigation in the field of contact mechanics was made by Hertz (1882) who analyzed the stresses in the contact of two elastic solids. Hertz's theory was initially intended to study the possible influence of elastic deformation on Newton's optical interference fringes in the gap between two glass lenses. This theory provided a basis for solution of many tribological problems. It led to methods for the calculation of the real contact area of rough surfaces and the contact stiffness of junctions, to the investigation of rolling and sliding contact, wear of cams and gears, to estimation of the limiting loads for rolling bearings, etc.

However, it is well known that the Hertz theory is based on some assumptions which idealize the properties of contacting bodies and the contact conditions. Among other things, it is assumed that

- the contacting bodies are elastic, homogeneous and isotropic;
- the strains are small;
- the surfaces are smooth and non-conforming;
- the surface shape does not change in time;

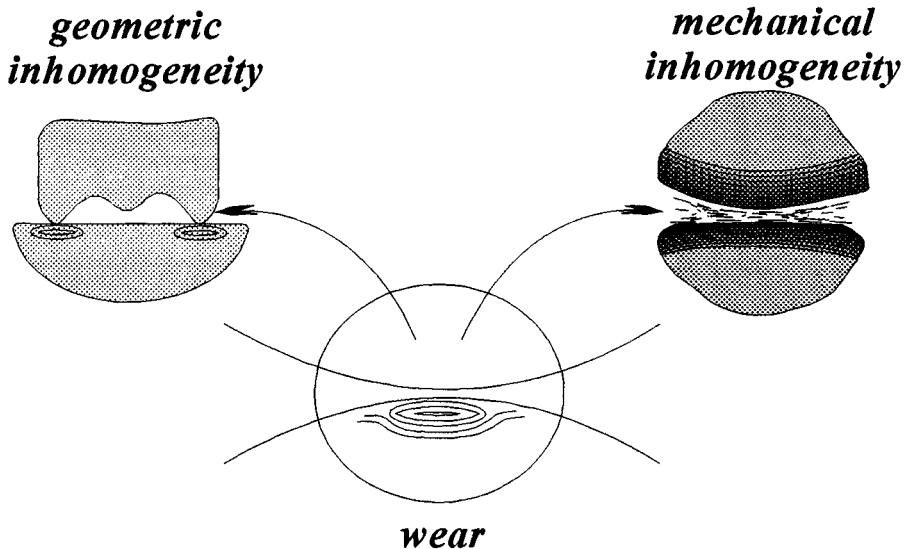


Figure 1.1: Scheme of contact of elastic bodies with geometric (a) and mechanical (b) inhomogeneities.

- the contact is frictionless.

These assumptions are often unwarranted in tribological problems. It is known for instance that, in contact interaction, stresses increase in a thin surface layer, the thickness of which is comparable with the size of contact region. Fig. 1.1 illustrates the scheme of contact and stresses near the surface. Due to the high stresses, cracks initiate and grow in this layer; this leads to particle detachment from the surface (wear). Thus, the properties of a thin surface layer play an important role in the subsurface stress and wear analysis.

Due to the surface treatment (heating, mechanical treatment, coating, etc.) the surface layer has different kinds of inhomogeneity. These significantly influence the stress distribution and wear in contact interaction.

*Geometric inhomogeneity*, such as macrodeviations, waviness or roughness (see Fig. 1.1(a)), which is a deviation of the surface geometry from the design shape, leads to discreteness of the contact between solid surfaces. Geometric inhomogeneity influences the contact characteristics (real pressure distribution, real contact area, etc.) and internal stresses in the surface layer. Due to the roughness of contacting bodies, the subsurface layer is highly and nonuniformly loaded, so there is a nonuniform internal stress distribution within this layer. These peculiarities of the stress field govern the type of fracture of the surface layer.

*Mechanical inhomogeneity* of materials of contacting bodies (see Fig. 1.1(b)) also arises due to different kinds of surface treatment, application of coatings and solid lubricants or in operating. Specifically, the mechanical properties of the surface layer are different from the bulk material. In spite of the small thickness of this layer, its characteristics can significantly influence the friction and wear processes.

*The intermediate medium* between the contacting bodies (third body) also influences the stress distribution in subsurface layers, e.g. application of a thin film of lubricant essentially decreases the friction and wear of surfaces.

These properties of friction contact prove that special problems of contact mechanics (contact problems) must be formulated to describe the phenomena important for tribological needs: problems which include complicated boundary conditions, the properties of the intermediate medium, surface inhomogeneity and so on.

## 1.2 Previous studies and the book outline

Contact mechanics has evolved from the consideration of simple idealised contact configurations to the analysis of complicated models of contacting bodies and boundary conditions.

The following fields of contact mechanics are well developed:

- contact problems with friction;
- contact problems for layered and inhomogeneous elastic bodies;
- contact problems for anisotropic elastic bodies;
- thermoelastic contact problems;
- contact problems for viscoelastic and elasto-plastic bodies.

These fields of contact mechanics have been considered in monographs by Staierman (1949), Muskhelishvili (1949), Galin (1953, 1976b, 1980, 1982), Ling (1973), Vorovich, Aleksandrov and Babeshko (1974), Rvachev and Protsenko (1977), Gladwell (1980), Popov (1982), Aleksandrov and Mhitaryan (1983), Mossakovskiy, Kachalovskaya and Golikova (1985), Johnson (1987), Goryacheva and Dobychin (1988), Kalker (1990), etc.

The gap between contact mechanics and tribology has been narrowed; they have the same subject of investigation, i.e. friction contact. Contact problem formulations now include specific properties of friction contact such as surface microstructure, friction and adhesion, shape variation of contacting bodies during the wear process, surface inhomogeneity, etc.

### 1.2.1 Surface microstructure

To take into account the surface microstructure, such as roughness or waviness, Staierman (1949) proposed a model of a combined foundation. Surface displacement of this foundation under loading was represented as a sum of the elastic displacement of the body with given macroshape and an additional displacement due to the surface microstructure. This model became a basis for investigation of the contact of rough bodies which was further developed for nonlinear models of combined foundation and for various surface shapes of contacting bodies. Based on this approach, we can calculate the nominal (averaged) contact characteristics (nominal pressure and nominal contact area).

Another way of looking at the problem of the contact of rough bodies was developed by Archard (1951), Goodman (1954) Greenwood and Williamson (1966), Greenwood and Tripp (1967), Demkin (1970), Hisakado (1969, 1970), Rudzit (1975), Hughes and White (1980), Thomas (1982), Kagami, Yamada and Hatazawa (1983), Sviridenok, Chijik and Petrokovets (1990), Majumdar and Bhushan (1990, 1991), etc. They considered models of discrete contact of bodies with surface microgeometry which made it possible to calculate such important characteristics of the rough body contact as the real contact pressure and the real contact area. Note that the most of the discrete contact models include the assumption that the stress-strain state near each contact spot is determined only by the load applied to this contact spot, i.e. these models neglect the interaction between contact spots. This assumption is valid only for small loads when the density of contact spots is not too high.

Generally, the problem of the discrete contact of rough bodies is a three-dimensional boundary problem of contact mechanics for a system of contact spots comprising the real contact area. This problem is discussed in detail in Chapter 2 where the contact problem for bodies with surface microgeometry is formulated as a multiple contact problem for elastic bodies.

### 1.2.2 Friction

The other important property of contact interaction is the friction between contacting bodies. In classical formulation of contact problems, friction is introduced phenomenologically by a definite relation (friction law) between the tangential and normal stresses in the contact zone.

The method of complex variables developed by Muskhelishvili (1949), Galin (1953), Kalandiya (1975) is mainly used to determine the stress distribution for the 2-D contact problems in the presence of friction. The linear form of the friction law is normally used in the problem formulations.

If a tangential force  $T$  applied to the body satisfies the inequality  $T < \mu P$ , where  $P$  is the normal force and  $\mu$  is the friction coefficient, then partial slip occurs; this is characterized by the existence of slip and stick zones within the contact region. The friction is *static friction*. In slip zones the linear relation between the normal ( $p$ ) and tangential ( $\tau$ ) stresses is usually used, i.e.  $\tau = \mu p$ . In stick zones

the displacements of contacting bodies at each point are equal. Contact problems with partial slip in contact region were considered by Mindlin (1949), Galin (1945, 1953), Lur'e (1955), Spence (1973), Keer and Goodman (1976), Mossakovskiy and Petrov (1976), Mossakovskiy, Kachalovskaya and Samarsky (1986), Goldstein and Spector (1986), etc. The solution of the problems includes the determination of the positions and sizes of stick and slip zones for given loading conditions. In particular, it is shown that the area of stick zones decreases and tends to zero, if  $T \rightarrow \mu P$ .

If  $T = \mu P$ , there is limiting friction, and the condition of full slip occurs in the contact region. This case is also called *sliding friction*. Axisymmetric contact problems with limiting friction were investigated by Mindlin (1949), Lur'e (1955), Muki (1960), Westman (1965), Hamilton and Goodman (1966), Korovchinsky (1967), Gladwell (1980), etc. In most cases the assumption was made that the tangential stress in the contact region does not influence the contact pressure distribution. This assumption is valid for a small value of the parameter  $\varepsilon = \mu \vartheta^*$ , where

$$\vartheta^* = \frac{[(1 - 2\nu_1)/G_1] - [(1 - 2\nu_2)/G_2]}{2[(1 - \nu_1)/G_1] + [(1 - \nu_2)/G_2]},$$

$$G_i = \frac{E_i}{1 + \nu_i}, \quad i = 1, 2.$$

For contacting bodies of identical material, and also for the case  $\nu_1 = \nu_2 = \frac{1}{2}$ ,  $\varepsilon = 0$ , the assumption is true.

3-D contact problems with limiting friction (taking into account the influence of the tangential stress on the normal stress within the contact region) were investigated in Kravchuk (1980, 1981), Galin and Goryacheva (1983), Mossakovskiy, Kachalovskaya and Samarsky (1986).

Chapter 3 presents some solutions of contact problems in the 2-D and 3-D formulations with limiting friction which include the influence of the tangential stress on the contact pressure distribution and on the size and the position of contact region.

Amontons' friction law  $\tau = \mu p$ , where  $\tau$  and  $p$  are the tangential and normal contact stresses, is mainly used in formulation of the contact conditions in slip zones. From the standpoint of the molecular-mechanical theory of friction, Amontons' law takes into account only the mechanical component of friction force arising from the deformation of asperities of rough contacting bodies. Deryagin (1934), Bowden and Tabor (1950), Kragelsky (1965) showed that adhesion plays a key part in the friction force formation. Taking into account adhesion gives rise to Coulomb's law  $\tau = \tau_0 + \mu p$ . Chapter 3 also describes some results which follow from the solution of the contact problems with Coulomb's law.

### 1.2.3 Imperfect elasticity

Many phenomena taking place in friction interaction cannot be explained on the basis of elastic bodies. Specifically, they are the dependence of the friction force on

the temperature and velocity, self-oscillations during a friction process, etc. Thus, more complicated models taking into account imperfect elasticity of contacting bodies must be used in the analysis.

Among such investigations, there is the contact problem for a rigid cylinder rolling over a viscoelastic foundation considered by Ishlinsky (1940). The author used the one-dimensional Kelvin–Voigt model to describe the relation between the normal stress  $\sigma_y$  and the deformation  $\epsilon_y$  of the foundation:

$$\sigma_y = E\epsilon_y + HT_\epsilon \dot{\epsilon}_y,$$

where  $E$ ,  $H$  and  $T_\epsilon$  are characteristics of the viscoelastic body. The results showed that the dependence of the friction force  $T$  on the rolling speed  $V$  had a nonmonotone character: for low speed it was described by

$$T = \frac{HT_\epsilon VP}{ER},$$

while for high speed

$$T = \frac{2}{3} \sqrt{\frac{P^3 l_0}{HT_\epsilon VRl}},$$

where  $l$  and  $R$  are the length and the radius of the cylinder, and  $l_0$  is a characteristic length.

It is interesting to note, that if these two asymptotic formulae had been obtained earlier, they might have brought an end to the discussion raised between Dupuit (1837) and Morin (1853) in the nineteenth century concerning the dependence of the friction force on the radius of the roller. Dupuit suggested that  $T \sim R^{-1/2}$ , and Morin thought that  $T \sim R^{-1}$ . Ishlinsky's formulae support both suggestions.

More complicated and also more realistic models of viscoelastic bodies are based on the mechanics of solids. The methods of solution of some contact problems for viscoelastic solids have been presented in May, Morris and Atack (1959), Lee and Radok (1960), Hunter (1960, 1961), Morland (1962, 1967, 1968), Galin and Shmatkova (1968), Ting (1968), Braat and Kalker (1993), etc. and also in monographs by Il'ushin and Pobedrya (1970), Ling (1973), Rabotnov (1977), etc. Some problems for inelastic solids concerning normal, sliding, and rolling contact and impact are discussed by Johnson (1987).

The analysis of the contact problem solutions taking into account inelastic properties of solids and friction allows the establishment of the dependence of the contact characteristics on the mechanical properties of bodies and the contact conditions. It also makes possible to determine the conditions that allow us to use the simplified models.

Some rolling and sliding contact problems for viscoelastic bodies are also presented in Chapter 3. The solutions of these problems are used to calculate the mechanical component of friction force and to analyze its dependence on the sliding velocity.

### 1.2.4 Inhomogeneous bodies

Since specific surface properties of contacting bodies considerably influence the stress distribution near the contact region and the friction force, the solution of contact problems for bodies with elastic parameters which vary with depth is of great interest for tribology. A review of early works devoted to investigation of contact problems for inhomogeneous elastic bodies may be found in Galin (1976b) and Gladwell (1980). Most of these works are concerned with the special forms of the functions describing the dependence of elastic moduli (the Young modulus and the Poisson ratio) on the depth.

Different kinds of coatings and surface modification are widely used in friction components to decrease friction, to increase the wear resistance and to prevent seizure between contacting surfaces. The lifetime of coatings and their tribological characteristics (friction coefficient, wear resistance, etc.) depend on the mechanical properties of coatings, their thickness and structure and on the interface adhesion. It is important for tribologists to choose the optimal mechanical and geometrical characteristics of coatings for any particular type of junctions.

Contact mechanics of layered bodies can help to solve this problem. Many researches in this field are reviewed in monographs by Nikishin and Shapiro (1970, 1973), Vorovich, Aleksandrov and Babeshko (1974), Aleksandrov and Mhitarian (1983). They give solutions of plane and axisymmetric contact problems for an elastic layer bonded to or lying without friction on an elastic or rigid foundation.

Considerable attention has been focussed recently on the production of thin coatings, the thickness of which is commensurable with the typical size and distance between asperities. This initiated the investigation of contact problems for layered bodies with rough surfaces. Problems of this kind are considered in detail in Chapter 4. The effect of the boundary conditions at the interface between the coating and the substrate is also analyzed in that chapter. This analysis elucidates the influence of the interface adhesion on the internal stresses and the fracture of coating.

Chapter 4 also includes contact problems for viscoelastic layered elastic bodies. Solving these problems for rolling or sliding elastic indenter with smooth or rough surface is very important for studying the dependence of the friction force on the speed for junctions operating in the boundary lubrication condition or in the presence of solid lubricants.

What is the influence of a thin viscoelastic layer on the stress distribution in the lubricated contact of two elastic rollers? This question is also discussed in Chapter 4 where the model of lubricated contact includes equations from hydrodynamics, viscoelasticity and elasticity. This model allows us to analyze the dependence of the friction coefficient on speed for variable mechanical and geometrical characteristics of the surface layer.

### 1.2.5 Surface fracture

Investigation of the contact problems taking into account friction, microstructure, presence of surface layers and an intermediate medium allows us to determine contact and internal stresses in a thin subsurface layer, where the cracks initiate. Such analysis becomes a basis for prediction of the surface fracture process (wear) in friction interaction.

The methods and models of fracture mechanics are most commonly used to model the fracture of surface layer in friction process. However, modelling of fracture in tribology has specific features. First, to predict the type of wear, we must know both bulk and surface strength characteristics of materials. Secondly, detachment of one wear particle from the surface does not mean the failure of the junction; the volume of wear particles detached from the surface during the life of junction may be considerable. The surface fracture process changes surface properties (the shape of the surface and its microgeometry, mechanical properties, damage characteristics, etc.). The variable surface properties influence, in turn, the wear process. Some problems of contact fracture mechanics are discussed in monographs by Marchenko (1979), Waterhouse (1981), Kolesnikov and Morozov (1989), Hills and Nowell (1994), and Menčík (1996) and in papers by Miller, Keer and Cheng (1985), Hattori et al. (1988), Waterhouse (1992), Liu and Farris (1994), Szolwinski and Farris (1996), etc.

The models of delamination of the surface layer and wear particle detachment in friction of rough surfaces are presented in Chapter 5. They are based on the theory of fatigue damage accumulation in cyclic loading.

### 1.2.6 Wear contact problems

Wear of surfaces leads to the continuous irreversible changes of the surface macroshape in time. Consideration of these changes requires new contact problem formulations and solution methods. All contact characteristics (pressure distribution, shape variation, size and position of contact region, approach of bodies) are unknown functions of time in this case. Calculation of the wear process for different junctions is a necessary condition for design of long-life machines.

The first formulation of the wear contact problem suggested by Pronikov (1957) (see also Pronikov, 1978) did not take into account the deformation of contacting bodies; the contact conditions included only the irreversible surface displacements due to wear.

The contact problem for elastic bodies taking into account the surface shape variations during the wear process was formulated by Korovchinsky (1971). In this work the displacements of the surface due to wear are supposed to be commensurable with the elastic displacements. At any instant of time, the shape of the surface is determined by wear at each point, and simultaneously influences the contact pressure. The wear rate at each point of the contact region at any instant of time is, in turn, a function of the contact pressure at this point. Thus, all functions (pressure distribution, wear and elastic displacements of the surface,

etc.) in the wear contact problem are time-dependent and interconnected.

The system of equations governing wear contact problems includes a wear equation which can be found experimentally or can be obtained by modelling the wear process (an example of such model is presented in the Chapter 4).

After the fundamental works by Galin (1976a, 1977, 1980), wear contact problems were intensively investigated in Russia. The methods of solution of the 2-D and 3-D wear contact problems for the contacting bodies of different shape (half-space, strip, beam, parabolic indenter, cylinder, etc.), for various models of deformable bodies (elastic, viscoelastic, etc.) under different loading conditions and a type of motion were presented in Aleksandrov and Kovalenko (1978, 1982), Goryacheva (1979a, 1980, 1987, 1989), Bogatin, Morov and Chersky (1983), Teply (1983), Soldatenkov (1985, 1987), Galakhov and Usov (1990), etc.

Some of these problems are discussed in Chapters 6 – 8 of this book. These chapters include general formulations of the wear contact problems and methods for their solution, the analysis of such particular problems as wear of thin coatings, wear of bodies with variable wear coefficient, wear of discrete contact, etc. Some applications of the methods to the analysis of the wear kinetics of components (plane journal bearing, wheel and rail, abrasive and cutting tools, etc.) are also presented there. The results can be used to predict the lifetime of these components and to optimize the wear process.

The close connection between tribology and contact mechanics has led to new fields in contact mechanics. These fields are the theoretical basis for further investigations in tribology and in the modelling of the phenomena that occur in friction interaction. Some of them are discussed in the chapters that follow.

# Chapter 3

## Friction in Sliding/Rolling Contact

### 3.1 Mechanism of friction

The causes of friction have been explored for many years. According to the modern conception of tribology there are two main causes of energy dissipation which give rise to a resistance in sliding contact.

The first one is associated with the work done in making and breaking adhesion bonds formed in the points of contact of sliding surfaces. The force necessary to shear these bonds is termed the adhesive (molecular) component of the friction force. The mechanism for the formation of adhesion bonds depends on the properties of the contacting bodies and on the friction conditions. For sliding contact of metal surfaces, it is realized as the rupture of the welded *bridges* between the contacting surfaces. For sliding contact of rubbers and rubber-like polymers, the energy dissipation takes place in the process of thermal jumping of the molecular chains from one equilibrium state to another. The adhesive component of the friction force depends on the surface properties of both contacting bodies. An interesting approach to modelling of the adhesive interaction in sliding contact was developed in papers by Godet (1984), Alekseev and Dobychin (1994), where the motion of the substance of the *third-body* was investigated. The third-body is a thin layer at the interface between the contacting bodies. Its properties depend on the mechanical properties of the surface layers of the contacting bodies, the boundary film etc. However, up to now, there is no theoretical model for calculating the adhesive component of the friction force.

The adhesive friction is taken into account in the formulation of contact problems by some relationship between the stresses in the contact zone. The law of friction established experimentally by Coulomb (1785) is usually used to describe the relation between the normal  $p$  and tangential  $\tau$  stresses in the contact zone:

$$\tau = \tau_0 + \mu p \quad (3.1)$$

Here  $\tau_0$  and  $\mu$  are parameters of the friction law. It has been found that the value  $\tau_0$  is very small for polymers and boundary lubrication (see Kragelsky, Dobychin and Kombalov, 1982). Eq. (3.1) is used in the formulation of contact problems for elastic bodies in sliding contact (§ 3.2 and § 3.3).

The second cause of the energy dissipation is the cyclic deformation of the bodies in sliding contact. The resistive force connected with this process is termed the mechanical component of friction. It depends on the mechanical properties of the bodies in sliding contact, the geometry of their surfaces, the applied forces etc. Unlike the adhesive component, the mechanical component of friction force depends in the main on the deformation of the bodies in contact, and thus can be studied by the methods of contact mechanics.

Since there is no energy dissipation in the deformation of elastic bodies, the mechanical component of the friction force is equal to zero for elastic bodies. For example, in sliding contact of elastic cylinders the contact pressure is distributed symmetrically within the contact zone (which is also symmetrically placed with respect to the symmetry axis of the cylinder) for the case  $\tau = 0$  and so there is no resistance to the relative motion. To study the mechanical component of the friction force, imperfect elasticity of contacting bodies must be taken into account. This is the reason for considering contact problems for viscoelastic bodies in this Chapter.

In tribology, the adhesive and mechanical components of friction force are usually considered as independent. However there are some experimental results which argue against this statement (see Moore, 1975). It has been established that the relation between the components of the friction force depends on friction conditions, mechanical properties of contacting bodies etc. The investigation of the sliding contact of viscoelastic bodies (§ 3.4) makes it possible to analyze the dependence between the mechanical and adhesive components of the friction force.

Both causes of energy dissipation also occur in rolling contact. It has been shown theoretically and experimentally that the resistance to rolling is caused by the following:

1. Friction due to the relative slip of the surfaces within the contact area arising from the differences of the curvature of the contacting surfaces, and their different mechanical properties. Reynolds (1875) was the first to establish this fact. It was also supported by experimental results of Heathcote (1921), Konvisarov and Pokrovskaya (1955), Pinegin and Orlov (1961) etc.
2. Imperfect elasticity of the contacting bodies (Tabor, 1952, Flom and Bueche, 1959, Flom, 1962, etc.).
3. The adhesive forces in the contact (Tomlinson, 1929).

The question is what is the contribution of each process to rolling resistance for different operating conditions? To answer this question the rolling contact of viscoelastic bodies is considered, taking into account the partial slip in the contact zone (§ 3.5).

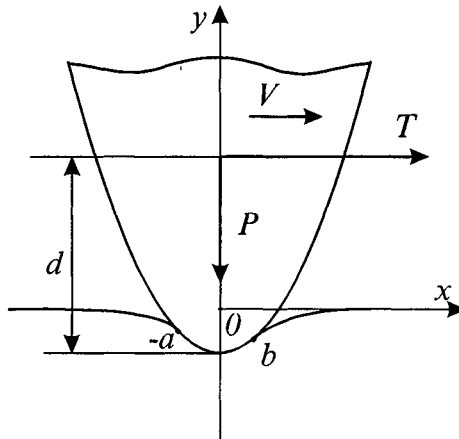


Figure 3.1: Sliding contact of a cylindrical punch and an elastic half-space.

As has been mentioned in Chapter 2, the roughness is usually modelled by a system of asperities described by some simple shape and a specific spatial distribution. The first stage of investigation of the contact of rough bodies is the consideration of the contact of two asperities. The methods of contact mechanics can be applied to this problem. So some of the results obtained in this Chapter can be used to describe the resistance to the relative motion of isolated asperities and rough surfaces.

## 3.2 Two-dimensional sliding contact of elastic bodies

### 3.2.1 Problem formulation

We consider a sliding contact of a rigid cylinder and an elastic half-space (Fig. 3.1). The shape of the rigid body is described by the function  $y = f(x)$ . External forces also are independent of the  $z$ -coordinate. This problem is considered as a two-dimensional (plane) problem for a punch and an elastic half-plane. The two-term friction law (3.1) is assumed to hold within the contact zone  $(-a, b)$ :

$$\tau_{xy}(x) = (\tau_0 + \mu p(x)) \operatorname{sgn} V, \quad (3.2)$$

where  $p(x) = -\sigma_y(x)$  and  $\tau_{xy}(x)$  are the normal pressure and tangential stress at the surface of the elastic half-plane ( $y = 0$ ), and  $V$  is the velocity of the cylinder.

Applied tangential  $T$  and normal  $P$  forces cause the body to be in the limiting equilibrium state, or to move with a constant velocity. This motion occurs so slowly that dynamic effects may be neglected.

In the moving coordinate system connected with the rigid cylinder, the follow-

ing boundary conditions hold ( $y = 0$ )

$$\begin{aligned}\sigma_y &= 0, \quad \tau_{xy} = 0, \quad (-\infty < x < -a, \quad b < x < +\infty), \\ v &= f(x) - D, \quad \tau_{xy} = (\tau_0 + \mu p) \operatorname{sgn} V, \quad (-a \leq x \leq b),\end{aligned}\quad (3.3)$$

where  $v$  is the normal displacement of the half-plane surface,  $D$  is the approach of the contacting bodies.

The relationship between stresses and the normal displacement gradient at the boundary  $y = 0$  of the lower half-plane has the form (Galin, 1980)

$$\frac{\pi E}{2(1-\nu^2)} \cdot \frac{\partial v}{\partial x} = \int_{-\infty}^{+\infty} \sigma_y \frac{dt}{t-x} - \frac{1-2\nu}{2-2\nu} \pi \tau_{xy}. \quad (3.4)$$

Using Galin's method (Galin, 1980), we introduce a function  $w_1(z)$  of a complex variable in the lower half-plane  $y \leq 0$

$$w_1(z) = U_1 - iV_1 = \int_{-\infty}^{+\infty} \sigma_y \frac{dt}{t-z}. \quad (3.5)$$

Using (3.3), (3.4) and the limiting values of the Cauchy integral (3.5) as  $z \rightarrow x - i0$ , we can derive the following boundary conditions for the function  $w_1(z)$

$$\begin{aligned}V_1 &= 0, \quad (-\infty < x < -a, \quad b < x < +\infty), \\ U_1 + \mu \vartheta V_1 \operatorname{sgn} V &= \pi F(x), \quad (-a \leq x \leq b),\end{aligned}\quad (3.6)$$

where

$$\begin{aligned}F(x) &= \vartheta \tau_0 \operatorname{sgn} V + \frac{f'(x)}{\pi K}, \\ K &= \frac{2(1-\nu^2)}{\pi E}, \quad \vartheta = \frac{1-2\nu}{2(1-\nu)}.\end{aligned}\quad (3.7)$$

So the problem is reduced to the determination of the analytic function  $w_1(z)$  (3.5) based on the relationships (3.6) between its real and imaginary parts  $U_1, V_1$  at the boundary of the region of its definition. This is a particular case of the Riemann–Hilbert problem.

The solution of this problem that satisfies the condition  $w_1(z) \sim \frac{P}{z}$  as  $z \rightarrow \infty$  and has the integrated singularities at the boundary is the following function

$$w_1(z) = \frac{\varrho}{X(z)} \int_{-a}^b F(t) X^+(t) \frac{dt}{t-z} + \frac{P}{X(z)}, \quad (3.8)$$

where

$$\begin{aligned}X(z) &= (z+a)^{1/2+\eta} (z-b)^{1/2-\eta}, \\ X^+(t) &= (t+a)^{1/2+\eta} (b-t)^{1/2-\eta},\end{aligned}$$

$$\varrho = \frac{1}{\sqrt{1 + \mu^2 \vartheta^2}}, \quad \eta = \frac{1}{\pi} \arctan(\mu \vartheta) \operatorname{sgn} V, \quad |\eta| < \frac{1}{2}. \quad (3.9)$$

Using the function (3.8), we can determine the stress-strain state of the elastic half-plane. For example, Eq. (3.5) implies that the normal stress at the  $x$ -axis  $\sigma_y(x, o)$  is the imaginary part of the function (3.8) as  $z \rightarrow x - i0$ . The limiting value of the Cauchy integral

$$\Phi(z) = \frac{1}{2\pi i} \int_{-\infty}^{+\infty} \varphi(t) \frac{dt}{t - z}$$

as  $z \rightarrow x - i0$  can be determined by the Plemelj (1908) formula (see also Muskhelishvili, 1949)

$$\Phi^-(x) = \frac{1}{2\pi i} \int_{-\infty}^{+\infty} \varphi(t) \frac{dt}{t - x} - \frac{1}{2} \varphi(x).$$

The limiting value of the function  $\frac{1}{X(z)}$  as  $z \rightarrow x - i0$  is determined by the formula

$$\begin{aligned} & \left[ \frac{1}{(z+a)^{1/2+\eta}(z-b)^{1/2-\eta}} \right]_{z=x-i0} = \\ & = \begin{cases} -\frac{1}{(-a-x)^{1/2+\eta}(b-x)^{1/2-\eta}}, & (-\infty < x < -a), \\ \frac{\sin \pi \eta + i \cos \pi \eta}{(x+a)^{1/2+\eta}(b-x)^{1/2-\eta}}, & (-a \leq x \leq b), \\ \frac{1}{(x+a)^{1/2+\eta}(x-b)^{1/2-\eta}}, & (b < x < +\infty). \end{cases} \end{aligned}$$

So the contact pressure  $p(x) = -\sigma_y(x, 0) = -\frac{1}{\pi} V_1(x, 0)$ , where  $V_1(x, 0)$  is the imaginary part of the function  $w_1(z)$  as  $z \rightarrow x - i0$ , is given by

$$\begin{aligned} p(x) &= -F(x)\varrho \sin \pi \eta + \\ & \frac{\varrho}{\pi} \cdot \frac{\cos \pi \eta}{X^+(x)} \int_{-a}^b F(t) X^+(t) \frac{dt}{t - x} + \frac{P \cos \pi \eta}{\pi X^+(x)}, \quad x \in (-a, b). \end{aligned} \quad (3.10)$$

### 3.2.2 Contact problem for a cylinder

We consider the particular case of a sliding contact of a rigid cylinder and an elastic half-space. For this case  $f(x) = \frac{x^2}{2R}$  and the function  $F(x)$  (3.7) becomes

$$F(x) = \tau_0 \vartheta \operatorname{sgn} V + \frac{x}{\pi K R}. \quad (3.11)$$

Substituting (3.11) in (3.10) and using the following relationships (Gradshteyn and Ryzhik, 1963)

$$\int_{-a}^b (a+t)^{-1/2+\eta} (b-t)^{-1/2-\eta} \frac{dt}{t-x} = \pi \tan \pi \eta (a+x)^{-1/2+\eta} (b-x)^{-1/2-\eta}, \quad (-a < x < b),$$

$$\int_{-a}^b (a+x)^{\mu-1} (b-x)^{\nu-1} dx = (a+b)^{\mu+\nu-1} B(\mu, \nu), \quad (\mu > 0, \nu > 0),$$

we obtain the expression for the contact pressure

$$\begin{aligned} p(x) &= \frac{\varrho L(x)}{(x+a)^{-1/2+\eta} (b-x)^{-1/2-\eta}}, \\ L(x) &= \frac{P}{\pi} + \frac{(a+b)^2 \left( \frac{1}{4} - \eta^2 \right)}{2\pi K R} + \tau_0 \vartheta(a+b) \left( \frac{1}{2} - \eta \right) \operatorname{sgn} V \\ &\quad + \frac{(a+b)x}{\pi K R} \left( \frac{1}{2} - \eta \right) - \tau_0 \vartheta(x+a) \operatorname{sgn} V + \frac{(a+x)x}{\pi K R}. \end{aligned} \quad (3.12)$$

The contact pressure (3.12) has to be bounded at the ends of the contact zone. Equation (3.12) shows that if it is bounded there, it must in fact be zero there, i.e.  $p(-a) = p(b) = 0$  and

$$l^2 = (a+b)^2 = \frac{2RPK}{\frac{1}{4} - \eta^2}, \quad (3.13)$$

$$\frac{a-b}{2} = l\eta + \tau_0 \vartheta K R \pi \operatorname{sgn} V. \quad (3.14)$$

So that

$$p(x) = \frac{\varrho}{\pi K R} (x+a)^{1/2-\eta} (b-x)^{1/2+\eta}. \quad (3.15)$$

The relationships (3.13), (3.14) and (3.15) determine the contact width, the shift of the contact zone and the contact pressure, respectively. Equations (3.13) and (3.15) coincide with the ones obtained by Galin (1953), where the contact problem in the analogous formulation with Amontons' (1699) law of friction  $\tau_{xy} = \mu \sigma_y$  was considered.

The results indicate that the magnitude  $\tau_0$  in the law (3.2) influences only the contact displacement (3.14).

It follows from Eq. (3.15) that the contact pressure is an unsymmetrical function. It provides the moment  $M$

$$M = \int_{-a}^b p(x)x dx = -P \left[ \frac{4}{3}l\eta + \pi\vartheta KR\tau_0 \operatorname{sgn} V \right], \quad (3.16)$$

where

$$P = \int_{-a}^b p(x) dx.$$

If there is no active moment applied to the cylinder, the moment  $M$  is equal to the moment of the tangential force  $T$

$$T = \int_{-a}^b \tau_{xy} dx = (\tau_0 l + \mu P) \operatorname{sgn} V. \quad (3.17)$$

In this case, it follows from the equilibrium conditions that the force  $T$  must be applied at the point  $(0, d)$  (Fig. 3.1):  $d = \left| \frac{M}{T} \right|$ .

Note that in most cases  $\mu\vartheta \ll 1$ , so that we may approximate Eq. (3.9) by

$$|\eta| \approx \frac{\mu}{\pi}\vartheta \ll 1.$$

Based on this estimation, it follows from Eqs. (3.13), (3.14) and (3.15) that the friction coefficient  $\mu$  has no essential influence on the contact pressure, the shift or the width of contact zone.

The analysis of subsurface stresses revealed that the effect of the parameter  $\tau_0$  on the stress-strain state in an elastic body is similar to a friction coefficient  $\mu$ : it moves the point where the maximum principal shear stress  $(\tau_1)_{\max}$  takes place closer to the surface, and it increases the magnitude of  $(\tau_1)_{\max}$  (Fig. 3.2).

Eqs. (3.13) – (3.16) can be used to determine contact characteristics (contact width and displacement, contact pressure etc.) for sliding contact of two elastic bodies with radii of curvature  $R_1$  and  $R_2$ . We replace the parameters  $K$ ,  $\vartheta$ ,  $R$  and  $\eta$  (see Eqs. (3.7) and (3.9)) by the parameters  $K^*$ ,  $\vartheta^*$ ,  $R^*$ ,  $\eta^*$ . For plane stress

$$K^* = \frac{2}{\pi} \left( \frac{1}{E_1} + \frac{1}{E_2} \right), \quad \vartheta^* = \frac{1}{K\pi} \left( \frac{1-\nu_2}{E_2} - \frac{1-\nu_1}{E_1} \right), \quad (3.18)$$

and for plane strain

$$\begin{aligned} K^* &= \frac{2}{\pi} \left( \frac{1-\nu_1^2}{E_1} + \frac{1-\nu_2^2}{E_2} \right), \\ \vartheta^* &= \frac{1}{K\pi} \left[ \frac{(1+\nu_2)(1-2\nu_2)}{E_2} - \frac{(1+\nu_1)(1-2\nu_1)}{E_1} \right], \end{aligned} \quad (3.19)$$

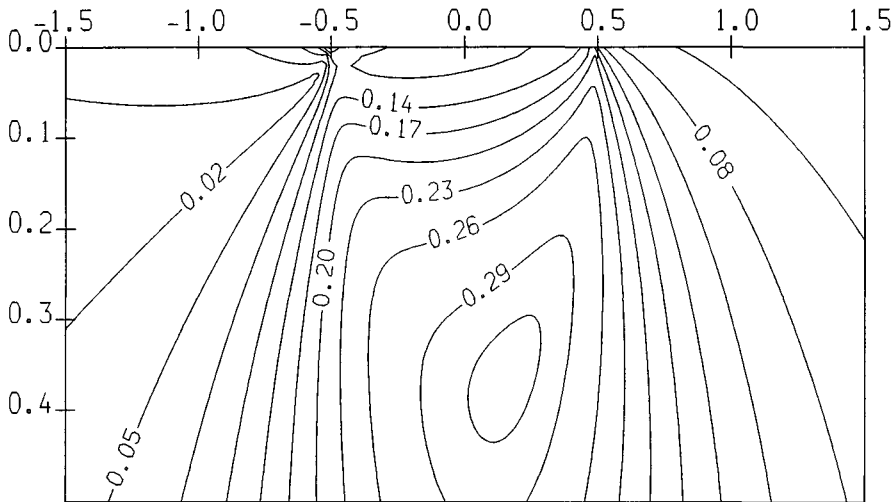


Figure 3.2: Contours of the principal shear stress beneath a sliding contact ( $\mu = 0$ ,  $\tau_0/p_0 = 0.1$ ).

and

$$\frac{1}{R^*} = \frac{1}{R_1} + \frac{1}{R_2}, \quad \eta^* = \frac{1}{\pi} \arctan(\mu \vartheta^*) \operatorname{sgn} V.$$

Provided that  $l \ll R_i$ , ( $i = 1, 2$ ) we can consider the cylinders as half-planes. So we use Eq. (3.4) to determine the gradient of normal displacement for both cylinders, taking into account the relationship:  $\tau_{xy}^{(1)} = -\tau_{xy}^{(2)}$ .

### 3.2.3 Contact problem for a flat punch

We consider sliding contact of a punch with a flat base (Fig. 3.3). Under the applied forces, the punch has the inclination  $\gamma$ . So the equation for the punch shape is  $f(x) = -\gamma x - D$ .

The function  $F(x)$  (3.7) has the following form

$$F(x) = \tau_0 \vartheta \operatorname{sgn} V - \frac{\gamma}{\pi K} \quad (-a \leq x \leq b). \quad (3.20)$$

We introduce the dimensionless parameter

$$\kappa = \frac{b}{P} \left( \tau_0 \vartheta \operatorname{sgn} V - \frac{\gamma}{\pi K} \right). \quad (3.21)$$

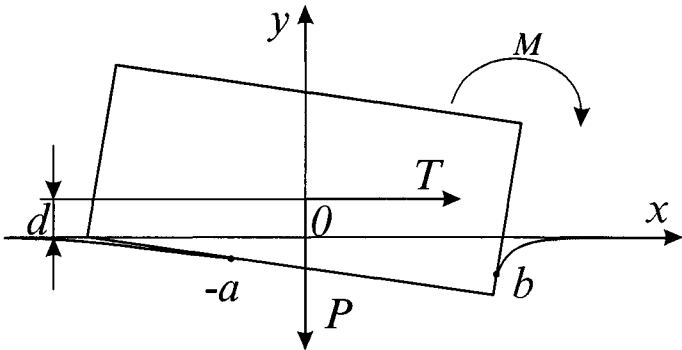


Figure 3.3: Sliding contact of a flat punch and an elastic half-plane.

Substituting Eq. (3.20) in Eq. (3.10) and transforming this equation, we have

$$p(x) = \frac{P\varrho}{\pi b} \cdot \frac{b + \pi\kappa \left[ b - x - \left( \frac{1}{2} + \eta \right) (a + b) \right]}{(x + a)^{1/2+\eta} (b - x)^{1/2-\eta}}. \quad (3.22)$$

Eq. (3.22) shows that the contact pressure near the ends of contact zone ( $x \rightarrow +0$ ) can be represented as

$$p(-a + x) = \frac{A_1}{x^{1/2+\eta}} + O\left(x^{1/2-\eta}\right),$$

$$A_1 = \frac{P\varrho}{\pi b} \cdot \frac{\left[ b + \pi\kappa(a + b) \left( \frac{1}{2} - \eta \right) \right]}{(a + b)^{1/2-\eta}}, \quad (3.23)$$

$$p(b - x) = \frac{A_2}{x^{1/2-\eta}} + O\left(x^{1/2+\eta}\right),$$

$$A_2 = \frac{P\varrho}{\pi b} \cdot \frac{\left[ b - \pi\kappa(a + b) \left( \frac{1}{2} + \eta \right) \right]}{(a + b)^{1/2+\eta}}. \quad (3.24)$$

We consider the case of a complete contact of a flat punch and an elastic half-plane. Setting  $a = b$  in Eq. (3.22) we have

$$p(x) = \frac{P\varrho}{\pi b} \cdot \frac{[b - \pi\kappa(x + 2b\eta)]}{(x + b)^{1/2+\eta} (b - x)^{1/2-\eta}}. \quad (3.25)$$

The contact pressure is a nonnegative function,  $p(x) \geq 0$  ( $-b \leq x \leq b$ ), and hence

$$\kappa_1 \leq \kappa \leq \kappa_2, \quad (3.26)$$

where

$$\kappa_1 = -\frac{1}{\pi(1 - 2\eta)}, \quad \kappa_2 = \frac{1}{\pi(1 + 2\eta)}. \quad (3.27)$$

The contact pressure  $p(x)$  given by Eq. (3.25) tends to infinity at the edges of the punch ( $x = \pm b$ ), if  $\kappa \in (\kappa_1, \kappa_2)$ . If  $\kappa = \kappa_1$  or  $\kappa = \kappa_2$ , the contact pressure is zero at the left end or at the right end of the contact zone, respectively.

If the parameter  $\kappa \notin [\kappa_1, \kappa_2]$ , there is only partial contact. If  $\kappa \leq \kappa_1 < 0$  the separation of the punch base from the half-plane appears at the left-hand end of the contact zone at the point  $x = -a$ . The contact width is found according to Eq. (3.23)

$$a + b = -\frac{b}{\pi\kappa\left(\frac{1}{2} - \eta\right)}. \quad (3.28)$$

Using Eqs. (3.22) and (3.28), we obtain the contact pressure

$$p(x) = \frac{P\varrho}{\pi b} \cdot \frac{\left[ b + \pi\kappa(b-x)\left(\frac{1}{2} - \eta\right) \right]}{\left(\frac{1}{2} - \eta\right)(x+a)^{1/2+\eta}(b-x)^{1/2-\eta}}. \quad (3.29)$$

If  $\kappa > \kappa_2 > 0$  the contact pressure is zero at the right-hand end of the contact zone at the point  $x = b$ , where  $|b| < a$  ( $a$  is the half-width of the punch in this case). Using (3.22) and (3.24), we find the equation for the contact pressure

$$p(x) = \frac{P\kappa\varrho}{b} \left( \frac{b-x}{x+a} \right)^{1/2+\eta}.$$

It follows from Eqs. (3.21) and (3.24) that the coordinate  $x = b$  is determined by the formula

$$b = -a + \frac{P}{\pi \left( \tau_0 \vartheta \operatorname{sgn} V - \frac{\gamma}{\pi K} \right) \left( \frac{1}{2} + \eta \right)}. \quad (3.30)$$

The contact pressure distributions for different values of the parameter  $\kappa$  are shown in Fig. 3.4. The curves 1 – 4 correspond to the cases of complete contact and pressure approaching to infinity at the ends of contact zone ( $\kappa = 0$ ), complete contact when  $p(-b) = 0$  ( $\kappa = \kappa_1$ , see Eqs. (3.25) and (3.27)), and partial contact ( $\kappa = -0.5$  and  $\kappa = -0.75$ ), respectively. For the calculations we used  $|\mu\vartheta| = 0.057$  ( $\mu = 0.2$ ,  $\nu = 0.3$ ). Note that for frictionless contact ( $\mu = 0$ ,  $\tau_0 = 0$ ) the results obtained in this part coincide with those obtained by Galin (1953).

The parameter  $\kappa$  depends on the inclination  $\gamma$  (see Eq. (3.21)). For definiteness, let us consider the punch moving in the  $x$ -axis direction ( $V > 0$ ). The parameter  $\gamma$  can be found using the equilibrium conditions for the punch. The normal load  $P$ , the tangential force  $T$ , and the active moment  $M$  are applied to the punch (see Fig. 3.3). The contact pressure  $p(x)$  and the tangential stress  $\tau_{xy}(x)$  form the resistance forces which satisfy the following equilibrium conditions:

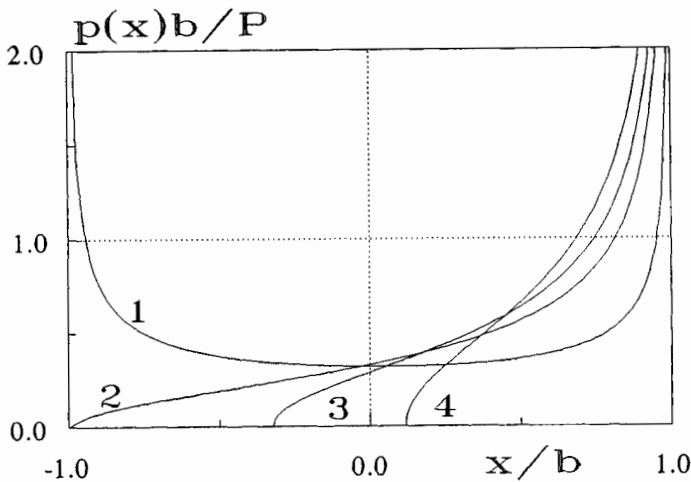


Figure 3.4: Contact pressure under a flat inclined punch sliding on an elastic half-plane ( $\mu\vartheta = 0.057$ );  $\kappa = 0$  (curve 1);  $\kappa = \kappa_1 = -0.33$  (curve 2);  $\kappa = -0.5$  (curve 3);  $\kappa = -0.75$  (curve 4).

$$P = \int_{-a}^b p(x)dx, \quad (3.31)$$

$$T = \int_{-a}^b \tau_{xy}(x)dx = \tau_0(a+b) + \mu P,$$

$$\int_{-a}^b (b-x)p(x)dx - Pb + Td - M = 0, \quad (3.32)$$

where  $(0, d)$  are the coordinates of the point where the force  $T$  is applied, and  $M$  is the active moment relative to the point  $x = b$ .

Using Eqs. (3.22) and (3.31), we can transform Eq. (3.32) to the following relation

$$-P(a+b)\left(\frac{1}{2} - \eta\right) + Pa + \frac{\pi P \kappa (a+b)^2}{2b} \left(\frac{1}{4} - \eta^2\right) + \tau_0(a+b)d + \mu P d - M = 0. \quad (3.33)$$

Eqs. (3.20) and (3.33) are used to determine the inclination  $\gamma$ , which depends on both quantities  $d$  and  $M$ .

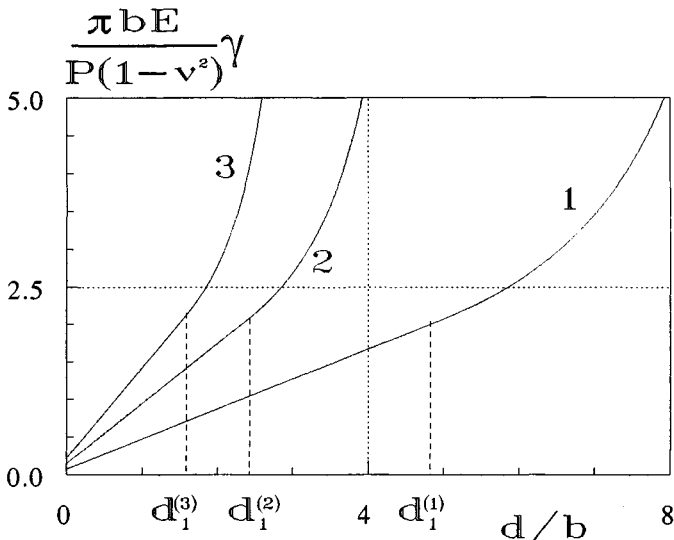


Figure 3.5: The effect of the position of the point of application of the tangential force  $T$  on the inclination of a punch ( $\nu = 0.3$ ,  $\tau_0 = 0$ );  $\mu = 0.1$  (curve 1),  $\mu = 0.2$  (curve 2),  $\mu = 0.3$  (curve 3);  $d_1^{(i)}$ , ( $i = 1, 2, 3$ ) indicates the transition point from complete to partial contact.

Let us consider the particular case  $M = 0$  and analyze the dependence of the inclination  $\gamma$  on the distance  $d$ . Using Eqs. (3.21), (3.26) and (3.33) we conclude that the complete contact occurs for  $d \in (0, d_1)$ , where

$$d_1 = \frac{Pb \left( \frac{1}{2} - \eta \right)}{2b\tau_0 + \mu P}. \quad (3.34)$$

The inclination  $\gamma$  for this case is

$$\gamma = \frac{2bP\eta + (2b\tau_0 + \mu P)d}{2b^2 \left( \frac{1}{4} - \eta^2 \right)} K + \tau_0 \pi \vartheta K. \quad (3.35)$$

If  $d \in (d_1, d_2)$ , the partial contact occurs with the separation point  $x = -a$ , where  $|a| < b$ ;  $d_2$  is determined by the condition  $-a = b$ , i.e. there is point contact. It follows from Eq. (3.33), that  $d_2 = \frac{b}{\mu}$ . The inclination  $\gamma$  of the punch for the case

$d_1 \leq d < d_2$  is determined from Eqs. (3.21), (3.28) and (3.33)

$$\gamma = \frac{P \left( \frac{1}{2} + \eta \right) + 2\tau_0 d}{2 \left( \frac{1}{2} - \eta \right) (b - \mu d)} K + \tau_0 \pi \vartheta K. \quad (3.36)$$

It follows from Eq. (3.36) that  $\gamma \rightarrow +\infty$  (the punch is overturned) as  $d \rightarrow d_2 - 0$ . Fig. 3.5 illustrates the dependence of the inclination  $\gamma$  on the distance  $d \in [0, d_2]$  for different magnitudes of the coefficient  $\mu$  and  $\tau_0 = 0$ . The Eqs. (3.35) and (3.36) have been used to plot the curves.

The results of this analysis can be used in the design of devices for tribological tests. If two specimens with flat surfaces come into contact, the hinge is used to provide their complete contact. The results show that the hinge must be fixed at a distance  $d \in (0, d_1)$  from the specimen base. The limiting distance  $d_1$  essentially depends on the friction coefficient  $\mu$ . If  $\tau_0 = 0$ , we obtain from Eq. (3.34)

$$\frac{d_1}{b} \approx \frac{1}{2\mu} - \frac{1 - 2\nu}{2\pi(1 - \nu)}.$$

### 3.3 Three-dimensional sliding contact of elastic bodies

We investigate three dimensional contact problems under the assumption that friction forces are parallel to the motion direction. This case holds if the punch slides along the boundary of an elastic half-space with anisotropic friction. The friction depends in magnitude and direction on direction of sliding. The description of the anisotropic friction has been made by Vantorin (1962) and Zmitrovic (1990). This friction occurs, for example, in sliding of monocrystals, which have properties in different directions which depend on the orientation of the crystal. Seal (1957) investigated friction between two diamond samples, and showed that the friction coefficient changes from 0.07 to 0.21, depending on the mutual orientation of the samples. A similar phenomenon was observed by Tabor and Wynne-Williams (1961) in experiments on polymers, where polymeric chains at the surface have special orientations.

For arbitrary surfaces, the assumption that friction forces are parallel to the motion direction is satisfied approximately.

#### 3.3.1 The friction law has the form $\tau_{xz} = \mu p$

We consider the contact of a punch sliding along the surface of an elastic half-space. We assume the problem to be quasistatic, which imposes a definite restriction on the sliding velocity, and we introduce a coordinate system  $(x, y, z)$  connected with

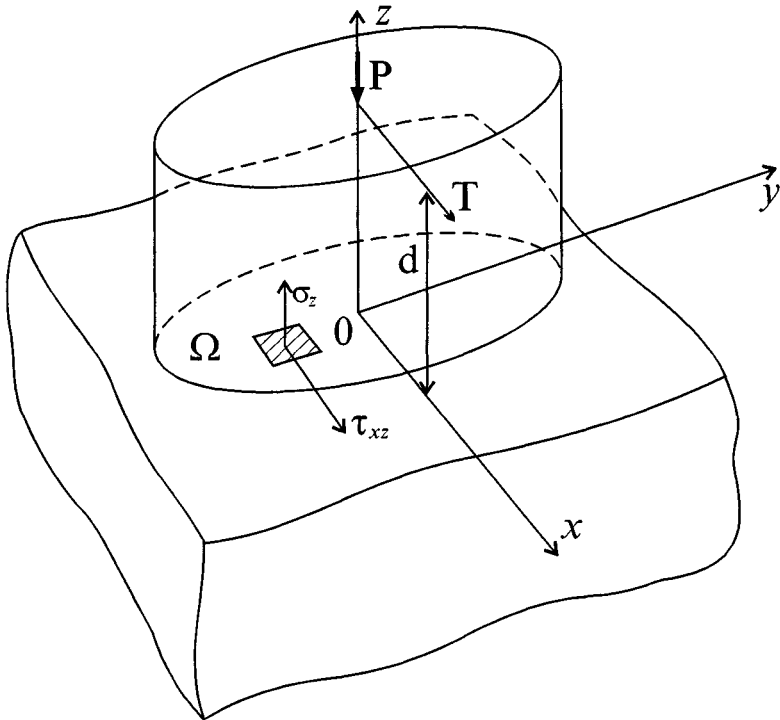


Figure 3.6: Sliding contact of a punch and an elastic half-space.

the moving punch (Fig. 3.6). The tangential stresses within the contact region  $\Omega$  are assumed to be directed along the  $x$ -axis, and  $\tau_{xz} = \mu p(x, y)$ , where  $p(x, y) = -\sigma_z(x, y, 0)$  is the contact pressure ( $p(x, y) \geq 0$ ). The boundary conditions have the form

$$\begin{aligned} w &= f(x, y) - D, & \tau_{xz} &= -\mu\sigma_z, & \tau_{yz} &= 0, & x, y \in \Omega, \\ \sigma_z &= \tau_{xz} = \tau_{yz} = 0, & & & & & x, y \notin \Omega. \end{aligned} \quad (3.37)$$

Here  $f(x, y)$  is the shape of the punch, and  $D$  is its displacement along the  $z$ -axis.

The displacement  $w$  of the half-space boundary in the direction of the  $z$ -axis can be represented as the superposition of the displacements caused by the normal pressure  $p(x, y)$  and the tangential stress  $\tau_{xz}$  within the contact zone. The solution of the problem for the elastic half-space loaded by a concentrated force at the origin with components  $T_x, T_z$  along the  $x$ - and  $z$ -axis, gives the vertical displacement

$w$  on the plane  $z = 0$  as

$$w = \frac{1 - \nu^2}{\pi E} \cdot \frac{T_z}{R} + \frac{(1 + \nu)(1 - 2\nu)}{2\pi E} \cdot \frac{xT_x}{R^2}, \quad (3.38)$$

$$\left( R = \sqrt{x^2 + y^2} \right).$$

Integrating (3.38) over the contact area  $\Omega$  and taking into account conditions (3.37), we obtain the following integral equation to determine the contact pressure  $p(x, y)$

$$\begin{aligned} \iint_{\Omega} \left[ \frac{1}{\sqrt{(x - x')^2 + (y - y')^2}} + \frac{\mu\vartheta(x - x')}{(x - x')^2 + (y - y')^2} \right] p(x', y') dx' dy' \\ = \frac{\pi E}{1 - \nu^2} [D - f(x, y)], \\ \vartheta = \frac{1 - 2\nu}{2 - 2\nu}. \end{aligned} \quad (3.39)$$

The coefficient  $\vartheta$  is equal to zero when  $\nu = 0.5$ , i.e. the elastic body is incompressible; in this case, friction forces do not affect the magnitude of the normal pressure. For real bodies, Poisson's ratio  $\nu$  satisfies the inequality  $0 < \nu < 0.5$ , hence the coefficient  $\vartheta$  varies between the limits  $0.5 > \vartheta > 0$ ; for example,  $\vartheta = 0.286$  for  $\nu = 0.3$ . Moreover, it should be remembered that the magnitude of the friction coefficient  $\mu$  is also small. For dry friction of steel on steel,  $\mu = 0.2$ . In the case  $\nu = 0.3$ ,  $\mu\vartheta \approx 0.057$ . For lubricated surfaces, the coefficient  $\mu\vartheta$  takes a still smaller value.

We investigate Eq. (3.39), assuming the parameter  $\mu\vartheta = \varepsilon$  to be small, and use the notation  $p_0(x, y)$  for the solution of the integral equation (3.39) in the case  $\mu\vartheta = 0$ . We represent the function  $p(x, y)$  in the form of the series

$$p(x, y) = p_0(x, y) + \varepsilon p_1(x, y) + \cdots + \varepsilon^n p_n(x, y) + \cdots. \quad (3.40)$$

Substituting the series (3.40) into the integral equation (3.39), we obtain a recurrent system of equations for the unknown functions  $p_n(x, y)$

$$A[p_n(x, y)] = B[p_{n-1}(x, y)], \quad n = 1, 2, \dots. \quad (3.41)$$

Here the following notations are introduced for operators

$$\begin{aligned} A[\omega] &= \iint_{\Omega} \frac{\omega(x', y') dx' dy'}{\sqrt{(x - x')^2 + (y - y')^2}}, \\ B[\omega] &= - \iint_{\Omega} \frac{\omega(x', y')(x - x') dx' dy'}{(x - x')^2 + (y - y')^2}. \end{aligned} \quad (3.42)$$

The convergence of the series (3.40) was proved (Galin and Goryacheva, 1983) for the case of a bounded function  $\omega$ .

As an illustration, let us consider sliding contact of an axisymmetric punch of circular planform,  $f(r) = \frac{r^2}{2R}$ , ( $r \leq a$ ,  $a$  is the radius of the contact region  $\Omega$ ,  $R$  is the radius of curvature of the punch surface). We introduce the polar coordinates  $(r, \theta)$ , i.e.

$$x = r \cos \theta, \quad y = r \sin \theta.$$

As is known (see, for example, Galin (1953) or Johnson (1987)), in this case the function  $p_0(x, y) = p_0(r)$  is

$$p_0(r) = \frac{4}{R\pi^2 K} \sqrt{a^2 - r^2}.$$

where  $K$  is determined in Eq. (3.7).

To find the next term  $p_1(r, \theta)$  in the series (3.40), first we find  $B[p_0(r)]$ , which is the result of integration

$$\begin{aligned} B[p_0(r)] &= b(r) \cos \theta, \\ b(r) &= \frac{8}{3R\pi K r} \left[ (a^2 - r^2)^{3/2} - a^3 \right]. \end{aligned}$$

Then we solve the equation

$$A[p_1(r, \theta)] = b(r) \cos \theta. \quad (3.43)$$

We will seek the solution of the equation (3.43) in the form

$$p_1(r, \theta) = q(r) \cos \theta.$$

Changing to polar coordinates in Eq.(3.42) we obtain

$$A[p_1(r, \theta)] = \int_0^{2\pi} \int_0^a \frac{q(r') \cos(\theta') r' dr' d\theta'}{\sqrt{r^2 + r'^2 - 2rr' \cos(\theta - \theta')}}.$$

Using tables of Gradshteyn and Ryzhik (1963, 3.674), we calculate the integral

$$\int_0^{2\pi} \frac{\cos(\theta') d\theta'}{\sqrt{r^2 + r'^2 - 2rr' \cos(\theta - \theta')}} = Q(r, r') \cos \theta,$$

where

$$Q(r, r') = \begin{cases} \frac{4}{r'} \left[ K\left(\frac{r'}{r}\right) - E\left(\frac{r'}{r}\right) \right], & r' < r, \\ \frac{4}{r} \left[ K\left(\frac{r}{r'}\right) - E\left(\frac{r}{r'}\right) \right], & r' > r. \end{cases}$$

$K(x)$  and  $E(x)$  are the complete elliptic integrals of the first and second kinds, respectively. So Eq.(3.43) reduces to the equation for determining the function  $q(r)$

$$\int_0^r \left[ K\left(\frac{r'}{r}\right) - E\left(\frac{r'}{r}\right) \right] q(r') dr' + \frac{1}{r} \int_r^a \left[ K\left(\frac{r}{r'}\right) - E\left(\frac{r}{r'}\right) \right] r' q(r') dr' = \frac{1}{4} b(r).$$

The other terms in the series (3.40) have the form (Galin and Goryacheva, 1983)

$$p_n(r, \theta) = \sum_{k=1}^n q_{nk}(r) \cos k\theta.$$

So in the case of sliding contact with friction, the contact pressure has the form  $p(r, \theta) = p_0(r) + \varepsilon q(r) \cos \theta + O(\varepsilon^2)$  which indicates, in particular, that the contact pressure is distributed nonsymmetrically, so that there is an additional moment  $M_y$  with respect to the  $y$ -axis:

$$M_y = \int_0^a \int_0^{2\pi} p(r, \theta) r^2 \cos \theta dr d\theta = \varepsilon \pi \int_0^a q(r) r^2 dr + O(\varepsilon^2).$$

It follows from the equilibrium condition that the force  $T$  directed along the  $x$ -axis that causes the punch motion, should be applied at a distance  $d = \left| \frac{M_y}{\mu P} \right|$  from the base. When this is not satisfied, the punch has an inclined base, which implies a change of the boundary conditions (3.37).

The contact problem for the punch with the flat circular base was investigated in the paper of Galin and Goryacheva (1983). It has been shown that the contact pressure can be presented in the form

$$p(r, \theta) = \frac{\psi(r, \theta)}{(a - r)^{1/2 + \eta}},$$

where  $\eta = \frac{1}{\pi} \arctan(\varepsilon \cos \theta)$ , and  $\psi(r, \theta)$  is a bounded and continuous function. To obtain this function, we again use the method of series-expansion with respect to the small parameter  $\varepsilon$ .

For the flat punch, the function  $w(r, \theta)$  in (3.37) has the form  $w(r, \theta) = \gamma r \cos \theta - D$ . The unknown coefficient  $\gamma$  governing the inclination of the punch can be found from the equilibrium condition for the moments acting on the punch (see § 3.2).

### 3.3.2 The friction law has the form $\tau_{xz} = \tau_0 + \mu p$

Consider the sliding contact of the punch and an elastic half-space, and assume that tangential stresses within the contact region are directed along the  $x$ -axis and

satisfy the friction law (3.1). Based on Eq. (3.38), we obtain the following integral equation for the contact pressure  $p(x, y)$

$$\begin{aligned} & \iint_{\Omega} \left[ \frac{1}{\sqrt{(x-x')^2 + (y-y')^2}} + \frac{\mu\vartheta(x-x')}{(x-x')^2 + (y-y')^2} \right] p(x', y') dx' dy' \\ & + \vartheta\tau_0 \iint_{\Omega} \frac{x - x'}{(x - x')^2 + (y - y')^2} dx' dy' = \frac{2}{K} [D - f(x, y)]. \end{aligned} \quad (3.44)$$

The second integral in the left-hand part of Eq. (3.44) can be calculated if the contact domain  $\Omega$  is given. For example, if  $\Omega$  is the circle of the radius  $a$ , we may change to polar coordinates, and find

$$\iint_{x'^2+y'^2 \leq a^2} \frac{(x - x') dx' dy'}{(x - x')^2 + (y - y')^2} = \int_0^a \int_0^{2\pi} \frac{(r \cos \theta - r' \cos \theta') r' dr' d\theta'}{r^2 + r'^2 - 2rr' \cos(\theta - \theta')}.$$

Using the relationship

$$\int_0^{2\pi} \frac{(r \cos \theta - r' \cos \theta') d\theta'}{r^2 + r'^2 - 2rr' \cos(\theta - \theta')} = \begin{cases} \frac{2\pi}{r} \cos \theta, & \left| \frac{r'}{r} \right| < 1, \\ 0, & \left| \frac{r'}{r} \right| > 1, \end{cases}$$

and the result of integration

$$\int_0^r \frac{2\pi}{r} \cos \theta r' dr' = \pi r \cos \theta = \pi x,$$

we reduce Eq. (3.44) to

$$\begin{aligned} & \iint_{\Omega} p(x', y') \left[ \frac{1}{\sqrt{(x-x')^2 + (y-y')^2}} + \frac{\mu\vartheta(x-x')}{(x-x')^2 + (y-y')^2} \right] dx' dy' \\ & = \frac{2}{K} [D - f(x, y)] - \pi\vartheta\tau_0 x. \end{aligned} \quad (3.45)$$

Eq. (3.45) differs from Eq. (3.39) only by the right side. The method of expansion with respect to the small parameter  $\varepsilon = \mu\vartheta$  can again be used to solve Eq. (3.45).

Let us analyze the influence of the parameter  $\frac{\tau_0}{E}$  on the solution of Eq. (3.45). At first, we consider the case of a smooth punch with surface described by the

function  $f(x, y) = \frac{x^2 + y^2}{2R}$ . Then the right side of Eq. (3.45) can be rewritten in the form

$$\frac{2}{K} [D - f(x, y)] - \pi \vartheta \tau_0 x = \frac{2}{K} \left[ D_1 - \frac{(x + e)^2 + y^2}{2R} \right], \quad (3.46)$$

where

$$e = \frac{\vartheta \tau_0 R \pi K}{2}, \quad D_1 = D + \frac{R \vartheta^2 \tau_0^2 \pi^2 K^2}{8}. \quad (3.47)$$

The relationships (3.47) indicate that the shift of the contact region  $e$  and the indentation of the punch  $D$  depend on the value of  $\frac{\tau_0}{E}$ .

Then let us consider the sliding contact of a punch with a flat base ( $f(x, y) = 0$ ,  $x^2 + y^2 \leq a^2$ ). In this case the right-hand side of Eq. (3.45) has the form

$$\frac{2}{K} [D - f(x, y)] - \pi \vartheta \tau_0 x = \frac{2}{K} D - \pi \vartheta \tau_0 x.$$

In this case the contact pressure distribution corresponds to the solution of Eq. (3.39) for the punch with inclined flat base; the angle of inclination is proportional to  $\pi \vartheta \tau_0$ .

This conclusion about the influence of  $\tau_0$  on the contact characteristics is in a good agreement with that made in the two-dimensional problem (see § 3.2).

### 3.4 Sliding contact of viscoelastic bodies

We consider a rigid cylinder moving over a viscoelastic base with a constant velocity  $V$  (Fig. 3.7). We assume that the velocity  $V$  is much smaller than the speed of sound in the viscoelastic body, which permits the inertial terms to be neglected in the equilibrium equations. Note that the typical values of the speed of sound ( $V_s$ ) are  $V_s \approx 5 \cdot 10^3$  m/s (for steels),  $V_s \approx 10^3$  m/s (for polymer materials),  $V_s \approx 30 - 50$  m/s (for soft rubbers).

### 3.4.1 Constitutive equations for the viscoelastic body

The relationships between the strain and stress components in an isotropic viscoelastic body are taken in the following form:

$$\begin{aligned}\varepsilon_{x^0} + T_\epsilon \frac{\partial \varepsilon_{x^0}}{\partial t} &= \frac{1 - \nu^2}{E} \left( \sigma_{x^0} + T_\sigma \frac{\partial \sigma_{x^0}}{\partial t} \right) \\ &\quad - \frac{\nu(1 + \nu)}{E} \left( \sigma_{y^0} + T_\sigma \frac{\partial \sigma_{y^0}}{\partial t} \right), \\ \varepsilon_{y^0} + T_\epsilon \frac{\partial \varepsilon_{y^0}}{\partial t} &= \frac{1 - \nu^2}{E} \left( \sigma_{y^0} + T_\sigma \frac{\partial \sigma_{y^0}}{\partial t} \right) \\ &\quad - \frac{\nu(1 + \nu)}{E} \left( \sigma_{x^0} + T_\sigma \frac{\partial \sigma_{x^0}}{\partial t} \right), \\ \gamma_{x^0 y^0} + T_\epsilon \frac{\partial \gamma_{x^0 y^0}}{\partial t} &= \frac{1 + \nu}{E} \left( \tau_{x^0 y^0} + T_\sigma \frac{\partial \tau_{x^0 y^0}}{\partial t} \right).\end{aligned}\tag{3.48}$$

Here  $T_\epsilon$  and  $T_\sigma$  are quantities characterizing the viscous properties of the medium,  $E$  and  $\nu$  are the Young's modulus of elasticity and Poisson's ratio, respectively. Plane strain is considered here; plane stress can be considered in the similar way.

Eqs. (3.48) constitute the two-dimensional extension of the Maxwell-Thomson model, for which  $H = \frac{T_\epsilon E}{T_\sigma}$  is the instantaneous modulus of elasticity,  $T_\epsilon > T_\sigma$ .

The parameter  $\frac{T_\epsilon}{T_\sigma}$  is equal to  $10^5 - 10^7$  for amorphic polymer materials,  $10 - 10^2$  for high level crystalline polymer materials,  $1.1 - 1.5$  for black metals;  $\frac{1}{T_\epsilon}$  is the coefficient of retardation.

Let us introduce a coordinate system  $(x, y)$  connected with the center of the cylinder (Fig. 3.7)

$$x = x^0 - Vt, \quad y = y^0.$$

The state of the viscoelastic medium is steady with respect to this coordinate system. The displacements and stresses depend on the coordinates  $(x, y)$  and are independent of time. i.e.  $u^0(x + Vt, t) \equiv u(x)$ ,  $v^0(x + Vt, t) \equiv v(x)$  etc. After differentiating the first identity with respect to  $t$  and  $x$ , we obtain

$$\frac{\partial u^0(x^0, t)}{\partial x^0} V + \frac{\partial u^0}{\partial t} = 0, \quad \frac{\partial u^0(x^0, t)}{\partial x^0} = \frac{\partial u(x)}{\partial x},$$

or

$$\frac{\partial u^0(x^0, t)}{\partial t} = -V \frac{\partial u(x)}{\partial x}.$$

The time derivative of the function  $v^0(x^0, t)$  and all components of stresses and strains in (3.48) can be found by the same procedure. Let us introduce the nota-

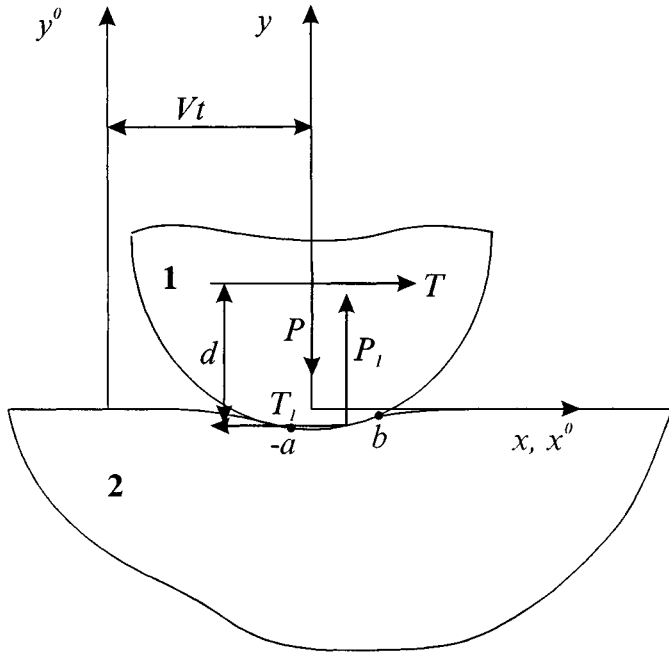


Figure 3.7: Scheme of the sliding contact of a cylinder and a viscoelastic half-space.

tions

$$\begin{aligned} \varepsilon_{ij}^0 + T_\varepsilon \frac{\partial \varepsilon_{ij}^0}{\partial t} &= \varepsilon_{ij} - T_\varepsilon V \frac{\partial \varepsilon_{ij}}{\partial x} = \varepsilon_{ij}^*, \\ \sigma_{ij}^0 + T_\sigma \frac{\partial \sigma_{ij}^0}{\partial t} &= \sigma_{ij} - T_\sigma V \frac{\partial \sigma_{ij}}{\partial x} = \sigma_{ij}^*, \\ u - T_\varepsilon V \frac{\partial u}{\partial x} &= u^*, \quad v - T_\varepsilon V \frac{\partial v}{\partial x} = v^*. \end{aligned} \quad (3.49)$$

The functions  $\varepsilon_x^*$ ,  $\varepsilon_y^*$ ,  $\gamma_{xy}^*$ ,  $\sigma_x^*$ ,  $\sigma_y^*$ ,  $\tau_{xy}^*$  introduced in this manner satisfy the equations equivalent to the equilibrium, strain compatibility and Hooke's law equations for an isotropic elastic body.

### 3.4.2 Problem formulation

Since the deformations are small, we describe the shape of the cylinder by the function  $f(x) = \frac{x^2}{2R}$ , and refer the boundary conditions to the undeformed surface ( $y = 0$ ). The relationship  $v = f(x) + \text{const}$  for the normal displacement  $v$  of the

half-plane ( $y = 0$ ) holds within the contact zone  $(-a, b)$ , hence

$$\frac{\partial v}{\partial x} = \frac{x}{R}, \quad (y = 0). \quad (3.50)$$

We suppose that there is limiting friction in the contact region. So the following relationship between the normal  $\sigma_y$  and tangential  $\tau_{xy}$  stresses (Amontons' law of friction, see Amontons, 1699) holds within the contact zone

$$\tau_{xy} = -\mu\sigma_y \operatorname{sgn} V, \quad (y = 0), \quad (3.51)$$

where  $\mu$  is the coefficient of sliding friction. The surface of the contacting bodies is stress free outside the contact area:

$$\sigma_y = \tau_{xy} = 0 \quad (-\infty < x < -a, \quad b < x < +\infty).$$

Using the notations (3.49), we find that Eqs. (3.50) and (3.51) give the following boundary conditions ( $y = 0$ )

$$\begin{aligned} \sigma_y^* &= \tau_{xy}^* = 0, \quad (-\infty < x < -a, \quad b < x < +\infty), \\ \frac{\partial v^*}{\partial x} &= \frac{x - T_\varepsilon V}{R}, \quad \tau_{xy}^* + \mu\sigma_y^* \operatorname{sgn} V = 0, \quad (-a \leq x \leq b). \end{aligned} \quad (3.52)$$

### 3.4.3 Analytical results

This boundary problem can be reduced to a Riemann-Hilbert problem by the method described by Galin (1953) and used in § 3.2. Then the real stresses and displacement can be found by solving of the differential equations (3.49). The solution of this problem in detail is published (Goryacheva, 1973) We give here only the final expressions.

The normal pressure  $p(x)$  at any point of contact zone is defined by the formula

$$\begin{aligned} p(x) &= -\sigma_y(x, 0) = -\frac{\varrho \exp(x/(T_\sigma V))}{T_\sigma V \pi K R} \times \\ &\times \int_{-a}^x \left[ \frac{(a+b)^2}{2} \left( \frac{1}{4} - \eta^2 \right) + PKR + (x' - T_\varepsilon V)(a+b) \left( \frac{1}{2} - \eta \right) - \right. \\ &\quad \left. (x' - T_\varepsilon V)(a+x') \right] \frac{\exp(-x'/(T_\sigma V)) dx'}{(a+x')^{1/2+\eta} (b-x')^{1/2-\eta}}, \end{aligned} \quad (3.53)$$

where  $K$ ,  $\varrho$  and  $\eta$  are determined by Eqs. (3.7) and (3.9),  $P$  is the normal force applied to the cylinder

$$P = \int_{-a}^b p(x) dx. \quad (3.54)$$

A tangential stress  $\tau_{xy}$  at the surface of the half-plane is determined by Eq. (3.51).

The width of the contact zone  $l = a + b$  is found as the solution of the following equation

$$\begin{aligned} & \left[ 1 - \left( \frac{l}{l_E} \right)^2 \right] \left[ \Psi \left( \frac{3}{2} + \eta, 3; 2\zeta \right) \Phi \left( \frac{1}{2} + \eta, 1; 2\alpha\zeta \right) + \right. \\ & \left. \frac{1}{2}\alpha \left( \frac{1}{2} - \eta \right) \Psi \left( \frac{1}{2} + \eta, 1; 2\zeta \right) \Phi \left( \frac{3}{2} + \eta, 3; 2\alpha\zeta \right) \right] + \\ & \left( \frac{l}{l_E} \right)^2 (1 - \alpha) \Psi \left( \frac{3}{2} + \eta, 3; 2\zeta \right) \Phi \left( \frac{3}{2} + \eta, 3; 2\alpha\zeta \right) = 0, \end{aligned} \quad (3.55)$$

where  $\zeta = \frac{l}{2T_\epsilon V}$  represents the ratio of the time taken for an element to travel through the semi-contact width  $\frac{l}{2}$  to the retardation time  $T_\epsilon$ ,  $l_E = \sqrt{2PKR / \left( \frac{1}{4} - \eta^2 \right)}$  is the contact width in sliding of the cylinder over the elastic half-plane under the normal force  $P$  if the elastic properties of the half-plane are characterized by the parameters  $K$  and  $\vartheta$  (see Eq. (3.7)),

$$\alpha = \frac{T_\epsilon}{T_\sigma},$$

and  $\Phi(\beta, \gamma; z)$  and  $\Psi(\beta, \gamma; z)$  are the confluent hypergeometric functions (see Gradshteyn and Ryzhik (1963, 9.210) or Janke and Emde (1944))

$$\Phi(\beta, \gamma; z) = 1 + \frac{\beta}{\gamma} \cdot \frac{z}{1!} + \frac{\beta(\beta+1)}{\gamma(\gamma+1)} \cdot \frac{z^2}{2!} + \frac{\beta(\beta+1)(\beta+2)}{\gamma(\gamma+1)(\gamma+2)} \cdot \frac{z^3}{3!} + \dots,$$

$$\Psi(\beta, \gamma; z) = \frac{\Gamma(1-\gamma)}{\Gamma(\beta-\gamma+1)} \Phi(\beta, \gamma; z) + \frac{\Gamma(\gamma-1)}{\Gamma(\beta)} z^{1-\gamma} \Phi(\beta-\gamma+1, 2-\gamma; z).$$

Eq. (3.55) shows that the contact width  $l$  depends on the viscoelastic properties of the half-plane, the normal force  $P$  applied to the cylinder, its radius  $R$  and also on the coefficient of friction  $\mu$ . Since the last term in Eq. (3.55) is negative ( $\alpha > 1$ ,  $|\eta| < \frac{1}{2}$ ), the first one is positive, and  $l^2 \leq l_E^2$ .

The shift  $\epsilon$  of the contact zone relative to the point  $(0, 0)$  can be found as

$$\epsilon = \frac{b-a}{b+a} = -2\eta + \frac{\left[ 1 - \left( \frac{l}{l_E} \right)^2 \right] \left( \frac{1}{2} - \eta \right) \Psi \left( \frac{1}{2} + \eta, 1; 2\zeta \right)}{2\zeta \left( \frac{l}{l_E} \right)^2 \Psi \left( \frac{3}{2} + \eta, 3; 2\zeta \right)}. \quad (3.56)$$

The ends of the contact zone  $-a$  and  $b$  can be found from Eqs. (3.55) and (3.56).

Fig. 3.7 illustrates the forces applied to the cylinder. The vertical component  $P_1$  of the reaction of the viscoelastic half-plane does not pass through the cylinder center. Hence, the moment

$$M_1 = \int_{-a}^b xp(x)dx = - \int_{-a}^b x\sigma_y^*(x, 0)dx - T_\sigma VP \quad (3.57)$$

resists the cylinder motion. To calculate the moment  $M_1$  we use

$$\int_{-a}^b x \frac{\partial \sigma_y(x, 0)}{\partial x} dx = P.$$

The last relation holds because of the continuity of the stresses at the boundary of the contact zone, Eq. (3.54) and the relation  $\sigma_y(x, 0) = -p(x)$ . The following expression for the moment  $M_1$  can be obtained by substituting Eq. (3.53) into Eq. (3.57)

$$\frac{M_1}{Pl} = \left( \frac{l}{l_E} \right)^2 \left( \frac{1}{2\zeta} - \frac{\epsilon}{2} - \frac{\eta}{3} \right) + \left( \frac{\epsilon}{2} - \frac{1}{2\zeta\alpha} - \eta \right). \quad (3.58)$$

The tangential forces  $T_1 = \mu P$  and  $T$  ( $|T| = |T_1|$ ) give rise to the moment  $M_2 = \mu Pd$ ,  $(0, d)$  is the point of application of the force  $T$  (see Fig. 3.7). The relations  $M_1 = M_2$   $\left( \text{or } d = \frac{M_1}{\mu P} \right)$  must hold, to provide the steady motion of the cylinder.

### 3.4.4 Some special cases

If we assume  $\eta = 0$  in the previous equations we obtain the solution of the frictionless problem for sliding of the rigid cylinder over the viscoelastic half-plane ( $\mu = 0$ ).

If we put  $\eta = 0$  in Eq. (3.53), we obtain the following expression for the contact pressure

$$p(x) = - \frac{\exp(x/(T_\sigma V))}{T_\sigma V \pi K R} \int_{-a}^x \frac{\frac{1}{8}(a+b)^2 + \frac{1}{2}(x' - T_\epsilon V)(b-a-2x') + PKR}{\exp(x'/(T_\sigma V)) \sqrt{(a+x')(b-x')}} dx'. \quad (3.59)$$

Since there is no friction, we have  $\tau_{xy} = 0$ .

If we put  $\eta = 0$  in Eqs. (3.55) and (3.56) we obtain

$$\begin{aligned} & \left[ 1 - \left( \frac{l}{l_0} \right)^2 \right] [I_0(\alpha\zeta)K_1(\zeta) + K_0(\zeta)I_1(\alpha\zeta)] + \\ & \frac{2}{\zeta} \left( \frac{1}{\alpha} - 1 \right) \cdot \left( \frac{l}{l_0} \right)^2 I_1(\alpha\zeta)K_1(\zeta) = 0, \end{aligned} \quad (3.60)$$

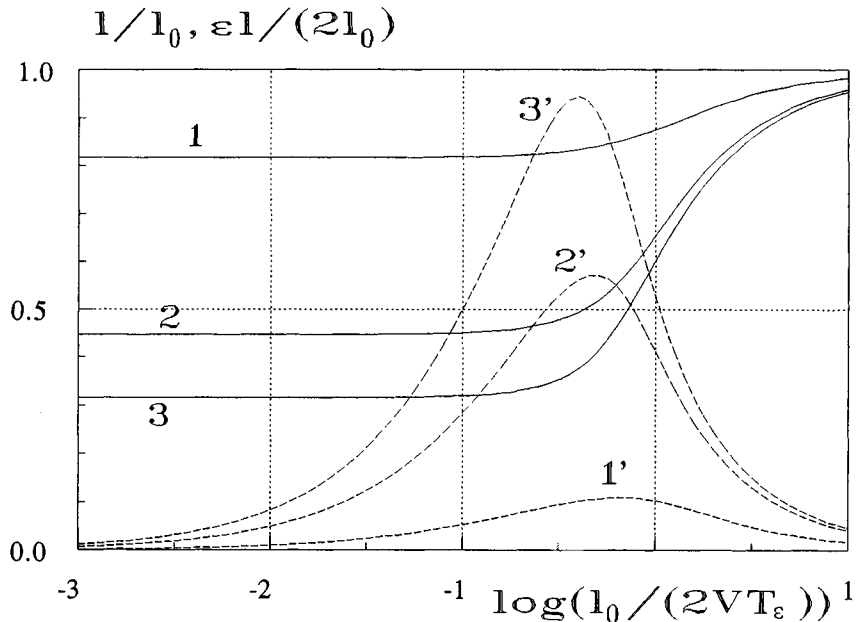


Figure 3.8: The contact width (solid lines) and the contact displacement (broken lines) in sliding/rolling contact ( $\mu\vartheta = 0$ ) of a cylinder and a viscoelastic half-space for various values of  $\alpha = T_\varepsilon/T_\sigma$ :  $\alpha = 1.5$  (curves 1, 1'),  $\alpha = 5$  (curves 2, 2'),  $\alpha = 10$  (curves 3, 3').

$$\epsilon = \frac{1}{2} \left( \left( \frac{l_0}{l} \right)^2 - 1 \right) \frac{K_0(\zeta)}{K_1(\zeta)}, \quad (3.61)$$

where  $l_0 = \sqrt{8KR_P}$  is the contact width in the corresponding problem for the elastic body, characterized by the parameter  $K$  (see Eq. (3.7)),  $I_\nu(x)$  and  $K_\nu(x)$  are modified Bessel functions. The following relationships (see Gradshteyn and Ryzhik (1963, § 8.4-8.5) or Janke and Emde (1944)) have been used to derive Eqs. (3.60) and (3.61)

$$\Phi\left(\frac{1}{2} + \nu, 1 + 2\nu; 2x\right) = 2^\nu \Gamma(\nu + 1) x^{-\nu} \exp(x) I_\nu(x),$$

$$\Psi\left(\frac{1}{2} + \nu, 1 + 2\nu; 2x\right) = \frac{1}{\sqrt{\pi}} \exp(x) (2x)^{-\nu} K_\nu(x).$$

The dependence of dimensionless contact width  $\frac{l}{l_0}$  and contact shift  $\frac{el}{2l_0}$  on the parameter  $\zeta_0 = \frac{l_0}{2T_\varepsilon V}$  have been calculated based on Eqs. (3.60) and (3.61).

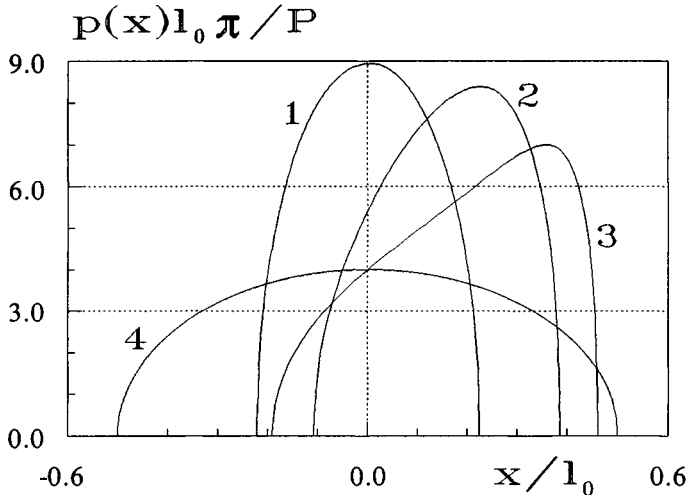


Figure 3.9: The pressure in sliding/rolling contact ( $\mu\vartheta = 0$ ) of a cylinder and a viscoelastic half-space ( $\alpha = 5$ ), for various values of  $\zeta_0$ :  $\zeta_0 = 10^{-3}$  (curve 1),  $\zeta_0 = 0.4$  (curve 2),  $\zeta_0 = 1$  (curve 3),  $\zeta_0 = 10^4$  (curve 4).

The parameter  $\zeta_0$  is the ratio of the contact duration at any point of the half-plane to the double retardation time  $T_\varepsilon$ . Fig. 3.8 illustrates the results calculated for the cases  $\alpha = 1.5$  (curve 1),  $\alpha = 5$  (curve 2) and  $\alpha = 10$  (curve 3). The results show that the contact width  $l$  changes within the limits  $l_H \leq l \leq l_0$ , where  $l_H = \sqrt{\frac{8KRP}{\alpha}}$ ,  $l_H$  is the contact width in the corresponding problem for the elastic body, having the instantaneous modulus of elasticity  $H = \alpha E$ . The contact shift  $\epsilon$  is a nonmonotonic function of the parameter  $\zeta_0$ , with its maximum lying in the range  $(0.1, 1)$ .

Fig. 3.9 illustrates the contact pressure distribution (Eq. (3.59)) for various parameters  $\zeta_0 = \frac{l_0}{2T_\varepsilon V}$ . For small values of this parameter ( $\zeta_0 = 10^{-3}$ , curve 1) the contact pressure is distributed symmetrically within the contact zone and it corresponds to the solution for elastic bodies having modulus  $H$ . For large values of the parameter ( $\zeta_0 = 10^3$ , curve 4), the contact pressure coincides with that for contact of elastic bodies having modulus  $E$ . If  $\zeta_0 \in (10^{-3}, 10^3)$ , the contact pressure becomes unsymmetrical (curves 2 and 3). The maximum contact pressure decreases as the parameter  $\zeta_0$  increases.

Equations (3.53), (3.55), (3.56) for  $T_\varepsilon = T_\sigma$  give the solution of the contact problem with limiting friction, for a rigid cylinder and an elastic half-plane (with elastic modulus  $E$ ). The following expressions can be obtained

$$p(x) = \frac{\varrho}{\pi K R} (a + x)^{1/2-\eta} (b - x)^{1/2+\eta}, \quad (3.62)$$

$$l = \sqrt{2KRP / \left( \frac{1}{4} - \eta^2 \right)}, \quad \epsilon = -2\eta. \quad (3.63)$$

The following relationship has been used to deduce Eq. (3.62)

$$I_0(x)K_1(x) + K_0(x)I_1(x) = \frac{1}{x}.$$

Eqs. (3.62) and (3.63) coincide with the results obtained in § 3.2 and in Galin (1980) and Johnson (1987).

## 3.5 Rolling contact of elastic and viscoelastic bodies

Contact problems for an elastic cylinder rolling along an elastic half-plane under the assumption of partial slip in the contact zone have been investigated by Carter (1926), Fromm (1927), Glagolev (1945), Poritsky (1950), Ishlinsky (1956), Johnson (1962), Mossakovskiy and Mishchishin (1967), Kalker (1990), etc.

The effect of imperfect elasticity of the contacting bodies has been investigated by Hunter (1961), Morland (1962), Kalker (1991), etc. They considered a rolling contact of a rigid or a viscoelastic cylinder and a viscoelastic half-plane.

We consider the simultaneous effect of sliding in contact and imperfect elasticity affecting the resistance to rolling.

### 3.5.1 Problem formulation

We consider this problem as two-dimensional and quasistatic. Suppose that a viscoelastic cylinder (1) of radius  $R$  rolls with a constant velocity  $V$  and angular velocity  $\omega$  over a base (2) of the same material (Fig. 3.7). As in the previous section, we consider a coordinate system  $(x, y)$  moving with the rolling cylinder. The relationship (3.50) holds within the contact zone  $(-a, b)$ . We assume that the contact zone  $(-a, b)$  consists of two parts: a slip region  $(-a, c)$  and a stick region  $(c, b)$ . The validity of this assumption in rolling contact problems for bodies of the same mechanical properties has been proved by Goryacheva (1974) and by Goldstein and Spector (1986).

The velocities of the tangential displacements of points of the cylinder and of the half-plane are equal within the stick zone  $(c, b)$ , i.e.

$$V - \omega R + \frac{\partial u_1^0}{\partial t} = \frac{\partial u_2^0}{\partial t}.$$

In the coordinate system  $(x, y)$  connected with the cylinder, this relation is written in the form:

$$\frac{du_2}{dx} - \frac{du_1}{dx} = \delta, \quad y = 0, \quad c < x < b, \quad \delta = \frac{\omega R - V}{V}. \quad (3.64)$$

Within the slip zone  $(-a, c)$  the Coulomb-Amontons' law of friction holds

$$\tau_{xy} = -\mu p(x) \operatorname{sgn} s_x, \quad p(x) > 0.$$

Here  $\mu$  is the coefficient of sliding friction, and  $s_x$  is the difference in velocities of tangential displacement of boundary points of a half-plane and cylinder:

$$s_x = \frac{\partial u_2}{\partial t} - \frac{\partial u_1}{\partial t} - V + \omega R = V \left( \delta + \frac{du_1}{dx} - \frac{du_2}{dx} \right).$$

The surface of the viscoelastic body is stress free outside the contact zone  $(-a, b)$ . The relations between the strain and stress components are taken in the form (3.48).

### 3.5.2 Solution

In the coordinate system  $(x, y)$ , the displacements and stresses do not depend explicitly on time and are functions only of the coordinates. As in § 3.4, we introduce the functions  $\epsilon_x^*, \epsilon_y^*, \gamma_{xy}^*, \sigma_x^*, \sigma_y^*, \tau_{xy}^*$  (3.49) which satisfy the equations equivalent to the equilibrium, strain compatibility and Hooke's law. To find these functions we use the method developed by Galin (1980). We introduce two functions of a complex variable  $w_1(z)$  and  $w_2(z)$  in the lower half-plane, which are Cauchy type integrals ( $z = x + iy$ )

$$w_1(z) = \int_{-a}^b \sigma_y^*(t, 0) \frac{dt}{t - z} = U_1(x, y) - iV_1(x, y),$$

$$w_2(z) = \int_{-a}^b \tau_{xy}^*(t, 0) \frac{dt}{t - z} = U_2(x, y) - iV_2(x, y).$$

Expressing the functions

$$\sigma_y^*(x, 0), \quad \tau_{xy}^*(x, 0), \quad \frac{du_i^*(x, 0)}{dx}, \quad \frac{dv_i^*(x, 0)}{dx}, \quad (i = 1, 2)$$

in terms of the real and imaginary parts of the functions  $w_1(z)$  and  $w_2(z)$  (see Galin, 1980) and substituting them into the boundary conditions, modified somewhat, taking account of (3.49), we obtain a conjugate problem: to find two functions  $w_1(z)$  and  $w_2(z)$  which are analytic in the lower half-plane and satisfy

$$V_1 = V_2 = 0, \quad x \notin (-a, b),$$

$$U_1 = -\frac{x - T_\varepsilon V}{KR}, \quad V_2 + \mu V_1 = 0, \quad x \in (-a, c),$$

$$U_1 = -\frac{x - T_\varepsilon V}{KR}, \quad U_2 = \frac{\delta}{K}, \quad x \in (c, b), \tag{3.65}$$

$$K = \frac{4(1 - \nu^2)}{\pi E}.$$

The functions satisfying the boundary conditions (3.65) are

$$\begin{aligned} w_1(z) &= -\frac{1}{X_1(z)} \int_{-a}^b \frac{t - T_\epsilon V}{\pi K R} X_1^+(t) \frac{dt}{t - z} - \frac{P}{X_1(z)}, \\ w_2(z) &= -\frac{X_2(z)}{\pi} \left[ \mu \int_{-a}^c V_1(t, 0) X_2^+(t) \frac{dt}{t - z} - \frac{\delta}{K} \int_c^b X_2^+(t) \frac{dt}{t - z} \right] - \frac{X_2(z)}{z - c} C_2. \end{aligned} \quad (3.66)$$

Here  $C_2$  is some constant and

$$\begin{aligned} X_1(z) &= \sqrt{(z + a)(z - b)}, \\ X_1^+(t) &= \sqrt{(a + t)(b - t)}, \\ X_2(z) &= \sqrt{\frac{z - c}{z - b}}, \\ X_2^+(t) &= \begin{cases} \sqrt{\frac{b - t}{c - t}}, & t \in (-a, c), \\ \sqrt{\frac{b - t}{t - c}}, & t \in (c, b), \end{cases} \\ P &= \int_{-a}^b p(x) dx = - \int_{-a}^b \sigma_y(x, 0) dx = - \int_{-a}^b \sigma_y^*(x, 0) dx. \end{aligned}$$

The last relation follows from Eq. (3.49) subject to the conditions  $\sigma_y(-a, 0) = \sigma_y(b, 0) = 0$ .

We can find  $\sigma_y^*(x, 0)$ ,  $\tau_{xy}^*(x, 0)$  by calculating the imaginary parts of the functions  $w_1(z)$  and  $w_2(z)$  on the real axis. Then true stresses  $p(x) = -\sigma_y(x, 0)$ ,  $\tau_{xy}(x)$  within the contact zone are found by solving the equations (3.49).

The function  $w_1(z)$  (3.66) shows that the tangential stress does not influence the pressure distribution for the contact of bodies having similar mechanical properties. The contact pressure in the problem under consideration is determined by Eq. (3.59) and can be represented by the curves in the Fig. 3.9.

Using the following relationships for the imaginary part  $V_1(x, 0)$  of the function  $w_1(z)$  as  $z \rightarrow x - i0$

$$V_1(x, 0) = \frac{F(x)}{\sqrt{(a + x)(b - x)}}, \quad x \in (-a, b),$$

where

$$F(x) = \frac{(a + b)^2}{8KR} + \frac{(x - T_\epsilon V)(b - a - 2x)}{2KR} + P \quad (3.67)$$

and the result of integration (see Gradshteyn and Ryzhik, 1963)

$$\int_c^b \sqrt{\frac{b-t}{t-c}} \cdot \frac{dt}{t-x} = \begin{cases} -\pi \left[ 1 - \sqrt{\left| \frac{b-x}{c-x} \right|} \right], & x \notin [c, b], \\ -\pi, & x \in (c, b), \end{cases} \quad (3.68)$$

we obtain the relationships for the imaginary part  $V_2(x, 0)$  of the function  $w_2(z)$  (3.66) as  $z \rightarrow x - i0$

$$\begin{aligned} V_2(x, 0) &= -\mu V_1(x, 0), \quad x \in (-a, c), \\ V_2(x, 0) &= -\mu V_1(x, 0) + \left[ \frac{\mu}{2KR} (b - c - 2x + 2T_\varepsilon V) + \frac{\delta}{K} \right] \times \\ &\quad \times \sqrt{\frac{x-c}{b-x}} + \frac{C_2}{\sqrt{(x-c)(b-x)}} = \pi \tau_{xy}^*(x, 0), \quad x \in (c, b). \end{aligned} \quad (3.69)$$

Then the tangential stresses  $\tau_{xy}(x)$  can be found by solving Eq. (3.49) (see Goryacheva, 1973):

- in the slip zone  $(-a, c)$

$$\tau_{xy}(x) = \mu p(x),$$

- in the stick zone  $(c, b)$

$$\begin{aligned} \tau_{xy}(x) &= \mu p(x) - \frac{\mu \exp(x/(T_\sigma V))}{2\pi KRT_\sigma V} \times \\ &\quad \int_c^x \left( b - c - 2t + 2T_\varepsilon V + \frac{2R\delta}{\mu} \right) \sqrt{\frac{t-c}{b-t}} \exp\left(-\frac{t}{T_\sigma V}\right) dt - \\ &\quad \frac{C_2}{\pi T_\sigma V} \exp\left(\frac{x}{T_\sigma V}\right) \int_c^x \frac{\exp(-t/(T_\sigma V))}{\sqrt{(t-c)(b-t)}} dt. \end{aligned} \quad (3.70)$$

For determining the constant  $C_2$  and the point  $c$  of transmission of slip to stick zone we use two conditions. The first one is the relation (3.64), which can be written at  $x = b$  in the form

$$\int_b^{+\infty} U_2(x, 0) \exp\left(-\frac{x}{T_\varepsilon V}\right) dx = \frac{\delta T_\varepsilon V}{K} \exp\left(-\frac{b}{T_\varepsilon V}\right), \quad (3.71)$$

where  $U_2(x, 0)$  is a real part of the function  $w_2(z)$  as  $z \rightarrow x - i0$ .

$$\begin{aligned} U_2(x, 0) &= - \left[ \frac{\mu}{2KR} (b - c - 2x + 2T_\varepsilon V) + \frac{\delta}{K} \right] \sqrt{\frac{x-c}{x-b}} + \\ &\quad \frac{\delta}{K} + \frac{\mu F(x)}{\sqrt{(x+a)(x-b)}} - \frac{C_2}{\sqrt{(x-c)(x-b)}}, \quad x \in (b, +\infty), \end{aligned}$$

where  $F(x)$  is defined by Eq. (3.67). The second one is the relation  $\tau_{xy}(b, 0) = 0$ , which holds because of the continuity of the stresses at the ends of the contact zone, and gives the equation

$$\int_{-a}^b V_2(x, 0) \exp\left(-\frac{x}{T_\sigma V}\right) dx = 0. \quad (3.72)$$

Using Eqs. (3.69), (3.71) and (3.72) we obtain

$$C_2 = \frac{\mu(b-c)}{4KR} \left[ b + c - 2T_\epsilon V - \frac{2R\delta}{\mu} + \left( b + c + \frac{2R\delta}{\mu} \right) \frac{K_1\left(\frac{b-c}{2T_\epsilon V}\right)}{K_0\left(\frac{b-c}{2T_\epsilon V}\right)} \right].$$

### 3.5.3 The contact width and the relation between the slip and stick zones

The unknown ends of the contact  $-a$  and  $b$ , and the transition point  $c$  can be determined by satisfying the conditions for the real stresses and displacements at the boundary of the elastic bodies. Goryacheva (1973) showed that the relationships for the contact width  $l = a + b$  and the contact shift  $\epsilon = \frac{b-a}{b+a}$  are the same as (3.60) and (3.61) which hold in the sliding problem for the rigid cylinder and the viscoelastic half-plane. The plots of these functions are presented in Fig. 3.8.

Using Eqs. (3.71) and (3.72) we can derive the following equation for determining the width  $\beta = \frac{b-c}{b+a}$  of the stick zone

$$\begin{aligned} & \left(1 + \epsilon - \beta - \frac{2R\delta}{\mu l}\right) [I_0(\alpha\beta\zeta)K_1(\beta\zeta) + I_1(\alpha\beta\zeta)K_0(\beta\zeta)] + \\ & \frac{1}{\zeta} \left(\frac{1}{\alpha} - 1\right) I_1(\alpha\beta\zeta)K_0(\beta\zeta) = 0. \end{aligned} \quad (3.73)$$

### 3.5.4 Rolling friction analysis

The cylinder is subjected to the normal load  $P$ , tangential load  $T$  and moment  $M$ . The reaction forces  $P_1$  and  $T_1$  are due to the normal and tangential stress distributions caused by the contact of the cylinder with the viscoelastic body (see Fig. 3.7). The condition for moment equilibrium about the center of the cylinder is

$$M + M_1 + T_1 R = 0,$$

where

$$M_1 = \int_{-a}^b xp(x) dx$$

and

$$T_1 = \int_{-a}^b \tau_{xy} dx = \int_{-a}^b \tau_{xy}^* dx = \frac{1}{\pi} \int_{-a}^b V_2(x, 0) dx,$$

$$(\tau_{xy}(-a) = \tau_{xy}(b) = 0).$$

Eqs. (3.57), (3.67) and (3.69) show that the equations for  $M_1$  and  $T_1$  can be transformed to the following expressions

$$\frac{M_1}{Pl} = \frac{\epsilon}{2} \left( 1 - \left( \frac{l}{l_0} \right)^2 \right) + \frac{1}{2\zeta} \left( \left( \frac{l}{l_0} \right)^2 - \frac{1}{\alpha} \right), \quad (3.74)$$

$$\frac{T_1}{\mu P} = 1 - \left( \frac{\beta l}{l_0} \right)^2 - 2\beta \left( \frac{l}{l_0} \right)^2 \left( 1 + \epsilon - \beta - \frac{2\delta R}{\mu l} \right) \frac{K_1(\beta\zeta)}{K_0(\beta\zeta)}. \quad (3.75)$$

Provided that the contact width  $l$  is in the limits  $l_H \leq l \leq l_0$  ( $l_H^2 = \frac{l_0^2}{\alpha}$ ), both terms in the side of (3.74) are nonnegative and so  $M_1 \geq 0$ . The sum of the moments of the normal and tangential contact stress with respect to the center of the cylinder gives the rolling friction moment  $M^* = M_1 + T_1 R$ .

The rolling friction is characterized by the rolling friction coefficient, which gives the relation between the moment of friction  $M^*$  and the normal load  $P$ . Using Eqs. (3.62), (3.73), (3.74) and (3.75) we obtain

$$\begin{aligned} \mu_r = \frac{M^*}{Pl} &= \left( \left( \frac{l_0}{l} \right)^2 - 1 \right) \frac{K_0(\zeta)}{4K_1(\zeta)} + \\ &\quad \frac{1}{2\zeta} \left( \left( \frac{l}{l_0} \right)^2 - \frac{1}{\alpha} \right) + \frac{\mu R}{l} \left( 1 - \frac{\beta^2 l^2}{l_0^2} \right) - \\ &\quad \frac{2\mu\beta R l \left( 1 - \frac{1}{\alpha} \right) I_1(\alpha\beta\zeta) K_0(\beta\zeta)}{l_0^2 \zeta [I_0(\alpha\beta\zeta) K_1(\beta\zeta) + I_1(\alpha\beta\zeta) K_0(\beta\zeta)]}. \end{aligned}$$

Free rolling occurs if  $T = 0$  and  $M = M_1$ . Fig. 3.10 illustrates the dependence of the coefficient  $\mu_r$  of a rolling friction on the parameter  $\zeta_0 = \frac{l_0}{2T_\epsilon V}$  for free rolling. The results indicate that the maximum value of the friction coefficient takes place for  $\zeta_0 \approx 1$ . The maximum value of  $\mu_r$  depends essentially on the parameter  $\alpha$  characterizing viscous properties of contacting bodies.

The analysis of Eqs. (3.74), (3.75) and the equilibrium conditions show that tangential contact stresses acting on the half-plane are parallel to the velocity  $V$  ( $\mu > 0$ ) if  $M > M_1$ . If  $M < M_1$  the tangential stresses have the opposite direction ( $\mu < 0$ ), in this case the active tangential force  $T$  in the direction of motion is applied to the cylinder. Eqs. (3.73) and (3.75) show that the width of stick zone

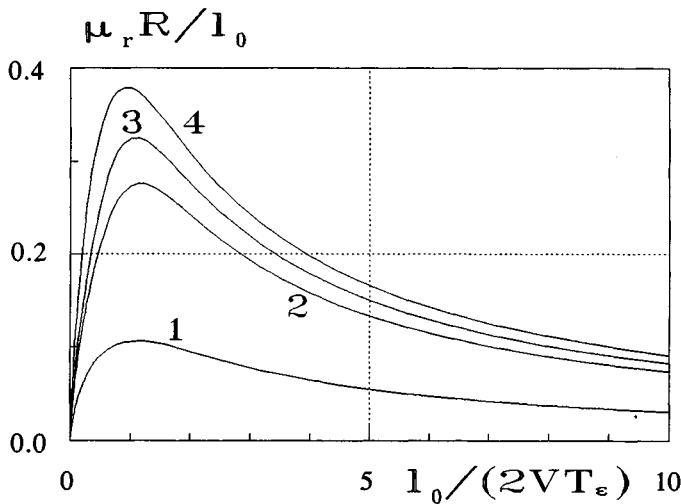


Figure 3.10: The rolling resistance of a viscoelastic cylinder on a viscoelastic half-space (similar materials,  $\mu = 0$ ) for various value of the parameter  $\alpha = T_\epsilon/T_\sigma$ :  $\alpha = 1.5$  (curve 1),  $\alpha = 5$  (curve 2),  $\alpha = 10$  (curve 3),  $\alpha = 100$  (curve 4).

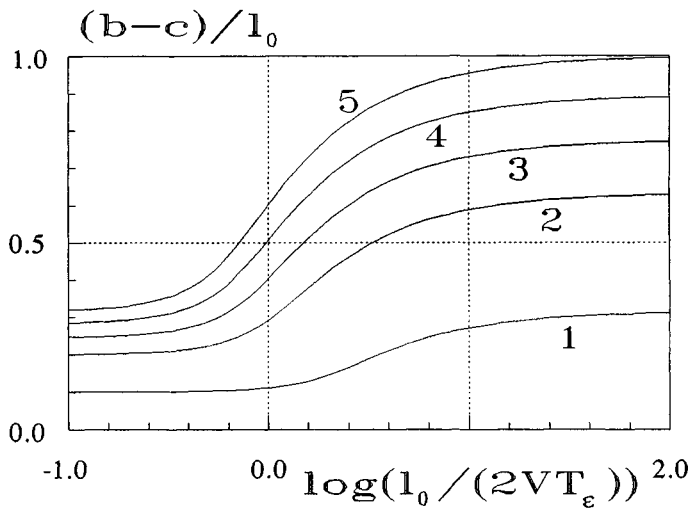


Figure 3.11: The effect of the parameter  $\zeta_0$  on the width of stick region for  $\alpha = 10$  and for various values of the parameter  $C = T_1/\mu P$ :  $C = 0.9$  (curve 1),  $C = 0.6$  (curve 2),  $C = 0.4$  (curve 3),  $C = 0.2$  (curve 4),  $C = 0$  (curve 5).

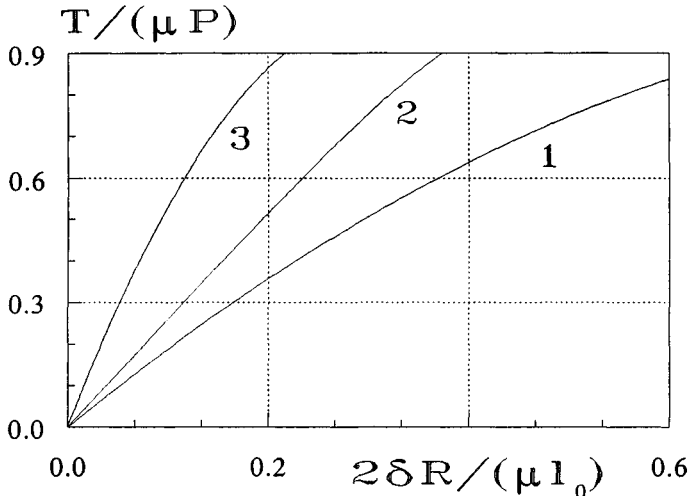


Figure 3.12: Creep curves for a tractive rolling contact of a viscoelastic cylinder on a viscoelastic half-space (similar materials,  $\alpha = 10$ ) for various values of the parameter  $\zeta_0 = l_0/2T_\varepsilon V$ :  $\zeta_0 = 10^2$  (curve 1),  $\zeta_0 = 10^{-1}$  (curve 2),  $\zeta_0 = 10^{-4}$  (curve 3).

depends on the ratio  $C = \frac{T_1}{\mu P}$ . Eq. (3.73) has been solved for various parameters  $C$ . The plots are shown in Fig. 3.11. The width of the stick zone increases as the parameter  $C$  decreases. For  $C = 0$ , the stick region is spread within the whole of the contact zone.

The creep ratio  $\delta$  for the rolling cylinder can be found from Eq. (3.75). Fig. 3.12 illustrates the dependence of the parameter  $C$  on the creep ratio for various parameters  $\zeta_0$ . The results show that for a fixed value of the parameter  $C$ , the creep ratio decreases as the parameter  $\zeta_0$  decreases (the velocity  $V$  increases).

### 3.5.5 Some special cases

If  $\alpha = 1$ , then the equations obtained above yield the solution of the problem of rolling of an elastic cylinder over a base of the same material, with elastic modulus  $E$ .

We obtain the following expressions for the normal and tangential stresses within the contact zone  $(-a, a)$  which is symmetrical in this case ( $\epsilon = 0$ )

$$p(x) = \frac{\sqrt{a^2 - x^2}}{\pi K R} \quad (-a < x < a),$$

$$\tau_{xy}(x) = \begin{cases} \frac{\mu}{\pi K R} \sqrt{a^2 - x^2}, & (-a < x < c), \\ \frac{\mu}{\pi K R} [\sqrt{a^2 - x^2} - \sqrt{(a-x)(x-c)}], & (c < x < a). \end{cases}$$

The contact width is  $l = 2a = \sqrt{8KRP}$ , the width of the stick zone is  $\beta = 1 - \frac{\delta R}{\mu a}$ .

The contact pressure distribution is symmetrical ( $M_1 = 0$ ). The tangential force  $T$  is calculated by the formula

$$\frac{T}{\mu P} = \frac{\delta R}{\mu a} \left( 2 - \frac{\delta R}{\mu a} \right).$$

Note that the relative width of the stick zone does not depend on the elastic properties of contacting bodies, and it is calculated by

$$\beta = \sqrt{1 - \frac{T}{\mu P}}.$$

If  $\alpha \neq 1$ , the contact characteristics for viscoelastic bodies approach those for elastic bodies with the elasticity moduli  $E$  and  $H = \alpha E$ , as  $T_\epsilon V \rightarrow 0$  and  $T_\epsilon V \rightarrow +\infty$ , respectively.

## 3.6 Mechanical component of friction force

We investigated the sliding contact of a rigid cylinder and an viscoelastic half-space in § 3.4. The results show that there is a resistance to the motion of the cylinder, even though we assume that the tangential stresses are zero at the interface. Under the same boundary conditions, there is no resistance to the motion in sliding contact of elastic bodies (see § 3.2 and § 3.3). The reason is that the deformation is reversible for elastic bodies so that both the contact region and stress distribution are symmetrical relative the axis of symmetry of the cylinder. This is not so for viscoelastic bodies. The center of the contact region, and the point where the maximum pressure takes place, are shifted towards the leading edge of the contact (see § 3.2). It is precisely these phenomena that are responsible for the resistance in sliding.

Let us calculate the tangential force  $T$  that has to be applied to the cylinder to provide its steady motion (Fig. 3.13). We assume that the tangential stress is negligible within the contact zone ( $\tau_{xy} = 0$ ). This enables us to study the mechanical friction component alone. Since the normal stress is directed to the center of the cylinder, the reaction force  $F$  is also directed to the center (see Fig. 3.13(a)). Let us calculate the  $x$ - and  $y$ - components  $T_d$  and  $P_1$  of the reaction force  $F$ . Taking into account that the contact width  $l = a + b$  is much less than the radius  $R$ , we can write

$$P_1 = \int_{-a}^b p(x) \cos \varphi(x) dx \approx \int_{-a}^b p(x) dx, \quad (3.76)$$

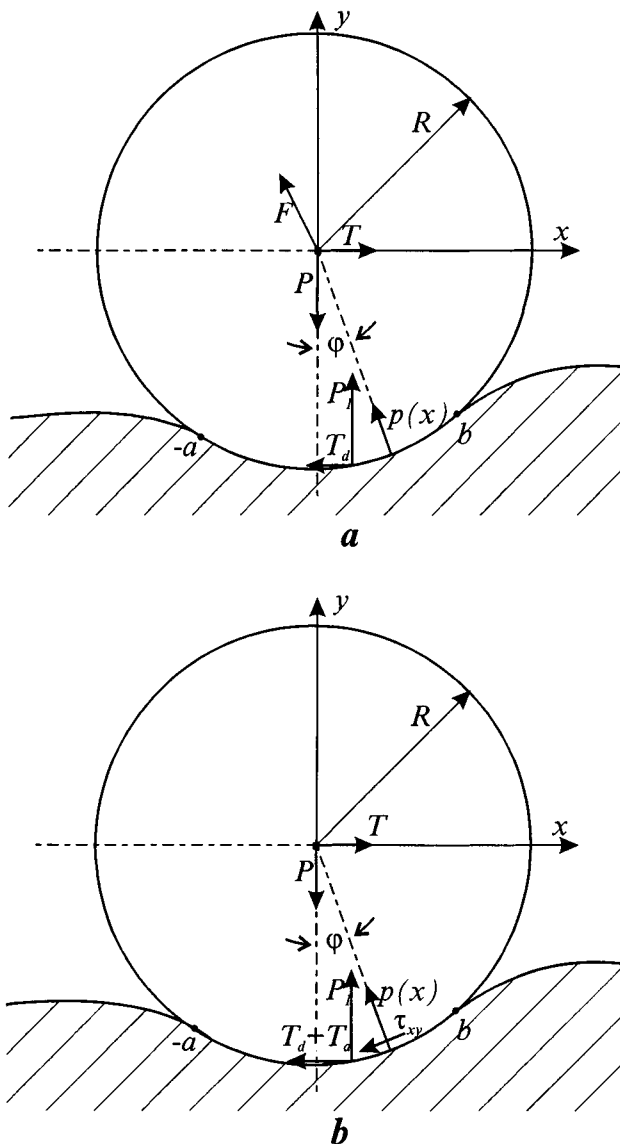


Figure 3.13: Scheme of the forces applied to the cylinder in sliding contact: frictionless contact (a), contact with friction (b).

$$T_d = \int_{-a}^b p(x) \sin \varphi(x) dx \approx \frac{M}{R}, \quad (3.77)$$

where

$$M = \int_{-a}^b xp(x) dx.$$

The equations of equilibrium show that  $T_d = T$  and  $P_1 = P$ . The force  $T_d$  is called the mechanical friction component. The mechanical friction coefficient  $\mu_d$  can be obtained by dividing the equation (3.77) by the equation (3.76), with the result

$$\mu_d = \frac{T_d}{P} = \frac{M}{PR}, \quad (3.78)$$

where  $M$  is estimated from (3.58) provided that  $\eta = 0$  ( $l_E = l_0$  if  $\eta = 0$ ). Hence the expression for  $\mu_d$  can be written in the form

$$\mu_d = \alpha_h \frac{l_0}{R}, \quad (3.79)$$

where

$$\alpha_h = \frac{\varepsilon l}{2l_0} \left( 1 - \left( \frac{l}{l_0} \right)^2 \right) + \frac{\left( \frac{l}{l_0} \right)^2 - \frac{1}{\alpha}}{2\zeta_0}. \quad (3.80)$$

It is worth noting that the mechanical friction coefficient  $\mu_d$  (Eq (3.79)) coincides with the coefficient of rolling friction for free rolling of a viscoelastic cylinder over a viscoelastic half-space. This conclusion follows from the fact that Eq.(3.80) is similar to Eq. (3.74) divided by  $\frac{l_0}{l}$ . So the curves in Fig. 3.10 illustrate the dependence of the mechanical friction coefficient  $\mu_d$  on the parameter  $\zeta_0$ . The dependence is not monotonic, and has a maximum when  $\zeta_0 \approx 1$ , i.e. the semi-contact time is roughly equal to the retardation time. The mechanical component of friction force tends to zero for small or large values of the parameter  $\zeta_0$ .

Tabor (1952) was the first who proposed to determine the mechanical friction coefficient from a rolling contact test. Later experiments supported his idea. Fig. 3.14 illustrates the experimental results obtained by Greenwood and Tabor (1958). The rolling and sliding contact of steel balls over high-hysteresis rubber specimens was investigated. A soap was used as lubricant in sliding contact to decrease the adhesive component of the friction force. The results in sliding (solid symbols) and in rolling (open symbols) agree very closely. For a nominal pressure less than  $3 \cdot 10^4 Pa$ , they are in a good agreement with the theoretical curve based on the hysteresis theory of friction. According to this theory elaborated for the rolling friction, the coefficient of rolling friction is determined from the expression (3.79). It is supposed that the coefficient  $\alpha_h$  is dependent on the viscoelastic properties of material and the rolling velocity. The value of the coefficient  $\alpha_h$  is determined from experiments of cyclic loading of the material.

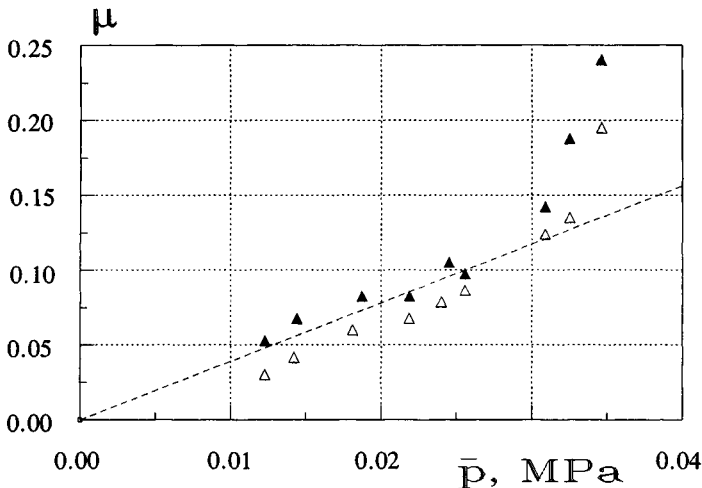


Figure 3.14: The friction coefficient of a steel sphere on well-lubricated rubber, as a function of the average contact pressure in rolling contact (open symbols) and in sliding contact (solid symbols) (the experimental results, Greenwood and Tabor, 1958). The broken line is a theoretical curve obtained from the hysteresis theory of friction (Tabor, 1955).

The investigation of contact problems for a cylinder and a viscoelastic half-space (see § 3.4 and § 3.5) makes it possible to analyze the dependence of the coefficient  $\alpha_h$  (3.80) in a sliding/rolling contact on the viscoelastic characteristics of the material ( $E$ ,  $\nu$ ,  $T_\sigma$ ,  $T_\epsilon$ ) and the sliding/rolling velocity. An analysis of the equation (3.80) shows that the magnitude of  $\alpha_h$  also depends on the normal load  $P$  because of  $l_0 \sim \sqrt{P}$ . The discrepancy between the theoretical and experimental results (see Fig. 3.14) may be explained by the neglect in the calculations of the dependence of  $\alpha_h$  on pressure (the theoretical curve corresponds to  $\alpha_h = 0.35$ ).

It was suggested in the previous analysis that the energy dissipation due to irreversible deformation is the only reason for the friction force. Considering that both of the causes of energy dissipation (adhesion and deformation) are simultaneously realized in sliding contact, it is important to investigate their joint influence on the friction force. Are there mutual influences between the adhesive and mechanical components of the friction force? Some results obtained in this chapter (see § 3.4) make it possible to answer this question.

We consider the cylinder of radius  $R$  sliding with friction ( $\tau_{xy}(x) = \mu_a p(x)$ ) over viscoelastic body (Fig. 3.13(b)). In this case the adhesive component of the

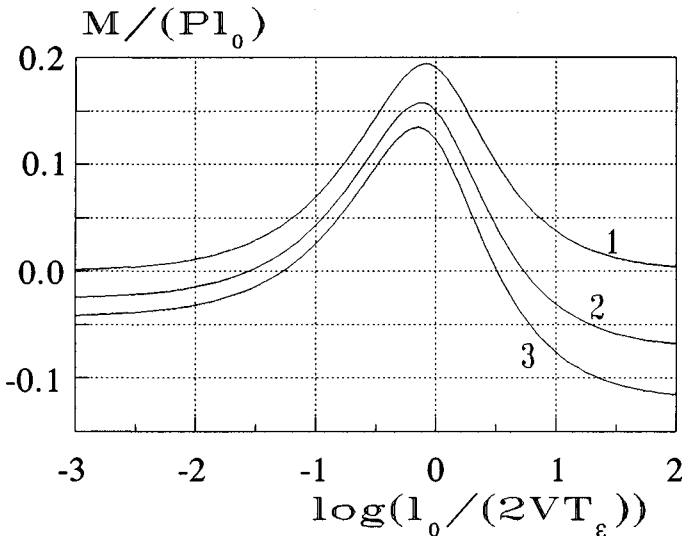


Figure 3.15: The mechanical component of friction force for different friction coefficients  $\mu_a$ :  $\mu_a = 0$  (curve 1),  $\mu_a = 0.3$  (curve 2),  $\mu_a = 0.6$  (curve 3),  $\alpha = 5$ .

friction force  $T_a$  can be written as

$$T_a = \int_{-a}^b \tau_{xy} \cos \varphi(x) dx \approx \mu_a \int_{-a}^b p(x) dx = \mu_a P. \quad (3.81)$$

The equation of equilibrium shows that

$$T = T_a + T_d = \mu_a P + \frac{M}{R}.$$

Hence the total friction coefficient is given by the expression

$$\mu = \frac{T}{P} = \mu_a + \frac{M}{PR}. \quad (3.82)$$

The second term in (3.82) is generally classified as the coefficient of the mechanical component of the friction force. The moment  $M$  is given by Eq. (3.58). Since the moment  $M$  depends on the parameter  $\eta$  (see Eqs. (3.55), (3.56) and (3.58)), and  $\eta$  in turn is a function of the adhesive friction coefficient  $\mu_a$  (see Eq. (3.9)), the mechanical component is governed by the adhesive one. Fig. 3.15 illustrates

the dependence of the dimensionless moment  $\frac{M}{Pl_0}$ , which is proportional to the mechanical component of friction force, on the parameter  $\zeta_0$  for different friction coefficients  $\mu_a$ . The results show that the coefficient  $\mu_a$  decreases the mechanical component. For small values of the parameter  $\zeta_0$ , the mechanical component becomes negative as the coefficient  $\mu_a$  increases.

# Chapter 2

## Mechanics of Discrete Contact

### 2.1 Multiple contact problem

#### 2.1.1 Surface macro- and micro- geometry

Contact problems in the classical formulation are posed for topographically smooth surfaces; this ensures that the contact region will be continuous.

In fact, contact between solid surfaces is *discrete* (discontinuous) due to deviations of the surface geometry from the design shape (*macrogeometry*). So a real contact region consists of contact spots, the total area of which (*the real contact area*) is a small fraction of the *nominal contact area* which is the minimal connected region enclosing all the contact spots. The size and arrangement of the contact spots depend on contact interaction conditions (load, kind of motion, etc.), materials, surface macrogeometry and the deviations from it.

These deviations (*asperities*) have various sizes and shapes. Their heights vary within wide limits: from a fraction of a nanometer (for example, the surface deviations of magnetic disks, Majumdar and Bhushan, 1990) to several millimeters. Depending on the scale, they are called macrodeviations, waviness or roughness. For example, *macrodeviations* are characterized by a small height and asperities with gentle slopes; they are caused by an imperfect calibration of an instrument, its wear, etc. *Waviness* is used to describe surface conditions which lie between macrodeviations and roughness. For waviness, the ratio of the distance between asperities (asperity pitch) to the height of an asperity is usually more than 40 (Sviridenok, Chijik and Petrokovets, 1990). *Roughness* is defined as a conglomeration of asperities with a small pitch relative to the base length. It forms a *surface microgeometry* which has a complex statistical character. It is usually a result of the surface treatment. Microgeometry of a surface can also be created artificially to provide the optimal conditions for frictional components to operate. Surfaces

with artificial microgeometry are widely applied in devices used for processing and storing information (Sviridenok and Chijik, 1992).

To obtain the complete information on the microshape deviations, various methods of surface topography measurement are used; they may, or may not, involve contact. Devices such as profilometers, optical interferometers, tunnel and atomic-force microscopes make it possible to describe the microgeometry of a given element of the surface, and to determine its roughness characteristics: the mean height, and the mean curvature of asperities, the number of asperities per unit area of the surface, etc.

Surface deviations from macroshape influence contact characteristics (real pressure distribution, real contact area, etc.) and internal stresses in subsurface layers. To estimate these effects, it is necessary to solve a *multiple contact problem*, that is a boundary problem in the mechanics of solids for a system of contact spots comprising a real contact area.

### 2.1.2 Problem formulation

We consider a contact interaction of a deformable half-space and a counter-body, the shape of which is described by the function  $z = -F(x, y)$  in the system of coordinates connected with the half-space (the plane  $Oxy$  coincides with the half-space surface in the undeformed state, and the  $z$ -axis is directed into the half-space). After deformation a finite number  $N$  or an infinity of contact spots  $\omega_i$  occur at the surface  $z = 0$  of the half-space within the nominal contact region  $\Omega$ . If  $N \rightarrow \infty$ , the region  $\Omega$  coincides with the plane  $z = 0$ .

The real contact pressure  $p_i(x, y)$  acts at each contact spot  $(x, y) \in \omega_i$ . We assume here that tangential stresses are negligibly small. The contact pressure provides the displacement of the half-space surface along the  $z$ -axis. This displacement  $u_z(x, y)$  depends on the pressure  $p_i(x, y)$  applied to all contact spots

$$u_z = A [p_1, p_2, \dots, p_N]. \quad (2.1)$$

The operator  $A$  is determined by the model of the deformable bodies in contact. For the contact between a rigid body with a rough surface and an elastic half-space, the relation (2.1) is

$$u_z(x, y) = \frac{1 - \nu^2}{\pi E} \sum_{i=1}^N \iint_{\omega_i} \frac{p_i(x', y') dx' dy'}{\sqrt{(x' - x)^2 + (y' - y)^2}}, \quad (2.2)$$

where  $E$  and  $\nu$  are the Young's modulus and Poisson's ratio of the half-space, respectively.

The contact condition must be satisfied within each contact spot  $\omega_i$

$$u_z(x, y) = D - F(x, y), \quad (x, y) \in \omega_i, \quad (2.3)$$

where  $D$  is the displacement of the rigid body along the  $z$ -axis. If  $D$  is not given in advance, but the total load  $P$ , applied to the bodies and directed along the  $z$ -axis

is known, we add to Eqs. (2.2) and (2.3) the equilibrium equation

$$\sum_{i=1}^N \iint_{\omega_i} p_i(x, y) dx dy = P. \quad (2.4)$$

The system of equations (2.2), (2.3) and (2.4) can be used to determine the real contact pressure  $p_i(x, y)$  within the contact spots  $\omega_i$ . However, the solution of this multiple contact problem is very complicated, even if we know the sizes and the arrangement of contact spots. In the general case we must determine also the number  $N$ , and the positions and shapes of the contact spots  $\omega_i$  for any value of load  $P$ . For a differentiable function  $F(x, y)$  we can use the condition  $p_i(x, y) \Big|_{x, y \in \partial \omega_i} = 0$  to determine the region  $\omega_i$  of an individual contact.

### 2.1.3 Previous studies

The contact problem formulated in § 2.1.2 can be solved numerically. In this case the faithfulness of the stress-strain state so determined depends on the accuracy of the numerical procedure. A computer simulation has been used to solve a contact problem for a rough body and an elastic homogeneous half-space (3-D state) in Seabra and Berthe, (1987) and for coated elastic half-plane (2-D state) in Sainsot, Leroy and Villechase, (1990) and in Cole and Sales, (1991). In these studies a function  $F(x, y)$  was obtained experimentally (for example, in the 2-D contact problem, the surface profile was determined by stylus profilometry).

It is worth noting that there is little point in developing the exact solution of the multiple contact problem formulated in § 2.1.2, because the function  $F(x, y)$  is usually determined approximately by measurements of some small surface element before deformation. There are basic constraints on the accuracy of measurements of a surface microgeometry by different devices. The function  $F(x, y)$  may vary from element to element. In addition, the function  $F(x, y)$  can change during contact interaction (for example, in a wear process). Not only do such numerical solutions consume computer time, but they are not universal. A solution for one set of contact characteristics and environment (load, temperature, etc.) cannot be used for another set.

For these reasons, the multiple contact problem for rough surfaces is usually investigated in a simplified formulation. First of all, some model of a real rough surface is considered. The model and the real surface are assumed to be adequate if some chosen characteristics of the real surface coincide with the corresponding characteristics of the model one.

The theory of random functions is widely used to model a rough surface (Sviridenok, Chijik and Petrokovets, 1990). This theory is used to determine the parameters needed to calculate contact characteristics. It was developed by Nayak (1971) for an isotropic surface and by Semenyuk and Sirenko (1980a, b, c), Semenyuk (1986a, b) for anisotropic surfaces.

Fractal geometry seems to be appropriate for rough surface modelling, because of the property of self-similarity of surface microgeometry. Majumdar and Bhushan (1990, 1991) showed experimentally that many rough surfaces have a fractal geometry, and they developed a procedure for determining fractal dimensions of rough surfaces.

It is traditional for tribology to model a rough surface as a system of asperities of a regular shape, the space distribution of which reflects the distribution of material in the surface rough layer. Researchers use various shapes of asperities in their models. A complete list of asperity shapes, with their advantages and disadvantages, is given in Kragelsky, Dobychin and Kombalov (1982). The shape of each asperity is determined by a number of parameters: a sphere by its radius, an ellipsoid by the lengths of its axes. These parameters are calculated from the measurement data of the surface microgeometry. The spacing of the asperities is calculated using the chosen asperity shape and the characteristics of the surface microgeometry obtained from the measurements (Demkin, 1970).

In addition to the approximate description of the surface microgeometry (its roughness), approximate methods of solution of Eqs. (2.1), (2.3) and (2.4) are used to analyse the multiple contact problem. The first investigations into the mechanics of discrete contact did not account for the interaction between contact spots, that is, the stress-strain state of bodies in the vicinity of one contact spot was determined by the load applied to this contact, neglecting the deformation caused by the loads applied to the remaining asperities. Under this assumption the operator  $A$  in Eq. (2.1) depends only on the function  $p_i(x, y)$ , if  $(x; y) \in \omega_i$ . This assumption gives good agreement between theory and experiment for low contact density, i.e. for low ratio of the real contact area to the nominal one. However, under certain conditions, there are discrepancies between experimental results and predictions. For example, investigating the contact area of elastomers, Bartenev and Lavrentiev (1972) revealed the effect of saturation, that is, the real contact area  $A_r$  is always smaller than the nominal contact area  $A_a$ , however great a compression load is used. Based on the experimental data, they obtained the following relation

$$\lambda = 1 - \exp\left(-\frac{\beta p}{E}\right), \quad (2.5)$$

where  $\lambda = \frac{A_r}{A_a}$  is the relative contact area,  $\beta$  is the parameter of roughness,  $p$  is

a contact pressure, and  $E$  is the elasticity modulus of the elastomers. It follows from Eq. (2.5) that  $\lambda < 1$  for a finite value of  $p$ .

However, if we use the simple theory neglecting the interaction between asperities, we may obtain  $\lambda = 1$ . For example, it follows from the Hertz solution that for waviness modelled by cylinders of radius  $R$  with axes parallel to the half-space surface and spaced at the distance  $l$  from each other,  $\lambda = 1$  if the load  $P$  applied

to unit of length of one cylinder is  $P = \frac{\pi E^* l^2}{16R}$ , where

$$E^* = \left( \frac{1 - \nu_1^2}{E_1} + \frac{1 - \nu_2^2}{E_2} \right)^{-1},$$

$E_1, \nu_1$  and  $E_2, \nu_2$  are the moduli of elasticity of the cylinders and the half-space, respectively.

In contact mechanics of rough surfaces, the method of calculation of contact characteristics developed by Greenwood and Williamson (1966) is widely used. They considered a model of a rough surface consisting of a system of spherical asperities of equal radii; the height of an asperity was a random function with some probability distribution. The deformation of each asperity obeyed the Hertz equation. The additional displacement of the surface because of the average (nominal) pressure distribution within the nominal contact area was also taken into account in this model.

For surfaces with regular microgeometry (for example, wavy surfaces) the methods of solution of periodic contact problems can be used to analyze Eqs. (2.2), (2.3) and (2.4). The 2-D periodic contact problem for elastic bodies in the absence of friction was investigated by Westergaard (1939) and Staierman (1949). Kuznetsov and Gorokhovsky (1978a, 1978b, 1980) obtained the solution of a 2-D periodic contact problem with friction force, and analysed the stress-strain state of the surface layer for different parameters characterizing the surface shape. Johnson, Greenwood and Higginson (1985) developed a method of analysis of a multiple contact problem for an elastic body, the surface of which in two mutually perpendicular directions was described by two sinusoidal functions; the counter body had a smooth surface.

We will start the investigation of a multiple contact problem from the analysis of a 3-D periodic contact problem for a system of asperities of regular shape.

## 2.2 Periodic contact problem

### 2.2.1 One-level model

We consider a system of identical axisymmetric elastic indenters ( $z = f(r)$ ) of the same height (one-level model), interacting with an elastic half-space (Fig. 2.1). The axes of the indenters are perpendicular to the half-space surface  $z = 0$  and intersect this surface at points which are distributed uniformly over the plane  $z = 0$ . As an example of such a system we can consider indenters located at the sites of a quadratic or hexagonal lattice.

Let us fix an arbitrary indenter and locate the origin  $O$  of a polar system of coordinates  $(r, \theta)$  in the plane  $z = 0$  at the point of intersection of the axis of this indenter with the plane  $z = 0$  (see Fig. 2.1(a)). The tops of the indenters have the coordinates  $(r_i, \theta_{ij})$  ( $i = 1, 2, \dots$ ;  $j = 1, 2, \dots, m_i$ , where  $m_i$  is the number of indenters located at the circumference of the radius  $r_i$ ,  $r_i < r_{i+1}$ ).

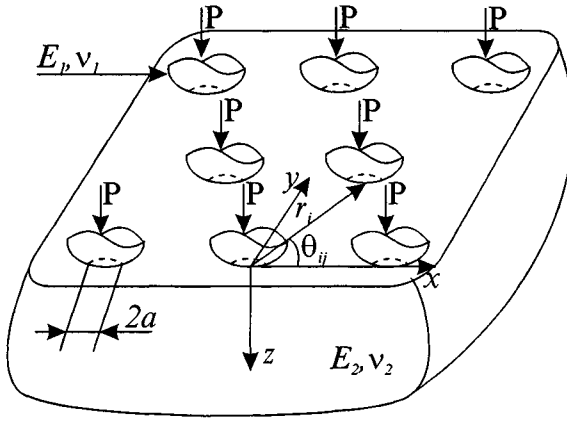
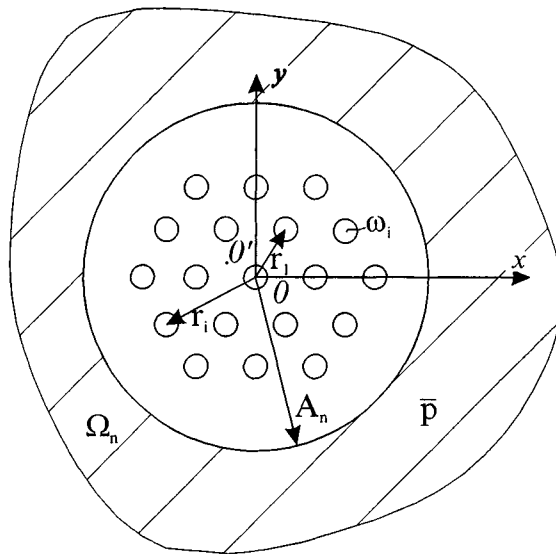
*a**b*

Figure 2.1: Scheme of contact of a periodic system of indenters and an elastic half-space (a) and representation of the contact region based on the principle of localization (b) (the nominal pressure  $\bar{p}$  is applied to the shaded region).

Due to the periodicity of the problem, each contact occurs under the same conditions. We assume that contact spots are circles of radius  $a$ , and that only normal pressure  $p(r, \theta)$  acts at each contact spot ( $r \leq a$ ) (the tangential stress is negligibly small). To determine the pressure  $p(r, \theta)$  acting at an arbitrary contact spot with a center  $O$ , we use the solution of a contact problem for an axisymmetric indenter ( $z = f(r)$ ) and an elastic half-space subjected to the pressure  $q(r, \theta)$ , distributed outside the contact region (Galin, 1953). The contact pressure  $p(r, \theta)$  ( $r \leq a$ ) is determined by the formula

$$p(r, \theta) = G(r) + \frac{c(\theta)}{\sqrt{a^2 - r^2}} - \frac{1}{\sqrt{a^2 - r^2}} \int_a^{+\infty} \int_0^{2\pi} q(r', \theta') H_2(r, \theta, r', \theta') r' dr' d\theta', \quad (2.6)$$

where

$$G(r) = \frac{E^*}{4\pi^2} \int_0^a \Delta f(r') H_1(r, r') dr', \quad (2.7)$$

$$H_1(r, r') = \int_0^{2\pi} \frac{2r'}{\sqrt{r^2 - 2rr' \cos \theta' + r'^2}} \arctan \frac{\sqrt{a^2 - r^2} \sqrt{a^2 - r'^2}}{a\sqrt{r^2 - 2rr' \cos \theta' + r'^2}} d\theta', \quad (2.8)$$

$$H_2(r, \theta, r', \theta') = \frac{\sqrt{r'^2 - a^2}}{\pi^2 [r^2 + r'^2 - 2rr' \cos(\theta - \theta')]} , \quad (2.9)$$

$$E^* = \left( \frac{1 - \nu_1^2}{E_1} + \frac{1 - \nu_2^2}{E_2} \right)^{-1}. \quad (2.10)$$

Here  $E_1$ ,  $\nu_1$  and  $E_2$ ,  $\nu_2$  are the moduli of elasticity of the indenters and the half-space, respectively. The function  $c(\theta)$  depends on a shape of the indenter  $f(r)$ . For example, if the indenter is smooth (the function  $f'(r)$  is continuous at  $r = a$ ), then the contact pressure is zero at  $r = a$ , i.e.  $p(a, \theta) = 0$ , and the function  $c(\theta)$  has the form

$$c(\theta) = \int_a^{+\infty} \int_0^{2\pi} q(r', \theta') H_2(a, \theta, r', \theta') r' dr' d\theta'. \quad (2.11)$$

The first term in Eq. (2.6) means the pressure that occurs under a single axisymmetric indenter of the shape function  $f(r)$  penetrating into an elastic half-space, the last two terms are the additional contact pressure occurring due to the pressure  $q(r, t)$  distributed outside the contact region.

For the periodic contact problem the function  $q(r, \theta)$  coincides with the pressure  $p(r, \theta)$  at each contact spot located at  $(r_i, \theta_{ij})$  ( $r_i > a$ ), and is zero outside

contact spots. So we obtain the following integral equation from Eq. (2.6), on the assumption that  $f'(r)$  is a continuous function ( $p(a, \theta) = 0$ ):

$$p(r, \theta) - \int_0^a \int_0^{2\pi} K(r, \theta, r', \theta') p(r', \theta') r' dr' d\theta' = G(r), \quad (2.12)$$

where

$$K(r, \theta, r', \theta') = \sum_{i=1}^{\infty} K_i(r, \theta, r', \theta'), \quad (2.13)$$

$$K_i(r, \theta, r', \theta') = \frac{1}{\pi^2 \sqrt{a^2 - r^2}} \sum_{j=1}^{m_i} [K_{ij}(a, \theta, r', \theta') - K_{ij}(r, \theta, r', \theta')], \quad (2.14)$$

$$\begin{aligned} K_{ij}(r, \theta, r', \theta') = \\ \frac{\sqrt{r_i^2 + r'^2 + 2r_i r' \cos(\theta_{ij} - \theta') - a^2}}{(r \cos \theta - r' \cos \theta' - r_i \cos \theta_{ij})^2 + (r \sin \theta - r' \sin \theta' - r_i \sin \theta_{ij})^2}. \end{aligned} \quad (2.15)$$

It is worth noting that similar reasoning can be used to obtain the integral equation for the system of punches with a given contact region (for example, cylindrical punches with a flat base); the equation will have the same structure as Eq. (2.12).

The kernel  $K(r, \theta, r', \theta')$  of Eq. (2.12) is represented as a series (2.13). A general term (2.14) of this series can be transformed to the form:

$$\begin{aligned} K_i(r, \theta, r', \theta') = \\ \frac{1}{\pi^2 \sqrt{a^2 - r^2}} \sum_{j=1}^{m_i} \left\{ \frac{2(a - r) \cos(\theta_{ij} - \theta)}{r_i^2} + \right. \\ \left. \frac{(a - r) [-a - r - 6r' \cos(\theta_{ij} - \theta') \cos(\theta_{ij} - \theta) + 2r' \cos(\theta' - \theta)]}{r_i^3} + O\left(\frac{1}{r_i^4}\right) \right\}. \end{aligned} \quad (2.16)$$

We assume that for the periodic system of indenters under consideration, each contact spot with center  $(r_i; \theta_{ij})$  has a partner with center at the point  $(r_i; \pi + \theta_{ij})$ . So the sum on the first line of Eq. (2.16) is zero. Hence, the general term of the series (2.13) has order  $O\left(\frac{1}{r_i^2}\right)$ , since  $m_i \sim r_i$ , and the series converges.

## 2.2.2 Principle of localization

In parallel with Eq. (2.12) we consider the following equation

$$\begin{aligned} p(r, \theta) - \int_0^a \int_0^{2\pi} \sum_{i=1}^n K_i(r, \theta, r', \theta') p(r', \theta') r' dr' d\theta' = \\ G(r) + \frac{2\bar{N}P}{\pi} \arctan \frac{\sqrt{a^2 - r^2}}{\sqrt{A_n^2 - a^2}}, \end{aligned} \quad (2.17)$$

where  $P$  is a load applied to each contact spot. This load satisfies the equilibrium equation

$$P = \int_0^a \int_0^{2\pi} p(r, \varphi) r dr d\varphi. \quad (2.18)$$

To obtain Eq. (2.17) we substitute integration over region  $\Omega_n$  ( $\Omega_n : r \geq A_n, 0 \leq \theta \leq 2\pi$ ) for summation over  $i > n$  in Eq. (2.13), taking into account that the centers of contact spots are distributed uniformly over the plane  $z = 0$  and their number per unit area is characterized by the value  $\bar{N}$ . Actually, the following transformation demonstrates the derivation Eq. (2.17)

$$\begin{aligned} J_n &= \sum_{i=n+1}^{\infty} K_i(r, \theta, r', \theta') \approx \\ &\bar{N} \int_{A_n}^{+\infty} \int_0^{2\pi} \frac{\sqrt{x^2 + r'^2 + 2xr' \cos(\phi - \theta') - a^2}}{\pi^2 \sqrt{a^2 - r^2}} \times \\ &\left[ \frac{1}{(a \cos \theta - r' \cos \theta' - x \cos \phi)^2 + (a \sin \theta - r' \sin \theta' - x \sin \phi)^2} - \right. \\ &\left. \frac{1}{(r \cos \theta - r' \cos \theta' - x \cos \phi)^2 + (r \sin \theta - r' \sin \theta' - x \sin \phi)^2} \right] x dx d\phi. \end{aligned}$$

Changing the variables  $y \cos \varphi = x \cos \phi + r' \cos \theta'$ ,  $y \sin \varphi = x \sin \phi + r' \sin \theta'$  and taking into account that  $r' \leq a \ll A_n$ , we finally obtain

$$\begin{aligned} J_n &\approx \frac{\bar{N}}{\pi^2 \sqrt{a^2 - r^2}} \times \\ &\int_{A_n}^{+\infty} \int_0^{2\pi} \sqrt{y^2 - a^2} \left[ \frac{1}{a^2 + y^2 - 2ay \cos \varphi} - \frac{1}{r^2 + y^2 - 2ry \cos \varphi} \right] y dy d\varphi = \\ &\frac{2\bar{N}}{\pi} \arctan \frac{\sqrt{a^2 - r^2}}{\sqrt{A_n^2 - a^2}}, \end{aligned}$$

where  $A_n$  is the radius of a circle in which there are  $\sum_{i=1}^n m_i + 1$  central indenters.

It is apparent that

$$A_n^2 = \frac{1}{\pi \bar{N}} \left( \sum_{i=1}^n m_i + 1 \right). \quad (2.19)$$

We note that the solution of Eq. (2.17) tends to the solution of Eq. (2.12) if  $n \rightarrow \infty$ .

Let us analyze the structure of Eq. (2.17). The integral term on the left side of Eq. (2.17) governs the influence of the real pressure distribution at the neighboring contact spots ( $r_i < A_n$ ), on the pressure at the fixed contact spot with center  $(0, 0)$  (local effect). The effect of the pressure distribution at the remaining contact spots which have centers  $(r_i, \theta_{ij})$ ,  $r_i > A_n$ , is taken into account by the second term in the right side of Eq. (2.17). This term describes the additional pressure  $p_a(r)$  which arises within a contact spot ( $r < a$ ) from the nominal pressure  $\bar{p} = PN$  in the region  $\Omega_n$  ( $r > A_n$ ). Indeed, from Eqs. (2.6) and (2.11) it follows that the additional pressure  $p_a(r)$  within the contact spot ( $r \leq a$ ) arising from the pressure  $q(r, \theta) = \bar{p}$  distributed uniformly in the region  $\Omega_n$  has the form

$$p_a(r) = \frac{\bar{p}}{\pi^2 \sqrt{a^2 - r^2}} \times \\ \int_{A_n}^{+\infty} \int_0^{2\pi} \sqrt{r'^2 - a^2} \left[ \frac{1}{a^2 + r'^2 - 2ar' \cos\theta} - \frac{1}{r^2 + r'^2 - 2rr' \cos\theta} \right] r' dr' d\theta = \\ \frac{2\bar{p}}{\pi} \arctan \frac{\sqrt{a^2 - r^2}}{\sqrt{A_n^2 - a^2}}.$$

Thus, the effect of the real contact pressure distribution over the contact spots  $\omega_i$  far away from the contact spot under consideration ( $\omega_i \in \Omega_n$ ) can be taken into account to sufficient accuracy by the nominal pressure  $\bar{p}$  distributed over the region  $\Omega_n$  (Fig. 2.1(b)).

This conclusion stated for the periodic contact problem is a particular case of a general contention which we call *a principle of localization*: in conditions of multiple contact, the stress-strain state near one contact spot can be calculated to sufficient accuracy by taking into account the real contact conditions (real pressure, shape of bodies, etc.) at this contact spot and at the nearby contact spots (in the local vicinity of the fixed contact), and the averaged (nominal) pressure over the remaining part of the region of interaction (nominal contact region). This principle will be supported by results of investigation of some particular problems considered in this chapter.

Eqs. (2.17) and (2.18) are used to determine the contact pressure  $p(r, \theta)$  and the radius  $a$  of each spot. The stress distribution in the subsurface region ( $z > 0$ ) arising from the real contact pressure distribution at the surface  $z = 0$  can then be found by superposition, using the potentials of Boussinesq (1885) or the particular solution of the axisymmetric problem given by Timoshenko and Goodier (1951).

To simplify the procedure, we can use the principle of localization for determination of internal stresses, substituting the real contact pressure at distant contact spots by the nominal contact pressure. We give here the analytical expressions for the additional stresses which occur on the axis of symmetry of any fixed contact

spot from the action of the nominal pressure  $\bar{p}$  within the region  $\Omega_n(r > A_n)$ .

$$\begin{aligned}\sigma_z &= -\frac{\bar{p}z^3}{(A_n^2 + z^2)^{3/2}}, \\ \sigma_r = \sigma_\theta &= \frac{\bar{p}z}{\sqrt{A_n^2 + z^2}} \left[ \frac{z^2}{2(A_n^2 + z^2)} - (1 + \nu) \right], \\ \tau_{rz} = \tau_{\theta z} = \tau_{r\theta} &= 0.\end{aligned}\quad (2.20)$$

### 2.2.3 System of indenters of various heights

The method described above is used to determine the real pressure distribution in contact interaction between a periodic system of elastic indenters of the various heights, and an elastic half-space. We assume that the shape of an indenter is described by a continuously differentiable function  $z = f_m(r) + h_m$ , where  $h_m$  is a height of indenters of a given level  $m$  ( $m = 1, 2, \dots, k$ ),  $k$  is the number of levels. An example of positions of indenters of each level for  $k = 3$  for a hexagonal lattice is shown in Fig. 2.2(a). We assume also that the contact spot of the  $m$ -th level is a circle of radius  $a_m$ .

Let us fix any indenter of the  $m$ -th level and place the origin of the polar system of coordinates at the center of its contact spot (Fig. 2.2(b)). Using the principle of localization, we take into account the real pressure  $p_j(r, \theta)$  ( $j = 1, 2, \dots, k$ ) at the contact spots which are inside the region  $\bar{\Omega}_m$  which is a circle of radius  $A_m$  ( $\bar{\Omega}_m : r \leq A_m$ ):

$$A_m^2 = \frac{1}{\pi} \left( \sum_{j=1}^k \frac{k_{jm}}{\bar{N}_j} + \frac{1}{\bar{N}_m} \right),$$

where  $k_{jm}$  is the number of indenters of the  $j$ -th level inside the region  $\bar{\Omega}_m$ ,  $\bar{N}_j$  is the density of indenters of the  $j$ -th level, which is the number of indenters at the  $j$ -th level for the unit area. It must be noted that the number of indenters of the  $m$ -th level ( $j = m$ ) inside the region  $\bar{\Omega}_m$  is  $k_{mm} + 1$ . Replacing the real contact pressure at the removed contact spots ( $r_i > A_m$ ) by the nominal pressure  $\bar{p}$  acting within the region ( $r > A_m$ )

$$\bar{p} = \sum_{j=1}^k \bar{N}_j \int_0^{a_j} \int_0^{2\pi} p_j(r', \theta') r' dr' d\theta',$$

we obtain the following relationship similar to Eq. (2.17)

$$\begin{aligned}p_m(r, \theta) - \sum_{j=1}^k \int_0^{a_j} \int_0^{2\pi} K_n(a_m, r, \theta, r', \theta') p_j(r', \theta') r' dr' d\theta' &= \\ G_m(r) + \frac{2\bar{p}}{\pi} \arctan \frac{\sqrt{a_m^2 - r^2}}{\sqrt{A_m^2 - a_m^2}}. &\end{aligned}\quad (2.21)$$

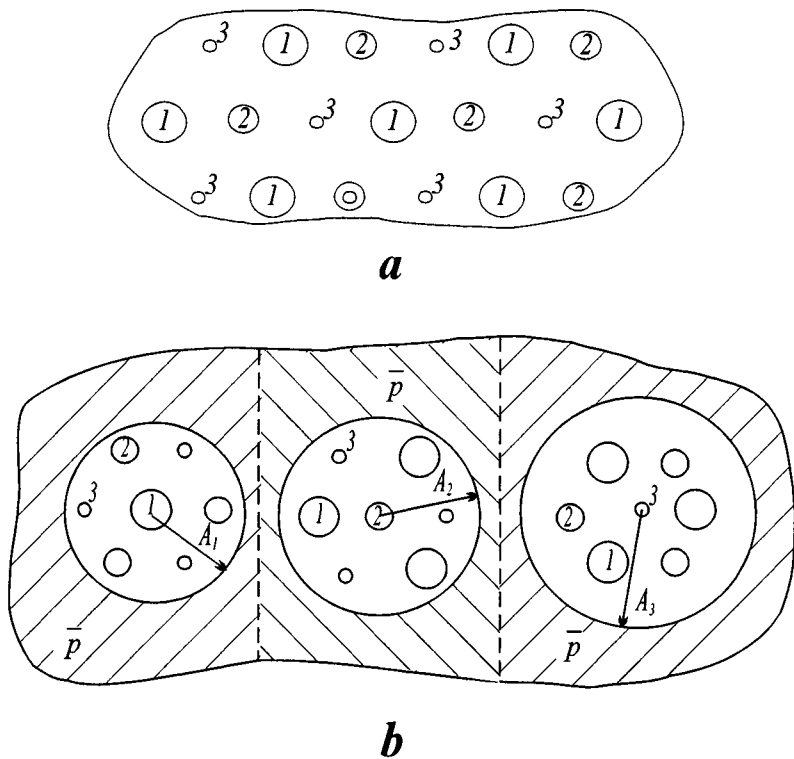


Figure 2.2: The location of indenters of each level in the model ( $k = 3$ ) (a) and scheme of calculations based on Eqs. (2.21)–(2.23) for  $n = 1$  (b).

The kernel of Eq. (2.21) has the form

$$K_n(a_m, r, \theta, r', \theta') = \sum_{i=1}^n K_i(a_m, r, \theta, r', \theta'),$$

where functions  $K_i(a_m, r, \theta, r', \theta')$  are determined by Eqs. (2.14) and (2.15), in which we must put  $a = a_m$ . The function  $G_m(r)$  is determined by Eq. (2.7), where  $a = a_m$  and  $f(r) = f_m(r)$ .

Repeating the same procedure for indenters of each level (see Fig. 2.2(b)), we obtain the system of  $k$  integral equations (2.21) ( $m = 1, 2, \dots, k$ ) for determination of the pressure  $p_m(r, \theta)$  within the contact spot ( $r \leq a_m$ ) of each level.

Usually the radius of a contact spot  $a_m$  is unknown. If an origin of a polar system of coordinates is placed in the center  $O_m$  of the  $m$ -th level contact spot,

we can write

$$h_m = \frac{1}{\pi E^*} \left[ \int_0^{a_m} \int_0^{2\pi} p_m(r, \theta) r dr d\theta + 2\pi \bar{p} (A_\infty - A_m) + \sum_{j=1}^k \sum_{i=1}^{k_{jm}} \int_0^{a_j} \int_0^{2\pi} \frac{p_j(r, \theta) r dr d\theta}{\sqrt{r^2 - 2rr_{ij}^{(m)} \cos(\theta - \theta_{ij}^{(m)}) + r_{ij}^{(m)2}}} \right], \quad (2.22)$$

where  $r_{ij}^{(m)}, \theta_{ij}^{(m)}$  are the coordinates with respect to the system  $(O_m r\theta)$  of the centers of contact spots located within the region  $\Omega_m$  ( $a_m < r_{ij}^{(m)} < A_m$ ,  $0 < \theta_{ij}^{(m)} < 2\pi$ ),  $A_\infty$  is a constant which can be excluded from the system of Eqs. (2.22) by consideration of differences of heights  $h_1 - h_m$ , where  $h_1$  is the largest height. The system of equations is completed if we add the equilibrium condition

$$\bar{p}\pi A_m^2 = \sum_{j=1}^k k_{jm} \int_0^{a_j} \int_0^{2\pi} p_j(r, \theta) r dr d\theta + \int_0^{a_m} \int_0^{2\pi} p_m(r, \theta) r dr d\theta. \quad (2.23)$$

It should be remarked that for given height distribution  $h_m$  all indenters enter into contact only if the nominal pressure reaches the definite value  $\bar{p}^*$ . For  $\bar{p} < \bar{p}^*$  there are less than  $k$  levels of indenters in contact.

## 2.2.4 Stress field analysis

We use the relationships obtained in § 2.2.1–2.2.3 to analyze a real contact pressure distribution and the internal stresses in a periodic contact problem for a system of indenters and the elastic half-space. Particular emphasis will be placed upon the influence of the geometric parameter which describes the density of indenter location, on the stress-strain state. This will allow us to determine the range of parameter variations in which it is possible to use the simplified theories which neglect the interaction between contact spots (the integral term in Eq. (2.12)) or the local effect of the influence of the real pressure distribution at the neighboring contact spots on the pressure at the fixed spot (the integral term in Eqs. (2.17)).

Numerical results are presented here for a system of spherical indenters,  $\left(f(r) = \frac{r^2}{2R}, R \text{ is a radius of curvature}\right)$ , located on a hexagonal lattice with a constant pitch  $l$ . Fig. 2.2(a) shows the location of indenters of different levels at the plane  $z = 0$  for a three-level model ( $k = 3$ ). We introduce the following dimensionless parameters and functions

$$\begin{aligned} \rho &= \frac{r}{R}, & A_n^1 &= \frac{A_n}{R}, & a^1 &= \frac{a}{R}, & l^1 &= \frac{l}{R}, \\ p^1(\rho, \theta) &= \frac{\pi p(\rho R, \theta)}{2E^*}, & P^1 &= \frac{\pi P}{2E^* R^2}. \end{aligned} \quad (2.24)$$

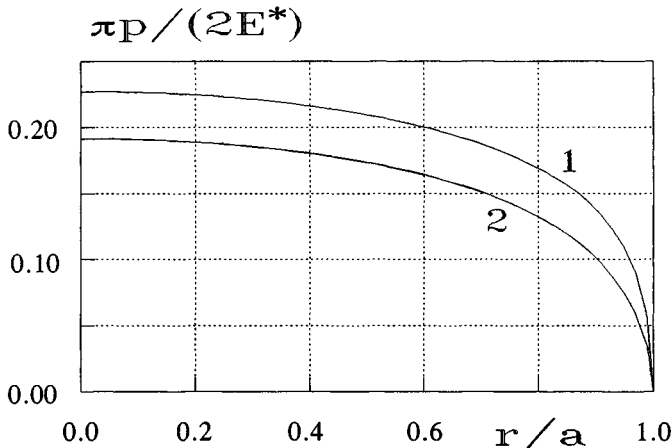


Figure 2.3: Pressure distribution within a contact spot, calculated from Eq. (2.17) for  $n = 0$  (curve 1),  $n = 1$  and  $n = 2$  (curve 2) and  $a/R = 0.1$ ,  $l/R = 0.2$  (one-level model).

The systems of Eqs. (2.17) and (2.18) for the one-level model and of Eqs. (2.21)-(2.23) for the three-level model are solved by iteration. The density  $\bar{N}_j$  of arrangement of indenters in the three-level model under consideration is determined by the formula

$$\bar{N}_j = \frac{2}{3l^2\sqrt{3}}, \quad (j = 1, 2, 3). \quad (2.25)$$

For the one-level model  $\bar{N} = 3\bar{N}_j = \frac{2}{l^2\sqrt{3}}$ .

For determination of the radius  $A_n$  of the circle ( $r \leq A_n$ ) where the real pressure distribution within a nearby contact spots is taken into account (local effect) and the corresponding value of  $n$  which gives an appropriate accuracy of the solution of Eq. (2.17), we calculated the contact pressure  $p^1(\rho, \theta)$  from Eqs. (2.17) and (2.18) for  $n = 0$ ,  $n = 1$ ,  $n = 2$  and so on. For  $n = 0$ , the integral term on the left of Eq. (2.17) is zero, so that the effect of the remaining contact spots surrounding the fixed one (with the center at the origin of coordinate system  $O$ ) is taken into account by a nominal pressure distributed outside the circle of radius  $A_0$  (the second term in the right side of Eq. (2.17)), where  $A_0$  is determined by Eq. (2.19). For  $n = 1$  we take into account the real pressure within 6 contact spots located at the distance  $l$  from the fixed one, for  $n = 2$  they are 12 contact spots, six located at the distance  $l$  and the another six at a distance  $l\sqrt{3}$ , and so on. Fig. 2.3 illustrates the results calculated for  $a^1 = 0.1$  and  $l^1 = 0.2$ , i.e.  $\frac{a}{l} = 0.5$ , this case corresponds to the limiting value of contact density. The results show that the contact pressure calculated for  $n = 1$  and  $n = 2$  differ from one another.

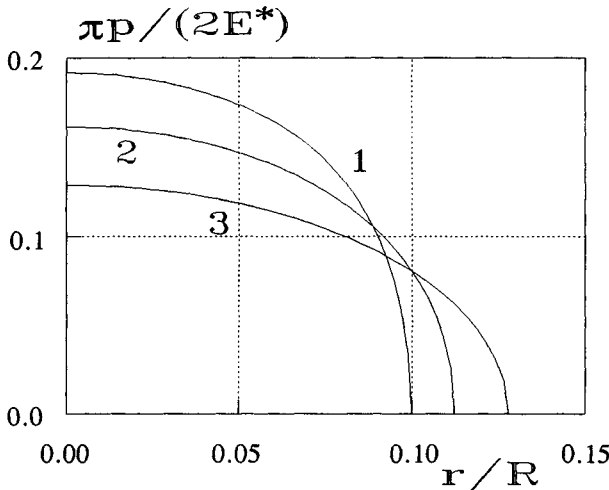


Figure 2.4: Pressure distribution under an indenter acted on by the force  $P^1 = 0.0044$  for the one-level model characterized by the various distances between indenters:  $l/R = 0.2$  (curve 1),  $l/R = 0.25$  (curve 2),  $l/R = 1$  (curve 3).

less than 0.1%. If contact density decreases ( $\frac{a}{l}$  decreases) this difference also decreases. Based on this estimation, we will take  $n = 1$  in subsequent analysis.

We first analyze the effect of interaction between contact spots and pressure distribution. Fig. 2.4 illustrates the contact pressure under some indenter of the one-level system for different values of the parameter  $l^1$  characterizing the distance between indenters. In all cases, the normal load  $P^1 = 0.0044$  is applied to each indenter. The results show that the radius of the contact spot decreases and the maximum contact pressure increases if the distance  $l$  between indenters decreases; the contact density characterized by the parameter  $\frac{a}{l}$  also increases ( $\frac{a}{l} = 0.128$  (curve 3),  $\frac{a}{l} = 0.45$  (curve 2),  $\frac{a}{l} = 0.5$  (curve 1)). The curve 3 practically coincides with the contact pressure distribution calculated from Hertz theory which neglects the influence of contact spots surrounding the fixed one. So, for small values of parameter  $\frac{a}{l}$ , it is possible to neglect the interaction between contact spots for determination of the contact pressure.

The dependencies of the radius of a contact spot on the dimensionless nominal pressure  $\bar{P}^1 = \frac{\bar{P}\pi}{2E^*}$  calculated for different values of parameter  $l^1$  and a one-level model are shown in Fig. 2.5 (curves 1, 2, 3). The results of calculation based on the Hertz theory are added for comparison (curves 1', 2', 3'). The results show that under a constant nominal pressure  $\bar{P}$  the radius of each contact spot and, hence

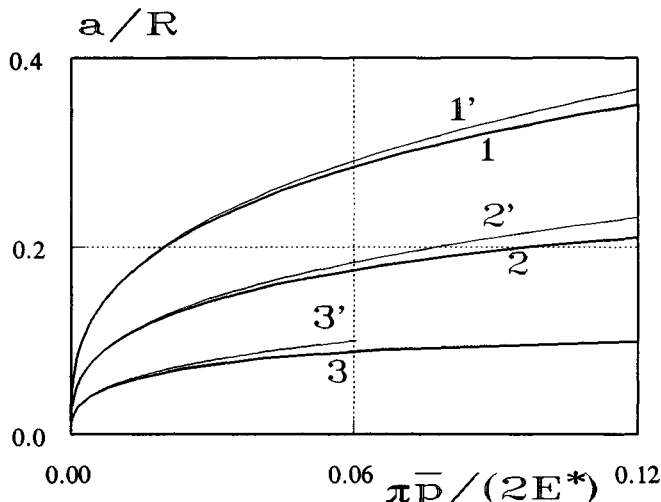


Figure 2.5: Dependence of the radius of a contact spot on the nominal pressure for  $l = 1$  (curves 1, 1'),  $l = 0.5$  (curves 2, 2'),  $l = 0.2$  (curves 3, 3'), calculated from Eq. (2.17) (1, 2, 3) and from Hertz theory (1', 2', 3').

the real contact area, decreases if the relative distance  $\frac{l}{R}$  between contact spots decreases. The comparison of these results with the curves calculated from Hertz theory makes it possible to conclude that for  $\frac{a}{l} < 0.25$  the discrepancy between the results predicted from the multiple contact theory and Hertz theory does not exceed 2.5%. For higher nominal pressure and, hence higher contact density, the discrepancy becomes serious. Thus, for  $l = 0.5$  (curves 2, 2') and  $\frac{a}{l} = 0.44$  the calculation of the real contact area from Hertz theory gives an error of about 15%.

Investigation of contact characteristics in the three-level model is a subject of particular interest because this model is closer to the real contact situation than is the one-level model. The multiple contact model developed in this section takes into account the influence of the density of contact spots on the displacement of the surface between contact spots, and so the load, which must be applied to bring a new level of indenters into contact, depends not only on the height difference of the indenters, but also on the contact density. The calculations were made for a model with fixed height distribution:  $\frac{h_1 - h_2}{R} = 0.014$  and  $\frac{h_1 - h_3}{R} = 0.037$ .

Fig. 2.6 illustrates the pressure distribution within the contact spots for each level if  $P^1 = 0.059$  where  $P^1$  is the load applied to 3 indenters ( $P^1 = P_1^1 + P_2^1 + P_3^1$ ). The curves 1, 2, 3 and the curves 1', 2', 3' correspond to the solutions of the periodic contact problem and to the Hertz problem, respectively. The results show that the smaller the height of the indenter, the greater is the difference between the contact pressure calculated from the multiple contact and Hertz theory.

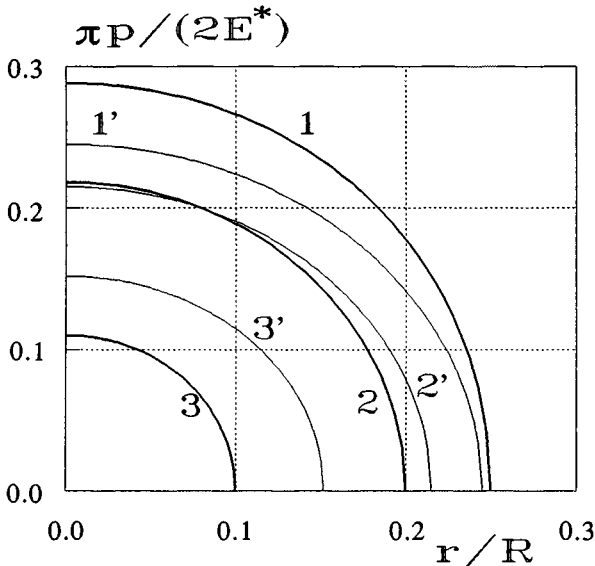


Figure 2.6: Pressure distribution at the contact spots of indenters with the heights  $h_1$  (curves 1, 1'),  $h_2$  (curves 2, 2') and  $h_3$  (curves 3, 3') for the three-level model  $((h_1-h_2)/R = 0.014, (h_1-h_3)/R = 0.037, P^1 = 0.059)$  calculated from Eqs. (2.21) – (2.23) (1, 2, 3) and from Hertz theory (1', 2', 3').

We also investigated the internal stresses for the one-level periodic problem and compared them with the uniform stress field arising from the uniform loading by the nominal pressure  $\bar{p}_n$ . It follows from the analysis that for periodic loading by the system of indenters, there is a nonuniform stress field in the subsurface layer, the thickness of which is comparable with the distance  $l$  between indenters.

The stress field features depend essentially on the contact density parameter  $\frac{a}{l}$ .

Fig. 2.7 illustrates the principal shear stress  $\frac{\tau_1}{\bar{p}}$  along the  $z$ -axis which coincides

with the axis of symmetry of the indenter (curves 1, 2) and along the axis  $O'z$  (curves 1', 2') equally spaced from the centers of the contact spots (see Fig. 2.1).

The results are calculated for the same nominal pressure  $\bar{p}^1 = 0.12$ , and the different distances  $\frac{l}{R}$  between the indenters:  $\frac{l}{R} = 1, \left(\frac{a}{R} = 0.35\right)$  (curves 1, 1') and

$\frac{l}{R} = 0.5 \left(\frac{a}{R} = 0.21\right)$  (curves 2, 2'). The maximum value of the principal shear stress is related to the nominal pressure; the maximum difference of the principal shear stress at the fixed depth decreases as the parameter  $\frac{a}{l}$  increases. The maximum value of the principal shear stress occurs at the point  $r = 0, \frac{z}{a} = 0.43$

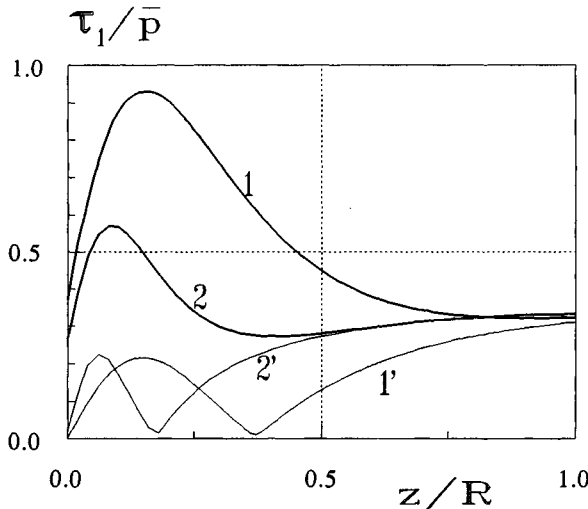


Figure 2.7: The principal shear stress  $\tau_1/\bar{p}$  along the axes  $Oz$  (curves 1, 2) and  $O'z$  (curves 1', 2') for  $l/R = 1$  (1, 1'),  $l/R = 0.5$  (2, 2'),  $\bar{p}^1 = 0.12$ .

for  $\frac{a}{l} = 0.35$  (curve 1) and at the point  $r = 0$ ,  $\frac{z}{a} = 0.38$  for  $\frac{a}{l} = 0.42$  (curve 2). At infinity the principal shear stresses depend only on the nominal stress  $\bar{p}$ . The results show that internal stresses differ noticeably from ones calculated from the

Hertz model if the parameter  $\frac{a}{l}$  varies between the limits  $0.25 < \frac{a}{l} \leq 0.5$ .

Fig. 2.8 illustrates contours of the function  $\frac{\tau_1}{\bar{p}}$  at the plane  $\frac{z}{R} = 0.08$ , which is parallel to the plane  $Oxy$ . The principal shear stresses are close to the maximum values at the point  $x = 0$ ,  $y = 0$  of this plane. Contours are presented within the region  $\left( -\frac{l^1}{2} < x < l^1, -\frac{l^1\sqrt{3}}{4} < y < \frac{l^1\sqrt{3}}{2} \right)$  for  $a^1 = 0.2$  and  $l^1 = 1$  (Fig. 2.8(a)) and  $l^1 = 0.44$  (Fig. 2.8(b)). The results show that the principal shear stress at the fixed depth varies only slightly if the contact density parameter is close to 0.5. Similar conclusions follow for all the components of the stress tensor.

Thus, as a result of the nonuniform pressure distribution at the surface of the half-space (discrete contact), there is a nonuniform stress field dependent on the contact density parameter in the subsurface layer. The increase of stresses in some points of the layer may cause plastic flow or crack formation. The results obtained here coincide with the conclusions which follow from the analysis of the periodic contact problem for the sinusoidal punch and an elastic half-plane (2-D contact problem) in Kuznetsov and Gorokhovsky (1978a, 1978b).

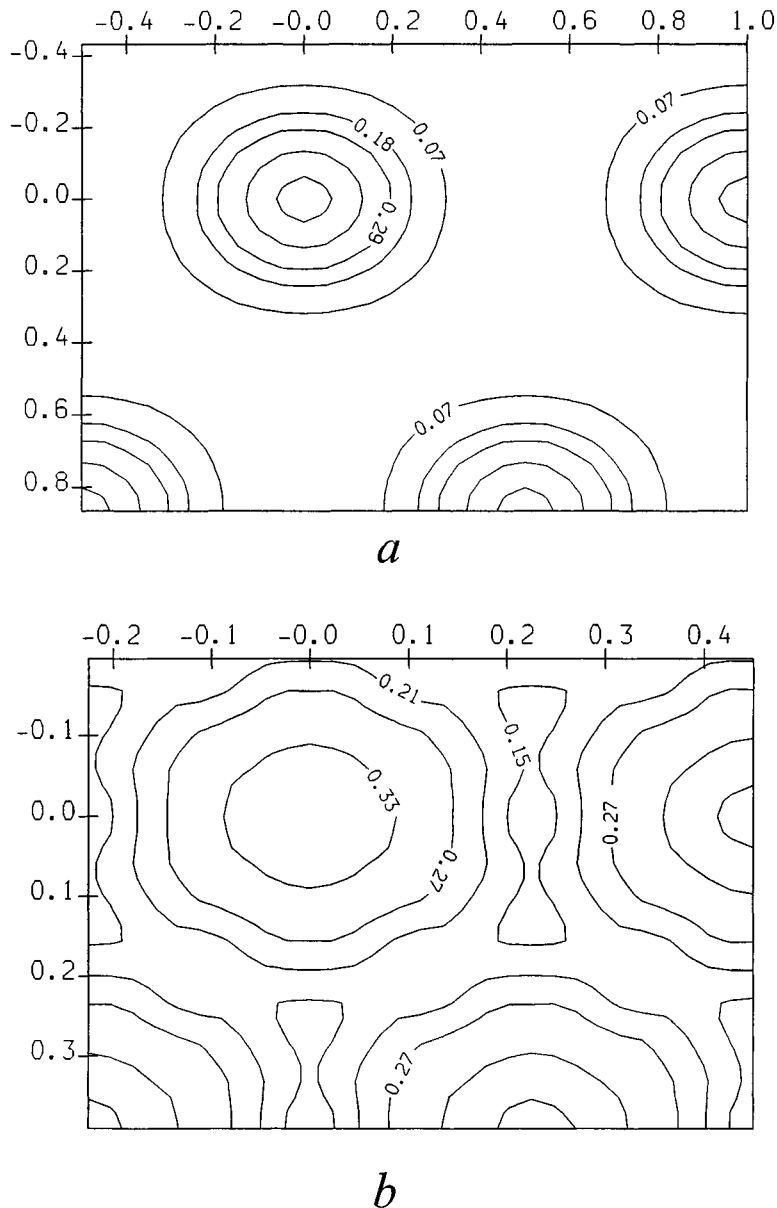


Figure 2.8: Contours of the function  $\tau_1/\bar{p}$  at the plane  $z/R = 0.08$  for  $l^1 = 1$  (a) and  $l^1 = 0.44$  (b);  $a^1 = 0.2$ .

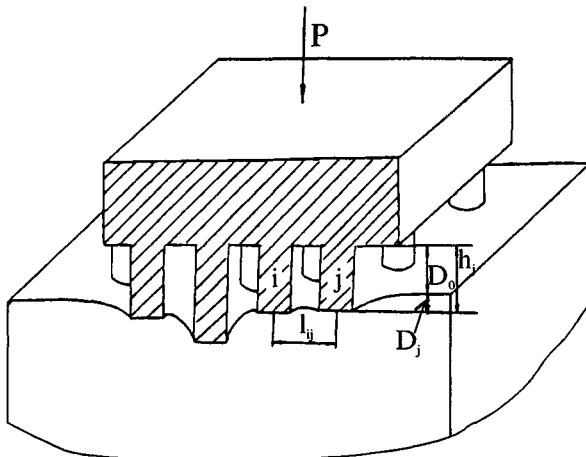


Figure 2.9: Scheme of contact of a system of punches and an elastic half-space.

## 2.3 Problem with a bounded nominal contact region

A distinctive feature of periodic contact problems is the uniform distribution of the nominal pressure on the half-space surface. The nominal pressure is the ratio of the load to the area, for one cell. Within one period, the load distribution between contact spots depends only on the difference of heights of indenters and variations in contact density.

For a finite number of indenters interacting with an elastic half-space, the nominal contact region is bounded. A nonuniform load distribution between indenters which are rigidly bonded, arises not only from the differences in indenter height and their arrangement density, but also from the different locations of the indenters within the nominal contact region. The load distribution for such a system of indenters is nonuniform even though all indenters have the same height and they are arranged uniformly within a bounded nominal contact region.

In what follows we will investigate the contact problem for a finite number of punches and an elastic half-space, and analyze the dependence of the contact characteristics (load distribution, real contact area, etc.) on the spatial arrangement of the punches.

### 2.3.1 Problem formulation

We consider the contact interaction of a system of punches with an elastic half-space (Fig. 2.9). The system of punches is characterized by:

- the total number  $N$ ;

- the shape of the contact surface of an individual punch  $f_j(r)$  (it is assumed that each punch is a body of revolution with its axis perpendicular to the undeformed surface of the half-space, and  $r$  is the polar radius for the coordinate system related to the axis of the punch);
- the distance  $l_{ij}$  between the axes of symmetry of the  $i$ -th and  $j$ -th punches;
- the heights of punches  $h_j$ .

The region of contact of the system of punches with the elastic half-space is a set of subregions  $\omega_i$  ( $i = 1, 2, \dots, N$ ). The remaining boundary of the half-space is stress free.

We introduce the coordinate system  $Oxyz$ . The  $Oz$ -axis is chosen to coincide with the axis of revolution of an arbitrary fixed  $i$ -th punch and the  $Oxy$  plane coincides with the undeformed half-space surface. For convenience, the directions of the axes  $Ox$  and  $Oy$  are chosen to coincide where possible with axes of symmetry of the system of punches.

Let us formulate the boundary conditions for the  $i$ -th punch and replace the action of the other punches on the boundary of the elastic half-space by the cor-

responding pressure, distributed over the aggregate region  $\bigcup_{\substack{j=1 \\ j \neq i}}^N \omega_j$ . The elastic

displacement of the half-space surface in the  $z$ -axis direction within the region  $\omega_i$  caused by the pressure  $p_j(x, y)$ ,  $(x, y) \in \omega_j$ , ( $j = 1, 2, \dots, N, i \neq j$ ) is calculated from Boussinesq's solution

$$u_z^i(x, y) = \frac{1 - \nu^2}{\pi E} \sum_{\substack{j=1 \\ j \neq i}}^N \iint_{\omega_j} \frac{p_j(x', y') dx' dy'}{\sqrt{(X_j + x' - x)^2 + (Y_j + y' - y)^2}}.$$

Generally speaking, the pressure  $p_j(x, y)$  is not known in advance. To simplify the problem, we approximate  $u_z^i(x, y)$  by the following function

$$u_z^{i1}(x, y) = \frac{1 - \nu^2}{\pi E} \sum_{\substack{j=1 \\ j \neq i}}^N \frac{P_j}{\sqrt{(X_j - x)^2 + (Y_j - y)^2}}, \quad (2.26)$$

where  $P_j$  is the concentrated force,  $P_j = \iint_{\omega_j} p_j(x, y) dx dy$ , which is applied at the center of the subregion with coordinates  $(X_j, Y_j)$ . The high accuracy of this approximation follows from the estimation made for the particular case of the

axially symmetric function  $p_j(x', y') = p(r)$ , ( $r \leq a$ )

$$\begin{aligned} & \int_0^{2\pi} \int_0^a \frac{p(r)r dr d\theta}{\sqrt{r^2 + l^2 - 2rl \cos \theta}} - \frac{P}{l} = \\ & \int_0^a p(r) \left[ \frac{4}{r+l} K\left(\frac{2\sqrt{rl}}{r+l}\right) - \frac{2\pi}{l} \right] r dr = 4 \int_0^a p(r) \frac{r}{l} \left[ K\left(\frac{r}{l}\right) - \frac{\pi}{2} \right] dr = \\ & \frac{\pi}{2} \int_0^a p(r) \left[ \left(\frac{r}{l}\right)^3 + O\left(\left(\frac{r}{l}\right)^5\right) \right] dr \leq \frac{P}{4} \left( \frac{a^2}{l^3} + O\left(\frac{a^4}{l^5}\right) \right), \end{aligned}$$

where  $l = \sqrt{(X_j - x)^2 + (Y_j - y)^2}$ ,  $P = 2\pi \int_0^a p(r)r dr$ ,  $K(x)$  is the elliptic integral of the first kind. The following relations have been used to obtain this estimation

$$\int_0^\pi \frac{d\theta}{\sqrt{r^2 + l^2 - 2rl \cos \theta}} = \frac{2}{r+l} K\left(\frac{2\sqrt{rl}}{r+l}\right), \quad (2.27)$$

$$K\left(\frac{2\sqrt{x}}{1+x}\right) = (1+x)K(x). \quad (2.28)$$

The superposition principle, which is valid for the linear theory of elasticity, makes it possible to present the displacements of the boundary of the elastic half-space along the axis  $Oz$  under the  $i$ -th punch, as the sum of the displacement  $u_z^{i1}(x, y)$  and the elastic displacement  $u_z^{i2}(x, y)$  due to the pressure  $p_i(x, y)$  distributed over the  $i$ -th punch base within the subregion  $\omega_i$ .

As a result, the pressure  $p_i(x, y)$  can be determined from the solution of the problem of the elasticity theory for the half-space with the mixed boundary conditions

$$\begin{aligned} u_z^{i1}(x, y) + u_z^{i2}(x, y) &= D_i - f_i(\sqrt{x^2 + y^2}), \\ \tau_{zx} = \tau_{zy} &= 0, \quad (x, y) \in \omega_i, \\ \sigma_z = \tau_{zx} = \tau_{zy} &= 0, \quad (x, y) \notin \omega_i, \end{aligned} \quad (2.29)$$

where  $D_i$  is the displacement of the punch along the  $z$ -axis.

For further consideration it is necessary to determine the relation between the loads  $P_i$ , acting upon the punches, and the depths of penetration of punches  $D_i$ . We use Betti's theorem to obtain this relation. We assume that the contact region  $\omega_i$  of an axially symmetric punch with the curved surface of the elastic half-space is close to a circular one of radius  $a_i$ . For an axisymmetric punch with a flat base of radius  $a_i$ , penetrating into the half-space to a depth  $D^*$ , the pressure  $p^*(r)$

$(r = \sqrt{x^2 + y^2})$  is determined by the formula (see, for example, Galin, 1953 or

Gladwell, 1980)

$$p^*(r) = \frac{ED^*}{\pi(1-\nu^2)\sqrt{a_i^2 - r^2}}.$$

From Betti's theorem it follows that

$$\int_0^{2\pi} \int_0^{a_i} p_i(r, \theta) D^* r dr d\theta = \int_0^{2\pi} \int_0^{a_i} p^*(r) u_z^{i2}(r, \theta) r dr d\theta \quad (\theta = \arctan \frac{y}{x})$$

or

$$P_i = \frac{E}{\pi(1-\nu^2)} \int_0^{2\pi} \int_0^{a_i} \frac{u_z^{i2}(r, \theta) r dr d\theta}{\sqrt{a_i^2 - r^2}}. \quad (2.30)$$

Substituting Eqs. (2.26) and (2.29) in the right-hand side of Eq. (2.30) we calculate the integrals using Eqs. (2.27), (2.28) and the following relations

$$\begin{aligned} \int_0^x \frac{dx'}{\sqrt{(x^2 - x') (1 - x' \sin^2 \phi)}} &= \frac{1}{\sin \phi} \ln \frac{1 + x \sin \phi}{1 - x \sin \phi}, \quad (|x| < 1), \\ \int_0^{\pi/2} \frac{1}{\sin \phi} \ln \frac{1 + x \sin \phi}{1 - x \sin \phi} d\phi &= \pi \arcsin x. \end{aligned}$$

Then we get from Eq. (2.30)

$$P_i = \frac{2E}{1-\nu^2} \int_0^{a_i} (D_i - f(r)) \frac{r dr}{\sqrt{a_i^2 - r^2}} - \frac{2}{\pi} \sum_{\substack{j=1 \\ j \neq i}}^N P_j \arcsin \frac{a_i}{l_{ij}}, \quad (2.31)$$

where  $l_{ij} = \sqrt{X_j^2 + Y_j^2}$ .

Considering the relations (2.31) for each punch of the system in combination with the contact condition

$$D_i = h_i - D_0, \quad (2.32)$$

( $D_0$  is the approach of bodies under the load  $P$  (Fig. 2.9)), we get  $2N$  equations for determining the values of  $D_i$  and  $P_i$  ( $i = 1, 2, \dots, N$ ).

If the approach of the bodies  $D_0$  is unknown, and the load  $P$  is given, then in order to determine  $D_0$  one should add to Eqs. (2.31) and (2.32) the equilibrium condition

$$\sum_{i=1}^N P_i = P. \quad (2.33)$$

When we study the contact interaction of a system of smooth axially symmetric punches with the elastic half-space, the radius of each contact spot  $a_i$  is the unknown value. We can find this value from the condition

$$p(a_i, \theta) = 0, \quad 0 < \theta \leq 2\pi.$$

It follows from this relation and the equilibrium equation

$$P_i(a_i) = \int_0^{a_i} \int_0^{2\pi} p(r, \theta) r dr d\theta$$

that  $\frac{\partial P_i}{\partial a_i} = 0$ . Differentiation of Eq. (2.31) with respect to  $a_i$  gives

$$D_i = -a_i \int_0^{a_i} \frac{f'(r) dr}{\sqrt{a_i^2 - r^2}} + \frac{1 - \nu^2}{\pi E} \sum_{\substack{j=1 \\ j \neq i}}^N \frac{P_j}{\sqrt{l_{ij}^2 - a_i^2}}. \quad (2.34)$$

Eqs. (2.34) in conjunction with Eqs. (2.31) and (2.32) give the complete system of equations to determine the values of  $D_i$ ,  $a_i$  and  $P_i$  for a system of punches, the shapes of which are described by a continuously differentiable function.

### 2.3.2 A system of cylindrical punches

We consider a system of cylindrical punches with flat bases of radii  $a_i$  ( $f(r) = 0$ ) penetrating into the elastic half-space, and assume that the contact is complete, that is, it occurs within the subregion  $\omega_i$ , ( $r \leq a_i$ ). Then we obtain from Eqs. (2.31) the following relationship for the  $i$ -th punch penetration ( $i = 1, 2, \dots, N$ )

$$D_i = \frac{P_i (1 - \nu^2)}{2a_i E} + \frac{1 - \nu^2}{\pi a_i E} \sum_{\substack{j=1 \\ j \neq i}}^N P_j \arcsin \frac{a_i}{l_{ij}}. \quad (2.35)$$

It follows from Eq. (2.35) that the penetration of the punch depends only on the total load applied to the punches located at the distant  $l_{ij}$  from the fixed one (circumference of radius  $l_{ij}$ ).

Eqs. (2.35) in combination with the contact condition (2.32) and the equilibrium equation (2.33) are used to calculate the load distribution  $P_i$  between punches. Then the pressure at the  $i$ -th contact spot can be approximately determined from the formula (2.6), by substitution of the concentrated loads  $P_j = \iint_{\omega_j} p_j(x, y) dx dy$ , applied to the centers of the contact spots  $\omega_j$ , ( $j \neq i$ ) for the real pressure  $p_j(x, y)$

$$p_i(x, y) = \frac{ED_i}{\pi(1 - \nu^2)\sqrt{a^2 - x^2 - y^2}} - \frac{1}{\pi^2 \sqrt{a^2 - x^2 - y^2}} \sum_{\substack{j=1 \\ j \neq i}}^N \frac{P_j \sqrt{X_j^2 + Y_j^2 - a_i^2}}{(x - X_j)^2 + (y - Y_j)^2}.$$

For definiteness we consider a system of  $N$  cylindrical punches which are rigidly bonded and acted on by the force  $P$  directed along the  $z$ -axis. Each punch has a flat base of radius  $a$ . We introduce the following notation

$$\Theta_j = \frac{1 - \nu^2}{2aED_0} P_j, \quad \delta_j = \frac{h_j}{D_0} - 1, \quad b_{ij} = \begin{cases} 1, & j = i, \\ \frac{2}{\pi} \arcsin \frac{a}{l_{ij}}, & j \neq i. \end{cases} \quad (2.36)$$

In this case Eqs. (2.32), (2.33) and (2.35) take the form

$$B\Theta = \delta, \quad (2.37)$$

where  $B$  is a square nonsingular matrix with elements  $b_{ij}$ ,  $\delta$  is a column vector with elements  $\delta_i > 0$ ,  $\Theta$  is a column vector with elements  $\theta_i$ . We assume that the column vector  $\delta$  provides the conditions  $\Theta_j > 0$  ( $j = 1, 2, \dots, N$ ) which occur if all punches are in contact with the elastic half-space.

In view of nonsingularity of matrix  $B$  it follows from Eq. (2.37) that

$$\Theta = B^{-1}\delta. \quad (2.38)$$

Adding up  $N$  equations in the system (2.38) and taking into account the equilibrium equation (2.33), we obtain

$$\frac{1 - \nu^2}{2aED_0} P = \sum_{i=1}^N \sum_{j=1}^N \tilde{b}_{ij} \delta_i, \quad (2.39)$$

where  $\tilde{b}_{ij}$  are the elements of the inverse matrix  $B^{-1}$ . Eq. (2.39) makes it possible to determine the relation between the load  $P$  applied to the system of punches, and its penetration  $D$  for different spatial arrangement of punches (their height distribution  $h_j$  and location within the nominal region  $\Omega$ ).

The system of equations (2.37) and the relationship (2.39) have been used for calculation of loads acting on the punches, and for determination of the relation between the total load and the depth of penetration for a system of  $N$  cylindrical punches of radius  $a$  that are embedded in a rigid plate. The traces of the axes of the cylinders form a hexagonal lattice with a constant pitch  $l$ , and the flat faces of the cylinders are at the same level  $h_j = h$  for all  $j = 1, 2, \dots, N$ . The punches are located symmetrically relative to the central punch, so the nominal region is close to a circle. The density of the contact is determined by the parameter  $\frac{a}{l}$ .

The scheme of the punch arrangement is presented in Fig. 2.13.

Fig. 2.10 illustrates the loads acting on the punches located at the various distances  $\frac{l_{1j}}{l}$  from the central punch, for different values of the parameter  $\frac{a}{l}$  and  $N = 91$ . The results show that for high density ( $\frac{a}{l} = 0.5$ , dark-coloured rectangles) the punches in the outlying districts are acted on by a load rough-

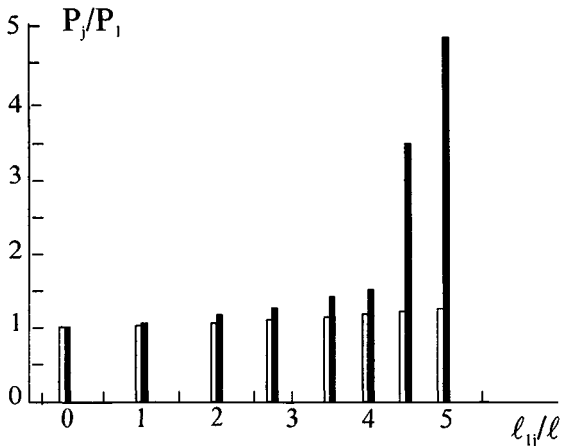


Figure 2.10: Load distribution between the cylindrical punches located at the distance  $\ell_{ij}$  from the central punch. The model parameters are  $N = 91$ ,  $a/l = 0.5$  (dark-coloured rectangles),  $a/l = 0.2$  (light-coloured rectangles). A schematic diagram of an arrangement of the punches is shown in Fig. 2.13.

ly 5 times greater than the load acting on the central punch; for lower density  $\left(\frac{a}{l} = 0.2\right)$ , (light-coloured rectangles) this ratio is equal to 1.14.

It follows from Eq. (2.39), that for the system of punches under consideration the relation between the total load  $P$  and the depth of penetration  $D$  ( $D = h - D_0$ ) has the form

$$P = j_0 \beta D, \quad (2.40)$$

where  $j_0 = \frac{2aE}{1-\nu^2}$  is the ratio of the load acting on an isolated cylindrical punch of radius  $a$ , to its penetration (contact stiffness of an isolated cylindrical punch),  $\beta = \sum_{i=1}^N \sum_{j=1}^N \tilde{b}_{ij}$ . The value  $\beta$  can be approximated by the function (Goryacheva and Dobychin, 1988)

$$\beta = k N^\alpha, \quad 0.5 \leq \alpha \leq 1, \quad (2.41)$$

where the coefficient  $k$  and the power  $\alpha$  depend on the parameter  $\frac{a}{l}$ . For  $\frac{a}{l} = 0.5$ , i.e. the punches are arranged with a maximum possible density,  $\alpha = 0.5$ . We can reason as follows. If we arrange the punches with the maximum possible density, the whole system of punches can be regarded as a single punch having radius  $r_N$ ; obviously, in that case  $\pi r_N^2 \approx \pi a^2 N$  or  $r_N \sim \sqrt{N}$ . Since the stiffness of an isolated punch is proportional to its radius, the stiffness of the whole system must be proportional to  $\sqrt{N}$ . On the other hand, if the punches are thinly scattered

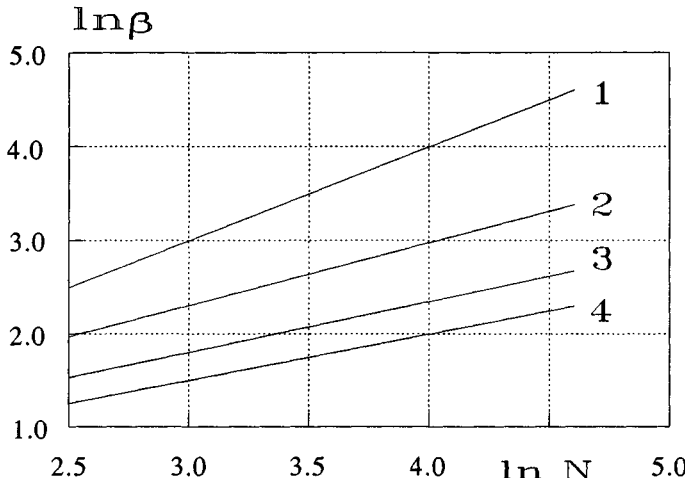


Figure 2.11: The dependence of  $\beta$  upon  $N$  for the various values of parameter  $a/l$ :  $a/l = 0$  (curve 1),  $a/l = 0.125$  (curve 2),  $a/l = 0.3$  (curve 3),  $a/l = 0.5$  (curve 4).

$(\frac{a}{l} \rightarrow 0)$ , their mutual influence is practically negligible,  $P_j = \frac{P}{N}$  and, as follows from Eq. (2.40),  $\beta = N$ . The variations of  $\beta$  with  $N$ , calculated from Eq. (2.40) for different values of the parameter  $\frac{a}{l}$  are presented in Fig. 2.11. The estimated values in the system of coordinates  $\ln \beta - \ln N$  cluster near the straight lines, which testifies to the appropriateness of the approximation function (2.41).

Thus, when the interaction of contact spots is neglected (the second term in Eq. (2.35) becomes zero and, hence,  $P = j_0 ND$ ) the contact stiffness  $\frac{P}{D}$  of the system of punches is overestimated, the error grows with the number of punches and the density of contact.

The approach described above has been used to analyze the relation between the load and the depth of penetration for different shapes of nominal region in which the punches are arranged (ellipses with different eccentricity are considered). For the models under consideration, the number  $N$  of punches and the contact density  $\frac{a}{l}$  were all the same. The results of calculation showed that as the eccentricity of the nominal region increases, the contact stiffness of the model increases moderately, the contact stiffness difference for an elongated contour and circular one is small (Goryacheva and Dobychin, 1988). It is interesting to note that the same result was obtained by Galin (1953) for an isolated punch with a flat base of an elliptic shape.

For calculations of the depth of penetration and the real area of contact of bodies with surface microgeometry, of great interest is the case when the tops of

Layer number	1	2	3	4	5	6	7	8
Number of punches	1	6	6	6	12	6	6	12
$\frac{h}{h_{\max}} (1)$	0.9	0.7	0.5	0.3	1.0	0.6	0.8	0.4
$\frac{h}{h_{\max}} (2)$	0.9	0.7	0.5	0.3	0.4	0.6	0.8	1.0

Table 2.1: The parameters of the model with different spatial arrangement of punches (the layer number is counted from the center to the periphery).

the punches are distributed in height rather than lying at the same level. Numerical calculations were carried out for a system of 55 flat-ended cylindrical punches which were located at sites of a hexagonal lattice (see Fig. 2.13). Different variants of the spatial arrangement of punches were considered. Two of them are presented in the Table 2.1. The punches of the  $j$ -th layer are located at the same distance  $l_{1j}$  from the central punch of the system. For the models under consideration, the number of punches that are intersected by the plane located at an arbitrary distance from the faces of the highest punches (with the height  $h_{\max}$ ), was the same in all variants (the layers of the model with given heights changed positions, but the number of punches in the layers was the same), i.e. the models were characterized by the same height distribution function. The results of the calculations have been described in details in the monograph by Goryacheva and Dobychin (1988). Fig. 2.12 shows the dependence of the real area of contact  $\frac{A_r}{A_r^*}$  ( $A_r^* = 55\pi a^2$ ) upon load  $\frac{P}{P^*}$  ( $P^*$  is the smallest load necessary for the complete contact of all the punches of the system in case of  $\frac{a}{l} = 0$ ) for  $\frac{a}{l} = 0$  (solid line) and  $\frac{a}{l} = 0.45$  (broken line). It must be noted that the dependence is a piecewise-constant function for the model under consideration. The broken line represents an averaged curve which reflects the ratio of the contact area and the load for the different variants of punch positions (the variants 1 and 2, presented in the Table 2.1 are indicated by triangles and squares, respectively).

The calculations showed that as the parameter  $\frac{a}{l}$  increases, the load which is necessary for the complete contact of all punches of the system also increases.

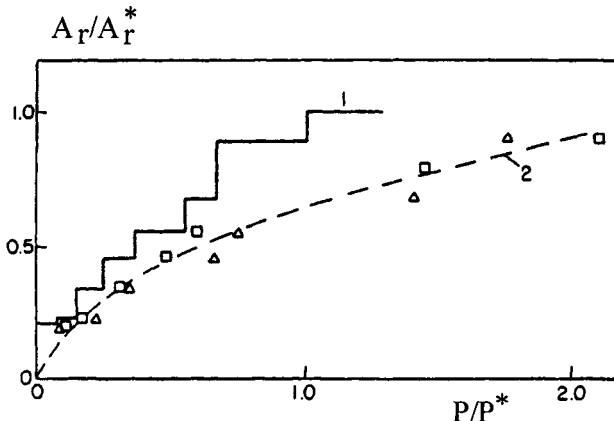


Figure 2.12: Real area of contact as a function of load (cylindrical punches distributed in height):  $a/l = 0$  (curve 1),  $a/l = 0.45$  (curve 2).

This can be explained by the interaction between the individual contact spots in the contact problem for the system of punches and the elastic half-space.

In order to evaluate the contribution of the simplifying assumptions made in the present model, experiments were made to study the dependence of the load upon the depth of penetration for a system of cylindrical punches with flat bases in contact with an elastic half-space.

The test sample was a steel plate with pressed-in steel cylinders of diameter  $2a = 3$  mm. When viewed from the top, the traces of the axes of the cylinders form a hexagonal lattice with a constant pitch  $l$ , and the flat faces of the cylinders are all at the same level. Two samples with  $\frac{a}{l} = 0.25$  and with  $\frac{a}{l} = 0.125$  were tested. The number of punches in each model was  $N = 55$ . A block of rubber was used as the elastic body. Its elastic constant had been estimated in advance:  $\frac{E}{1 - \nu^2} = 21.2$  MPa. Fig. 2.13 shows the results of experiments for these two samples. The theoretical dependencies obtained from Eq. (2.40) are given for comparison.

Thus, in full accord with the theory, the relation between the depth of penetration and the load is linear. The theoretical angular coefficients of these dependences, which are equal to 1.37 and 0.86 N/m, respectively, are sufficiently close to the experimental values (1.44 and 0.93, respectively). A slight difference between the theoretical and experimental data can be accounted for by the influence of the tangential stresses on the contact surfaces, which are not taken into account in the statement of the problem, but are not excluded by the experimental conditions. There will also be an error arising from the simplifying assumptions of the model, by which the real pressure distribution at neighboring punches is replaced by

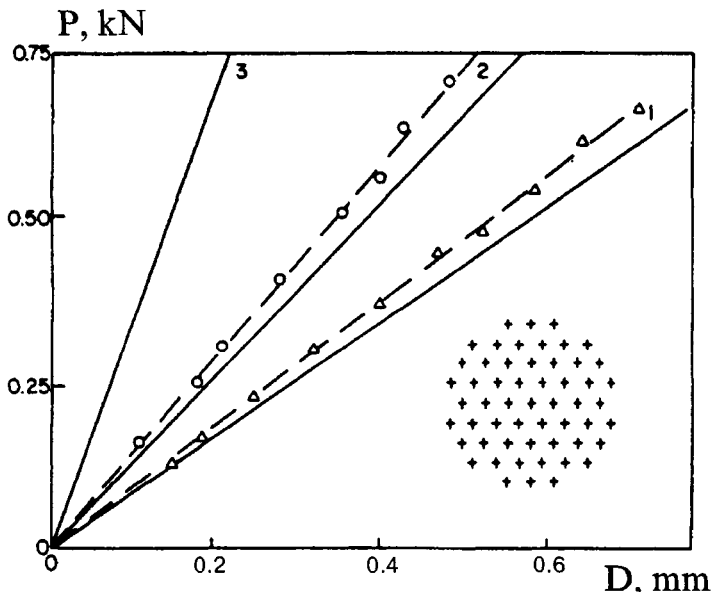


Figure 2.13: Relation between the normal load and the depth of penetration for  $a/l = 1/4$  (1),  $a/l = 1/8$  (2),  $a/l = 0$  (3); (solid line – theory, broken line – experiment). In the lower right-hand corner a schematic diagram of an arrangement of cylindrical punches on the test sample is shown.

concentrated forces.

The present model has been used to predict experimental results obtained by Kendall and Tabor (1971). The theoretical and experimental results are in good agreement (Goryacheva and Dobychin, 1980).

### 2.3.3 A system of spherical punches

For punches with a spherical contact surface of radius  $R$ ,  $f(r) = \frac{r^2}{2R}$ , and the given spatial arrangement Eqs. (2.31)–(2.33) take the form

$$\begin{aligned}
 h_i - D_0 &= \frac{a_i^2}{R} + \frac{1-\nu^2}{\pi E} \sum_{\substack{j=1 \\ j \neq i}}^N \frac{P_j}{\sqrt{l_{ij}^2 - a_i^2}}, \\
 P_i &= \frac{4Ea_i^3}{3R(1-\nu^2)} + \frac{2}{\pi} \sum_{\substack{j=1 \\ j \neq i}}^N P_j \left[ \frac{a_i}{\sqrt{l_{ij}^2 - a_i^2}} - \arcsin \frac{a_i}{l_{ij}} \right], \\
 P &= \sum_{i=1}^N P_i, \quad i = 1, 2, \dots, N.
 \end{aligned} \tag{2.42}$$

The system (2.42) determines the distribution of forces  $P_i$  among  $N$  punches, which are loaded with the total force  $P$  and interact with the elastic half-space, the radii  $a_i$  of the contact subregions  $\omega_i$ , the total real area of contact  $A_r = \pi \sum_{i=1}^N a_i^2$  and the dependence of the approach upon load  $D_0(P)$ .

It follows from the second group of Eqs. (2.42) that the radius of the  $i$ -th contact spot can be determined with accuracy of order  $\left(\frac{a_i}{l_{ij}}\right)^3$  by the Hertz formula

$$a_i = \sqrt[3]{\frac{3RP_i(1-\nu^2)}{4E}}.$$

Then the real area of contact can be approximated by the formula

$$A_r = \pi \sum_{i=1}^N \sqrt[3]{\left[\frac{3RP_i(1-\nu^2)}{4E}\right]^2},$$

where  $P_i$  is determined from the first group of Eqs. (2.42).

Fig. 2.14 shows plots of the relative area of contact  $\frac{A_r}{A_a}$  ( $A_a$  is the nominal area of contact) versus the pressure  $\bar{p} = \frac{P}{A_a}$  calculated from Eqs. (2.42) (curve 1) for the system of  $N = 52$  spherical punches of radius  $R$ , located at the same height and distributed at the sites of square lattice ( $l$  is the lattice pitch) with  $\frac{l}{R} = 0.5$ . Curve 2 is calculated using the Hertz theory and neglecting the redistribution of the loads applied to each contact spot due to the interaction between contact spots. From  $\frac{A_r}{A_a} = 0.3$  there is a noticeable error in the calculation of the real area of contact from the theory which ignores interaction.

Fig. 2.15 shows the dependence of the depth of penetration  $D$  upon the load  $P$  for the system of spherical asperities. The higher is the contact density (i.e. the smaller is the parameter  $\frac{l}{R}$ ), the smaller is the load required to achieve the given depth of penetration. Analogous results were obtained theoretically and experimentally when studying the interaction of a system of cylindrical punches, located at the same level, with an elastic half-space (Fig. 2.13).

From the results of the analysis we conclude that the calculation methods which do not take into account the interaction of the contact spots give overestimated values for the contact stiffness  $\frac{dP}{dD}$  and the real area of contact  $A_r$ ; the error increases with the number of contacts and their density.

The geometrical imperfections of a surface, in particular its waviness and distortion, which are caused by inaccurate conjunctions and deviations from the ideal system of external loads, lead to the localization of contact spots within the so-called contour regions. The nominal region can include a few or many contour

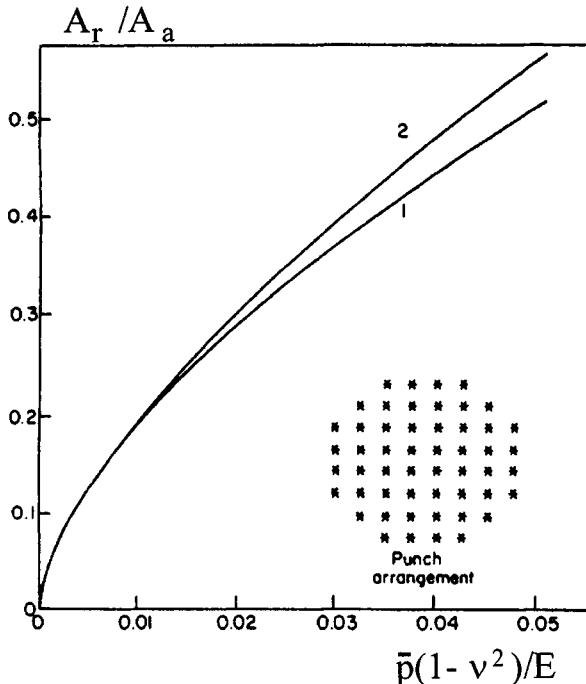


Figure 2.14: The dependence of the relative area of contact upon nominal pressure at  $l/R = 0.5$  calculated from the multiple contact model (curve 1) and the Hertz model (curve 2). A schematic diagram of the punch arrangement is shown in the lower right-hand corner.

regions, where the density of contact spots is high. So even a moderate load provides a high relative contact area within the contour regions, and the error of calculation based on the simplified theory can be large.

It is worth noting that the investigation of the multiple contact problem based on the approach described in this section and in § 2.2 necessitates the knowledge of the additional parameter characterizing the density of the arrangement of contact spots. This parameter can be determined, in particular, from modelling of rough surfaces based on the theory of random functions (Sviridenok, Chijik and Petrokovets, 1990).

## 2.4 The additional displacement function

### 2.4.1 The function definition

We again direct our attention to Eq. (2.2), which determines the displacement  $u_z(x, y)$  of the half-space surface loaded by the pressure  $p_i(x, y)$  within contact

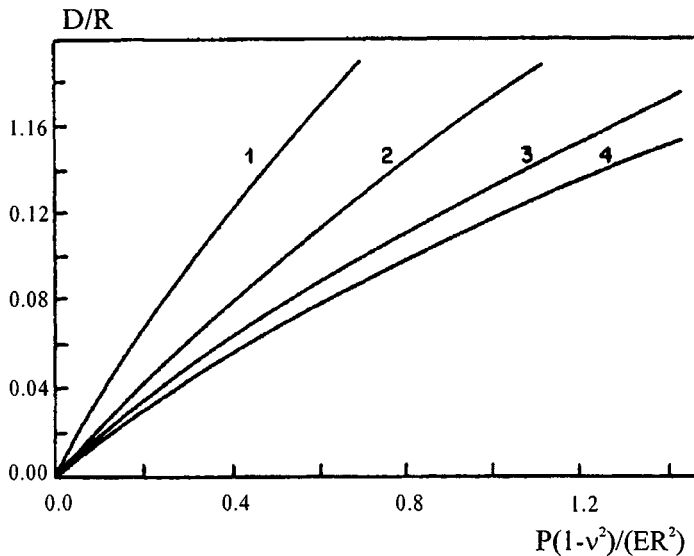


Figure 2.15: The dependence of the depth of penetration upon the load for the various values of the parameter  $l/R$ :  $l/R = 0.5$  (curve 1),  $l/R = 1$  (curve 2),  $l/R = 1.5$  (curve 3),  $l/R = 2$  (curve 4).

spots  $\omega_i$ , and substitute the nominal pressure  $p(x, y)$  within the region  $\Omega \setminus \Omega_0$  ( $\Omega_0$  is the circle with the center  $(x, y)$ ) for the real pressure distributed within the contact spots  $\omega_i \in \Omega \setminus \Omega_0$ , i.e.

$$\frac{\pi E}{1 - \nu^2} u_z(x, y) = \sum_{i=1}^n \iint_{\omega_i} \frac{p_i(x', y') dx' dy'}{\sqrt{(x' - x)^2 + (y' - y)^2}} + \iint_{\Omega \setminus \Omega_0} \frac{p(x', y') dx' dy'}{\sqrt{(x' - x)^2 + (y' - y)^2}}, \quad (2.43)$$

where  $\omega_i \in \Omega_0$  ( $i = 1, 2, \dots, n$ ).

The principle of localization formulated in § 2.2.2 shows that this substitution can be carried out with a high degree of accuracy. The radius  $R_0$  of the region  $\Omega_0$  can be determined from the following limiting estimate. We assume that there are  $N$  concentrated normal forces  $P_i$  ( $i = 1, 2, \dots, N$ ) within the annular domain ( $\Omega_{R_0} : R_0 < r < R_1$ ), and the nominal pressure is uniformly distributed within this region, i.e.  $p(x, y) = \bar{p}$  (see Fig. 2.16). This simulates the limiting case of a discrete contact. We determine the difference  $\Delta u_z$  of displacements at the center  $(x, y)$  of the annulus  $\Omega_{R_0}$  which arises from the concentrated forces on the one hand, and from the nominal pressure on the other hand, which are distributed

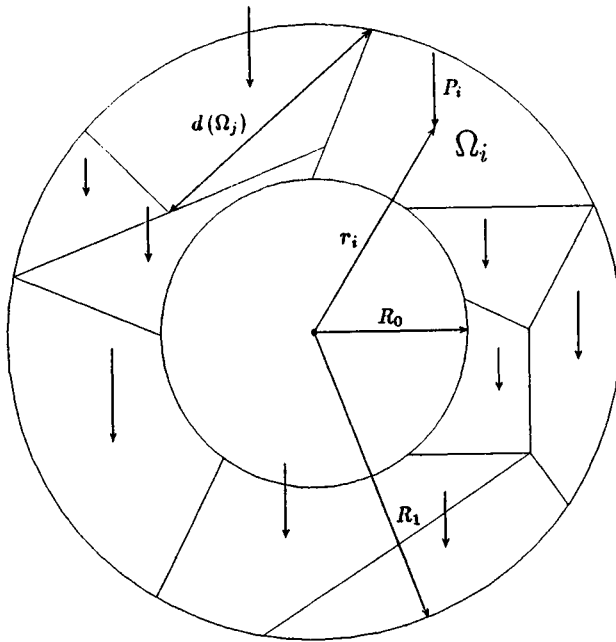


Figure 2.16: Scheme of an arrangement of the concentrated normal forces inside the nominal region  $\Omega_{R_0}$ .

within the region  $\Omega_{R_0}$ , that is

$$\frac{\pi E}{1 - \nu^2} \Delta u_z = \sum_{i=1}^N \frac{P_i}{r_i} - \iint_{\Omega_{R_0}} \frac{\bar{p} r dr d\varphi}{r}, \quad (2.44)$$

where  $r_i$  is the distance from the point  $(x, y)$  to the point where the concentrated force  $P_i$  is applied. We divide the region  $\Omega_{R_0}$  into  $N$  subregions  $\Omega_i$  so that only one force is within each subregion and the condition  $\bar{p} = \frac{P_i}{A_{\Omega_i}}$  is satisfied ( $A_{\Omega_i}$  is the area of  $\Omega_i$ ). Then we obtain on the basis of the law of the mean

$$\iint_{\Omega_i} \frac{\bar{p} r dr d\varphi}{r} = \frac{P_i}{\tilde{r}_i}, \quad (2.45)$$

where  $\tilde{r}_i$  is the distance from the point  $(x, y)$  to some point inside the subregion  $\Omega_i$ . Then it follows from Eqs. (2.44) and (2.45), and conditions  $r_i \geq R_0$ ,  $\tilde{r}_i \geq R_0$  that

$$\frac{\pi E}{1 - \nu^2} \Delta u_z = \sum_{i=1}^N \left( \frac{1}{r_i} - \frac{1}{\tilde{r}_i} \right) P_i \leq \frac{\max_i d(\Omega_i)}{R_0^2} \max_i P_i,$$

where  $d(\Omega_i)$  is the characteristic linear size of the region  $\Omega_i$ .

If concentrated forces with the same value  $P_i = P$  are uniformly distributed over the region  $\Omega_{R_0}$ , this estimate takes a simple form

$$\frac{\pi E}{1 - \nu^2} \Delta u_z \leq \frac{2P}{R_0^2} \sqrt{\frac{R_1^2 - R_0^2}{N}}.$$

We write the contact condition (2.3) in the following form

$$u_z(x, y) = D - f(x, y) + h(x, y), \quad x, y \in \omega_0, \quad (2.46)$$

where the function  $f(x, y)$  describes the macroshape of the indenter, and the function  $h(x, y)$  describes the shape of an asperity within the contact spot  $\omega_0$ .

From Eqs. (2.43) and (2.46), and substituting the integral over  $\Omega \setminus \Omega_0$  in Eq. (2.43) by the difference of integrals over regions  $\Omega$  and  $\Omega_0$ , we can derive the following integral equation

$$D - f(x, y) = \beta(x, y) + \frac{1 - \nu^2}{\pi E} \iint_{\Omega} \frac{p(x', y') dx' dy'}{\sqrt{(x' - x)^2 + (y' - y)^2}}, \quad (2.47)$$

where

$$\begin{aligned} \beta(x, y) = & -h(x, y) + \\ & \frac{1 - \nu^2}{\pi E} \left[ \sum_{i=1}^n \iint_{\omega_i} \frac{p_i(x', y') dx' dy'}{\sqrt{(x' - x)^2 + (y' - y)^2}} - \iint_{\Omega_0} \frac{p(x', y') dx' dy'}{\sqrt{(x' - x)^2 + (y' - y)^2}} \right]. \end{aligned} \quad (2.48)$$

The function  $\beta(x, y)$  depends only on the parameters of loading and microgeometry in the vicinity of the point  $(x, y)$  (within the region  $\Omega_0$ ).

It should be noted that there are two length scales in the problem: the macroscale connected with the nominal contact area and the macroshape of the indenter, and the microscale related to the size and distance between the contact spots. In what follows, we assume that all functions related to the macroscale, i.e.  $p(x, y)$ ,  $f(x, y)$ ,  $\beta(x, y)$ , etc., change negligibly little for distances of the order of the distance between neighbouring contact spots.

We will demonstrate below that under this assumption the function  $\beta(x, y)$  (we call it *the additional displacement*) can be presented as a function  $C(p)$  of the nominal pressure  $p(x, y)$ , and determine the form of this function for some particular models of surface microgeometry.

## 2.4.2 Some particular cases

We consider Eq. (2.48) at the point  $(x_0, y_0) \in \omega_0$ , where the top of an asperity with height  $h_0$  is located. Taking into account the assumption concerning two geometry scales for the problem under consideration, we suppose that the nominal pressure within the region  $\Omega_0$  which is a circle of radius  $R_0$  with a center at the

point  $(x_0, y_0)$  is uniform and equal to  $p(x_0, y_0)$ . Inside the region  $\Omega_0$  we consider also the real pressure distribution at the contact spots  $\omega_i \in \Omega_0$  ( $i = 1, 2, \dots, n$ ) (local effect). Then Eq. (2.48) can be reduced to the form

$$\beta(x_0, y_0) = -h_0 + \frac{1 - \nu^2}{\pi E} \left[ \sum_{i=0}^n \iint_{\omega_i} \frac{p_i(x', y') dx' dy'}{\sqrt{(x' - x_0)^2 + (y' - y_0)^2}} - 2\pi R_0 p(x_0, y_0) \right]. \quad (2.49)$$

So the value  $\beta(x_0, y_0)$  characterizes the additional displacement of the region  $\Omega_0$  (which is acted by the nominal pressure  $p(x_0, y_0)$ ) arising from the penetration of asperities into the elastic half-space inside this region. Since  $A_{\Omega_0} \ll A_\Omega$ , we can neglect the curvature of the surface at the point  $(x_0, y_0)$  when determining the value of  $\beta(x_0, y_0)$ . This suggests that it might be convenient to use the solution of the periodic contact problem for determination of  $\beta(x_0, y_0)$ . In this case the periodic contact problem must be considered for the system of indenters which models the real surface geometry in the region  $\Omega_0$  and which is loaded by the nominal pressure  $p(x_0, y_0)$ . It was shown in § 2.2 that for the given nominal pressure  $p$  and the known spatial arrangement of indenters we can uniquely determine the real contact pressure  $p_i(x, y)$  from the systems of equations (2.17) or 2.21 – 2.23 and, hence, the value  $\beta(x_0, y_0)$  from Eq. (2.49). So the dependence of the additional displacement upon the nominal pressure  $C(p)$  can be constructed at each point  $(x_0, y_0)$  based on Eq. (2.49).

We note that to sufficient accuracy the function  $C(p)$  can be written in analytical form for some surfaces with a regular microgeometry. Using the law of the mean, we reduce Eq. (2.49) to the following form

$$\beta(x_0, y_0) = -h_0 + \phi(P_0) + \frac{1 - \nu^2}{\pi E} \left[ \sum_{i=1}^n \frac{P_i}{l_{0i}} - 2\pi R_0 p(x_0, y_0) \right], \quad (2.50)$$

where

$$\phi(P_0) = \frac{1 - \nu^2}{\pi E} \iint_{\omega_0} \frac{p_0(x', y') dx' dy'}{\sqrt{(x' - x_0)^2 + (y' - y_0)^2}},$$

$$P_i = \iint_{\omega_i} p_i(x', y') dx' dy'$$

and  $l_{0i}$  is the distance from the point  $(x_0, y_0)$  to some internal point of the contact spot  $\omega_i \in \Omega_0$  ( $i = 1, 2, \dots, n$ ).

As an example, we consider a surface for which the microgeometry can be simulated by asperities of the same height located at the sites of a hexagonal lattice with constant pitch  $l$ . In § 2.2 it was shown that to sufficient accuracy we can take  $n = 6$  in Eq. (2.49). Then we obtain from Eq. (2.19)

$$R_0 = \sqrt{\frac{7}{\pi N}},$$

where  $\bar{N}$  is a number of asperities per unit area. For the hexagonal lattice we have  $\bar{N} = \frac{2}{l^2\sqrt{3}}$ . Since all asperities within the region  $\Omega_0$  are undergoing the same conditions, they are loaded uniformly and so the load  $P$  applied to one asperity is obtained from the equilibrium condition

$$P = \frac{1}{7} p(x_0, y_0) \pi R_0^2 = \frac{p(x_0, y_0)}{\bar{N}}.$$

For a cylindrical asperity with a flat base of radius  $a$ , the function  $\phi(P)$  in Eq. (2.50) has the form

$$\phi(P) = \frac{(1 - \nu^2) P}{2aE}.$$

Substituting the relations obtained above in Eq. (2.50) on the assumption that  $l_{0i} \approx l$ , gives the following form for the additional displacement function:

$$\begin{aligned} \frac{1}{l} C[p(x, y)] &= \frac{1}{l} \beta(x, y) = \\ \frac{1 - \nu^2}{E} p(x, y) &\left( \frac{\sqrt{3}}{4} \cdot \frac{l}{a} + \frac{3\sqrt{3}}{\pi} \cdot \frac{l}{a} \arcsin \frac{a}{l} - \sqrt{\frac{14\sqrt{3}}{\pi}} \right). \end{aligned} \quad (2.51)$$

The height of asperities  $h$  is not present in Eq. (2.51) because this value can be taken into account in the right side of Eq. (2.47) for models with asperities of the same height.

For elastic asperities of spherical shape, i.e.  $f(r) = \frac{r^2}{2R}$ , located at the sites of a hexagonal lattice with a pitch  $l$ , the function  $C(p)$  can be reduced in a similar way based on the results of § 2.2. The final expression has the form

$$\begin{aligned} \frac{C[p(x, y)]}{R} &= \frac{\beta(x, y)}{R} = \frac{p(x, y)}{E^*} \cdot \frac{l}{R} \left( \frac{3\sqrt{3}}{\pi} - \sqrt{\frac{14\sqrt{3}}{\pi}} \right) + \\ &4 \cdot \left( \frac{l}{R} \right)^{\frac{4}{3}} \left( \frac{p(x, y)}{E^*} \right)^{\frac{2}{3}} \left( 1 + \frac{p(x, y)}{E^*} \cdot \frac{R}{l} \cdot \frac{3\sqrt{3}}{2\pi} \right)^{\frac{1}{3}}. \end{aligned} \quad (2.52)$$

### 2.4.3 Properties of the function

The equation of the type (2.47) was first introduced by Staierman (1949) for determination of the nominal pressure and nominal contact area for the contact of rough bodies. He proposed that for contact interaction of bodies with a surface microstructure, it is necessary to take into account the additional compliance (analogous to soft interlayer) caused by asperity deformation. As a rule, it is taken to be a linear or power additional displacement function in Eq. (2.47)

$$C[p(x, y)] = B p^\kappa(x, y), \quad \kappa \leq 1. \quad (2.53)$$

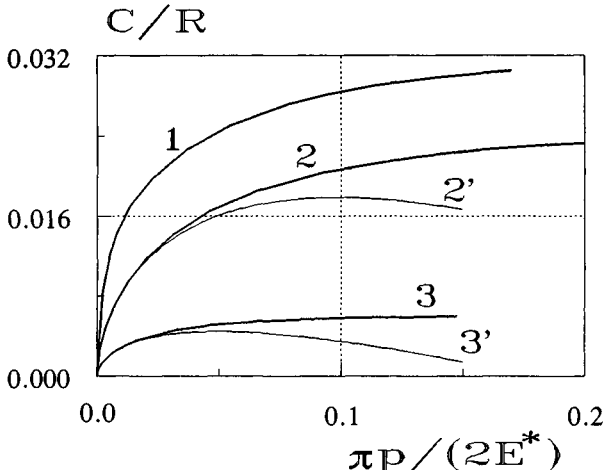


Figure 2.17: The additional displacement function for the three-level model (1) and the one-level model with  $l/R = 0.6$  (2, 2') and  $l/R = 0.3$  (3, 3'), calculated from Eqs. (2.17) and (2.21)–(2.23) (curves 1, 2, 3) and from Eq. (2.52) (curves 2', 3').

The coefficient  $B$  and the exponent  $\kappa$  are usually obtained experimentally. However the experimental determination of the function  $C[p(x, y)]$  for rough bodies is a complicated and laborious problem.

The method developed above makes it possible to calculate the additional displacement function for different kinds of surface microgeometry. It is based on the model representation of the microgeometry of rough surfaces. Fig. 2.17 illustrates the functions  $C(p)$  calculated for the three-level system of spherical indenters of radius  $R$  located at the sites of a hexagonal lattice with pitch  $\frac{l}{R} = 0.6$  and characterized by the following relative difference in the heights of the levels:  $\frac{h_0 - h_1}{R} = 0.01$ ,  $\frac{h_0 - h_2}{R} = 0.015$  (curve 1); and for the one-level system of spherical indenters located at the sites of a hexagonal lattice with the pitch  $\frac{l}{R} = 0.6$  (curve 2) and  $\frac{l}{R} = 0.3$  (curve 3). The calculations were based on Eq. (2.49), where the functions  $p_i(x, y)$  were obtained from the integral equations (2.17) and (2.21) – (2.23) for the one-level model and three-level one, respectively. The results indicate that the rate of change of the function  $C(p)$  decreases as the nominal pressure  $\bar{p}$  increases. If the real contact area is close to saturation, i.e.  $\frac{A_r}{A_a} \approx 1$ , the additional displacement function is close to a constant value, i.e.  $\frac{dC}{dp} = 0$ .

The curves 2 and 3 in Fig. 2.17 calculated for the one-level model illustrate this conclusion. The results calculated from Eq. (2.52) for the corresponding models are also presented in Fig. 2.17 (curves 2' and 3'). The coincidence of the curves 2, 2' and 3, 3' for relatively small values of the nominal pressure shows that it is possible to use the approximate analytical relationship (2.52) for calculation of the additional displacement, if  $\frac{a}{l} < 0.2$ . The discrepancy between the results for the higher values of the parameter  $\frac{a}{l}$  is explained by the essential effect of the real pressure distribution at the contact spots nearest to the chosen one. This effect in Eq. (2.52) is taken into account approximately by the corresponding values of the concentrated forces applied to these contact spots.

Thus, as the nominal pressure increases, the additional compliance  $\frac{dC}{dp}$  caused by the existence of a surface microgeometry, is progressively reduced and tends to zero in going from the discrete to continuous contact.

We note that the power function (2.53) does not describe this process, so it can be used only for low values of the nominal pressure, for which continuous contact does not occur.

## 2.5 Calculation of contact characteristics

### 2.5.1 The problem of continuous contact

We consider the contact of two elastic bodies with the macroshape described by the function  $z = f(x, y)$  and take into account parameters of their surface microgeometry. There are two scales of size in the problem: the characteristic dimension  $R_a$  of the nominal contact region  $\Omega$ , and the characteristic distance  $l_a$  between contact spots. The relation between  $R_a$  and  $l_a$  can vary in the contact interaction. For small loads it is conceivable that  $R_a \sim l_a$ , i.e. there are a finite number of asperities in the contact. In this case the method described in § 2.3 can be used for the determination of the contact characteristics (the nominal and real contact area, the load distribution between contact spots, the real pressure distribution, etc.).

If  $l_a \ll R_a$  there are many asperities within the nominal contact region. In this case the nominal (averaged) pressure can be determined from the integral equation (2.47) in which  $C(p)$  is the additional displacement function. The method for its determination is described in § 2.4. Eq. (2.47) completely determines the nominal pressure  $p(x, y)$  if the nominal contact region  $\Omega$  and the penetration  $D$  are prescribed. If the nominal contact region is not known in advance, the problem is reduced to the determination of the nominal contact pressure  $p(x, y)$  and the

region  $\Omega$  with its boundary  $\partial\Omega$  from the system of equations

$$\begin{aligned} u_z(x, y) &= C(p(x, y)) + \iint_{\Omega} K(x, y, x', y') p(x', y') dx' dy', \\ p(x, y) > 0, \quad \text{if } &u_z(x, y) = D - f(x, y), \quad (x, y) \in \Omega, \\ p(x, y) = 0, \quad \text{if } &(x, y) \in \partial\Omega, \\ p(x, y) = 0, \quad \text{if } &u_z(x, y) > D - f(x, y), \quad (x, y) \notin \Omega. \end{aligned} \tag{2.54}$$

The equilibrium equation

$$P = \iint_{\Omega} p(x', y') dx' dy' \tag{2.55}$$

is added to this system to obtain the unknown value  $D$  if the load  $P$  applied to the indenter is known in advance. Eq. (2.47) or the system of equations (2.54) have been analyzed in Staierman (1949), Popov and Savchuk (1971), Aleksandrov and Kudish (1979), Goryacheva (1979b), Galanov (1984), etc. for different types of the function  $C(p)$  and different kernels  $K(x, y, x', y')$  of the integral operator which are typical for contact problems. In what follows we will describe the method of investigation of these equations for plane and axisymmetric contact problems.

## 2.5.2 Plane contact problem

We consider the contact of a strip punch or a long elastic cylinder, with an elastic layer of thickness  $h$  ( $|x| < \infty$ ,  $0 < z < h$ ), lying on a rigid foundation (Fig. 2.18). This problem can be analyzed in a 2-D formulation. The indenter macroshape is given by the equation  $z = f(x)$ . The load  $P$  is applied to the indenter in the  $z$ -axis direction. The tangential stress within the contact region is supposed to be negligibly small. We investigate two types of contact conditions at the boundary between the strip (layer) and foundation ( $z = h$ ):

1. The strip lies on the rigid foundation without friction; then

$$\tau_{xz}(x, h) = 0, \quad u_z(x, h) = 0, \quad |x| < +\infty.$$

2. The strip is bonded with the foundation; then

$$u_x(x, h) = u_z(x, h) = 0.$$

The boundary conditions at the surface  $z = 0$  are

$$\begin{aligned} \tau_{xz}(x, 0) &= 0, \quad \sigma_z(x, 0) = 0, \quad a < |x| < \infty, \\ \tau_{xz}(x, 0) &= 0, \quad u_z(x, 0) = D - f(x), \quad |x| < a. \end{aligned} \tag{2.56}$$

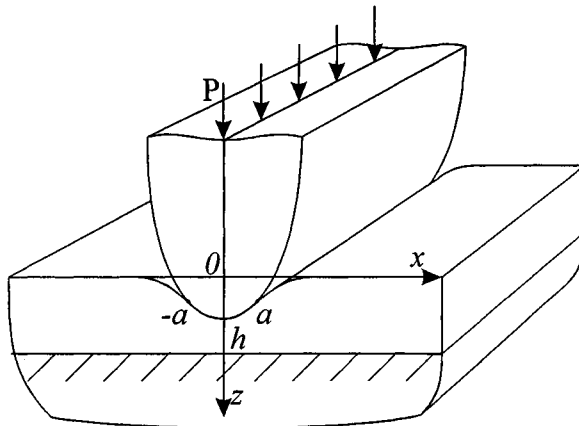


Figure 2.18: Scheme of the contact of a rough punch and an elastic layer lying on a rigid foundation.

The main integral equation (2.54) taking into account the additional displacement  $C(p)$  caused by the surface roughness of the contacting bodies takes the following form for the problem under consideration

$$D - f(x) = C(p(x)) + \frac{2(1-\nu^2)}{\pi E} \int_{-a}^a k\left(\frac{x'-x}{h}\right) p(x') dx'. \quad (2.57)$$

It has been shown in Vorovich, Aleksandrov and Babeshko (1974), that the kernel of the integral operator in Eq. (2.57) has the form

$$k(t) = \int_0^{+\infty} \frac{L(u)}{u} \cos ut du. \quad (2.58)$$

The form of the function  $L(u)$  depends on the boundary conditions at the plane  $z = h$ .

In case 1

$$L(u) = \frac{\cosh 2u - 1}{\sinh 2u + 2u}. \quad (2.59)$$

In case 2

$$L(u) = \frac{2\kappa_* \sinh 2u - 4u}{2\kappa_* \cosh 2u + 4u^2 + 1 + \kappa_*^2}, \quad \kappa_* = 3 - 4\nu. \quad (2.60)$$

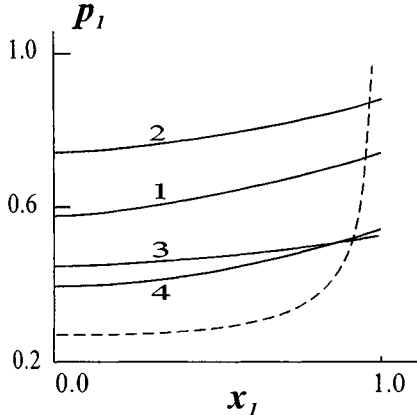


Figure 2.19: The pressure in the contact of a punch with flat rough base and a thick elastic strip, for various roughness parameters (solid lines) and for a smooth surface (broken lines).

We rewrite Eq. (2.57) and the equilibrium condition (2.55) in dimensionless form. To do this, we introduce the following notation:

$$\begin{aligned} x_1 &= \frac{x}{a}, & \delta &= \frac{D}{a}, \quad \lambda = \frac{a}{h}, \\ f_1(x_1) &= \frac{f(ax_1)}{a}, & C_1(p_1(x_1)) &= \frac{C(p(ax_1))}{a}, \\ p_1(x_1) &= \frac{2(1-\nu^2)}{\pi E} p(ax_1), & P_1 &= \frac{2(1-\nu^2) P}{\pi E a}. \end{aligned} \quad (2.61)$$

Then we obtain

$$\int_{-1}^1 k(\lambda(t-x_1)) p_1(t) dt + C_1(p_1(x_1)) = \delta - f_1(x_1), \quad (2.62)$$

$$\int_{-1}^1 p_1(x) dx = P_1. \quad (2.63)$$

If the contact half-width  $a$  is known in advance, Eqs. (2.62) and (2.63) form the complete system of equations for the determination of the dimensionless contact pressure  $p_1(x_1)$  and the penetration  $\delta$  of the indenter.

Eq. (2.62) is an equation of Hammerstein type. It can be reduced to canonical form. To do this, we introduce the function

$$\psi(x_1) = C_1(p_1(x_1)) + f_1(x_1) - \delta. \quad (2.64)$$

Then

$$\int_{-1}^1 k(\lambda(t - x_1)) C_1^{-1}(\psi(t) - f_1(t) + \delta) dt + \psi(x_1) = 0, \quad (2.65)$$

where  $C_1^{-1}(x)$  is the inverse function to  $C_1(x)$ .

To solve this equation, we can use iteration. We take  $\psi_0(x_1) = 0$  as the initial solution and then calculate the subsequent values from the recurrence relation

$$\psi_{n+1}(x_1) = - \int_{-1}^1 k(\lambda(t - x_1)) C_1^{-1}(\psi_n(t) - f_1(t) + \delta) dt.$$

The convergence of the method can be proved for some particular forms of the function  $C(p)$ . It was indicated in § 2.4 that  $C(p)$  can be approximated by the power function (2.53), valid for relatively low values of the nominal pressure  $p$  and, hence, for the case in which the real contact area is much less than the nominal contact area. For the function  $C(p) = Bp^\kappa$  (2.53), successive approximations  $\psi_n(x_1)$  converge to the unique solution of the equation (2.65), if the parameters of the problem satisfy to the following inequality (Goryacheva, 1979b)

$$\left( \frac{1}{\kappa B_1^{1/\kappa}} \right)^2 \int_{-1}^1 [\delta - f_1(x)]^{2/\kappa-2} \left[ \int_{-1}^1 k^2(\lambda(t - x)) dt \right] dx < 1, \quad (2.66)$$

where

$$B_1 = \frac{B}{2a} \left[ \frac{\pi E}{2(1-\nu^2)} \right]^\kappa. \quad (2.67)$$

For the other values of parameters, the Newton–Kantorovich method (Kantorovich and Krylov, 1952) can be used to solve the problem. Then the dimensionless pressure can be found from the formula (2.64). If the penetration  $D$  of the indenter is not known in advance, we use also Eq. (2.63) to solve the problem.

The study makes it apparent that for the function  $C(p)$  (2.53), the contact pressure does not tend to infinity at the ends of the contact region. To prove this fact, we anticipate that pressure has an integrable singularity of the type  $(1 - x_1)^{-\theta}$  ( $0 < \theta < 1$ ) at the point  $x_1 = 1$ . We take into account also that the kernel of the integral operator has a singularity of the type  $\ln(1 - x_1)$ . Then we conclude that the left side of Eq. (2.62) has a singularity of the form  $(1 - x_1)^{-k\theta}$ , whereas there is no singularity at the right side of the equation. This contradiction proves the proposition mentioned above. Thus, the consideration of the additional displacement caused by the asperity penetration leads to the disappearance of the singularity of the contact pressure at the ends of the contact zone which occurs for the problem formulation neglecting the surface microgeometry, for bodies whose macroshape  $f(x)$  provides a discontinuity of the derivative of the surface displacement  $u'_z(x)$  at the ends of the contact region (for example,  $f'(x) = 0$  for  $x < a$ ).

For linear contact of elastic cylindrical bodies with rough surfaces we use the additional condition that the contact pressure is equal to zero at the ends of the contact region, i.e.  $p_1(-1) = p_1(1) = 0$ , and also the relation  $C(0) = 0$ . Then the integral equation (2.62) for the nominal contact pressure determination can be reduced to the form

$$\int_{-1}^1 (k(\lambda(t - x_1)) - k(\lambda(t - 1))) p_1(t) dt + C_1(p_1(x_1)) = f_1(1) - f_1(x_1), \quad (2.68)$$

where

$$p_1(x_1) = \frac{2}{\pi E^*} p(ax_1). \quad (2.69)$$

This is also a Hammerstein type integral equation which can be solved by iteration or the Newton-Kantorovich method.

The solution of Eq. (2.68) with the function  $C(p)$  of the form (2.53), where  $0 < \kappa < 1$ , has zero derivative at the ends of the contact region, i.e.  $p'_1(-1) = p'_1(1) = 0$ . This can be proved as follows. Upon differentiating Eq. (2.68) with respect to  $x_1$  and setting  $x_1 = -1$  (the case  $x_1 = 1$  can be analyzed in a similar manner), we obtain

$$\int_{-1}^1 (-\lambda k'(\lambda(t - x_1))) p_1(t) dt + B_1 \kappa p_1^{\kappa-1}(-1) p'_1(-1) = -f'_1(-1), \quad (2.70)$$

where  $B_1$  is determined from Eq. (2.67).

Since the function  $p_1(x_1)$  is continuously differentiable,  $p_1(-1) = p_1(1) = 0$ , and the kernel  $k(t)$  (2.58) is presented as (see Vorovich, Aleksandrov and Bershko, 1974)

$$k(t) = -\ln|t| + F(t),$$

where  $F(t)$  is an analytical function, the integral term on the left side of Eq. (2.70) is bounded. The second term in the left side of this equation has to be also bounded, as the value  $f'_1(-1)$  is bounded on the right side of Eq. (2.70). This holds for  $0 < \kappa < 1$ , only if  $p'_1(-1) = 0$ .

As an example, we consider the problem of frictionless contact between a thick rough layer and a punch with the flat base,  $f(x) = 0$ . For the nominal pressure determination, we use Eq. (2.62) in which  $f_1(x_1) = 0$ , and the kernel  $k(t)$  has the form  $k(t) = -\ln|t| + a_0$ ;  $a_0 = -0.352$  for case 1, and  $a_0 = -0.527$  for case 2 ( $\nu = 0.3$ ) (Vorovich et al., 1974). This asymptotic representation of the kernel holds for the comparatively thick layer  $\left(\lambda \leq \frac{1}{2}\right)$ . The function  $C(p)$  is used in the form of Eq. (2.53).

The problem is attacked by solving Eq. (2.65) by iteration. Then we obtain the nominal contact pressure as

$$p_1(x_1) = B_1^{-\frac{1}{\kappa}} [\psi(x_1) + \delta]^{\frac{1}{\kappa}},$$

where  $\psi(x_1)$  is the limit of the function sequence  $\{\psi_n(x_1)\}$  determined by

$$\psi_{n+1}(x_1) = B_1^{-\frac{1}{\kappa}} \int_{-1}^1 (\ln |t - x_1| + c_0) [\psi_n(t) + \delta]^{\frac{1}{\kappa}} dt,$$

$$c_0 = \ln \left( \frac{a}{h} \right) - a_0.$$

This limit exists if the condition (2.66) holds, which has the following form in this case

$$\frac{\delta^{\frac{2}{\kappa}} - 2(2c_0^2 - 3c_0 + 3.5)}{\kappa^2 B_1^{\frac{2}{\kappa}}} < 1.$$

For the numerical calculation, the following values of parameters are used:  $\kappa = 0.4$ ,  $c_0 = -3.352$ . Fig. 2.19 illustrates the pressure distribution for different values of the dimensionless load  $P_1$  and the roughness parameter  $B_1$ . The curves 1 and 2 are drawn for  $B_1 = 1$  and  $P_1^{(1)} = 0.6 \cdot 10^{-2}$  (curve 1) and  $P_1^{(2)} = 0.75 \cdot 10^{-2}$  (curve 2). Penetration for the cases  $P_1^{(1)}$  and  $P_1^{(2)}$  are  $\delta^{(1)} = 0.15$ ,  $\delta^{(2)} = 0.17$ . The results indicate that for the same roughness parameter, the pressure increases especially at the periphery of the contact region, as the load increases. For fixed load  $0.41 \cdot 10^{-2}$ , the penetration and the pressure distribution depend on the roughness parameters  $B_1$  and  $\kappa$ . For the case  $B_1 = 0.75$  ( $\kappa = 0.4$ ), the penetration is  $\delta = 0.1$ ; for  $B_1 = 0.35$  (the smoother surface) the penetration is smaller,  $\delta = 0.06$ . The graphs of pressure distribution for the cases are shown in Fig. 2.19 by the curves 3 and 4, respectively; the pressure distribution for the smooth punch is shown by the broken line. The calculation showed the fast convergence of the iteration method. For an accuracy of  $10^{-5}$ , it is sufficient to take 15–20 iterations.

### 2.5.3 Axisymmetric contact problem

We consider the contact of an axisymmetric punch or elastic indenter with the macroshape described by the function  $z = f(r)$  ( $f(0) = 0$ ), and the elastic half-space ( $z < 0$ ). The contact region  $\Omega$  is a circle of the radius  $a$ . Using the Boussinesq's solution (see Galin, 1976b, Gladwell, 1980, etc.), we write the integral term in Eq. (2.54) which indicates the elastic displacements  $u_z^{(n)}$  of the half-space surface caused by the nominal pressure  $p(r)$  distributed within the circle of the radius  $a$ , in the following form

$$u_z^{(n)} = \frac{1}{\pi E^*} \int_0^a \int_0^{2\pi} \frac{p(r') r' dr' d\theta}{\sqrt{r^2 + r'^2 - 2rr' \cos \theta}} = \frac{1}{\pi E^*} \int_0^a H(r, r') p(r') r' dr',$$

where

$$H(r, r') = \frac{4}{r + r'} K \left( \frac{2\sqrt{rr'}}{r + r'} \right),$$

and  $K(t)$  is the complete elliptic integral of the first kind.

To write the integral equation in dimensionless form, we introduce the notation

$$\rho = \frac{r}{a}, \quad \delta = \frac{D}{a}, \quad f_1(\rho) = \frac{f(\rho a)}{a},$$

$$p_1(\rho) = \frac{p(\rho a)}{\pi E^*}, \quad P_1 = \frac{P}{\pi E^* a^2},$$

$$C_1(p_1(\rho)) = \frac{C(p(\rho a))}{a}.$$

If we consider the contact of a rough punch and an elastic half-space, and the radius  $a$  of the contact region is fixed due to the special punch shape (for example, if the punch has a flat base), the integral equation for the determination of the nominal pressure has the form

$$\int_0^1 H(\rho, \rho') p(\rho') \rho' d\rho' + C_1(p_1(\rho)) = \delta - f_1(\rho). \quad (2.71)$$

If the radius of the contact is not known in advance ( $f_1(\rho)$  is a smooth function), we use the additional conditions  $p_1(1) = 0$  and  $C(0) = 0$ , and obtain the following integral equation

$$\int_0^1 [H(\rho, \rho') - H(1, \rho')] p(\rho') \rho' d\rho' + C_1(p_1(\rho)) = f_1(1) - f_1(\rho). \quad (2.72)$$

Since the elliptic integral  $K(t)$  for  $t \approx 1$  has a logarithmic singularity of the same kind as the principal part of the kernel analyzed in § 2.5.2, Eqs. (2.71) and (2.72) can be analyzed in the same way as in § 2.5.2 for the given function  $C(p)$ . The conclusions of § 2.5.2 concerning the properties of the function  $p_1(\rho)$  at the boundary of the contact region for the function  $C(p)$  of the form (2.53) are valid also for axisymmetric contact problems, i.e. the value  $p(a)$  is always bounded above and  $p(a) = p'(a) = 0$  if  $f'(\rho)$  is continuous at  $\rho = a$ .

We note that for a linear additional displacement function, i.e.  $C = Bp$ , Eq. (2.54) is a Fredholm integral equation of the second kind, which can be solved by standard methods (for example, reduction to the linear algebraic equations). The dependence of the penetration of a punch with flat base upon the load is linear in this case. The results of calculations show that the contact stiffness  $\frac{P}{D}$  decreases as the roughness coefficient  $B$  increases.

## 2.5.4 Characteristics of the discrete contact

The nominal pressure obtained from Eq. (2.54) or its particular forms (Eqs. (2.57) and (2.71)) can be used to determine the characteristics of a discrete contact

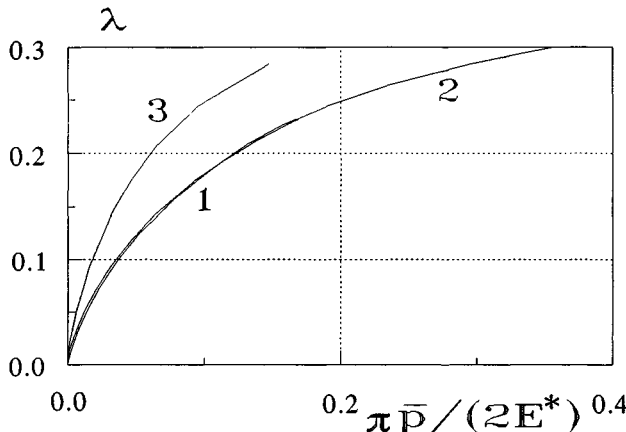


Figure 2.20: The dependence of the relative real area of contact on the nominal pressure for various models of the surface microgeometry.

which are needed for the study of friction and wear in the contact interaction (see Chapters 3, 5), or for calculation of the contact electric and heat conductivity, leak-proofness of seals, etc.

We describe the method of calculation of the discrete contact characteristics on the example of the calculation of the real area of contact  $A_r$ . For the given parameters characterizing the surface microgeometry of the contacting bodies, we can obtain the additional displacement  $C(p)$  and the relative area of contact  $\lambda(p)$  as functions of the nominal contact pressure  $p$  from the solution of the multiple contact problem. For example, for microgeometry modelled by a uniformly distributed system of asperities of different or the same height, these functions can be determined from the periodic contact problem for the system of asperities and the elastic half-space using the methods of §§ 2.2 and 2.4. The functions  $C(p)$  for some given values of the microgeometry parameters are shown in Fig. 2.17. Fig. 2.20 illustrates the variation of the relative real area of contact  $\lambda = \frac{4\pi(a_1^2 + a_2^2 + a_3^2)}{l^2\sqrt{3}}$

with the dimensionless nominal contact pressure  $\bar{p}^1 = \frac{\pi p}{2E^*}$  calculated for the one-level ( $a_1 = a_2 = a_3$ ) and the three-level models of asperity arrangement for the same parameters of surface microgeometry as in Fig. 2.17.

The function  $C(p)$  calculated for the given parameters of the surface microgeometry is then used to determine the nominal contact pressure  $p(x, y)$  and the nominal contact region  $\Omega$  from Eqs. (2.54) and (2.55) if we know the macroshapes of contacting bodies and the load applied to them. Thus, for the given parameters which describe the surface macroshape and microgeometry, the real area of contact

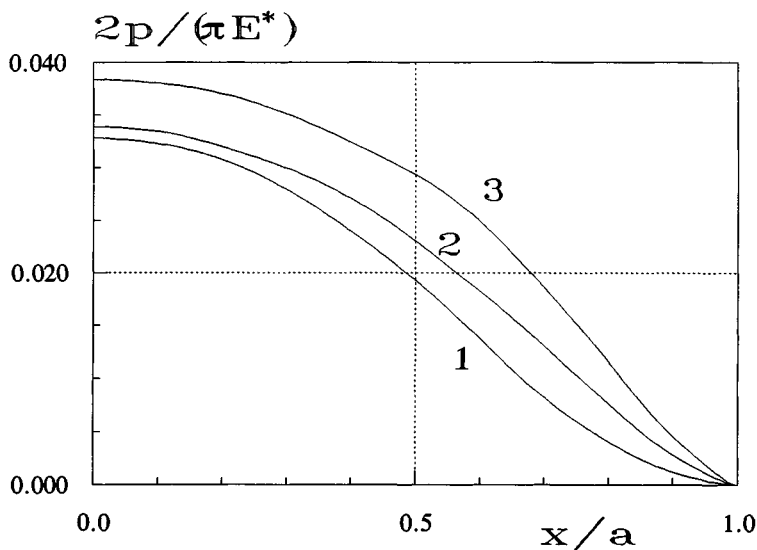


Figure 2.21: Nominal pressure distribution for the contact of a rough cylinder and a thick elastic layer for various microgeometry parameters.

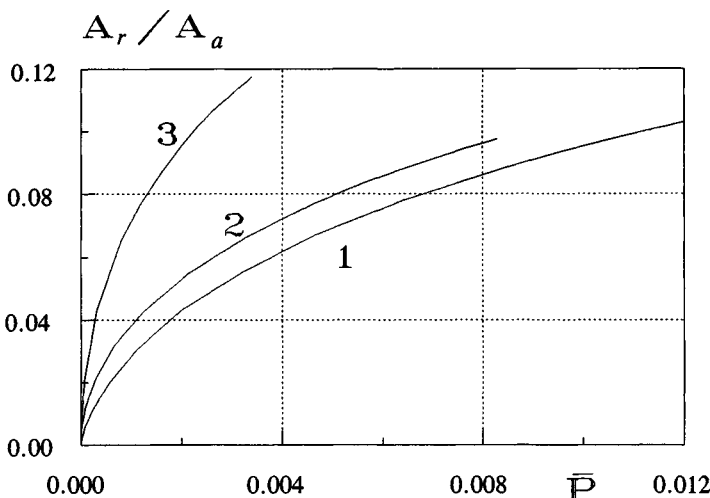


Figure 2.22: The variation of the relative real contact area with the load applied to the cylinder for the various microgeometry parameters.

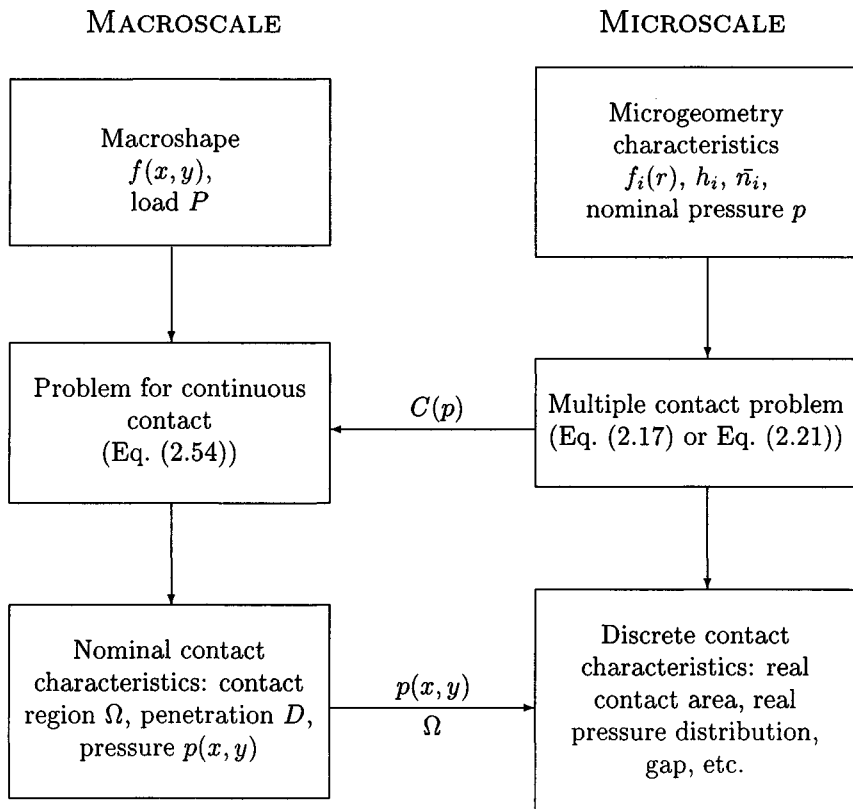


Figure 2.23: Scheme of the analysis of the contact characteristics, taking into account micro- and macro- geometry of the bodies in contact.

is determined from the formula

$$A_r = \iint_{\Omega} \lambda(p(x,y)) dx dy. \quad (2.73)$$

By way of example, let us consider the 2-D contact problem for an elastic cylinder whose macroshape is described by the function  $f(x) = \frac{x^2}{2R_0}$  ( $R_0$  is the radius of the cylinder), and an elastic thick layer bonded with a rigid foundation, for the various parameters characterizing their surface microgeometry. We investigate the microgeometry modelled by the one-level or three-level systems of spherical indenters uniformly distributed over the surface of the contacting body. The functions  $C(p)$  and  $\lambda(p)$  for these kinds of microgeometry with given parameters of the density of asperity arrangement are shown in Fig. 2.17 and in Fig. 2.20, respectively.

Using the function  $C(p)$ , we determine the nominal pressure  $p(x)$  and the contact half-width  $\frac{a}{R_0}$  from Eqs. (2.63) and (2.68) for the given value of the dimensionless load  $\bar{P}$   $\left(\bar{P} = \frac{2(1-\nu^2)P}{\pi ER_0}\right)$  applied to the cylinder. Fig. 2.21 illustrates the nominal pressure distribution within the nominal contact region for  $\bar{P} = 3.2 \cdot 10^{-3}$  and the functions  $C(p)$  presented in Fig. 2.17. The number of curves in Fig. 2.17 and Fig. 2.21 correspond to the particular model of the surface microgeometry. The half-widths of the nominal contacts for the models under consideration are  $\frac{a}{R_0} = 0.09$  (curve 1),  $\frac{a}{R_0} = 0.08$  (curve 2),  $\frac{a}{R_0} = 0.065$  (curve 3).

Then the relative real area of contact  $\frac{A_r}{A_a}$  where  $A_r$  is determined by Eq. (2.73) and  $A_a$  is the width of the nominal contact region ( $A_a = 2a$ ) is

$$\frac{A_r}{A_a} = \int_{-1}^1 \lambda(p(x)) dx.$$

Fig. 2.22 illustrates the variation of the relative area of contact  $\frac{A_r}{A_a}$  with the dimensionless load  $\bar{P}$  for the various parameters describing the surface microgeometry (the curves with the same number in Fig. 2.17, Fig. 2.21 and Fig. 2.22 correspond to the same parameters of the surface microgeometry).

In a similar way it is possible to calculate the gap between the contacting bodies arising from their surface microgeometry, the number of asperities in contact, etc.

The estimation of the real contact pressure and its maximum values in contact of rough bodies is of interest in studies of internal stresses in the thin subsurface layers and the surface fracture (the wear) of bodies in contact interaction (see Chapter 5). If the microgeometry of the contacting bodies has a homogeneous structure along the surface, the maximum value of the real pressure occurs at the contact spots where the nominal pressure reaches its peak. This can be calculated from the multiple contact problem solution for the given maximum value of the nominal pressure.

Fig. 2.23 illustrates the general stages in calculation of the characteristics of the nominal and the real contact described above by the example of the determination of the relative real area of contact.

# Chapter 6

## Wear Contact Problems

### 6.1 Wear equation

One of the principal results of wear is that there are irreversible changes in the shape of the surfaces. These changes are comparable to elastic deformations and thus should be taken into account in the estimation of the contact characteristics of the bodies in sliding contact (distribution of stresses, dimensions of contact area etc.).

In order to solve those problems it is necessary to have information about the wear laws for materials. Such laws in tribology are called wear equations: they establish a relation between some characteristics of wear and a set of parameters characterizing the properties of friction surfaces and operating conditions.

#### 6.1.1 Characteristics of the wear process

Among a great number of characteristics of wear processes analyzed in tribology, we select two of them which are convenient for contacting body wear estimation: *wear rate* and *wear intensity*.

The selection of these characteristics can be defended by several arguments. First, they are based on continuity of the wear process in time and they are described by continuous functions; the space-time discreteness of the wear process does not need to be taken into account at this scale. Secondly, these characteristics are directly related to the changes in the surface shape.

*The wear rate* is defined as the volume of material that is worn from a unit area of surface per unit time.

Generally, different points of the surface have different wear rates, and thus it is reasonable to speak about the wear rate at the given surface point  $(x, y)$ , which can be estimated according to the definition as follows:

$$\frac{dw_*}{dt} = \lim_{\Delta t \rightarrow 0} \lim_{\Delta A \rightarrow 0} \frac{\Delta v_w(x, y)}{\Delta A \Delta t} = \lim_{\Delta t \rightarrow 0} \frac{\Delta w_*(x, y)}{\Delta t}, \quad (6.1)$$

Friction unit, part	Wear resistance class
Cylinder-piston groups of automobiles	11–12
Gauges	10–11
Slideways of machine tools	9–10
Cutting tools	7–8
Brake shoes	6–7
Sliding bearings	5–8

Table 6.1: Wear resistance classes for some parts and joints

where  $\Delta A$  is the surface element in the vicinity of point  $(x, y)$ ,  $\Delta v_w(x, y)$  is the volume of the material worn from the surface element  $\Delta A$  during the time interval  $\Delta t$  (wear time),  $\Delta w_*(x, y)$  is the linear wear at the point  $(x, y)$ , which characterizes the depth of the layer worn during the time interval  $\Delta t$ .

The quantity  $\frac{dw_*}{dt}$  has a dimension of velocity; it gives the rate of change of the surface position due to wear.

If all points of the rubbing surface are wearing under similar conditions, the ratio  $\frac{\Delta v_w}{\Delta A}$  will not depend on the coordinates on the surface, and will be equal to the ratio of the material volume worn from the rubbing surface, to the area of this surface.

In addition to the wear rate, the *wear intensity* factor is used. This is defined as the volume of the material worn from the rubbing surface unit, per sliding distance unit, i.e.,

$$\frac{dw_*}{dl} = \lim_{\Delta l \rightarrow 0} \lim_{\Delta A \rightarrow 0} \frac{\Delta v_w}{\Delta A \Delta l} = \lim_{\Delta l \rightarrow 0} \frac{\Delta w_*}{\Delta l}, \quad (6.2)$$

where  $\Delta l$  is a sliding distance.

The wear intensity is a dimensionless quantity. It can vary from  $10^{-3}$  to  $10^{-13}$  according to material properties and operating conditions. We notice that  $\frac{dw_*}{dl} = 10^{-9}$  means that a layer of  $1 \mu\text{m}$  thickness is worn during sliding for a distance 1 km. Based on the wear intensity characteristics, the system of wear resistance classes has been created in Russia to evaluate the wear resistance of friction components. Wear resistance is defined as  $I = \left(\frac{dw_*}{dl}\right)^{-1}$ . The lowest class of wear resistance is the third one ( $I = 10^3 \div 10^4$ ), the highest class is the twelfth one ( $I = 10^{12} \div 10^{13}$ ). The typical classes of wear resistance for some parts and friction units are presented in Table 6.1.

The following relation exists between  $\frac{dw_*}{dt}$  and  $\frac{dw_*}{dl}$ , if  $V = \text{const.}$

$$\frac{dw_*}{dt} = V \frac{dw_*}{dl}. \quad (6.3)$$

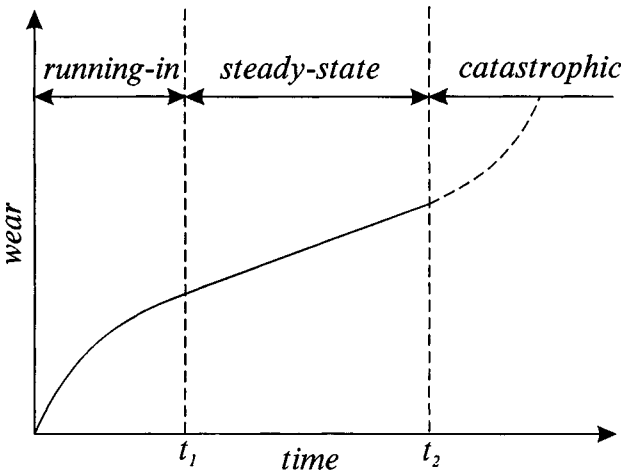


Figure 6.1: A typical dependence of wear on testing time.

Thus the wear characteristics of each friction component can be estimated from Eqs. (6.1) and (6.2). Are they characteristics of the material, or something else? We can answer this question by using a systematic approach to the investigation of tribological joints developed by Molgaard and Czichos (1977) and Czichos (1980). Generally the linear wear  $w_*$  is a function of structural parameters  $\{S\}$  and input parameters  $\{X\}$ , i.e.

$$w_* = F(S, X), \quad (6.4)$$

where  $\{S\}$  includes the following: structure elements (bodies in contact, interfacial and environment medium), properties of structure elements (aggregate state, geometric characteristics, volume, surface and bulk properties) and interaction of the elements;  $\{X\}$  includes load, velocity, time, temperature, etc. Consequently, the wear characteristics of the material depend on individual properties of the material as well as on the properties of the system as a whole.

### 6.1.2 Experimental and theoretical study of the wear characteristics

A relation of the type (6.4) is the wear equation in its integral form. In the profound investigation by Meng and Ludema (1995) devoted to the history of the wear problems, it is noted that there are roughly 200 relations which can be classified as wear equations. It is well known that the wear characteristics depend on more than one hundred parameters.

There are two different methods for establishing these relations: empirical and mathematical simulation.

*Empirical wear equations* are established by extension of testing results. We will list some peculiarities of tribological tests on wear study.

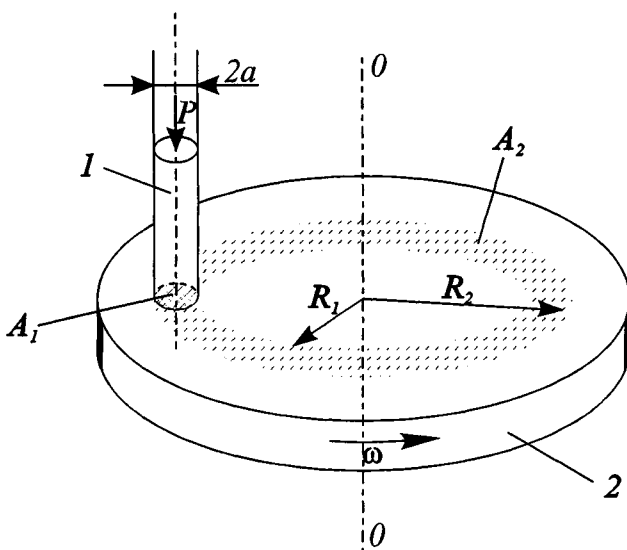


Figure 6.2: Scheme of pin-on-disk wear testing apparatus.  $A_2$  is an annular wear scar.

Fig. 6.1 illustrates a typical dependence of linear wear on testing time.

The first period of the wear process  $0 < t < t_1$  is called *running-in*. This is a very important stage of the wear process. During the running-in period, as a rule, the equilibrium (stable) surface roughness is provided, the chemical content of the surface (oxidation, diffusion) is established, and the temperature field of the friction pair is stabilized, i.e. the self-organizing processes of the system hold (Bershadsky, 1981, Polzer, Ebeling and Firkovsky, 1988 and Bushe, 1994). During the running-in period the wear intensity changes with time; this stage can last a long time.

The running-in period gives way to the *steady-state stage* of wear. For this time period ( $t_1 < t < t_2$ ) the wear is directly proportional to the test time or the sliding distance, i.e. the wear rate (intensity) does not change. It is at this stage of wear that the wear characteristics which appear in the wear equation are registered.

In some cases, especially for inhomogeneous materials and for modified surfaces, there is a stage of *catastrophic wear* ( $t > t_2$ ), when the wear rate increases radically.

When estimating wear rate, we must take into account that the rubbing surfaces of two interacting bodies may have different wear conditions. Let us consider the pin-on-disk friction testing apparatus (a common device for tribological tests) to illustrate this conclusion (see Fig. 6.2). When the pin (1) slides on the disk (2), the pin rubbing area is  $A_1$ , which coincides with the nominal area of contact  $A_1 = \pi a^2$ ; for the disk, the rubbing surface is a ring with area  $A_2 = \pi (R_2^2 - R_1^2)$ . The time of the wear for the pin  $\Delta t_1$  and for the disk  $\Delta t_2$  will be also different.

During the test time interval  $\Delta t$ , any point of the pin surface is in friction

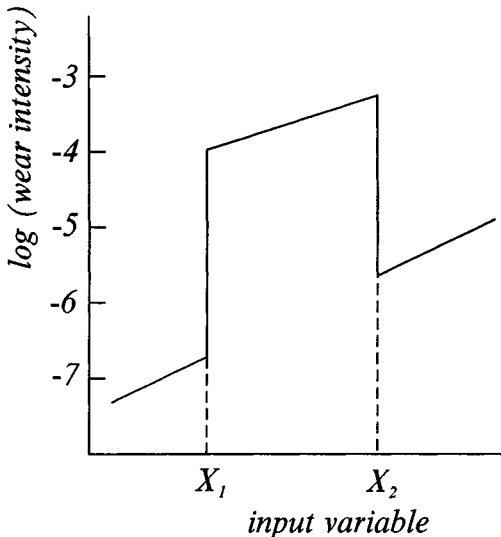


Figure 6.3: A typical dependence of wear intensity on an input parameter (for example, load, velocity, temperature, etc.);  $X_1$  and  $X_2$  are critical values of the parameter.

interaction for the whole of this time, i.e. for the pin the wear time  $\Delta t_1$  is equal to  $\Delta t$ . For the disk, during the time interval  $\Delta t$  any point is in friction interaction with the pin during the time interval  $\Delta t_2 = \frac{2a\Delta t}{\pi(R_1 + R_2)}$ . Thus the wear rates of materials 1 and 2 in the testing apparatus (Fig. 6.2) can be estimated by the formulae:

$$\left( \frac{dw_*}{dt} \right)_1 = \frac{\Delta(v_w)_1}{\pi a^2 \Delta t_1}, \quad \left( \frac{dw_*}{dt} \right)_2 = \frac{\Delta(v_w)_2}{4a^2 \Delta t_1}, \quad (6.5)$$

where  $\Delta(v_w)_1$  and  $\Delta(v_w)_2$  are experimentally measured volumes of worn material of the pin and the disk, respectively.

When studying the dependence of wear on the input parameters of tribological system (loads, velocities, temperature, etc.), we can observe the phenomenon of abrupt variation of wear rate under smooth variation of input parameters. Fig. 6.3 illustrates this phenomenon. Points  $X_1$  and  $X_2$  are called critical or transition points of the tribosystem. At these values there is a change of wear mechanism, and the wear rate changes.

Based on the test results, we describe the relationship between wear characteristics and input variables. The wear equations may be also constructed by a *mathematical simulation* of the processes which occur at rubbing surfaces (see Chapter 5).

The simplest approach developed by Holm (1946) and Archard (1953) was based on the idea that the wear rate is proportional to the real area of contact of rough bodies. The coefficient of proportionality was estimated in wear tests.

Author	Wear equation	Material; friction part; conditions	Cause of wear
Lewis (1968)	$\frac{dv_w}{dt} = KPV$	filled PTFE; piston rings; unlubricated contact	adhesion
Khrushchov and Babichev (1970)	$\frac{dv_w}{dt} = K \frac{PV}{H}$	metals; unlubricated contact	micro-cutting
Rhee (1970)	$v_w = KP^\alpha V^\beta t^\gamma$	polymer-bonded friction mate- rials (asbestos- reinforced poly- mers); breaks	adhesion with thermal process
Lancaster (1973)	$\frac{dv_w}{dt} = K k_1 k_2 k_3 k_4 PV,$ $k_1, k_2, k_3, k_4$ are wear-rate correction factors dependent on the operating conditions	filled thermoplastics; filled PTFE; dry rubbing bearings	
Larsen-Basse (1973)	$v'_w = K \frac{PV}{f},$ $f$ is a frequency of impact, $v'_w$ is a worn volume for one impact	carbide materials; drill bits	thermal fatigue, polishing of car- bide grains (low drilling rates), transgranular fracturing (high drilling rates)
Moor, Walker and Appl (1978)	$\frac{dv_w}{dt} = KV^\beta P(v_c),$ $v_c$ is a volume of rock removed per unit sliding distance, $\beta = 1.8$	diamond inserts; rotary drag bits	burning by superficial graftization, breakage by impact, matrix erosion

$K$  is specific coefficient for each wear equation,  $H$  is a hardness,  $P$  is a normal load.

Table 6.2: Empirical wear equations

Author	Wear equation	Mechanism of wear
Holm (1946)	$\frac{dw_*}{dt} = K \frac{pV}{H}$	adhesive
Archard (1953)	$\frac{dw_*}{dt} = K \frac{pV}{H}$	adhesive
Kragelsky (1965)	$\frac{dw_*}{dt} = K p^\alpha V \ (\alpha > 1)$	fatigue
Rabinowicz (1965)	$\frac{dw_*}{dt} = K \frac{pV}{H}$	abrasive
Rabinowicz (1971)	$\frac{dw_*}{dt} = K \frac{pV}{H}$	fretting
Harricks (1976)	$\frac{dw_*}{dt} = K pV$	fretting

$K$  is specific coefficient for each wear equation,  $H$  is a hardness.

Table 6.3: Theoretical models

A rich variety of wear equations based on fracture mechanics has been suggested in the last 20 years. These equations include the quantities relating to fatigue strength (Kragelsky, 1965), critical magnitude of energy absorbed by material (Fleischer, 1973), shear failure determined by a slip line analysis (Challen and Oxley, 1979), brittle fracture characteristics (Evans and Marshall, 1981). These theories considerably extend the number of parameters that have an influence on the wear, including the parameters which characterize the properties of materials.

As will be shown in § 6.2, for investigation of the kinetics of contact characteristics of junctions in wear process, we need to know the dependence of a wear rate on the contact pressure  $p$  and the relative sliding velocity  $V$ . Analysis of a number of wear equations obtained theoretically and experimentally shows that in many cases this dependence can be presented in the form

$$\frac{dw_*}{dt} = K_w p^\alpha V^\beta, \quad (6.6)$$

where  $K_w$  is the wear coefficient, and  $\alpha$  and  $\beta$  are parameters which depend on material properties, friction conditions, temperature, etc.

We present some wear equations obtained in wear tests with different materials (Table 6.2) and in theoretical models (Table 6.3). Based on these results, we can evaluate the parameters  $\alpha$  and  $\beta$  and the wear coefficient  $K_w$  in Eq. (6.6) for different mechanisms of wear.

## 6.2 Formulation of wear contact problems

The irreversible shape changes of bodies in contact arising from the wear of their surfaces, are taken into consideration for mathematical formulation of wear contact problems. The value of the linear wear  $w_*$  (change of the linear dimension of the body in the direction perpendicular to the rubbing surface) is often used to describe the wear quantitatively. Generally, the surfaces are worn nonuniformly, hence the linear wear  $w_*(x, y)$  should be considered at each point  $(x, y)$  of the rubbing surface.

### 6.2.1 The relation between elastic displacement and contact pressure

We assume that the irreversible surface displacement  $w_*(x, y)$  is small, and comparable to the elastic displacement  $w(x, y)$ . Hence for the determination of the stress state of the contacting bodies, the boundary conditions are posed on undeformed surfaces, neglecting both the elastic displacement  $w(x, y)$  and the surface wear  $w_*(x, y)$ .

Under this assumption the pressure  $p(x, y, t)$  within the contact region and the elastic displacement  $w(x, y, t)$  for an arbitrary instant of time  $t$  are related by operator  $A$  which is analogous to the operator relating the pressure and elastic displacement in the corresponding contact problem when the wear does not occur, i.e.

$$w(x, y, t) = A [p(x, y, t)]. \quad (6.7)$$

For example, Eq.(6.7) has the following form for frictionless contact of a cylindrical punch and an elastic half-space

$$w(x, t) = \frac{2(1-\nu^2)}{\pi E} \int_{-a(t)}^{a(t)} \ln|x - x'| p(x', t) dx' + \text{const}, \quad (6.8)$$

$$-a(t) < x < a(t).$$

If the size of the contact zone does not change during the wear process, the operator  $A$  is time-independent; this occurs, for example, in the contact problem for the punch with a flat face and an elastic foundation. Otherwise the unknown contact area should be obtained at each instant of time from the condition

$$p(x, y, t) \Big|_{x, y \in \Gamma} = 0,$$

which holds on the boundary  $\Gamma$  of the contact region  $\Omega(t)$ . This condition is needed to ensure the continuity of the surface displacement gradient at the boundary of the contact zone, for a punch whose shape is described by a smooth function.

It must be noted that the requirement of a small value of  $w_*(x, y, t)$  follows from the functional restrictions for components operating, for example, at precision

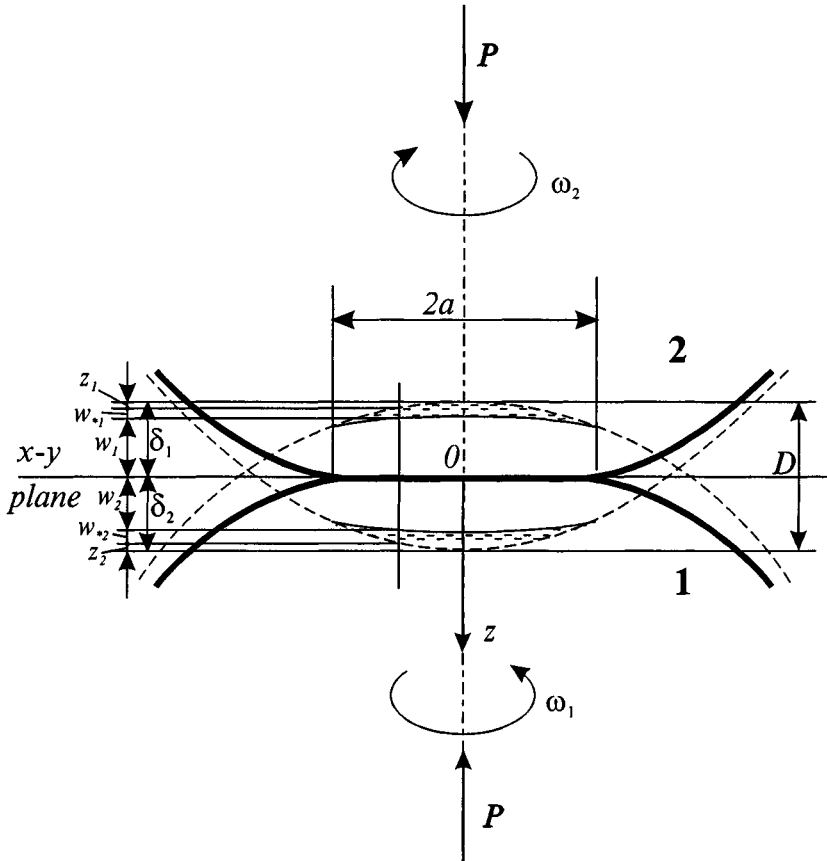


Figure 6.4: Elastic and wear displacements in the contact of two bodies.

junctions. For some wear contact problems, the value of the linear wear  $w_*(x, y, t)$  is comparable to the size of the body in contact; now the relation (6.7) between the elastic displacement and pressure becomes more complex and time-dependent. In particular, it can depend on the geometry of the worn body. We describe such a problem in § 6.7 where we investigate a contact of a punch and an elastic half-space coated by a thin elastic layer.

### 6.2.2 Contact condition

We consider a contact of two elastic bodies (Fig. 6.4). We take the rectangular coordinate axis  $Oxyz$  connected with the body 1. The origin  $O$  is the point where the surfaces touch at  $t = 0$  if they are brought into contact by a negligibly small force. The  $Oz$  axis is chosen to coincide with the common normal to the two surfaces at  $O$ . The undeformed shapes of two surfaces are specified by the

functions

$$z_1 = f_1(x, y), \quad z_2 = -f_2(x, y).$$

During the compression, the surface of each body is displaced parallel to  $Oz$  by an elastic displacement  $w_i(x, y, t)$ , ( $i = 1, 2$ ) (measured positive into each body) due to the contact pressure. So the following relation takes place within the contact zone at the initial instant of time  $t = 0$ :

$$w_1(x, y, 0) + w_2(x, y, 0) = D(0) - [f_1(x, y) + f_2(x, y)], \quad (6.9)$$

where  $D(t)$  is the approach of the bodies.

Let us consider any allowable changes in the relative position of the contacting bodies in friction process. We assume for the time being that there is no change of the body shapes due to their wear. If the contact condition (6.9) for any point of body 1 is valid after any relative displacement of body 2, we can use this equation to describe the contact condition at an arbitrary instant of time. Taking into account the shape changes of the bodies during wear process, we obtain

$$\begin{aligned} w_1(x, y, t) + w_{*1}(x, y, t) + w_2(x, y, t) + w_{*2}(x, y, t) \\ = D(t) - [f_1(x, y) + f_2(x, y)]. \end{aligned} \quad (6.10)$$

Wear contact problems with the contact condition in the form (6.10) are denoted as class  $\mathcal{A}$  problems. Many practical problems fall into this category: the wear of axisymmetric bodies rotating about their common axis of symmetry; the wear in contact of a long cylinder, sliding back and forth along its generatrix on an elastic half-space. The last problem can be considered in a two-dimensional (plane) formulation.

We will classify the problem as type  $\mathcal{B}$  if the form of the contact condition (6.9) changes because of relative displacement of the body 2 allowed by the considered friction process. For the problems of the type  $\mathcal{B}$ , the contact condition at an arbitrary instant of time depends on relative displacement of body 2. For example, if the punch with the shape function  $z = f_2(x, y)$  moves in the direction of the  $y$ -axis with the constant velocity  $V$  over the elastic half-space (the body 1, which is worn due to friction), the contact condition for the fixed point  $(x, y)$  of the elastic half-space has the form

$$\begin{aligned} w_1(x, y, t) + w_{*1}(x, y, t) = D(t) - f(x, y - Vt), \quad a(x, t) < y < b(x, t), \\ t_* = \frac{b(x, t) - a(x, t)}{V}. \end{aligned} \quad (6.11)$$

Here  $a(x, t)$  and  $b(x, t)$  indicate the ends of the contact region,  $t_*$  is the contact time of the given point  $(x, y)$  in a single pass. We will consider wear contact problems of type  $\mathcal{B}$  for different kinds of junctions in § 6.6 and § 8.2.

It is worth noting that the wear contact problem for one junction can be referred to class  $\mathcal{A}$  or  $\mathcal{B}$ , depending on which component and its wear is under investigation. For example, for the junctions presented in Fig. 6.2, the contact problem is one of

type  $\mathcal{B}$  if we study the wear of the disk, while it is the problem of the type  $\mathcal{A}$  if we analyze the wear of the pin and neglect the shape change of the disk surface in the wear process.

To complete the mathematical model of the wear contact problem, we must know the dependence of the linear wear  $w_*(x, y, t)$  on the contact pressure  $p(x, y, t)$  and on the sliding velocity  $V(x, y, t)$ . The dependence generally can be described by an operator involving these functions. Since the linear wear at the given point  $(x, y)$  at instant  $t$  is the total displacement, which is the accumulation of the elementary displacements which have taken place for instants  $t' \leq t$ , this operator is of hereditary type, and can be written as an integral operator

$$w_*(x, y, t) = \int_0^t K(t, t') f[p(x, y, t'), V(x, y, t')] dt'. \quad (6.12)$$

In wear contact problem formulation, we often use the simplest forms of Eq. (6.12). It was pointed out in § 6.1 that, for different mechanisms of wear, the dependence of a wear rate on the contact pressure and the sliding velocity (the wear equation) has the following form

$$\frac{\partial w_*}{\partial t} = K_w p^\alpha(x, y, t) V^\beta(x, y, t), \quad (6.13)$$

It follows from Eq. (6.13) that the linear wear is determined by the formula

$$w_*(x, y, t) = K_w \int_0^t p^\alpha(x, y, t') V^\beta(x, y, t') dt'. \quad (6.14)$$

Eqs. (6.7), (6.10) (or Eq. (6.11)), (6.13) provide the complete system of equations for determining the contact pressure  $p(x, y, t)$ , the shape of the worn surface  $w_*(x, y, t)$ , and the elastic displacement  $w(x, y, t)$ . It must be noted that if the approach function  $D(t)$  is not given, but we know the total normal load  $P(t)$  applied to the contacting bodies, we can use the equilibrium equation to complete the system of equations

$$\iint_{\Omega} p(x, y, t) dx dy = P(t). \quad (6.15)$$

## 6.3 Wear contact problems of type A

### 6.3.1 Steady-state wear for the problems of type A

Let us examine the system of equations (6.7), (6.10) and (6.13) to investigate changes in contact characteristics for problems of type  $\mathcal{A}$ . At first we consider the case

$$V(x, y, t) = V_\infty(x, y), \quad \Omega(t) = \Omega_\infty, \quad \frac{dD(t)}{dt} = D_\infty, \quad (6.16)$$

i.e. these functions are time-independent in the wear process. Then the system of equations can be rewritten in the form

$$w(x, y, t) = A[p(x, y, t)], \quad (6.17)$$

$$\frac{\partial w_*}{\partial t} = K_w p^\alpha(x, y, t) V_\infty^\beta(x, y), \quad (6.18)$$

$$w(x, y, t) + w_*(x, y, t) = D(0) + D_\infty t - f(x, y), \quad (6.19)$$

where

$$w(x, y, t) = w_1(x, y, t) + w_2(x, y, t),$$

$$f(x, y) = f_1(x, y) + f_2(x, y),$$

$$w_*(x, y, t) = w_{*1}(x, y, t) + w_{*2}(x, y, t).$$

The system of equations (6.17), (6.18), (6.19) has a steady-state solution which determines the contact pressure  $p_\infty(x, y) = \lim_{t \rightarrow +\infty} p(x, y, t)$  in the steady-state wear process

$$p_\infty(x, y) = \left[ \frac{D_\infty}{K_w V_\infty^\beta(x, y)} \right]^{1/\alpha}. \quad (6.20)$$

From Eq. (6.19) we obtain the following condition for the steady-state wear process

$$\frac{\partial w_*(x, y, t)}{\partial t} = \frac{dD(t)}{dt} = D_\infty,$$

i.e. the steady-state wear is characterized by a uniform wear rate within the contact region. The equation of the shape of the worn surface  $f_\infty(x, y)$  of the body 1 follows from Eqs. (6.17), (6.19) and (6.20)

$$f_\infty(x, y) = \lim_{t \rightarrow +\infty} [f_1(x, y) + w_*(x, y, t) - f_1(x^0, y^0) - w_*(x^0, y^0, t)] = \\ -f_2(x, y) + f_2(x^0, y^0) - A[p_\infty](x, y) + A[p_\infty](x^0, y^0), \quad (6.21)$$

where  $(x^0, y^0) \in \Omega_\infty$ ,  $A[p_\infty](x, y)$  is the value of an operator  $A$ , calculated at the point  $(x, y)$ , for the function  $p_\infty$  determined by Eq. (6.20).

Substituting Eq. (6.20) into the equilibrium equation (6.15) we obtain the formula for determining the steady-state normal load  $P_\infty$

$$P_\infty = \left( \frac{D_\infty}{K_w} \right)^{1/\alpha} \iint_{\Omega_\infty} \frac{dx dy}{V_\infty^{\beta/\alpha}(x, y)}. \quad (6.22)$$

### 6.3.2 Asymptotic stability of the steady-state solution

Let us represent the general solution of Eqs. (6.17), (6.18) and (6.19) in the form

$$p(x, y, t) = p_\infty(x, y) + \varphi(x, y, t), \quad (6.23)$$

where  $p_\infty(x, y)$  is the steady-state solution determined by Eq. (6.20). It is an asymptotically stable steady-state solution if the function  $\varphi(x, y, t)$  satisfies the condition

$$\lim_{t \rightarrow +\infty} \varphi(x, y, t) = 0. \quad (6.24)$$

In the linear problem formulation ( $\alpha = 1$ ) we can note the sufficient conditions for the representation of the solution in the forms of Eqs. (6.23) and (6.24). Under the assumption that the linear operator  $A$  is time-independent, i.e. validity of the relation

$$\frac{\partial}{\partial t} A[p] = A \left[ \frac{\partial p}{\partial t} \right], \quad (6.25)$$

it follows from relations (6.17), (6.18), (6.19), (6.20) and (6.23) that the function  $\varphi(x, y, t)$  satisfies the equation

$$A \left[ \frac{\partial \varphi(x, y, t)}{\partial t} \right] = -K_w \varphi(x, y, t) V_\infty^\beta(x, y). \quad (6.26)$$

We shall seek the solution of this equation in the form

$$\varphi(x, y, t) = \psi(x, y) T(t). \quad (6.27)$$

Then we obtain

$$\dot{T}(t) A[\psi(x, y)] = -K_w V_\infty^\beta(x, y) \psi(x, y) T(t)$$

or

$$\dot{T}(t) + \lambda T(t) = 0, \quad (6.28)$$

$$q(x, y) - \lambda A_1[q(x, y)] = 0, \quad (6.29)$$

where

$$q(x, y) = K_w V_\infty^\beta(x, y) \psi(x, y),$$

$$A_1[q(x, y)] = A \left[ \frac{q(x, y)}{K_w V_\infty^\beta(x, y)} \right]. \quad (6.30)$$

We denote the system of eigenvalues of Eq. (6.29) by  $\Lambda \equiv \{\lambda_n\}_{n=1}^\infty$ . It follows from Eq. (6.28) that

$$T(t) = T(0) \exp(-\lambda_n t). \quad (6.31)$$

To find the function  $\psi(x, y, t)$  we should study the spectrum  $\Lambda$  of the operator  $A_1$ . The particular solutions  $\varphi(x, y, t)$  of Eq. (6.26) satisfy the condition (6.24) if all  $\lambda_n > 0$ . This occurs if the operator  $A_1$  is self-adjoint and positive semi-definite (Tricomi, 1957).

In § 6.4 and § 6.5 we will investigate some wear contact problems, in which the operator  $A_1$  satisfies the sufficient conditions listed here for existence of asymptotically stable steady-state wear.

A necessary condition for the asymptotic stability of the steady-state solution in a non-linear wear contact problem ( $\alpha \neq 1$  in Eq. (6.18)) is discussed in § 8.4.

### 6.3.3 General form of the solution

We assume that  $A_1$  is a totally continuous, self-adjoint, positive semi-definite linear operator. As a consequence, the system of its eigenfunctions  $U_n(x, y)$  is complete and orthonormalized in the space of continuous functions. The eigenvalues  $\lambda_n$  of this operator are positive.

According to Eqs. (6.23), (6.27) and (6.31), we can write the contact pressure at an arbitrary instant of time in the form

$$p(x, y, t) = p_\infty(x, y) + \frac{1}{K_w V_\infty^\beta(x, y)} \sum_{n=1}^{\infty} A_n U_n(x, y) \exp(-\lambda_n t). \quad (6.32)$$

The coefficients  $A_n$  are found by the expansion of the contact pressure at the initial instant of time  $t = 0$  in the series of eigenfunctions  $U_n(x, y)$

$$p(x, y, 0) = p_\infty(x, y) + \frac{1}{K_w V_\infty^\beta(x, y)} \sum_{n=1}^{\infty} A_n U_n(x, y). \quad (6.33)$$

The shape of the worn surface at an arbitrary instant of time is determined by the equation obtained from Eq. (6.18) for  $\alpha = 1$  and Eq. (6.32)

$$w_*(x, y, t) = D_\infty t + \sum_{n=1}^{\infty} \frac{A_n}{\lambda_n} U_n(x, y) (1 - \exp(-\lambda_n t)). \quad (6.34)$$

If the functions  $V(x, y, t)$ ,  $\Omega(t)$ ,  $D(t)$  are time-dependent and satisfy the conditions  $\lim_{t \rightarrow +\infty} V(x, y, t) = V_\infty(x, y)$ ,  $\lim_{t \rightarrow +\infty} \Omega(t) = \Omega_\infty$  and  $\lim_{t \rightarrow +\infty} \frac{dD(t)}{dt} = D_\infty$  (or  $\lim_{t \rightarrow +\infty} P(t) = P_\infty$ ), then the solution of the system of Eqs. (6.7), (6.10) and (6.13) approaches to that determined by Eqs.(6.32) and (6.34) as  $t \rightarrow +\infty$ . So the necessary conditions for the existence of a steady-state regime of wear process for the contact problems of the type  $\mathcal{A}$  is the stabilization of the external characteristics (approach of the contacting bodies  $D(t)$ , normal load  $P(t)$  etc.) in time. If  $P_\infty = 0$  or  $D_\infty = 0$ , then the contact pressure  $p_\infty(x, y) = 0$ .

## 6.4 Contact of a circular beam and a cylinder

Let us examine the problem of type  $\mathcal{A}$ , in which  $A$  (see Eq. (6.7)) is a time-independent differential operator, and use the method described in § 6.3 for determining the changes of contact characteristics in wear process.

### 6.4.1 Problem formulation

We will investigate a contact of an initially bent circular beam 1 and the inside surface of a rigid cylinder 2 (Fig. 6.5). The beam takes the form of an open circular ring; the size of the gap at the cut is negligibly small. In the course of displacement

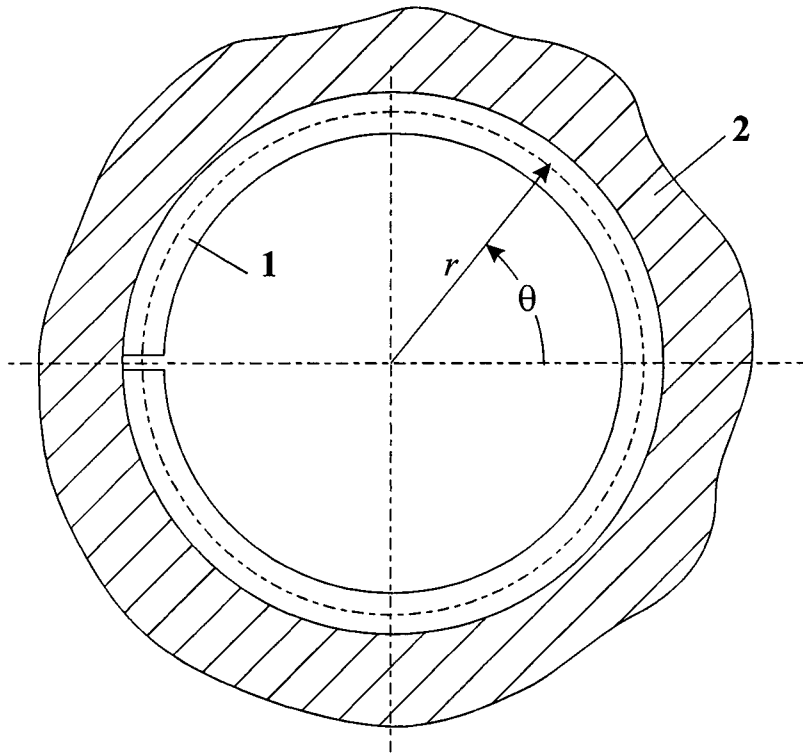


Figure 6.5: Scheme of contact of an open ring inserted into a cylinder liner.

of the ring along the cylinder generatrix, wear occurs both at the surface of the cylinder and at the surface of the ring.

We assume that the rate of wear  $\frac{\partial w_*(\theta, t)}{\partial t}$  of the ring and the cylinder surfaces at any point is proportional to the pressure  $p(\theta, t)$  between the ring and the cylinder

$$\frac{\partial w_*(\theta, t)}{\partial t} = K_w p(\theta, t).$$

Here  $\theta$  is the polar angle (see Fig. 6.5); the wear coefficient  $K_w$  can depend on sliding velocity, temperature, etc.

As the result of wear, the thickness of the ring will decrease. In determining the radial elastic deflection  $u_r(\theta, t)$  of the ring we neglect these variations and assume that the moment of inertia  $J$  of the ring remains roughly constant while it is in operation.

Under this assumption, the radial deflection  $u_r(\theta, t)$  can be obtained from the following equation which is valid for bending of circular beams of small curvature

(Timoshenko, 1943):

$$\frac{1}{r^2} \cdot \frac{\partial^2 u_r(\theta, t)}{\partial \theta^2} + \frac{u_r(\theta, t)}{r^2} = -\frac{M(\theta, t)}{EJ}. \quad (6.35)$$

Here  $M(\theta, t)$  is the bending moment in the beam, which is taken to be positive if it sets up compressive stresses in the exterior fibers of the beam;  $r$  is the radius of curvature of the ring,  $E$  is the Young's modulus.

We assume that the ends of the beam at the gap site ( $\theta = \pm\pi$ ) are free of forces, i.e., at these points the bending moment and tensile forces are equal to zero. Then the bending moment at an arbitrary cross section of the ring is set up by the pressure  $p(\theta, t)$  between the cylinder and the ring, i.e.

$$M(\theta, t) = -r^2 \int_{-\pi}^{\theta} p(\theta', t) \sin(\theta - \theta') d\theta', \quad -\pi \leq \theta \leq \pi. \quad (6.36)$$

Thus, the pressure  $p(\theta, t)$ , the radial deflection  $u_r(\theta, t)$  and the total wear of the ring and the cylinder  $w_*(\theta, t)$  are determined from the following system of equations

$$\frac{\partial^2 u_r(\theta, t)}{\partial \theta^2} + u_r(\theta, t) = \frac{r^4}{EJ} \int_{-\pi}^{\theta} p(\theta', t) \sin(\theta - \theta') d\theta', \quad (6.37)$$

$$\frac{\partial w_*(\theta, t)}{\partial t} = K_w p(\theta, t), \quad u_r(\theta, t) = u_r(\theta, 0) - w_*(\theta, t). \quad (6.38)$$

The last equation is the condition for the contact of the ring and the cylinder.

Let us introduce the following dimensionless variable and functions

$$t_1 = \frac{K_w E J t}{r^4}, \quad p_1(\theta, t_1) = \frac{p(\theta, t) r^3}{E J},$$

$$u_{r1}(\theta, t_1) = \frac{u_r(\theta, t)}{r}, \quad w_{*1}(\theta, t) = \frac{w_*(\theta, t)}{r}.$$

Then the system of equations (6.37) and (6.38) can be rewritten as

$$\frac{\partial^2 u_{r1}(\theta, t_1)}{\partial \theta^2} + u_{r1}(\theta, t_1) = \int_{-\pi}^{\theta} p_1(\theta', t_1) \sin(\theta - \theta') d\theta', \quad (6.39)$$

$$\frac{\partial u_{r1}(\theta, t_1)}{\partial t_1} = -p_1(\theta, t_1). \quad (6.40)$$

## 6.4.2 Solution

We apply the differential operator  $\frac{\partial^2(\cdot)}{\partial \theta^2} + (\cdot)$  to Eq. (6.39), and obtain

$$\frac{\partial^4 u_{r1}(\theta, t_1)}{\partial \theta^4} + 2 \frac{\partial^2 u_{r1}(\theta, t_1)}{\partial \theta^2} + u_{r1}(\theta, t_1) = p_1(\theta, t_1). \quad (6.41)$$

The equation for determining the ring deflection  $u_{r1}(\theta, t_1)$  follows from Eqs. (6.40) and (6.41), namely

$$\frac{\partial^4 u_{r1}(\theta, t_1)}{\partial \theta^4} + 2 \frac{\partial^2 u_{r1}(\theta, t_1)}{\partial \theta^2} + \frac{\partial u_{r1}(\theta, t_1)}{\partial t_1} + u_{r1}(\theta, t_1) = 0. \quad (6.42)$$

We will solve Eq. (6.42) by the method of a separation of variables. The unknown function  $u_{r1}(\theta, t_1)$  can be written in the form

$$u_{r1}(\theta, t_1) = U(\theta)T(t_1), \quad T(0) = 1. \quad (6.43)$$

The functions  $T(t_1)$  and  $U(\theta)$  are determined from the equations

$$\frac{dT}{dt_1} + \lambda^2 T = 0, \quad (6.44)$$

$$\frac{d^4 U}{d\theta^4} + 2 \frac{d^2 U}{d\theta^2} + U(1 - \lambda^2) = 0, \quad (6.45)$$

where  $\lambda$  is the unknown parameter. The solutions of Eqs. (6.44) and (6.45) are

$$\begin{aligned} T(t_1) &= \exp(-\lambda^2 t_1), \\ U(\theta) &= A \sinh \Lambda_1 \theta + B \cosh \Lambda_1 \theta + C \sin \Lambda_2 \theta + D \cos \Lambda_2 \theta, \\ \Lambda_1 &= \sqrt{\lambda - 1}, \quad \Lambda_2 = \sqrt{\lambda + 1}, \quad \lambda > 1. \end{aligned} \quad (6.46)$$

The function  $u_r(\theta, t)$  satisfies the condition  $u_r(-\theta, t) = u_r(\theta, t)$ , so that

$$A = C = 0. \quad (6.47)$$

The coefficients  $B$  and  $D$  can be found by satisfying the equilibrium equations for the ring. The equilibrium equation for the forces applied to the ring is

$$\int_{-\pi}^{\pi} p_1(\theta, t_1) \cos \theta d\theta = 0. \quad (6.48)$$

Using Eqs. (6.40), (6.43), (6.46), (6.47) and (6.48), we obtain

$$B \int_{-\pi}^{\pi} \cosh \Lambda_1 \theta \cos \theta d\theta + D \int_{-\pi}^{\pi} \cos \Lambda_2 \theta \cos \theta d\theta = 0.$$

Upon integrating, we can rewrite this equation as

$$B \Lambda_1 \sinh \Lambda_1 \pi + D \Lambda_2 \sin \Lambda_2 \pi = 0. \quad (6.49)$$

The second equation for determining the coefficients  $B$  and  $D$  can be obtained from the following condition

$$M(-\pi, t) = M(\pi, t) = 0. \quad (6.50)$$

We consider the equation (6.50) at the instant  $t = 0$  and take into account Eq. (6.35), and obtain

$$\frac{d^2U}{d\theta^2} \Big|_{\theta=\pi} + U(\pi) = 0,$$

or, substituting Eq. (6.46) and taking into account Eqs. (6.47), we have

$$B \cosh \Lambda_1 \pi - D \cos \Lambda_2 \pi = 0. \quad (6.51)$$

The system of equations (6.49) and (6.51) is used to find the coefficients  $B$  and  $D$ . The system has a solution different from zero, if eigenvalues  $\lambda_n$  satisfy the characteristic equation

$$\Lambda_2 \sin \Lambda_2 \pi \cosh \Lambda_1 \pi + \Lambda_1 \cos \Lambda_2 \pi \sinh \Lambda_1 \pi = 0. \quad (6.52)$$

Substituting the coefficients  $B$  and  $D$  determined by Eqs. (6.49) and (6.51) for  $\lambda_n > 1$  in Eq. (6.46), we obtain the particular solutions in the form

$$U_n(\theta) = \frac{\cos \Lambda_{2n} \pi}{\cosh \Lambda_{1n} \pi} \cosh \Lambda_{1n} \theta + \cos \Lambda_{2n} \theta, \quad \Lambda_{1n} = \sqrt{\lambda_n - 1}, \quad \Lambda_{2n} = \sqrt{\lambda_n + 1}. \quad (6.53)$$

It is easy to check that  $\lambda = 1$  does not satisfy Eq. (6.45). For  $\lambda < 1$  the solution of Eq. (6.45) can be written in the form

$$U(\theta) = A \cos L_2 \theta + B \cos L_1 \theta, \quad \left( L_1 = \sqrt{1 - \lambda}, \quad L_2 = \sqrt{1 + \lambda} \right). \quad (6.54)$$

The system of equations for determining the coefficients  $A$  and  $B$  follows from the relationships (6.48) and (6.50). The characteristic equation of the system is

$$-L_2 \sin L_2 \pi \cos L_1 \pi + L_1 \sin L_1 \pi \cos L_2 \pi = 0. \quad (6.55)$$

It is evident that  $\lambda_0 = 0$  is the solution of Eq. (6.55). The second root of Eq. (6.55) is  $\lambda_1 = 0.80$  calculated to the second decimal place. The particular solutions corresponding to the eigenvalues  $\lambda_0$  and  $\lambda_1$  have the form

$$\begin{aligned} U_0(\theta) &= \cos \theta, \\ U_1(\theta) &= \cos L_{21} \theta + \frac{\cos L_{21} \pi}{\cos L_{11} \pi} \cos L_{11} \theta, \\ L_{11} &= \sqrt{1 - \lambda_1}, \quad L_{21} = \sqrt{1 + \lambda_1}. \end{aligned} \quad (6.56)$$

The functions  $U_n(\theta)$  determined by Eqs. (6.53) and (6.56) are mutually orthogonal. To prove this, we consider two particular solutions (6.53) for  $\lambda_n \neq \lambda_m$

$$\int_{-\pi}^{\pi} U_m(\theta) U_n(\theta) d\theta = \frac{4 \cos \Lambda_{2n} \pi \cos \Lambda_{1m} \pi}{\lambda_m^2 - \lambda_n^2} [F(\lambda_m) - F(\lambda_n)],$$

$$F(\lambda) = \lambda [\Lambda_1 \tanh \Lambda_1 \pi + \Lambda_2 \tan \Lambda_2 \pi].$$

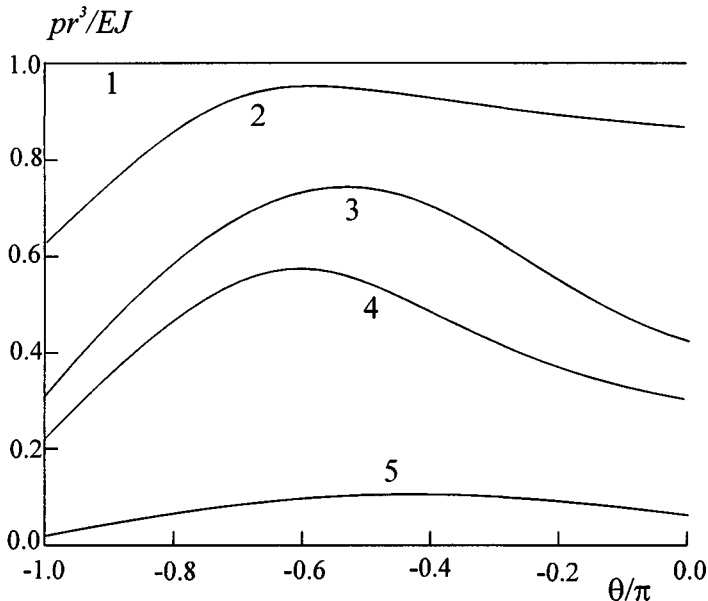


Figure 6.6: The time variation caused by wear of pressure distribution in contact of an open ring with a cylinder liner;  $t_1 = 0$  (curve 1),  $t_1 = 0.1$  (curve 2),  $t_1 = 0.5$  (curve 3),  $t_1 = 1.0$  (curve 4),  $t_1 = 5.0$  (curve 5);  $t_1 = K_w E J t / r^4$ .

The right side of this relationship is equal to zero in view of Eq. (6.52). The orthogonality of the other particular solutions can be proved in a similar manner.

Expanding the known function  $u_{r1}(\theta, 0)$  (which is determined by the shape of the ring in the free state) into a series in the complete orthonormal system of functions  $U_n(\theta)$ , we find the coefficients  $A_n$ :

$$u_{r1}(\theta, 0) = A_0 \cos \theta + \sum_{n=1}^{\infty} A_n U_n(\theta).$$

Then taking into account Eqs. (6.43) and (6.46) we obtain the relationship for determining the ring deflection  $u_{r1}(\theta, t_1)$  at succeeding instants in time

$$u_{r1}(\theta, t_1) = A_0 \cos \theta + \sum_{n=1}^{\infty} A_n U_n(\theta) \exp(-\lambda_n^2 t_1). \quad (6.57)$$

The equation for determining the pressure  $p_1(\theta, t_1)$  follows from Eqs. (6.40) and (6.57), namely

$$p_1(\theta, t_1) = \sum_{n=1}^{\infty} A_n \lambda_n^2 U_n(\theta) \exp(-\lambda_n^2 t_1), \quad (6.58)$$

The expressions for functions  $U_n(\theta)$  are given by formulae (6.53) and (6.56).

The analysis of the characteristic equation (6.52) shows that the eigenvalues  $\lambda_n$  form a rapidly increasing sequence:  $\lambda_1 = 0.80$ ,  $\lambda_2 = 2.32$ ,  $\lambda_3 = 6.69$ ,  $\lambda_4 = 13.16$ ,  $\lambda_5 = 21.63$ ,  $\lambda_6 = 32.12$ , etc., (with an accuracy of 0.0005). This makes possible to sum only the first few terms of series (6.58) to determine the pressure distribution for instants of time not close to zero.

Fig. 6.6 illustrates the pressure between the ring and the cylinder for different times. The initially uniform pressure distribution becomes nonuniform in the wear process. Wear can produce a gap between the ring and the cylinder.

The solution obtained here can be applied to study sealing properties of a piston ring, and to evaluate its useful life.

## 6.5 Contact problem for an elastic half-space

In this part we develop a general method for solving 2-D and 3-D wear contact problems of type  $\mathcal{A}$ , for the case of a constant contact region in a wear process (elasticity operator  $A$  (6.7) is time-independent). The linear relation between a wear rate and a contact pressure is used; this allows us to reduce the problems to linear integral equations.

### 6.5.1 Problem formulation

Consider a punch rotating or sliding back and forth over an elastic half-space. The shape function of the punch is described by the equation  $z = f(x, y)$ . In a system of coordinates attached to the punch, the relation between the elastic displacement  $w(x, y, t)$  in the  $z$ -axis direction and the contact pressure  $p(x, y, t)$  (see Eq. (6.7)) has the form of the integral equation

$$w(x, y, t) = \iint_{\Omega} K(x, y, x', y') p(x', y', t) dx' dy'. \quad (6.59)$$

The kernel  $K(x, y, x', y')$  does not depend on time, so that Eq. (6.59) holds at each instant of time. As was mentioned in § 6.2, this assumption is valid if the wear displacement and the elastic displacement of the half-space surface are small and of comparable size. In this case, we can consider both relative to the undeformed surface of the elastic half-space. Eq. (6.59) also holds at an arbitrary instant of time if only the punch experiences wear. There is no restriction on the magnitude of the punch linear wear  $w_*(x, y, t)$  in this case.

The kernel  $K(x, y, x', y')$  is generally symmetric and positive. The kernel symmetry is explained by the fact that it is a function of the distance between the point with coordinates  $(x, y)$  where the displacement is measured and the point with coordinates  $(x', y')$  where the normal load  $p(x', y', t) dx' dy'$  is applied. To prove the kernel positiveness, let us consider the functional  $J[q]$

$$J[q] = \iint_{\Omega} q(x, y) \left[ \iint_{\Omega} K(x, y, x', y') q(x', y') dx' dy' \right] dx dy,$$

where  $q(x, y)$  is any continuous function not identically zero within the region  $\Omega$ . The functional  $J(q)$  can be rewritten in the form which follows from Eq. (6.59)

$$J(q) = \iint_{\Omega} q(x, y) w_q(x, y) dx dy.$$

Thus the functional  $J(q)$  represents the total work done by an arbitrary pressure  $q(x, y)$  on the corresponding displacements  $w_q(x, y)$  of the points of the contact region,  $(x, y) \in \Omega$ . If the pressure is not zero, the work is always nonnegative. So  $J(q) \geq 0$  for any function  $q(x, y)$ , not identically zero. This establishes that the kernel is positive semi-definite.

The contact condition (6.10) of the punch ( $w_1(x, y) = 0$ ) and the elastic half-space at an arbitrary instant of time can be written as

$$w(x, y, t) + w_*(x, y, t) = D(t) - f(x, y). \quad (6.60)$$

Here  $w_*(x, y, t)$  is the irreversible displacement due to wear of the punch or elastic foundation in the direction of the  $z$ -axis. We assume that the function  $w_*(x, y, t)$  satisfies the wear equation (6.18).

The equations (6.18), (6.59) and (6.60) are used for determining the contact pressure  $p(x, y, t)$ , the elastic displacement  $w(x, y, t)$  and the wear displacement  $w_*(x, y, t)$  if the approach  $D(t)$  is a known function.

If the normal load  $P(t)$  applied to the punch is given, then to determine the unknown function  $D(t)$  we must add the equilibrium equation to the system of Eqs. (6.10), (6.59) and (6.60)

$$P(t) = \iint_{\Omega} p(x, y, t) dx dy. \quad (6.61)$$

Based on the analysis presented in §6.3, we can write the necessary conditions of the existence of the steady-state wear regime described by Eqs. (6.20) and (6.21). There is steady-state wear if the rate  $\frac{dD}{dt}$  of the approach of the contacting bodies and the normal load  $P(t)$  have the asymptotic values

$$\lim_{t \rightarrow +\infty} \frac{dD(t)}{dt} = \lim_{t \rightarrow +\infty} \frac{\partial w_*(x, y, t)}{\partial t} = D_{\infty}, \quad (6.62)$$

and

$$\lim_{t \rightarrow +\infty} \frac{dP}{dt} = P_{\infty},$$

where  $P_{\infty}$  is determined by Eq. (6.22).

$$P_{\infty} = \left( \frac{D_{\infty}}{K_w} \right)^{1/\alpha} \iint_{\Omega} \frac{dx dy}{V_{\infty}^{\beta/\alpha}(x, y)}.$$

If  $P_\infty = 0$  or  $D_\infty = 0$ , then the contact pressure  $p_\infty(x, y) = 0$ .

The equation of the shape of the worn punch surface  $f_\infty(x, y)$  follows from Eqs. (6.21) and (6.59)

$$f_\infty(x, y) = - \iint_{\Omega} [K(x, y, x', y') - K(x^0, y^0, x', y')] \left[ \frac{D_\infty}{K_w V_\infty^\beta(x', y')} \right]^{1/\alpha} dx' dy', \quad (6.63)$$

where  $(x^0, y^0) \in \Omega$ .

From this equation and the analysis presented in § 6.3 it follows that the kinetics of the wear process depends essentially on the type of punch motion.

### 6.5.2 Axisymmetric contact problem

Consider an axisymmetric contact problem for a punch of annular form in plan, rotating about its axis with a constant angular velocity  $\omega$ , and pressed into an elastic half-space (Fig. 6.7). The shape of the punch is described by the equation  $z = f(r)$ . The force  $P(t)$  and moment  $M(t)$  applied to the punch are generally time-dependent functions. A solution of the problem can be used to calculate the wear of such junctions as thrust sliding bearings, end face seals, clutches, disk brakes and others.

The contact occurs within the annular region  $a \leq r \leq b$ . We assume that the inner  $a$  and external  $b$  radii do not change during the wear process. This is precisely so for a punch with a flat base, and approximately true if the variations of the contact region due to wear are small compared to its width.

As the punch rotates, tangential stresses  $\tau_{z\theta}$  appear within the contact region. They coincide in direction with the direction of rotation, i.e. they are perpendicular to the radius of the contact region and

$$\tau_{z\theta}(r, t) = \mu p(r, t),$$

where  $p(r, t)$  is the normal pressure within the contact region, and  $\mu$  is the coefficient of friction. Because of the wear process, all components of stress and displacement are functions of time  $t$ .

The stress state of the elastic half-space at an arbitrary instant in time satisfies the following boundary conditions:

- within the contact region  $r \in [a, b]$

$$u_z = w(r, t), \quad \tau_{z\theta} = \mu p(r, t), \quad \tau_{zr} = 0, \quad (6.64)$$

- outside the contact region  $r \notin [a, b]$

$$\sigma_z = \tau_{z\theta} = \tau_{zr} = 0.$$

Here  $w(r, t)$  is the elastic displacement of the half-space in the  $z$ -axis direction at any instant in time.

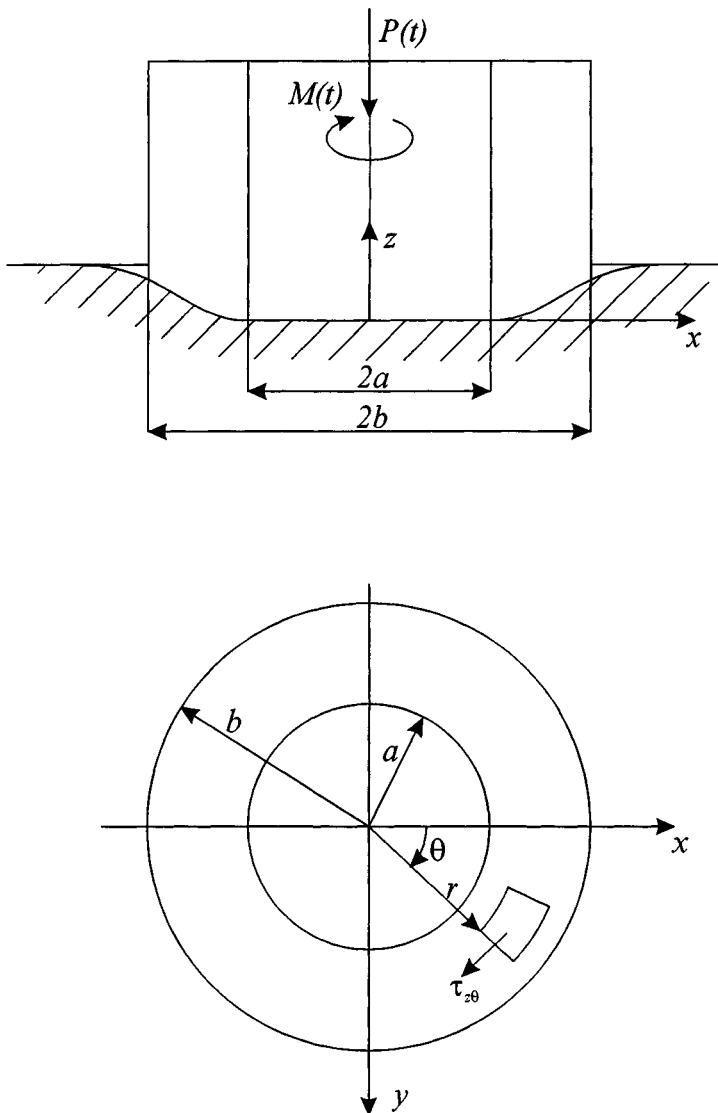


Figure 6.7: Scheme of contact of an annular cylindrical punch rotating on an elastic half-space surface.

Galin (1953) showed that the stress state corresponding to this boundary conditions can be broken down into two independent states:  $\sigma_z = \sigma_z^{(1)} + \sigma_z^{(2)}$ ,  $\tau_{z\theta} = \tau_{z\theta}^{(1)} + \tau_{z\theta}^{(2)}$ , etc., satisfying the boundary conditions (problem 1)

$$\begin{aligned} u_z^{(1)} &= w(r, t), \quad \tau_{z\theta}^{(1)} = \tau_{zr}^{(1)} = 0, \quad r \in [a, b], \\ \sigma_z^{(1)} &= \tau_{z\theta}^{(1)} = \tau_{zr}^{(1)} = 0, \quad r \notin [a, b]. \end{aligned} \quad (6.65)$$

and (problem 2)

$$\begin{aligned} u_z^{(2)} &= 0, \quad \tau_{z\theta}^{(2)} = -\mu\sigma_z^{(1)}, \quad \tau_{zr}^{(2)} = 0, \quad r \in [a, b], \\ \sigma_z^{(2)} &= \tau_{z\theta}^{(2)} = \tau_{zr}^{(2)} = 0, \quad r \notin [a, b]. \end{aligned} \quad (6.66)$$

Eq. (6.65) shows that  $\sigma_z^{(1)}$ ,  $\tau_{z\theta}^{(1)}$ , etc. are determined by the solution of the frictionless contact problem for the punch and the elastic half-space. The solution of the contact problem with the boundary conditions (6.66) shows that  $u_z^{(2)} = 0$  and  $\sigma_z^{(2)} = 0$  at the elastic half-space surface. So the relationship between the normal displacement  $w(r, t) = u_z = u_z^{(1)}$  and the contact pressure  $p(r, t) = -\sigma_z = -\sigma_z^{(1)}$  follows from the solution of the problem 1, and has the form

$$w(r, t) = \frac{1}{\pi E^*} \int_a^b \int_0^{2\pi} \frac{p(r', t)r'dr'd\varphi}{\sqrt{r^2 + r'^2 - 2rr' \cos \varphi}}, \quad (6.67)$$

where

$$E^* = \frac{E}{1 - \nu^2}.$$

The tangential stress at the half-space surface is determined by the equation following from the solution of problem 2:

$$\tau_{z\theta} = \tau_{z\theta}^{(2)} = \mu p(r, t). \quad (6.68)$$

The shape of the elastic half-space surface changes during the wear process. We use the wear equation in the form (6.18) to determine the wear displacement  $w_*(r, t)$  in the  $z$ -axis direction. This equation for  $\beta = 1$  is written as

$$\frac{\partial w_*}{\partial t} = K_w \omega r p(r, t), \quad (6.69)$$

We assume that, from  $t = 0$  to time  $t$ , the punch shifts by a distance  $D(t)$  along its axis, and that there is no change in the position of the punch axis. Then at an arbitrary instant in time, the contact condition for the punch and the half-space has the form

$$w(r, t) + w_*(r, t) = D(t) - f(r). \quad (6.70)$$

Substituting Eq. (6.67) into Eq. (6.70) and taking Eq. (6.69) into account, we obtain an integral equation for determining the contact pressure in the wear process

$$\frac{1}{\pi E^*} \int_a^b \int_0^{2\pi} \frac{p(r', t) r' dr' d\varphi}{\sqrt{r^2 + r'^2 - 2rr' \cos \varphi}} = D(t) - f(r) - K_w \omega r \int_0^t p(r, \tau) d\tau. \quad (6.71)$$

Based on the general method described in §6.3, we introduce the new function  $q(r, t) = rp(r, t)$ , which we seek in the following form:

$$q(r, t) = q_\infty + \sum_{n=1}^{\infty} q_n(r) \exp(-\lambda_n \omega t). \quad (6.72)$$

Substituting Eq. (6.72) into Eq. (6.71) we obtain the following equation

$$\begin{aligned} & \sum_{n=1}^{\infty} [1 - \exp(-\lambda_n \omega t)] \left[ \frac{K_w}{\lambda_n} q_n(r) - \right. \\ & \left. \frac{1}{\pi E^*} \int_a^b \int_0^{2\pi} \frac{q_n(r') dr' d\varphi}{\sqrt{r^2 + r'^2 - 2rr' \cos \varphi}} \right] = D(t) - D(0) - K_w \omega q_\infty t. \end{aligned} \quad (6.73)$$

Let us look at various possible cases of this problem. If the punch does not move along its axis, i.e.  $D(t) = D(0)$ , Eq. (6.73) shows that the contact pressure approaches zero ( $q_\infty = 0$ ). To find the unknown functions  $\bar{q}_n(\rho) = \frac{q_n(\rho b)}{b E^*}$  and the values  $\lambda_n$  we have a homogeneous Fredholm integral equation of the second kind ( $\rho = \frac{r}{b}$ )

$$\bar{q}_n(\rho) - \lambda_n \int_{a/b}^1 H(\rho, \rho') \bar{q}_n(\rho') d\rho' = 0 \quad (6.74)$$

with symmetric positive semi-definite kernel

$$H(\rho, \rho') = \frac{1}{\pi E^* K_w} \int_0^{2\pi} \frac{d\varphi}{\sqrt{\rho^2 + \rho'^2 - 2\rho\rho' \cos \varphi}} = \frac{4}{\pi E^* K_w (\rho + \rho')} K\left(\frac{2\sqrt{\rho\rho'}}{\rho + \rho'}\right), \quad (6.75)$$

where  $K(x)$  is the complete elliptic integral of the first kind. In the asymptotic case  $\frac{b-a}{a} \ll 1$ , i.e. if the ring width is far less of its radius, the kernel  $H(\rho, \rho')$  takes the simple form

$$H(\rho, \rho') = \frac{2}{\pi E^* K_w} \ln \frac{8a}{|\rho - \rho'|b}.$$

The eigenvalues  $\lambda_n$  determined by Eq. (6.74) are all real and positive since the kernel (6.75) is real, symmetric and positive semi-definite. The eigenfunctions of Eq. (6.74) are orthogonal by virtue of the symmetry of the kernel.

The contact pressure  $p(r, 0)$  at the initial instant in time can be found by solving the frictionless contact problem for the axisymmetric annular punch and an elastic half-space. This problem has been investigated by Gubenko and Mossakovskiy (1960), Collins (1963), Aleksandrov (1967), Gladwell and Gupta (1979); see also the monographs by Galin (1976) and Gladwell (1980). For instance, if the punch has a flat base ( $f(r) = f = \text{const}$ ) and the annular width is much more than its inner radius  $\frac{b-a}{a} \gg 1$  the relation given by Gubenko and Mossakovskiy (1960) can be used ( $a < r < b$ )

$$p(r, 0) = \frac{2fE^*}{\pi^2} \left[ \frac{1}{\sqrt{b^2 - r^2}} \arctan \frac{b\sqrt{r^2 - a^2}}{a\sqrt{b^2 - r^2}} + \frac{a}{b\sqrt{r^2 - a^2}} \right]. \quad (6.76)$$

Expanding the known function  $\bar{q}(\rho, 0) = \rho p(\rho b, 0)/E^*$  into a series in the complete orthonormal system of eigenfunctions  $U_n(\rho)$  of Eq. (6.74), we find the coefficients  $A_n$ :

$$\bar{q}(\rho, 0) = \sum_{n=1}^{\infty} A_n U_n(\rho).$$

Then the contact pressure  $\bar{p}(\rho, t) = p(\rho, t)/E^*$  at succeeding instants in time is calculated from the formula

$$\bar{p}(\rho, t) = \frac{1}{\rho} \sum_{n=1}^{\infty} A_n U_n(\rho) \exp(-\lambda_n \omega t). \quad (6.77)$$

The linear-wear case, i.e.  $D(t) = D(0) + D_{\infty}t$ , also necessitates solution of the integral equation (6.74). The solution of the problem takes the following form

$$\bar{p}(\rho, t) = \frac{1}{\rho} \left[ \bar{q}_{\infty} + \sum_{n=1}^{\infty} A_n U_n(\rho) \exp(-\lambda_n \omega t) \right], \quad (6.78)$$

where  $\bar{q}_{\infty} = \frac{D_{\infty}}{K_w \omega b E}$ . Using the equilibrium equation (6.61) we obtain the normal load function  $P(t)$  in this case

$$P(t) = P_{\infty} + \sum_{n=1}^{\infty} A_n P_n \exp(-\lambda_n \omega t),$$

where

$$P_{\infty} = \frac{2\pi D_{\infty}(b-a)}{K_w \omega}, \quad (6.79)$$

$$P_n = 2\pi b^2 E^* \int_{a/b}^1 U_n(\rho) d\rho.$$

If the known functions  $D(t)$  or  $P(t)$  have another form, and satisfy the conditions

$$D(t) = D(0) + D_\infty t + D_*(t), \quad D_*(t) \leq A \exp(-\lambda_1 \omega t),$$

$$P(t) = P_\infty + P_*(t), \quad P_*(t) \leq B \exp(-\lambda_1 \omega t),$$

where  $A$  and  $B$  are some constants, the problem can be solved using a similar technique (Goryacheva, 1988) and is reduced to the investigation of the inhomogeneous Fredholm integral equations.

The method can also be used to solve the wear contact problem for a punch which has a circular contact region of radius  $b$ . However, in this case Eq. (6.69) shows that the displacement due to wear will be zero at the center of the contact region. This should lead to increasing contact pressure at this point; this in turn will cause irreversible plastic deformation at the center of the contact region. Thus, although irreversible changes of surface shape occur over the whole contact region, the solution based on the theory of elasticity given below will be valid for the whole contact zone except for a small region of radius  $a$  near its center. The eigenfunctions  $U_n(\rho)$  in Eq. (6.78) can be found from the analysis of Eq. (6.74) with the symmetric and positive semi-definite kernel (6.75) for  $\frac{a}{b} \ll 1$ .

The initial contact pressure  $p(r, 0)$  can be determined by the formula (Galin, 1953):

$$p(r, 0) = \frac{E^*}{4\pi} \int_0^b \Delta f(r') L(r, r') dr',$$

where

$$L(r, r') = \int_0^{2\pi} \frac{2r'}{\pi \sqrt{r^2 + r'^2 - 2rr' \cos \varphi}} \arctan \frac{\sqrt{b^2 - r^2} \sqrt{b^2 - r'^2}}{b \sqrt{r^2 + r'^2 - 2rr' \cos \varphi}} d\varphi,$$

$$\Delta = \frac{1}{r'} \cdot \frac{\partial}{\partial r'} + \frac{\partial^2}{\partial r'^2}.$$

Kellogg's method (see, for example, Mikhlin and Smolitsky, 1967) was used to determine eigenfunctions  $U_k(r)$  and eigenvalues  $\lambda_k$  of the Fredholm equation (6.74) with the real symmetric and positive semi-definite kernel (6.75). Successive approximations at the  $k$ -th step were calculated from the formula

$$\tilde{U}_k^{(n+1)}(\rho) = \int_{a/b}^1 H(\rho, \rho') \left[ U_k^{(n)}(\rho') - U_k^{(n)}(\rho) \right] d\rho' + U_k^{(n)}(\rho) \int_{a/b}^1 H(\rho, \rho') d\rho'.$$

$n$	$k_n \left( \frac{a}{b} = 0.0005 \right)$	$k_n \left( \frac{a}{b} = 0.5 \right)$	$n$	$k_n \left( \frac{a}{b} = 0.0005 \right)$	$k_n \left( \frac{a}{b} = 0.5 \right)$
1	0.03643	0.18286	12	1.91324	6.62237
2	0.06730	0.90155	13	2.17578	7.48047
3	0.15221	1.57259	14	2.42712	8.23339
4	0.29421	2.22609	15	2.76887	8.46120
5	0.46936	2.79990	16	2.91857	9.62898
6	0.63901	3.41897	17	3.32462	11.06820
7	0.77450	3.83968	18	3.75936	12.86998
8	0.99863	4.37473	19	4.22465	15.48172
9	1.25300	5.06344	20	4.80057	19.90402
10	1.39264	5.67423	21	8.06343	30.73539
11	1.69633	6.18522			

Table 6.4: The eigenvalues of integral equation (6.74)

Here the first integral has no singularity at  $\rho' = \rho$  and can be calculated numerically, the second integral is calculated analytically. The function  $\tilde{U}_k^{(0)}(\rho)$  for each  $k$ -th step was taken in the orthogonal complement to the linear hull of the eigenfunctions  $U_1(\rho), U_2(\rho), \dots, U_{k-1}(\rho)$ , corresponding to the eigenvalues  $0 < \lambda_1 < \lambda_2 < \dots < \lambda_{k-1}$ , which were found at the previous steps. Then the eigenvalue  $\lambda_k$  is determined as

$$\lambda_k = \lim_{n \rightarrow \infty} \lambda_k^{(n)} = \lim_{n \rightarrow \infty} \frac{\|U_k^{(n)}\|_{L^2}}{\|U_k^{(n+1)}\|_{L^2}}.$$

Table 6.4 shows the numerical results of eigenvalue calculations for the cases  $\frac{a}{b} = 5 \cdot 10^{-4}$  and  $\frac{a}{b} = 5 \cdot 10^{-1}$ . The values  $k_n = \lambda_n / (\pi E^* K_w)$  increase rapidly with  $n$ . This makes it possible to consider just the first few terms of the series (6.72) in determining the contact pressure for large time.

Fig. 6.8 illustrates the contact pressure distribution under the ring punch with flat face at the initial instant of time (curve 1) and in the steady-state wear, i.e.  $t \rightarrow +\infty$  (curve 2). Note that the singularity of the pressure distribution at the ends of the contact zone, which is present when  $t = 0$  disappears for  $t > 0$ .

The proposed method can be used to analyze the wear both of the elastic foundation and of the punch. The shape of the worn punch surface in the steady-

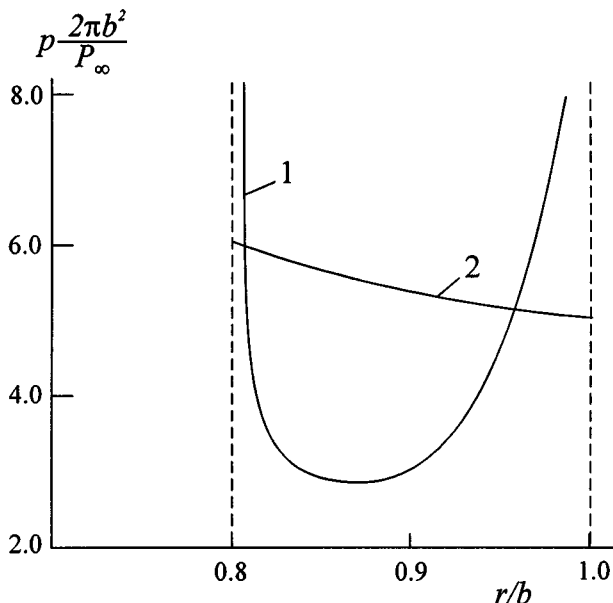


Figure 6.8: The initial (curve 1) and steady-state (curve 2) pressure distributions in contact of a flat-ended annular cylindrical punch with an elastic half-space.

state wear is calculated from the formula which follows from Eq.(6.63), namely

$$f_\infty(r) - f_\infty(a) = \frac{2P_\infty}{\pi^2 E^*(b-a)} \left[ \int_{a/r}^1 K(x) dx - \int_{a/b}^{r/b} \frac{K(x)}{x} dx \right] \quad (6.80)$$

where  $K(x)$  is a complete elliptic integral of the first kind.

### 6.5.3 The case $V(x, y) = V_\infty$

Now we investigate a wear contact problem for a strip punch (3) sliding back and forth on a surface of an elastic layer (1). This problem is considered in a two-dimensional formulation (Fig. 6.9). The solution of the problem can be used for the prediction of the durability of different types of slideways.

The integral equation for the problem is written as

$$\frac{2}{\pi E^*} \int_a^a H_1 \left( \frac{x-x'}{h_0} \right) p(x', t) dx' = D(t) - f(x) - K_w V_\infty^\beta \int_0^t p(x, t') dt'.$$

Here  $f(x)$  is a shape of the punch contacting surface,  $D(t)$  is the punch penetration into the layer due to wear,  $h_0$  is the layer thickness,  $V_\infty$  is the punch sliding velocity,

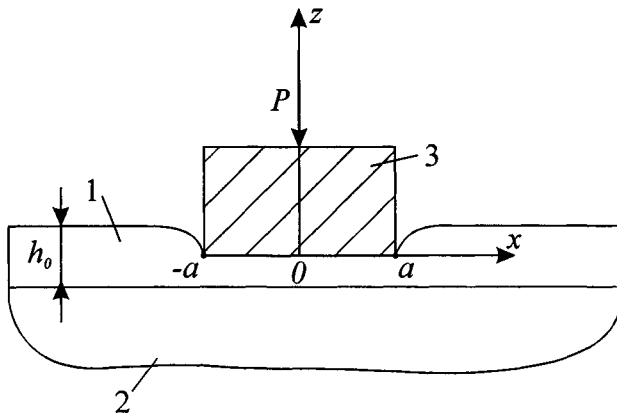


Figure 6.9: Scheme of contact of a cylindrical punch and a layered elastic half-space.

$p(x, t)$  is the pressure distribution,  $K_w, \beta$  are the parameters in the wear equation which is described by the relation

$$\frac{\partial w_s(x, t)}{\partial t} = K_w p(x, t) V_\infty^\beta.$$

The kernel  $H_1(y)$  can be represented as Galin (1976))

$$H_1(y) = \int_0^{+\infty} \frac{L(u)}{u} \cos(uy) du,$$

where

$$L(u) = \frac{\cosh 2u - 1}{\sinh 2u + 2u}$$

in the problem for the elastic layer placed on the rigid substrate (2) in the absence of tangential stresses between the layer and substrate;

$$L(u) = \frac{2\kappa \sinh 2u - 4u}{2\kappa \cosh 2u + 4u^2 + 1 + \kappa^2}, \quad \kappa = 3 - 4\nu$$

in the problem for the elastic layer bonded to a rigid substrate.

This wear contact problem can also be reduced to a Fredholm integral equation by the method described in § 6.5.2 (Goryacheva, 1988). Here we give only the formula for the worn punch shape  $f_\infty$  in the steady state wear which follows from Eq.(6.63)

$$f_\infty(x) - f_\infty(0) = \frac{P_\infty}{\pi E^* a} \int_{-a}^a \left[ H_1 \left( \frac{x' - x}{h_0} \right) - H_1 \left( \frac{x'}{h_0} \right) \right] dx'. \quad (6.81)$$

Using the expansion of the kernel  $H_1(y)$  into series, given by Aleksandrov (1968), we can reduce this relationship to the following form which is valid for  $\left(\frac{a}{h_0}\right)^4 \ll 1$

$$\left(\xi = \frac{x}{a}\right)$$

$$f_{\infty 1}(\xi) = \frac{[f_{\infty}(a\xi) - f_{\infty}(0)]\pi E^*}{P_{\infty}} = -(1-\xi)\ln(1-\xi) + (1+\xi)\ln(1+\xi) + 1.432 \left(\frac{a\xi}{h_0}\right)^2.$$

Note that if the punch has the shape function given by Eq. (6.81) at the initial instant of time, and the contact region is restricted by the shape of the punch and is independent of time, this initial punch shape does not change in the wear process. Wear is uniform within the contact region. This conclusion follows from the analysis presented in § 6.23. So the specimen with the shape described by Eq. (6.81) provides the uniform wear condition, and can be used for the study of wear equation in tests.

The same conclusion could be drawn from the analysis of Eq. (6.80) which holds for a spin motion of an annular punch.

## 6.6 Contact problems of type $\mathcal{B}$

The mathematical formulation of the wear contact problem of type  $\mathcal{B}$  includes Eqs. (6.7), (6.11) and (6.12). It follows from this system of equations that the contact conditions at any given point of the body 1 change in time, so the linear wear is determined by integrating the contact pressure function within the region of the contact, depending on the type of motion. Note that for some problems of this type, wear takes place only during a limited time.

We will illustrate the method of solution of the problems of type  $\mathcal{B}$  by considering two particular problems.

### 6.6.1 The wear of an elastic half-space by a punch moving translationally

We consider the punch moving in the direction of the  $x$ -axis with a constant velocity  $V$  (Fig. 6.10). The contact of the punch and the elastic half-space takes place within the region  $\Omega \equiv \{x, y : x \in (-a, a), y \in (-b, b)\}$  in the system of coordinates  $(x, y)$  attached to the moving punch. The punch has a rectangular cross-section at the plane  $x = \text{const}$ . The normal load  $P$  is applied to the punch.

The wear of the elastic half-space occurs when the punch moves. The shape changes of the half-space surface can be determined from the wear equation (6.13). In the system of coordinates  $x_1, y_1, z_1$ , related to the half-space surface, it can be written as

$$\frac{\partial w_*(x_1, y_1, t)}{\partial t} = K_w p^\alpha(x_1, y_1, t) V^\beta. \quad (6.82)$$

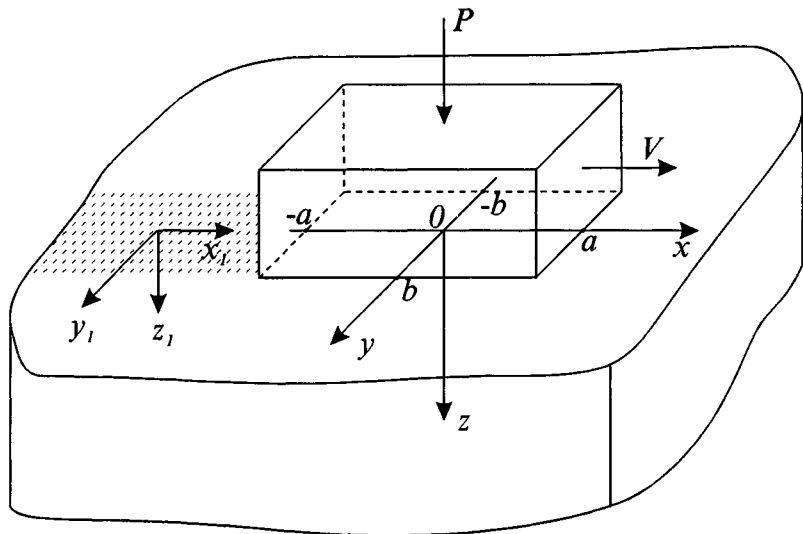


Figure 6.10: Wear of an elastic half-space by a punch of the rectangular form in plane.

It was proved by Galin (1953), that the pressure  $p(x, y)$  within a contact area  $\Omega$  which is a long rectangle ( $a \gg b$ ) can be presented by the relation

$$p(x, y) = \frac{p_1(x)}{\pi \sqrt{b^2 - y^2}} \quad (6.83)$$

where the function  $p_1(x)$  depends linearly on the elastic displacement  $w(x, 0) = w_1(x)$  in the  $z$ -axis direction. Thus

$$p_1(x) = kw_1(x), \quad (6.84)$$

where

$$k = \frac{\pi E}{2(1-\nu^2) \log(a/b)}.$$

This relation is similar to that found for a Winkler foundation model.

By virtue of Eq. (6.84) and the fact that the punch moves along the  $x$ -axis, the wear contact problem can be considered in a two-dimensional formulation on the coordinate plane  $y = 0$ .

We will investigate the steady-state wear process and fix some point  $(x_1, 0)$  of the boundary of the half-space, take  $t = 0$  to be the instant that point  $(x_1, 0)$  arrives at the contact ( $x_1 = a$ ), and denote by  $t(x)$  the instant at which the point  $(x_1, 0)$  will have coordinates  $(x, 0)$  in the  $(x, y)$  system. Then we obtain

$$t(x) = \frac{a - x}{V},$$

We introduce the functions  $W_*(x)$  and  $\tilde{p}(x)$  which are time independent in the system of coordinates  $x, z$ , by

$$w_*(a, 0, t(x)) = W_*(x), \quad W_*(x) = 0 \quad \text{if } x > a,$$

$$p(a, 0, t) = \tilde{p}(a - Vt).$$

Using these relations and Eq. (6.82), we obtain the following relationship between  $W_*(x)$  and  $\tilde{p}(x)$

$$W_*(x) = K_w V^\beta \int_0^{t(x)} \tilde{p}^\alpha(a - Vt') dt' = K_w V^{\beta-1} \int_x^a \tilde{p}^\alpha(s) ds. \quad (6.85)$$

The contact condition of the punch and the worn half-space at the section  $y = 0$  has the following form in the moving system of coordinates  $x, z$

$$W_*(x) + w_1(x) = D - f(x), \quad (6.86)$$

where  $f(x)$  is the shape function of the punch at the plane  $y = 0$ ,  $D$  is its penetration.

On differentiating Eqs. (6.84), (6.85) and (6.86) and substituting Eqs. (6.84) and (6.85) into Eq. (6.86), we obtain

$$K_* \tilde{p}^\alpha(x) - \frac{\pi b}{k} \tilde{p}'(x) = f'(x), \quad (6.87)$$

where

$$K_* = K_w V^{\beta-1}. \quad (6.88)$$

Eq. (6.87) and the equilibrium equation

$$\int_{-a}^a \tilde{p}(x) dx = P_0$$

provide the complete system of equations to determine the function  $p(x)$ . The value  $P_0$  can be determined from Eq. (6.83) if the normal load  $P$  applied to the punch is known.

The solution of the problem for the case  $\alpha = 1$  has the following dimensionless form

$$\tilde{p}_1(\xi) = \left[ C - \int_{-1}^{\xi} f'_1(\xi') \exp(-\kappa\xi') d\xi' \right] \exp(\kappa\xi), \quad (6.89)$$

$$C = \frac{P_{01} - \int_{-1}^1 [1 - \exp(\kappa(1 - \xi'))] f'_1(\xi') d\xi'}{2 \sinh \kappa},$$

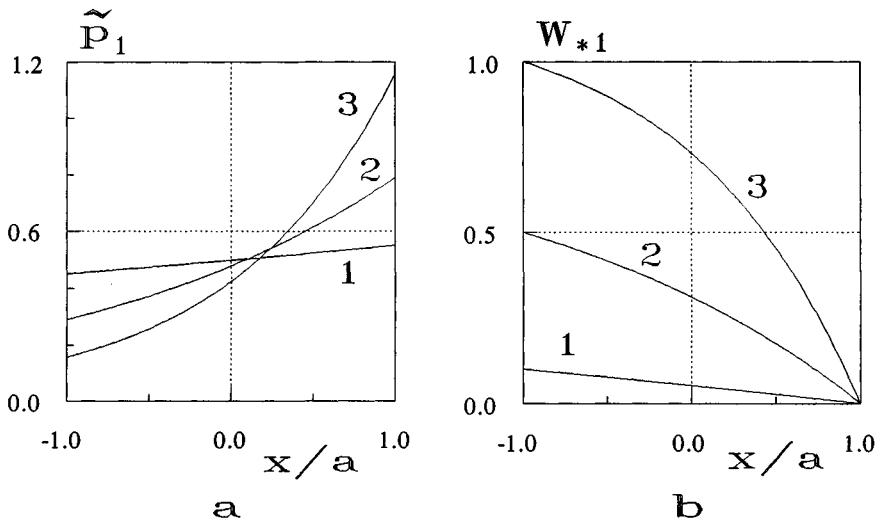


Figure 6.11: The steady-state pressure  $\tilde{p}_1$  (a) and the shape of the worn surface  $W_{*1}$  (b) of an elastic half-space within the contact region for different values of parameter  $\kappa = \frac{K_w V^{\beta-1} E a}{2(1-\nu^2) b \log a/b}$ :  $\kappa = 0.1$  (curves 1),  $\kappa = 0.5$  (curves 2),  $\kappa = 1$  (curves 3) and  $\alpha = 1$ .

where

$$\tilde{p}_1(\xi) = \frac{\pi b \tilde{p}(a\xi)}{ka}, \quad \xi = \frac{x}{a}, \quad \kappa = \frac{K_* a k}{\pi b}, \quad P_{01} = \frac{K_* P_0}{a}, \quad f_1(\xi) = \frac{f(\xi a)}{a}.$$

Fig. 6.11 illustrates the contact pressure  $\tilde{p}_1(\xi)$  and the shape of the worn surface  $W_{*1}(\xi) = \frac{W_*}{a}$  of the half-space within the contact region, for the contact problem of a punch with flat face ( $f'(x) = 0$ ) and the elastic half-space. Based on Eqs. (6.85) and (6.89), the function  $W_*(x)$  is calculated from the formula

$$W_{*1}(\xi) = \frac{P_{01}}{2 \sinh \kappa} (\exp(\kappa) - \exp(\kappa \xi)).$$

It is interesting to note that Eq. (6.87) can also be used to find the shape of the moving punch which has uniform wear in the steady-state wear of the elastic half-space. As mentioned above, the investigation of punch wear relates to problems of type  $\mathcal{A}$ . The steady-state wear of the punch moving translationally with a constant velocity  $V$  occurs only if the contact pressure is distributed uniformly within the contact region, and does not change in the wear process, i.e.  $p(x, y) = p_0$ , where  $p_0 = \frac{P}{4ab}$  (see § 6.3). Then the equation for the punch shape  $f_0(x)$  which will not

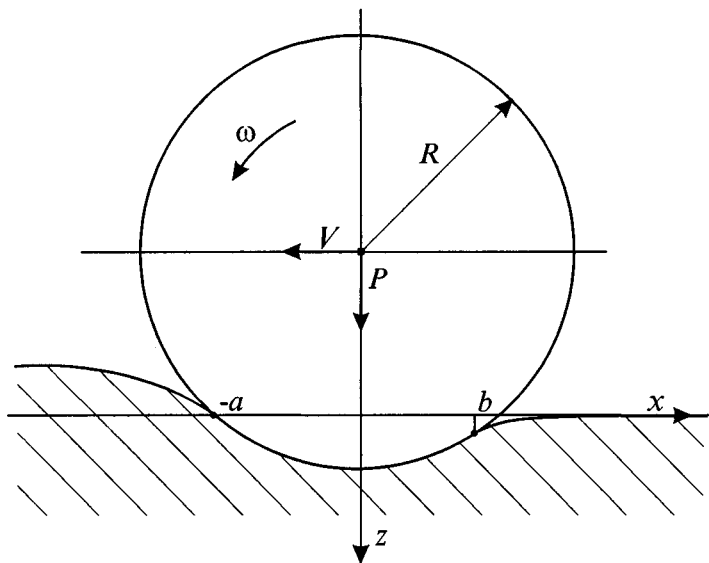


Figure 6.12: Wear of a half-plane by a disk executing translational and rotational motion.

change in the wear process follows from Eq. (6.87)

$$f_0(x) = K_* p_0^\alpha x + \text{const},$$

where  $K_*$  is determined by Eq. (6.88).

### 6.6.2 Wear of a half-plane by a disk executing translational and rotational motion

A more complicated contact problem of type  $B$  is considered by Soldatenkov (1989).

A rigid disk of radius  $R$  is pressed into an elastic half-plane, and moves translationally to the left along it (see Fig. 6.12) with a constant velocity  $V > 0$ , while at the same time rotating with a constant angular velocity  $\omega$ . The positive direction of rotation is shown in the figure. The normal force  $P$  is applied to the disk.

We will take into account the wear of the half-plane by the disk. We assume that the linear wear  $w_*(x_1, t)$  is determined from Eq. (6.13), which can be written as

$$\frac{\partial w_*(x_1, t)}{\partial t} = K_w |\omega R - V| p(x_1, t). \quad (6.90)$$

Here  $(x_1, z_1)$  is the coordinate frame fixed in the half-plane.

We will investigate the steady-state wear following the procedure described above. Based on Eq. (6.90), we establish the relationship between the linear wear  $W_*(x)$  and contact pressure  $p(x)$  determined in the moving system of coordinates

$x, z$ . Assuming that the point  $x_1$  arrives at the contact zone, i.e.  $x_1 = -a$ , at the instant  $t = 0$ , we denote the instant of time  $t(x)$  at which the point  $x_1$  will have coordinate  $x$  in the moving system. Then we have

$$\begin{aligned} t(x) &= \frac{a+x}{V}, \\ w_*(-a, t(x)) &= W_*(x), \quad W_*(x) = 0 \quad \text{if } x \leq -a, \\ p(-a, t) &= \tilde{p}(-a + Vt), \end{aligned}$$

$$W_*(x) = K_w |\omega R - V| \int_0^{t(x)} p(-a + Vt') dt' = K_w \frac{|\omega R - V|}{V} \int_{-a}^x p(s) ds. \quad (6.91)$$

The contact condition between the disk and the half-plane is

$$W'_*(x) + w'(x) = -f'(x), \quad x \in [-a, b], \quad (6.92)$$

where  $w(x)$  is the elastic displacement of the half-plane along the  $z$ -axis (in the  $x, z$  system);  $f(x)$  is the shape of the contacting surface of the disk which can be represented by the equation  $f(x) = \frac{x^2}{2R}$  valid for  $a + b \ll R$ ; the prime denotes differentiation with respect to  $x$ .

Under the assumption that the wear  $W_*(x)$  and the velocity  $V$  are small, the derivative  $w'(x)$  can be expressed by the relation corresponding to the static problem of deformation of a half-plane (see Galin (1953) or Johnson (1987))

$$w'(x) = K \int_{-a}^b p(s) \frac{ds}{s-x} + \pi \vartheta K \tau_{xz}(x), \quad (z=0), \quad (6.93)$$

$$K = \frac{2(1-\nu^2)}{\pi E}, \quad \vartheta = \frac{1-2\nu}{2(1-\nu)},$$

where  $\tau_{xz}(x)$  is the tangential contact stress, which can be expressed in terms of the contact pressure in accordance with Coulomb's law (see § 3.1):

$$\tau_{xz}(x) = (\mu p(x) + \tau_0) \operatorname{sgn}(\omega R - V).$$

Substituting Eqs. (6.91) and (6.93) into Eq. (6.92) leads to the following equation for  $p(x)$ :

$$mp(x) + K \int_{-a}^b p(s) \frac{ds}{s-x} = F(x), \quad (6.94)$$

$$F(x) = -f'(x) - \pi \vartheta K \tau_0 \operatorname{sgn}(\omega R - V), \quad (6.95)$$

$$m = \pi \vartheta K \mu \operatorname{sgn}(\omega R - V) + \frac{K_w}{V} |\omega R - V|. \quad (6.96)$$

In addition, we have the equilibrium equation

$$P = \int_{-a}^b p(x) dx. \quad (6.97)$$

The solution  $p(x)$  of Eq. (6.94) can readily be obtained by using the technique described in § 3.2 and in Muskhelishvili's (1946) and Johnson's (1987) books. Assuming that function  $p(x)$  belongs to the Hölder class within  $[-a, b]$  and is bounded at the ends of the contact region, we have

$$\begin{aligned} p(x) &= \frac{m}{m^2 + (\pi K)^2} F(x) - \frac{K}{m^2 + (\pi K)^2} (a+x)^{1/2-\eta} (b-x)^{1/2+\eta} \times \\ &\times \int_{-a}^b \frac{F(s) ds}{(a+s)^{1/2-\eta} (b-s)^{1/2+\eta} (s-x)}, \quad x \in [-a, b] \end{aligned} \quad (6.98)$$

under the condition

$$\int_{-a}^b \frac{F(x) dx}{(a+x)^{1/2-\eta} (b-x)^{1/2+\eta}} = 0, \quad (6.99)$$

$$\eta = \frac{1}{\pi} \arctan \frac{m}{\pi K}, \quad |\eta| < \frac{1}{2}. \quad (6.100)$$

Taking into account Eq. (6.95), we reduce Eqs. (6.98) and (6.99) to

$$p(x) = \frac{(a+x)^{1/2-\eta} (b-x)^{1/2+\eta}}{Rm \sqrt{1 + \left(\pi \frac{K}{m}\right)^2}}, \quad (6.101)$$

$$\frac{a-b}{a+b} = 2\eta + \frac{2\pi\vartheta K}{a+b} R\tau_0 \operatorname{sgn}(\omega R - V). \quad (6.102)$$

From Eqs. (6.97)–(6.101) we obtain

$$(a+b)^2 = \frac{2PRK}{\left(\frac{1}{4} - \eta^2\right)}. \quad (6.103)$$

Eqs. (6.101)–(6.103) completely specify the distribution of the contact pressure  $p(x)$ . By integrating Eq. (6.101) in accordance with Eq. (6.91), we can determine the wear distribution  $W_*(x)$ . In the general case,  $W_*(x)$  is expressed in terms of a hypergeometric function.

Let us analyze Eqs. (6.101)–(6.103), and consider some cases.

First we note that in the absence of wear,  $K_w = 0$  and  $\omega = 0$ , Eqs. (6.101)–(6.103) coincide with the solution obtained in § 3.2 for the contact problem for a parabolic punch with limiting friction.

Wear affects both the contact pressure distribution  $p(x)$  and the position of the contact region. In particular, Eqs. (6.96), (6.100), (6.102) and (6.103) show that wear causes the center of the contact region to shift in the direction of translation of the disk (opposite to the  $x$ -axis), thus decreasing the displacement of the center of the contact region arising from friction forces for  $\omega R - V < 0$ , and increasing this displacement for  $\omega R - V > 0$ .

Of interest is the case  $\frac{\omega R}{V} = 1 - \frac{\pi\vartheta K\mu}{K_w}$ , for  $\frac{\omega R}{V} < 1$ , when, by virtue of Eq. (6.96),  $m = 0$ , and hence  $\eta = 0$ . In this case the contact pressure has the same distribution as in the case of parabolic punch in the frictionless contact with the elastic half-plane (Galin, 1953). The only exception is that the center of the contact region is shifted by an amount  $\pi\vartheta K R \tau_0$  opposite to the direction of translation of the disk (in the  $x$  direction). The corresponding wear distribution  $W_*(x)$ , in accordance with Eq. (6.91), has the form

$$W_*(x) = \frac{K_w |\omega R - V|}{\pi RVK} \left\{ \frac{1}{2} \left( x - \frac{b-a}{2} \right) \sqrt{(a+x)(b-x)} + \frac{(a+b)^2}{8} \left[ \arcsin \left( 2 \frac{x+a}{a+b} - 1 \right) + \frac{\pi}{2} \right] \right\}.$$

Note also that, in the absence of rotation of the disk ( $\omega = 0$ ), solution (6.101)–(6.103) is independent of the translation velocity  $V$  of the disk.

The solution obtained here can be used to analyze the process of wearing of a material by an abrasive tool.

## 6.7 Wear of a thin elastic layer

The method described in § 6.4 can be used to investigate the wear kinetics of a thick layer bonded to an elastic foundation. If the irreversible displacement of the layer surface due to wear is commensurate with the elastic displacement, and much less than the thickness of the layer, we can use the same relationship between elastic displacement and contact pressure as in the contact problem without wear. In this case the operator  $A$  in Eq. (6.7) does not depend on time under the supplementary assumption that the contact area remains constant during the wear process.

However it is not possible to use this method to investigate the wear process of thin coatings. For thin coatings, the wear displacement can be commensurate with the thickness of the coating. For instance, it is important in practice to know the lifetime of the coating, which is estimated by the time when the wear displacement at any point is equal to the thickness of the coating.

It is difficult to obtain the exact solution of this problem, because we do not know the operator  $A$  (see Eq. (6.7)) for the contact problem with a complex shaped

boundary. Below, we examine an approximate solution which makes it possible to analyze the kinetics of changes of all the contact characteristics and the coating thickness during the wear process.

### 6.7.1 Problem formulation

We investigate a contact of a cylindrical punch and a layered elastic foundation. The coordinate system ( $Oxyz$ ) is connected with the punch (3) (see Fig. 6.9), which has a shape function  $z = f(x)$ ,  $f(-x) = f(x)$ . This problem can be considered as two-dimensional. We assume that the elastic modulus of the coating (1) less than that of the foundation (2). The coating is modeled as an elastic strip lying on the elastic half-plane without friction (problem 1), or bonded to the elastic half-plane (problem 2).

The strip is worn by the punch sliding along the  $y$ -axis. We assume that  $h(x, 0) = h_0$ , and the wear rate  $\frac{\partial h(x, t)}{\partial t}$  is proportional to the contact pressure  $(p(x, t))^\alpha$ :

$$\frac{\partial h(x, t)}{\partial t} = -K_w \left[ \frac{p(x, t)}{p^*} \right]^\alpha, \quad (6.104)$$

where  $K_w$  is the wear coefficient and  $p^*$  is a standard pressure.

The punch is loaded by a constant normal force  $P$ . The tangential stress within the contact region is directed along the  $y$ -axis, so that  $\tau_{xz} = 0$ . The component  $\tau_{yz}$  of the tangential stress does not influence the contact pressure distribution, which can be found as the solution of a plane contact problem. The component  $\tau_{yz}$  influences the wear rate and can be taken into account by the wear coefficient  $K_w$ .

The contact condition of the points of the punch and the worn strip surface for  $x \in (-a, a)$  at any instant in time has a form

$$h(x, t) - h(0, t) + (w(x, t) - w(0, t)) = f(x), \quad f(0) = 0, \quad (6.105)$$

where  $w(x, t)$  is the elastic displacement of the strip surface in the direction of the  $z$ -axis,  $a$  is the half-contact width, which is assumed to be fixed in the wear process.

The displacement gradient  $w'_x(x, 0) = \frac{\partial w(x, 0)}{\partial x}$  of the elastic strip loaded by a normal pressure  $p(x, 0)$  can be obtained from the following equation given by Aleksandrova (1973)

$$\int_{-a}^a p(x', 0) K \left( \frac{x' - x}{h_0} \right) dx' = \pi h_0 E_1^* w'_x(x, 0), \quad |x| \leq a, \quad (6.106)$$

$$E_i^* = \frac{E_i}{2(1 - \nu_i^2)},$$

where  $E_i$ ,  $\nu_i$  are Young's moduli and Poisson's ratios of the strip ( $i = 1$ ) and the half-plane ( $i = 2$ ), respectively.

The kernel of the integral equation (6.106) has the form

$$K(t) = \int_0^{+\infty} N(u) \sin tu du, \quad (6.107)$$

where for problem 1

$$N(u) = \frac{\cosh 2u - 1 + n(2u + \sinh 2u)}{2u + \sinh 2u + n(\cosh 2u - 1 - 2u^2)},$$

and for problem 2

$$N(u) = \frac{M + 4u \exp(-2u) - L \exp(-4u)}{M - (1 + 4u^2 + LM) \exp(-2u) + L \exp(-4u)},$$

$$M = \frac{\mu_2 \kappa_1 + n \mu_1}{n \mu_1 - \mu_2}, \quad L = \frac{n \mu_1 \kappa_2 - \mu_2 \kappa_1}{n \mu_1 \kappa_2 + \mu_2},$$

where

$$\mu_i = 1 - \nu_i, \quad \kappa_i = 3 - 4\nu_i, \quad n = \frac{E_1^*}{E_2^*}.$$

We can use the representation of the kernel  $K(t)$  given by Aleksandrova (1973), which is valid for large  $t$  and small  $n$

$$K(t) \sim \frac{n}{t} - A\pi\delta'(t), \quad (6.108)$$

where

$$A = \frac{1}{2} - \text{for problem 1},$$

$$A = \frac{2(1-n)(\kappa-1)(2-n+n\kappa)}{(\kappa+1)^2} - \text{for problem 2} \quad (6.109)$$

if  $\nu_1 = \nu_2 = \nu, \quad \kappa_1 = \kappa_2 = \kappa,$

$\delta(t)$  – Dirac's function.

Substituting Eq. (6.108) in Eq. (6.106), we can obtain the integral equation

$$\frac{Ah}{E_1^*} p'(x, 0) + \frac{1}{\pi E_2^*} \int_{-a}^a \frac{p(x', 0) dx'}{x' - x} = -w'(x, 0). \quad (6.110)$$

Aleksandrova (1973) showed that this equation holds for a thin strip  $\left(\frac{h}{a} \ll 1\right)$ , and  $n \leq 2$ .

Integrating both sides of Eq. (6.110) with respect to  $x$ , we obtain

$$\begin{aligned} & -\frac{Ah_0}{E_1^*} [p(x, 0) - p(0, 0)] + \\ & \frac{1}{\pi E_2^*} \int_{-a}^a p(x', 0) \ln \left| \frac{x' - x}{x'} \right| dx' = w(x, 0) - w(0, 0). \end{aligned} \quad (6.111)$$

The first term in the left side of this equation can be considered as the displacement of the strip surface which behaves like a Winkler elastic foundation with proportionality coefficient  $k = \frac{Ah_0}{E_1^*}$ . This interpretation of the first term in Eq. (6.111) makes sense if it is examined together with the second term, which is the substrate displacement  $w_2(x, 0)$ .

It was proved by Soldatenkov (1994) that for slight relative change of the strip thickness ( $h'(x) \ll 1$ ), Eq. (6.111) still holds, except that the first term takes the form

$$w_1(x, t) = -\frac{A}{E_1^*} [h(x, t)p(x, t) - h(0, t)p(0, t)]. \quad (6.112)$$

Eq. (6.111) with the first term  $w_1(x, t)$  in the form of Eq. (6.112) is the generalization of the foregoing interpretation of Eq. (6.111) to the case of variable  $h(x, t)$ . It can be written as

$$\begin{aligned} & -\frac{A}{E_1^*} [h(x, t)p(x, t) - h(0, t)p(0, t)] + \\ & \frac{1}{\pi E_2^*} \int_{-a}^a p(x', t) \ln \left| \frac{x' - x}{x'} \right| dx' = w(x, t) - w(0, t). \end{aligned} \quad (6.113)$$

Substituting Eq. (6.113) into Eq. (6.105), we obtain the equation for determining the contact pressure at an arbitrary instant of time

$$\begin{aligned} & h(x, t) - h(0, t) - \frac{A}{E_1^*} [h(x, t)p(x, t) - h(0, t)p(0, t)] + \\ & \frac{1}{\pi E_2^*} \int_{-a}^a p(x', t) \ln \left| \frac{x' - x}{x'} \right| dx' = f(x). \end{aligned} \quad (6.114)$$

The strip thickness at any instant of time is determined from Eq. (6.104)

$$h(x, t) = h_0 - K_w \int_0^t \left[ \frac{p(x, t')}{p^*} \right]^\alpha dt'. \quad (6.115)$$

In addition we have the equilibrium equation

$$\int_{-a}^a p(x, t) dx = P. \quad (6.116)$$

### 6.7.2 The dimensionless analysis

We note that if the function  $f(x)$  is symmetrical, we obtain symmetrical solutions  $p(x, t)$  and  $h(x, t)$  of Eqs. (6.114)–(6.116). We assume that the shape of the punch allows the contact region to be constant during the wear process (Fig. 6.9).

We introduce the dimensionless quantities

$$\xi = \frac{x}{a}, \tau = t \frac{K_w}{a}, \bar{P} = \frac{P}{aE_2^*},$$

$$\bar{h}_0 = \frac{h_0}{a}, \bar{h}(\xi, \tau) = \frac{1}{a} h \left( \xi a, \tau \frac{a}{K_w} \right), R = \frac{A}{n}, \quad (6.117)$$

$$\bar{p}(\xi, \tau) = \frac{1}{E_2^*} p \left( \xi a, \tau \frac{a}{K_w} \right), \bar{f}(\xi) = \frac{1}{a} f(\xi a).$$

The system of equations (6.115)–(6.116) can be rewritten in the dimensionless form

$$\bar{h}(\xi, \tau) = \bar{h}_0 - \int_0^\tau \left[ \frac{\bar{p}(\xi, \tau')}{\bar{p}^*} \right]^\alpha d\tau', \quad (6.118)$$

$$\bar{h}(\xi, \tau) - \bar{h}(0, \tau) - R [\bar{h}(\xi, \tau) \bar{p}(\xi, \tau) - \bar{h}(0, \tau) \bar{p}(0, \tau)] +$$

$$\frac{1}{\pi} \int_{-1}^1 \bar{p}(\xi', \tau) \ln \left| \frac{\xi' - \xi}{\xi'} \right| d\xi' = \bar{f}(\xi), \quad (6.119)$$

$$\int_{-1}^1 \bar{p}(\xi, \tau) d\xi = \bar{P}. \quad (6.120)$$

The solution of the wear contact problem is found from this system of equations.

### 6.7.3 Calculation techniques and numerical results.

To solve equations (6.118)–(6.120) we convert from continuous time to discrete time by breaking the time down into small intervals  $(\tau_k, \tau_{k+1})$ :  $\tau_{k+1} = \tau_k + \Delta\tau$ ,  $\tau_0 = 0$ ,  $k = 0, 1, \dots$ . Then the system (6.118)–(6.120) can be approximated by the following relations

$$\bar{h}_{k+1}(\xi) = \bar{h}_k(\xi) - \left[ \frac{\bar{p}_k(\xi)}{\bar{p}^*} \right]^\alpha \Delta\tau, \quad \bar{h}_0(\xi) = \bar{h}_0. \quad (6.121)$$

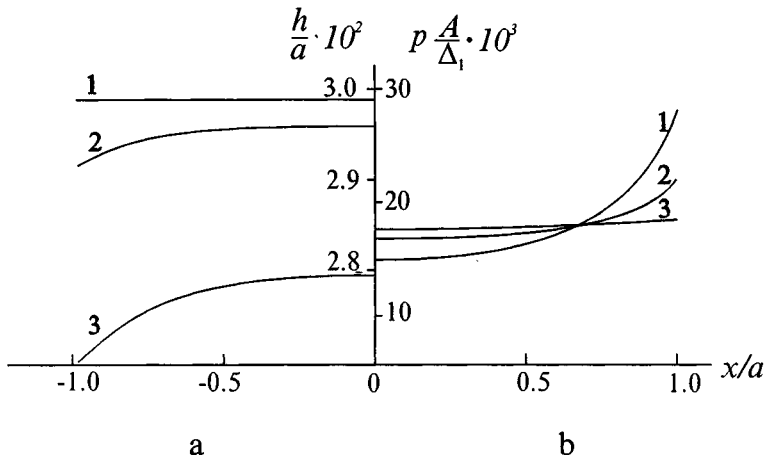


Figure 6.13: Profile of the worn surface of the layer (a) and pressure distribution (b) within the contact region during the wear process:  $\tau = 0$  (curve 1),  $\tau = 0.15$  (curve 2),  $\tau = 0.64$  (curve 3).

$$\bar{h}_k(\xi) - \bar{h}_k(0) - R [\bar{h}_k(\xi)\bar{p}_k(\xi) - \bar{h}_k(0)\bar{p}_k(0)] + \frac{1}{\pi} \int_{-1}^1 \bar{p}_k(\xi') \ln \left| \frac{\xi' - \xi}{\xi'} \right| d\xi' = \bar{f}(\xi), \quad (6.122)$$

$$\int_{-1}^1 \bar{p}_k(\xi) d\xi = \bar{P}, \quad (6.123)$$

which become the relations (6.118)–(6.120) as  $\Delta\tau \rightarrow 0$ . The function  $\bar{p}_k(\xi)$  found from Eqs. (6.122) and (6.123) determines in accordance with Eq. (6.121), the function  $\bar{h}_{k+1}(x)$  at the following moment. As a result we obtain the pressure distribution at various instants of discrete time in the strip wear process.

For the solution of the system of equations (6.122) and (6.123), we use the method of transformation of integral equations to finite-dimensional systems of linear equations (Kantorovich and Krylov, 1952).

For the numerical calculations, we assume that the strip is bonded to the substrate (problem 2) and that the rigidity of the strip is less than the substrate one. This case can be applied to investigate the wear of solid lubricant coatings.

For the calculation, we took the shape function  $\bar{f}(\xi) = 10^{-3}\xi^2$  and the following values of the dimensionless parameters:  $\alpha = 1.4$ ,  $R = 3.8$ ,  $\bar{p}^* = 0.26$ ,  $\bar{h}_0 = 3 \cdot 10^{-2}$ ,  $\bar{P} = 9 \cdot 10^{-3}$ .

Fig. 6.13 illustrates the contact pressure distribution and the worn surface profile at various times. In the wear process the contact pressure equalizes, i.e.

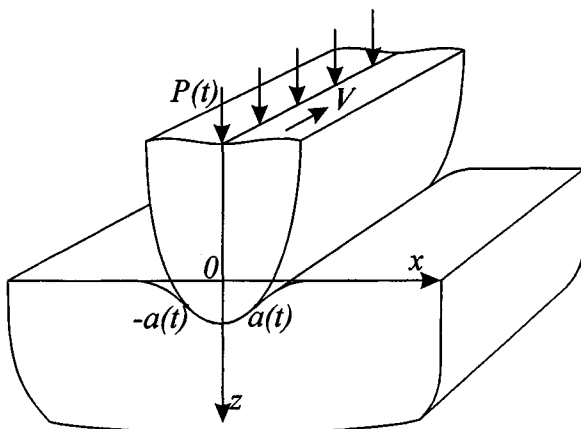


Figure 6.14: Scheme of the contact with time-dependent contact region in the wear process.

running-in of the rubbing surface occurs. The results show that equalization of the contact pressure is followed by the stabilization of the worn surface profile.

The analysis of the dependence of the running-in time on the initial layer thickness is presented in Goryacheva and Soldatenkov (1983). They also investigated the wear of the coating during the running-in time and the lifetime of coating for various values of the parameters of the problem.

## 6.8 Problems with a time-dependent contact region

Contact problems with a fixed contact region have been considered in § 6.3–§ 6.7. The contact area was determined by the punch shape, and did not change during the wear process. Generally the assumption of a constant contact region is roughly satisfied for small changes of the shape of contacting bodies in wear process.

If the contact region changes during the wear process, i.e.  $a = a(t)$ , the operator  $A$  in Eq. (6.7) depends on time. The contact problem becomes nonlinear even if the wear process (6.12) is linear. To analyze the main features of the wear process for this case, we use the simplest model of an elastic body which is a Winkler elastic foundation.

### 6.8.1 Problem formulation

We consider a cylindrical punch ( $z = f(x)$ , where  $f(x)$  is a differentiable function) which moves over the elastic foundation in the direction of  $y$ -axis with the velocity  $V$  (see Fig. 6.14). We assume that the elastic displacement  $w(x, t)$  in the direction

of the  $z$ -axis is determined by the formula

$$w(x, t) = kp(x, t), \quad (6.124)$$

where  $k = \frac{h}{K}$ ,  $K$  is the elastic modulus of the foundation,  $h$  is its depth,  $p(x, t)$  is a contact pressure.

We assume that the wear of the punch surface is considerably less than the wear of the foundation, so we take into account only the wear of the foundation. The wear equation is considered in the linear form

$$\frac{\partial w_*(x, t)}{\partial t} = K_w p(x, t), \quad (6.125)$$

where the wear coefficient  $K_w$  can depend on the velocity  $V$ , temperature, coefficient of friction, etc.

The condition that the points of the punch and foundation coincide within the contact zone  $(-a(t), a(t))$  at an arbitrary instant of time is written as

$$w(x, t) + w_*(x, t) = D(t) - f(x), \quad -a(t) \leq x \leq a(t). \quad (6.126)$$

Here  $D(t)$  is the displacement of the punch along the  $z$ -axis.

The force  $P(t)$  is applied to the punch (see Fig. 6.14), so the following equilibrium equation must be satisfied at an arbitrary instant of time

$$\int_{-a(t)}^{a(t)} p(x, t) dx = P(t). \quad (6.127)$$

The contact pressure is equal to zero at the ends of the contact region because of smoothness of the punch shape, so

$$p(\pm a(t), t) = 0. \quad (6.128)$$

The equations (6.124)–(6.128) are used to find the unknown functions  $p(x, t)$ ,  $w(x, t)$ ,  $w_*(x, t)$ ,  $a(t)$  and  $D(t)$ .

### 6.8.2 The cases of increasing, decreasing and constant contact region

Let us consider the Eq. (6.126) at the end of the contact region  $a(t)$ . Taking into account Eqs. (6.124) and (6.128), we obtain

$$w_*(a(t), t) = D(t) - f(a(t)). \quad (6.129)$$

Subtracting Eq. (6.129) from Eq. (6.126) gives

$$w(x, t) + w_*(x, t) - w_*(a(t), t) = f(a(t)) - f(x). \quad (6.130)$$

After differentiation Eq. (6.130) with respect to time and use of Eqs. (6.124) and (6.125) we obtain

$$k \frac{\partial p(x, t)}{\partial t} + K_w p(x, t) - K_w p(a, t) - \frac{\partial w_*(x, t)}{\partial a} \cdot \frac{da}{dt} = \frac{df}{da} \cdot \frac{da}{dt}. \quad (6.131)$$

Eq. (6.131) is valid within the contact region  $(-a(t), a(t))$ . Upon integrating Eq. (6.131) over this region, taking into account Eq. (6.128) and the relationship

$$\frac{d}{dt} \int_{-a}^a p(x, t) dx = \int_{-a}^a \frac{\partial p(x, t)}{\partial t} dx,$$

we have

$$kP'(t) + K_w P(t) = \left[ f'(a) + \frac{\partial w_*(x, t)}{\partial a} \right] \frac{da}{dt} 2a. \quad (6.132)$$

The conditions corresponding to the cases of increasing, decreasing and constant contact region can be obtained based on Eq. (6.132).

Let us consider the case of increasing contact region, i.e.  $\frac{da}{dt} > 0$ , and find the restriction imposed on the function  $P(t)$ . Eqs. (6.125) and (6.128) show that the relation  $w_*(a(t), t) = 0$  is valid for an arbitrary moment of time. Differentiating this identity with respect to time, we obtain

$$\frac{\partial w_*}{\partial t} + \frac{\partial w_*}{\partial a} \cdot \frac{da}{dt} = 0.$$

It follows from Eqs. (6.125) and (6.128) that  $\frac{\partial w_*}{\partial t} = 0$ . So

$$\frac{\partial w_*}{\partial a} \cdot \frac{da}{dt} = 0.$$

Then it follows from Eq. (6.132) that the rate of the contact width increase is calculated by

$$\frac{da}{dt} = \frac{kP'(t) + K_w P(t)}{2af'(a)}. \quad (6.133)$$

If the assumption is made that  $f'(a) > 0$ , the following conditions should be satisfied for the increase of the contact area

$$\frac{P'(t)}{P(t)} > -\frac{K_w}{k}. \quad (6.134)$$

As an example, let us consider the contact of a smooth punch with shape  $\frac{x^2}{2R}$  which is loaded by the constant force  $P(t) = P_0$ . It is evident that the condition (6.134) is fulfilled. To find the contact width at an arbitrary instant of time we can use the equation which follows from Eq. (6.133) in this particular case

$$\frac{da}{dt} = \frac{K_w P_0 R}{2a^2}.$$

Upon integrating this equation we obtain

$$a^3 - a_0^3 = \frac{3}{2} P_0 R K_w t, \quad a_0^3 = \frac{3}{2} P_0 R k$$

or

$$a = a_0 \sqrt[3]{1 + \frac{K_w}{k} t}.$$

Let us find now the condition on the function  $P(t)$  which provides constant contact width, i.e.  $a(t) = a_0$ . Eq. (6.132) for  $\frac{da}{dt} = 0$ , gives the following relation

$$kP'(t) + K_w P(t) = 0,$$

So the contact width is constant if the load changes exponentially with time

$$P(t) = P_0 \exp\left(-\frac{K_w}{k} t\right).$$

Differentiating Eq. (6.129) with respect to time, we obtain

$$\frac{\partial w_*(a(t), t)}{\partial t} + \left( \frac{\partial w_*(a(t), t)}{\partial a} + f'(a) \right) \frac{da}{dt} = D'(t),$$

If  $\frac{da}{dt} = 0$ , from this equation, taking into account Eqs. (6.125) and (6.128), it follows that  $D'(t) = 0$ . So, for the smooth punch, the constant contact width occurs if the approach between the punch and the foundation does not change during the wear process. The contact pressure  $p(x, t)$  is determined by the equation which follows from Eq. (6.131)

$$k \frac{\partial p(x, t)}{\partial t} + K_w p(x, t) = 0.$$

So the contact pressure tends to zero if  $t \rightarrow \infty$  and, as follows from Eq. (6.126), the shape of the worn surface is the same as the initial shape of the punch  $f(x)$ .

It is easy to show in a similar manner, that the contact width decreases, i.e.  $\frac{da}{dt} < 0$ , if the load  $P(t)$  satisfies the equation

$$\frac{P'(t)}{P(t)} < -\frac{K_w}{k}.$$

It should be noted that this analysis holds for the simple model described above. Similar analyses can be applied to investigate more complicated contact problems with time-dependent contact region.

The example of the solution of the wear contact problem with increasing contact width in wear process is given in § 8.1.

# Chapter 8

## Wear of Components

In this chapter we give some applications of the methods presented in Chapter 6 to the analysis of the wear kinetics of some components. Study of wear kinetics makes it possible to predict the durability of moving parts of machines during operation; this is one of the most important problems in tribology.

The first junction investigated in this chapter is the plain journal bearing. Recently considerable success has been gained in the calculation of the wear kinetics of journal bearings of different types. An algorithm accounting for wear of the journal only was developed in Blyumen, Kharach and Efros (1976) for a plain journal bearing with thick-wall sleeve. This study is based on Hertzian contact and a power-law dependence of the wear rate on the contact pressure. (This is the wear equation that is used in most studies.) A more complete solution of this problem was given by Usov, Drozdov and Nikolashev (1979), where journal and sleeve wear were both taken into account.

Journal bearings with antifriction coatings were studied by Bogatin and Kaniabolotsky (1980), Kuzmenko (1981), Kovalenko (1982), Goryacheva and Dobychin (1984a, 1984b), Soldatenkov (1985). The design of a sliding pair with a protective coating which prevents severe wear and decreases the friction losses is of interest for engineering. The wear of journal bearings depends on the coating location, either at the bush or at the shaft surface. In the calculation of wear of the journal bearing with coated bush the simplifying assumption is usually made that the thickness of the coating remains constant in the process of wear. Some researches ignore the coating when calculating the contact characteristics of bearings.

In § 8.1–§ 8.3 we discuss the wear of a thin antifriction coating in plain journal bearings when coating is either at the bush or at the shaft surface. In calculation of the wear kinetics we do not use the assumptions we just noted; this allows us to obtain a better model of journal bearings with antifriction coatings.

We also discuss the important rail-wheel contact problem in this chapter. In his monograph devoted to the mechanics of rolling contact Kalker (1990) stated: “The motion that rail and wheel perform with respect to each other is very complicated

and varied, yet it is found that the worn form of wheel and rail converge to standard forms. It would be interesting if such standards could arise from theoretical studies and simulations." Some approaches to rail and wheel wear analysis are presented in § 8.4.

In § 8.5 we discuss a model of the wear of a tool in rock cutting. This problem was investigated in a set of theoretical and experimental works. Some new approaches to the solution have been recently proposed by Hough and Das (1985) and Appl, Wilson and Landsman (1993). The model presented in this chapter was developed by Checkina, Goryacheva and Krasnik (1996). It is based on the analysis of worn tool profiles obtained experimentally. It takes into account the shape variation of both contacting bodies caused by the wear or cutting process. The model is used for calculation of the pressure distribution in a contact zone, and of the variation of forces during cutting process. The influence of tool wear on contact characteristics is also investigated.

We note that the wear kinetics of such widely used moving components as piston rings, slides and guides can be calculated by using the solutions of the wear contact problems described in § 6.2 and § 6.8.

## 8.1 Plain journal bearing with coating at the bush

### 8.1.1 Model assumptions

We consider the plain journal bearing with an antifriction element (coating) located at the bush (direct sliding pair, DSP). Fig. 8.1 illustrates the scheme of contact in the plain journal bearing consisting of the shaft  $S_1$ , the bush  $S_2$  and the coating  $S_0$ . The shaft  $S_1$  is loaded uniformly along its directrix with a load  $P$  per unit length. The shaft rotates with angular velocity  $\omega$  about the axis  $Oz$  which is perpendicular to the scheme plane. The wear occurs in the sliding process.

Before investigating the wear kinetics of this junction we make some assumptions. Usually the wear resistance of the shaft is greater than the wear resistance of the antifriction coating. So we neglect the wear of the shaft and assume that only the coating  $S_0$  wears.

It is typical for journal bearings that the elasticity modulus of the antifriction coating is 2-3 orders less than the moduli of the bush and shaft materials. Because of this we will assume that the bodies  $S_1$  and  $S_2$  are rigid and  $S_0$  is elastic.

Antifriction coatings, as a rule, have a thickness of  $10\text{--}100 \mu$ . Such small thickness of coatings can be explained by their low heat conductivity. The thinner the coating, the less is its size instability due to heat expansion and swelling and the greater is the stiffness of the junction. For this reason we will assume in what follows that the initial thickness of the antifriction coating  $h_0 = h(0)$  is small, i.e.  $h_0/R_0 \ll 1$ , where  $R_0$  is the inner radius of the coating.

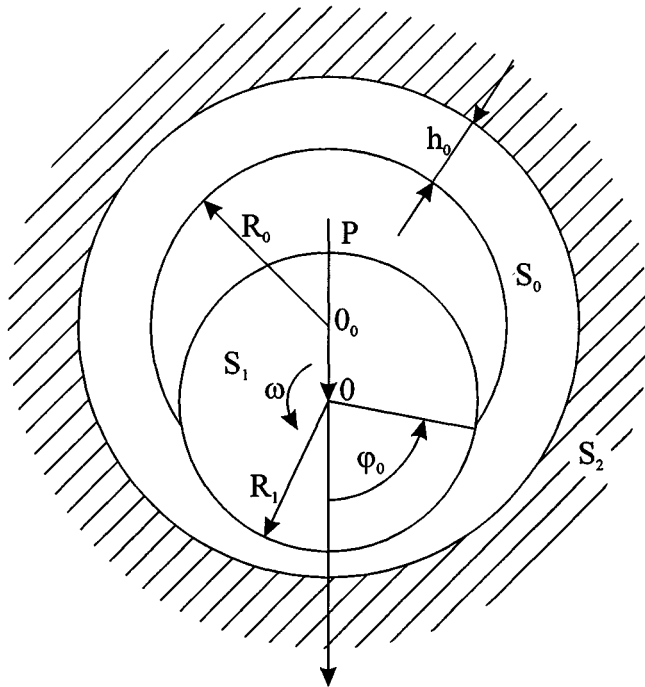


Figure 8.1: Scheme of plain bearing with coating applied on the bush (direct sliding pair, DSP)

### 8.1.2 Problem formulation

Under the assumptions of § 8.1.1 the wear kinetics of the journal bearing is reduced to a study of the wear of a thin coating \$S\_0\$ of initial thickness \$h\_0\$ applied on a rigid bush \$S\_2\$. The coating wears by contact interaction with a rigid shaft \$S\_1\$ (Fig. 8.1), loaded by the linear load \$P\$ and rotating with the angular velocity \$\omega\$.

We assume that the wear rate of the coating \$\partial h / \partial t\$ depends on the contact pressure \$p(\varphi, t)\$ and the linear velocity \$V = \omega R\_1\$ (\$R\_1\$ is the radius of the shaft) according to the relation

$$\frac{\partial h(\varphi, t)}{\partial t} = -K_w V p^\alpha(\varphi, t), \quad (8.1)$$

where \$K\_w\$ is a wear coefficient, \$K\_w = c p\_0^{-\alpha}\$, \$c\$, \$p\_0\$ and \$\alpha\$ are characteristics which depend on the mechanical properties of the contacting pair, roughness parameters and a friction coefficient, and can be determined theoretically from wear models or experimentally.

It was shown by Aleksandrov and Mhitaryan (1983) that for a thin elastic layer it is possible to neglect the influence of the tangential contact stress on the normal

one and to consider the thin elastic layer as a Winkler foundation for which the normal elastic displacement  $u(x)$  is proportional to the contact pressure  $p(x)$

$$u(x) = khp(x),$$

where  $h$  is the layer thickness,  $k$  is a coefficient characterizing the layer compliance; for the layer bonded to the rigid foundation it was determined by Aleksandrova (1973) as

$$k = \frac{1 - 2\nu}{2G(1 - \nu)}.$$

Here  $G$  and  $\nu$  are the shear modulus and the Poisson ratio for the layer, respectively ( $G = \frac{E}{2(1 + \nu)}$ ,  $E$  is the Young modulus).

It should be noted that due to nonuniform wear the layer thickness  $h$  varies along the contact region  $|\varphi| \leq \varphi_0$ , i.e.  $h = h(\varphi, t)$ . In previous studies of the wear of plain journal bearing these changes were neglected (see, for example, Kovalenko, 1982). Based on the method of § 6.8 we generalize the Winkler model and use the following relation to describe the layer compliance at an arbitrary instant of time:

$$u_r(\varphi, t) = kh(\varphi, t)p(\varphi, t), \quad (8.2)$$

where  $u_r(\varphi, t)$  is the radial displacement of the boundary points of  $S_0$ .

In the process of wear, not only the layer thickness changes, but the contact angle  $\varphi_0$  varies with a certain rate  $v = d\varphi_0/dt$ . Assuming that the rate  $v$  is positive, we will use the magnitude  $\varphi_0$  as a time parameter. In this case a real time  $t$  is determined by the formula:

$$t(\varphi_0) = \int_{\varphi_{0,0}}^{\varphi_0} \frac{d\varphi}{v(\varphi)}, \quad (8.3)$$

where  $\varphi_{0,0} = \varphi_0(0)$ .

Substituting the real time  $t$  by the parameter  $\varphi_0$  in Eqs. (8.2) and (8.1), we obtain

$$u_r(\varphi, \varphi_0) = kh(\varphi, \varphi_0)p(\varphi, \varphi_0), \quad (8.4)$$

$$\dot{h}(\varphi, \varphi_0) = -\frac{K_w V}{v(\varphi_0)} p^\alpha(\varphi, \varphi_0), \quad (8.5)$$

where

$$\dot{h}(\varphi, \varphi_0) = \frac{\partial h(\varphi, \varphi_0)}{\partial \varphi_0}, \quad h(\pm\varphi_0, \varphi_0) = h_0.$$

To Eqs. (8.4) and (8.5) we add the condition of contact of the bodies  $S_1$  and  $S_0$  within the region  $|\varphi| \leq \varphi_0$

$$h_0 - h(\varphi, \varphi_0) + u_r(\varphi, \varphi_0) = d(\varphi, \varphi_0), \quad (8.6)$$

where

$$d(\varphi, \varphi_0) = \Delta \left( \frac{\cos \varphi}{\cos \varphi_0} - 1 \right), \quad (8.7)$$

$\Delta$  is the initial clearance ( $\Delta = R_0 - R_1$ ).

Also we take into account the equilibrium equation

$$R_1 \int_{-\varphi_0}^{\varphi_0} p(\varphi, \varphi_0) \cos \varphi d\varphi = P. \quad (8.8)$$

Eqs. (8.4), (8.5), (8.6) and (8.8) comprise the basic system of equations of the problem.

### 8.1.3 Method of solution

We give the solution developed by Soldatenkov (1985).

From Eqs. (8.4) and (8.6) we derive the relationship for the contact pressure

$$p(\varphi, \varphi_0) = \frac{d(\varphi, \varphi_0) - h_0 + h(\varphi, \varphi_0)}{kh(\varphi, \varphi_0)}. \quad (8.9)$$

Substituting Eq. (8.9) in Eq. (8.8), we transform the equilibrium condition to the form

$$P = \frac{R_1}{k} \int_{-\varphi_0}^{\varphi_0} \frac{d(\varphi, \varphi_0) - h_0 + h(\varphi, \varphi_0)}{h(\varphi, \varphi_0)} \cos \varphi d\varphi. \quad (8.10)$$

Substituting  $\varphi_0 = \varphi_{0,0}$  and Eq. (8.7) in Eq. (8.10), and taking into account, that  $h(\varphi, \varphi_{0,0}) = h_0$ , we find the following relation between the problem characteristics

$$\frac{kPh_0}{R_1 \Delta} = \frac{\varphi_{0,0}}{\cos \varphi_{0,0}} - \sin \varphi_{0,0}. \quad (8.11)$$

It should be remarked that the elastic displacement at any point is always less than the layer thickness, i.e.  $u_r(\varphi, \varphi_0) < h(\varphi, \varphi_0)$ . From this condition it follows

$$\cos \varphi_0 > \frac{\Delta}{h_0 + \Delta}.$$

This is a restriction on the initial characteristics of the bearing.

Differentiating Eq. (8.10) with respect to the parameter  $\varphi_0$  and taking into account Eq. (8.5), we derive the following relationship to determine the rate of change of the contact angle  $\varphi_0$

$$v(\varphi_0) = \frac{VK_w \int_{-\varphi_0}^{\varphi_0} \frac{p^\alpha(\varphi, \varphi_0) [1 - kp(\varphi, \varphi_0)]}{h(\varphi, \varphi_0)} \cos \varphi d\varphi}{\Delta \cdot \frac{\sin \varphi_0}{\cos^2 \varphi_0} \int_{-\varphi_0}^{\varphi_0} \frac{\cos^2 \varphi d\varphi}{h(\varphi, \varphi_0)}}. \quad (8.12)$$

So we have the system of equations (8.5), (8.9) and (8.12) to calculate the functions  $p(\varphi, \varphi_0)$ ,  $h(\varphi, \varphi_0)$  and  $v(\varphi_0)$ . The real time  $t$  can be calculated from Eq. (8.3) where the initial contact angle  $\varphi_{0,0}$  is found from Eq. (8.11).

We introduce the dimensionless coordinate  $\bar{\varphi} = \varphi/\varphi_0$  and corresponding functions  $\bar{h}(\bar{\varphi}, \varphi_0) = h(\bar{\varphi}\varphi_0, \varphi_0)/h_0$ ,  $\bar{p}(\bar{\varphi}, \varphi_0) = p(\bar{\varphi}\varphi_0, \varphi_0)K_w^{1/\alpha}$ . Then Eq. (8.5) is transformed to the following

$$\frac{\partial \bar{h}(\bar{\varphi}, \varphi_0)}{\partial \varphi_0} - \frac{\bar{\varphi}}{\varphi_0} \frac{\partial \bar{h}(\bar{\varphi}, \varphi_0)}{\partial \bar{\varphi}} = -\frac{V}{h_0 v(\varphi_0)} \bar{p}^\alpha(\bar{\varphi}, \varphi_0). \quad (8.13)$$

The boundary conditions for Eq. (8.13) are  $\bar{h}(\bar{\varphi}, \varphi_{0,0}) = 1$ ,  $\bar{h}(\pm 1, \varphi_0) = 1$ .

The numerical calculation is based on step by step integration of the partial differential equation (8.13) along characteristics, taking into account the boundary conditions and Eqs. (8.3), (8.9), (8.10) and (8.12). That is, using the known values (on the first step - from initial conditions)  $\varphi_0$ ,  $\bar{h}(\bar{\varphi}, \varphi_0)$ ,  $\bar{p}(\bar{\varphi}, \varphi_0)$  and, consequently,  $v(\varphi_0)$  and  $d\varphi_0$ , we determine the increment of the function  $\bar{h}(\bar{\varphi}, \varphi_0)$  along the characteristics of Eq. (8.13). The characteristics are the family of hyperbolas  $\varphi_0 = C/\bar{\varphi}$ ;  $C$  is a parameter of the family. Then we determine the increment of the time  $dt$  from Eq. (8.3) and the new value of the pressure  $\bar{p}(\bar{\varphi}, \varphi_0 + d\varphi_0)$  from Eq. (8.9). Values of  $\varphi_0 + d\varphi_0$ ,  $t + dt$ ,  $\bar{h}(\bar{\varphi}, \varphi_0 + d\varphi_0)$ ,  $\bar{p}(\bar{\varphi}, \varphi_0 + d\varphi_0)$  are initial data for the next step in respect to the angle  $\varphi_0$ .

Based on this procedure we calculate the changes of the contact angle, contact pressure and thickness of the coating in time.

Note that Soldatenkov (1987) used a similar procedure to calculate the wear of a thin coating applied on the bush of a plain journal bearing, taking into account the elastic properties of the bush and the shaft.

#### 8.1.4 Wear kinetics

Calculations were carried out for the following values of the parameters:

$$\frac{kP}{R_1} = 0.9 \cdot 10^{-2}, \quad \frac{\Delta}{h_0} = 10^{-1}, \quad \alpha = 1, \quad \frac{k}{K_w} = 9 \cdot 10^5.$$

Fig. 8.2 illustrates the contact pressure distribution for times  $\bar{t} = \frac{tV}{h_0}$ . The dependence of the maximum contact pressure  $p_{\max}$ , the minimum value of the coating thickness  $h_{\min}$  and the contact angle  $\varphi_0$  on time are presented in Fig. 8.3. The results show that the maximum contact pressure and the average contact pressure decrease during the wear process.

Based on the results, we can divide the wear process of this type of journal bearing into two stages: the running-in ( $0 \leq t \leq T$ ), and steady-state stage ( $t > T$ ). In the running-in stage, the values of  $p_{\max}$  change considerably according to a non-linear law. It is evident that the running-in time  $T$  has to satisfy the condition  $T \ll T^*$ , where  $T^*$  is the bearing lifetime determined from the condition  $h(0, \varphi_0(T^*)) = 0$ .

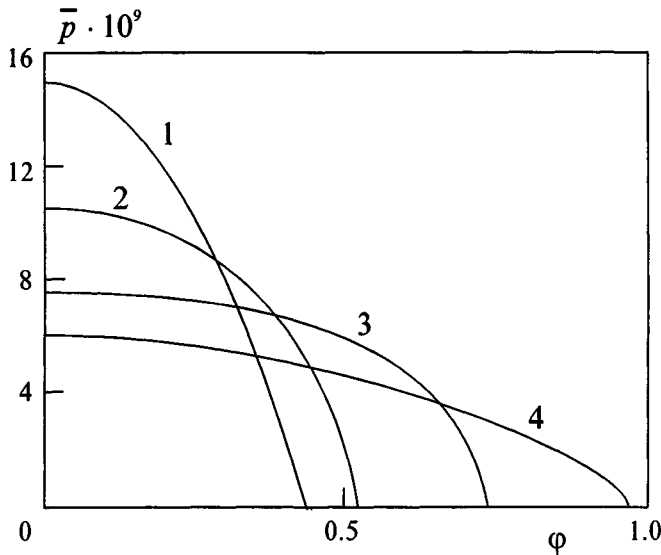


Figure 8.2: Pressure distribution within the contact region  $\varphi \leq \varphi_0$  ( $\varphi$  is expressed in radians) for the journal bearing (DSP) at different instants of time:  $\bar{t} = 0$  (curve 1);  $\bar{t} = 0.2 \cdot 10^7$  (curve 2);  $\bar{t} = 0.9 \cdot 10^7$  (curve 3);  $\bar{t} = 5.6 \cdot 10^7$  (curve 4).

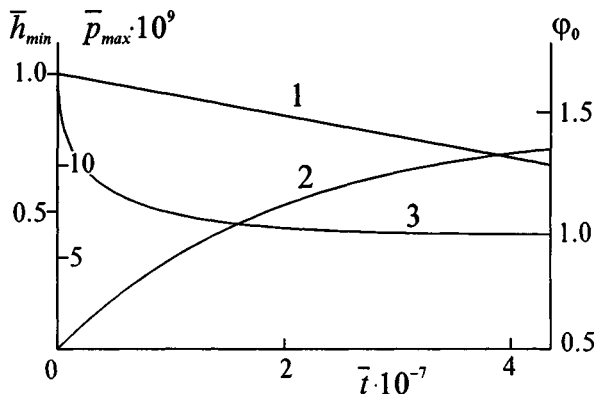


Figure 8.3: Dependence of the minimum value of the coating thickness  $\bar{h}_{min}$  (curve 1), the contact angle  $\varphi_0$  (curve 2) and the maximum contact pressure  $\bar{p}_{max}$  (curve 3) on time for the plain journal bearing (DSP).

The near-linear dependence of the value of  $h_{\min}$  on time makes it possible to calculate the lifetime  $T^*$  using linear interpolation of the function  $h_{\min}(t)$ . For the case under consideration  $\bar{T}^* = 1.5 \cdot 10^8$ .

In the steady-state stage the values of the maximum contact pressure  $p_{\max}$  change with an approximately constant rate. Due to this fact we can suggest some simplifications to the steady-state analysis.

### 8.1.5 Steady-state stage of wear process

For the bearing under consideration, the contact pressure cannot be stationary in the steady-state stage because the contact angle varies due to coating wear. However, the analysis of the numerical results shows that the contact pressure in the steady-state stage can be characterized by the stationary function  $p_s(\varphi, \varphi_0)$ , including the contact angle  $\varphi_0$  as parameter. This function can be determined from the following equation which is obtained by differentiating Eq. (8.6) with respect to  $\varphi_0$  and taking into account Eq. (8.5)

$$K_w V [p_s(\varphi, \varphi_0)]^\alpha \frac{1 - k p_s(\varphi, \varphi_0)}{\cos \varphi} = \Omega(\varphi_0), \quad (8.14)$$

where

$$\Omega(\varphi_0) = v(\varphi_0) \Delta \frac{\sin \varphi_0}{\cos^2 \varphi_0}. \quad (8.15)$$

We introduce the function

$$\varepsilon(\varphi_0) = \frac{\int_{-\varphi_0}^{\varphi_0} \left| K_w V [p(\varphi, \varphi_0)]^\alpha \frac{[1 - k p(\varphi, \varphi_0)]}{\cos \varphi} - \Omega(\varphi_0) \right| d\varphi}{\Omega(\varphi_0)} \quad (8.16)$$

which characterizes the deviation of the wear process from the steady-state stage. We assume that the steady-state stage begins at  $t(\tilde{\varphi}_0) = T$  if  $\varepsilon(\tilde{\varphi}_0) < 0.05$ .

The approximate formula and tables for calculation of the running-in time  $T$  and the contact angle  $\tilde{\varphi}_0$  corresponding to the time  $T$  are in Goryacheva and Dobychin (1988).

We will obtain here the characteristics of the steady-state stage of the wear process ( $t > T$ ), indicating these characteristics by the index  $S$ . To simplify the analysis we consider the case  $k p \ll 1$  which is most common in practice. From Eq. (8.14) we obtain

$$p_s(\varphi, \varphi_0) = \left( \frac{\Omega_S(\varphi_0)}{K_w V} \cos \varphi \right)^{\frac{1}{\alpha}}. \quad (8.17)$$

Substituting Eq. (8.17) into equilibrium condition (8.8), we find

$$P = R_1 \left( \frac{\Omega_S(\varphi_0)}{K_w V} \right)^{\frac{1}{\alpha}} \int_{-\varphi_0}^{\varphi_0} (\cos \varphi)^{\frac{1+\alpha}{\alpha}} d\varphi.$$

From this relationship we obtain

$$\Omega_S(\varphi_0) = K_w V \left( \frac{P}{R_1 C_\alpha(\varphi_0)} \right)^\alpha, \quad (8.18)$$

$$\text{where } C_\alpha(\varphi_0) = \int_{-\varphi_0}^{\varphi_0} (\cos \varphi)^{\frac{1+\alpha}{\alpha}} d\varphi.$$

Substituting Eq. (8.18) into Eq. (8.17) we obtain

$$p_S(\varphi, \varphi_0) = \frac{P}{R_1 C_\alpha(\varphi_0)} (\cos \varphi)^{\frac{1}{\alpha}}. \quad (8.19)$$

From Eqs. (8.15) and (8.18) we find the relationship for the rate  $v_S(\varphi_0)$

$$v_S(\varphi_0) = K_w V \left[ \frac{P}{R_1 C_\alpha(\varphi_0)} \right]^\alpha \frac{\cos^2 \varphi_0}{\Delta \cdot \sin \varphi_0}. \quad (8.20)$$

Then the real time  $t$  can be calculated from the following relationship obtained from Eq. (8.3)

$$t_S(\varphi_0) = \int_{\varphi_0}^{\varphi_0} \frac{d\varphi}{v_S(\varphi)} + T. \quad (8.21)$$

Eqs. (8.18)-(8.21) completely describe the steady-state stage of the wear process.

For  $\alpha = 1$  these equations take a simple form. In this case the function  $C_\alpha(\varphi_0) = C_1(\varphi_0)$  is

$$C_1(\varphi_0) = \varphi_0 + \frac{1}{2} \sin 2\varphi_0.$$

From Eqs. (8.19), (8.20) and (8.21) we obtain the contact pressure  $p_S(\varphi, \varphi_0)$ , the angle rate  $v_S(\varphi_0)$  and the time  $t_S(\varphi_0)$  in this case as

$$p_S(\varphi, \varphi_0) = \frac{P \cos \varphi}{R_1 (\varphi_0 + \sin \varphi_0 \cos \varphi_0)}, \quad (8.22)$$

$$v_S(\varphi_0) = \frac{K_w V P \cos^2 \varphi_0}{C_1(\varphi_0) R_1 \cdot \Delta \cdot \sin \varphi_0}, \quad (8.23)$$

$$t_S(\varphi_0) = \frac{R_1 \Delta}{K_w V P \left( \frac{\varphi_0}{\cos \varphi_0} - \sin \varphi_0 - \frac{\tilde{\varphi}_0}{\cos \tilde{\varphi}_0} + \sin \tilde{\varphi}_0 \right)} + T. \quad (8.24)$$

From Eq. (8.6) we can obtain the relationship for the limit contact angle  $\varphi_0^*$  which is found from the condition  $h(0, \varphi_0^*) = 0$ :

$$\varphi_0^* = \arccos \frac{\Delta}{h_0 + \Delta}. \quad (8.25)$$

Thus if we know the load  $P$  applied to the shaft, the geometric characteristics of the bearing ( $R_1$ ,  $\Delta$ ,  $h_0$ ), the shaft linear velocity  $V$ , the mechanical properties of the coating ( $k$ ) and the wear characteristics ( $K_w$  and  $\alpha$ ), we can calculate the lifetime of the bearing and the characteristics of the wear process using the method described above.

## 8.2 Plain journal bearing with coating at the shaft

Journal bearings in which the thin antifriction coating is located on the shaft are finding more and more applications.

The scheme of such a junction (inverse sliding pair, ISP) is presented in Fig. 8.4. As in the previous case, we assume that the coating wears, i.e. the wear of the bush is negligibly small compared to the wear of the soft antifriction coating. We assume also that in operation the coated shaft (journal) remains a circular cylinder with decreasing radius due to wear of the coating.

Thus, the geometry of the contact remains the same for any instant of time. So in the wear kinetics calculation we can use the solution of the same contact problem in which the thickness of the coating is determined from the wear equation at each step of the wear process. This distinguishes the problem from the contact problem for the coated bush and shaft described in the previous section where the equations (8.5), (8.9) and (8.12) were solved simultaneously.

That is why we will first describe the contact problem for the coated shaft and the bush, and then will study the wear kinetics of the junction taking into account the relationship between the contact characteristics and the magnitude of the wear.

### 8.2.1 Contact problem formulation

The plain journal bearing relates to a cylindrical joint with conforming surfaces. Such joints are widespread in engineering (journal bearing, hinges, piston liner assemblies etc.).

In this study we take into account elastic properties of a shaft and a bush. We consider an elastic infinite plate  $S_2$  (Fig. 8.4) with a round hole of radius  $R_2$  and an elastic disk  $S_1$  of radius  $R_1$  inserted into it. A thin layer  $S_0$  of initial thickness  $h_0$ , whose elastic properties differ from those of the disk, is applied on the disk surface. It is supposed that the radii  $R_2$  and  $R_0 = R_1 + h_0$  are close, i.e.  $(R_2 - R_0)/R_2 \ll 1$  and the layer thickness is small,  $h_0/R_1 \ll 1$ . In this joint the cylinder  $S_1$  with coating  $S_0$  is an analogue of the journal, the cylinder itself is an analogue of shaft, and the elastic body  $S_2$  is the model of the bush. The journal is loaded by a normal force uniformly distributed over its length, so that at each section perpendicular to the journal axis there is a linear load  $P$ . The journal rotates with angular velocity  $\omega$ .

Hertz theory applied to the calculation of the contact characteristics of this junction may lead to considerable errors, since in this case the condition that the dimension of the contact region must be small compared with the dimensions of each body is not always satisfied.

To solve the contact problem we use the method suggested by Kalandiya (1975). We introduce the system of coordinates ( $XOY$ ) related to the center  $O$  of the disk. Simultaneously we consider the plane of the complex variable  $z = x + iy$  where  $x = X/R_2$  and  $y = Y/R_2$ . In the  $x, y$ -plane the radii of the disk with coating and

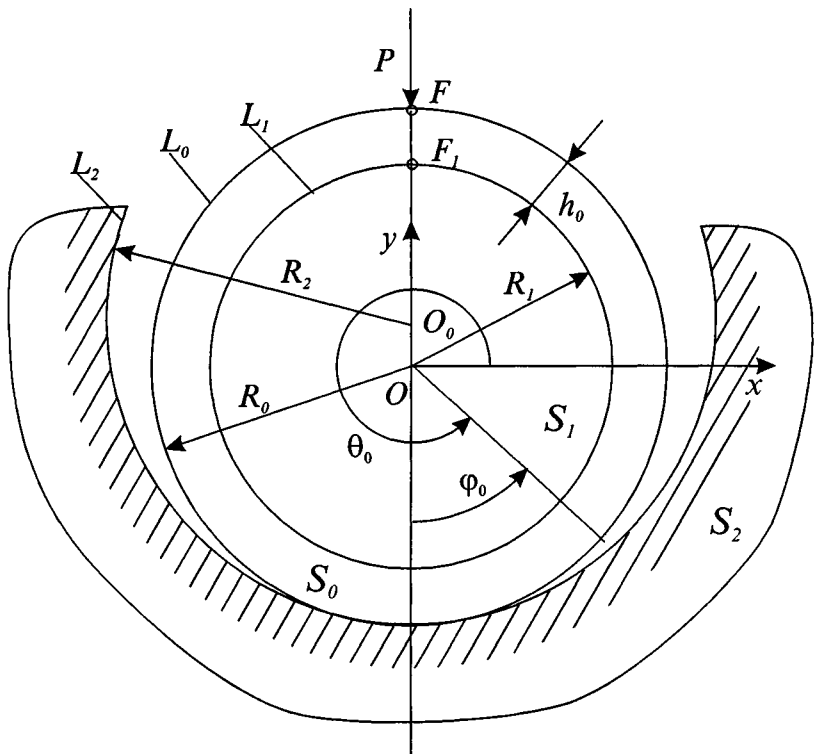


Figure 8.4: Scheme of a plain journal bearing with coating applied on the shaft (inverse sliding pair, ISP).

the hole are  $\rho = R_0/R_2$  ( $\rho < 1$ ) and 1, respectively. The center of the hole in the undeformed state is at the point  $z_0 = i(1 - \rho)$ . At the point  $F$  ( $z_F = i\rho$ ) the load  $P$  is applied. The load  $P$  direction passes through the point of initial contact of the bodies  $S_2$  and  $S_0$  opposite to the  $y$ -axis. The load presses the disk against the elastic plate  $S_2$  and as a result of elastic deformations they come into contact along the contact arc  $\gamma$  characterized by the angle  $2\varphi_0$ .

We denote the contours of the disk, the hole and the external contour of the layer by  $L_1$ ,  $L_2$  and  $L_0$ , respectively. Points on the contours  $L_0$  and  $L_2$  have coordinates  $t_0 = \rho e^{i\theta}$  and  $t_2 = e^{i\theta} + z_0$ , respectively;  $\theta$  is the polar angle calculated from the  $OX$  axis (see Fig. 8.4). To provide the contact of the bodies  $S_0$  and  $S_2$  along the contact arc  $\gamma$ , the dimensionless radial displacements  $u_r^{(0)}$ ,  $u_r^{(1)}$  and  $u_r^{(2)}$  of points on the contours  $L_0$ ,  $L_1$  and  $L_2$ , respectively, have to satisfy the following relationship which reflects the equality of curvatures within the contact region

$$u_r^{(0)}(\theta) + u_r^{(1)}(\theta) - u_r^{(2)}(\theta) = (1 - \rho)(1 + \sin \theta). \quad (8.26)$$

For a thin layer ( $h_0 \ll 2R_0\varphi_0$ , where  $\varphi_0$  is semi-contact angle) for which the modulus of elasticity of the layer  $S_0$  is smaller than that of the shaft, the radial

displacements  $u_r^{(0)}(\theta)$  are proportional to the layer thickness  $h_0$  and the normal contact stress  $\sigma_r(\theta)$ , i.e.

$$u_r^{(0)}(\theta) = k\delta_0\sigma_r(\theta), \quad (8.27)$$

where  $\delta_0 = \frac{h_0}{R_2}$ . It was shown by Aleksandrov and Mhitaryan (1983) that  $k = \frac{1-2\nu}{2G(1-\nu)}$ , where  $G$  and  $\nu$  are the shear modulus and the Poisson ratio for the layer  $S_0$ , respectively. The relation (8.27) corresponds to the Winkler model.

It should be noted here that alongside the normal stress  $\sigma_r(\theta)$  within the contact region  $\gamma$  there is a tangential stress  $\tau_{r\theta} = \mu\sigma_r(\theta)$  where  $\mu$  is the coefficient of friction, caused by friction of the surfaces. But due to the small value of the coefficient of friction  $\mu$  for the junction under consideration, it is possible to ignore the influence of the tangential stress on the normal stress within the contact region, i.e. to find the normal contact stress by neglecting the tangential one.

Then the following boundary conditions are satisfied on the contours  $L_0$  and  $L_2$

$$\begin{aligned} \tau_{r\theta}^{(0)}(t_0) &= \tau_{r\theta}^{(2)}(t_2) = 0, \quad t_0 \in L_0, \quad t_2 \in L_2, \\ \sigma_r^{(0)}(t_0) &= \sigma_r^{(2)}(t_2), \quad t_0 \in \gamma_0, \quad t_2 \in \gamma_2, \\ \sigma_r^{(0)}(t_0) &= 0, \quad t_0 \in L_0 \setminus \gamma_0, \quad t_0 \neq i\rho, \\ \sigma_r^{(2)}(t_2) &= 0, \quad t_2 \in L_2 \setminus \gamma_2, \end{aligned} \quad (8.28)$$

where  $\gamma_0$  and  $\gamma_2$  are the parts of the contours  $L_0$  and  $L_2$ , respectively, which are in contact after deformation;  $\sigma_r^{(i)}$  and  $\tau_{r\theta}^{(i)}$  are the normal and tangential stresses on the contour  $L_i$  ( $i = 0, 1, 2$ ).

Taking into account the boundary condition at  $L_0$  and the small thickness of the layer  $S_0$ , we obtain the following boundary condition on  $L_1$

$$\begin{aligned} \tau_{r\theta}^{(1)}(t_1) &= 0, \\ \sigma_r^{(1)}(t_1) &= \sigma_r^{(0)}(t_0). \end{aligned} \quad (8.29)$$

The equilibrium condition takes the form

$$\int_{\gamma_0} \sigma_r^{(0)}(t_0) dt_0 = -\frac{P}{R_2}. \quad (8.30)$$

## 8.2.2 The main integro-differential equation

To solve the problem we use the method suggested by Kalandiya (1975). Differentiating two times Eq. (8.26) and adding the result to the initial one, we obtain

$$\begin{aligned} \frac{d^2 u_r^{(0)}(\theta)}{d\theta^2} + u_r^{(0)}(\theta) + \frac{d^2 u_r^{(1)}(\theta)}{d\theta^2} + u_r^{(1)}(\theta) = \\ \frac{d^2 u_r^{(2)}(\theta)}{d\theta^2} + u_r^{(2)}(\theta) + 1 - \rho. \end{aligned} \quad (8.31)$$

Taking into account Eqs. (8.27)-(8.30), we can reduce Eq. (8.31) to the following integro-differential equation for the unknown function  $\sigma_r(t_1) = \sigma_r^{(1)}(t_1)$ ,  $t_1 \in \gamma'$  ( $\gamma'$  is a part of the contour  $L_1$  corresponding to the contact arc  $\gamma$ )

$$\begin{aligned} \eta\sigma_r(t_1) + \frac{t_1}{\pi i} \int_{\gamma'} \frac{\sigma'_r(t) dt}{t - t_1} - \frac{\lambda}{2\pi i} \int_{\gamma'} \frac{\sigma_r(t) dt}{t} + \\ u [t_1\sigma'_r(t_1) + t_1^2\sigma''_r(t_1)] = pH_1(t_1) + \\ \frac{qP}{2\pi} \left( \frac{\rho - \delta_0}{t_1} - \frac{t_1}{\rho - \delta_0} \right) - m(1 - \rho), \end{aligned} \quad (8.32)$$

where

$$\begin{aligned} \tau &= \frac{2}{\mu_2(\kappa_1 + 1)(\rho - \delta_0) + \mu_1(\kappa_2 + 1)}, \\ \eta &= \frac{1}{2}\tau [\mu_1(\kappa_2 - 1) - \mu_2(\kappa_1 - 1)(\rho - \delta_0) - 4\mu_1\mu_2k\delta_0], \\ \lambda &= \frac{1}{2}\tau\mu_1(\kappa_2 + 1), \quad u = 2\tau\mu_1\mu_2k\delta_0, \\ m &= 2\tau\mu_1\mu_2, \quad p = \tau\mu_2(\kappa_1 + 1)(\rho - \delta_0), \\ q &= \tau\kappa_2\mu_1, \quad \kappa_i = 3 - 4\nu_i, \quad \mu_i = \frac{E_i}{2(1 - \nu_i^2)}, \\ \sigma'_r(t) &= \frac{d\sigma_r}{dt}, \quad \sigma''_r(t) = \frac{d^2\sigma_r}{dt^2}. \end{aligned} \quad (8.33)$$

Here  $E_i$  and  $\nu_i$  are the Young's moduli and Poisson's ratios for the bodies  $S_1$  ( $i = 1$ ) and  $S_2$  ( $i = 2$ ).

The points  $t_1$  and  $t$  in Eq. (8.32) are on the contour  $L_1$ . However, it follows from Eq. (8.29) that the normal stresses found from Eq. (8.32) coincide with the stresses  $\sigma_r^{(0)}(t_0)$  occurring within the contact region  $\gamma$  at  $L_0$  for  $t_0 = \rho t_1 / (\rho - \delta_0)$ .

Note that if  $\delta_0 = 0$ , Eq. (8.32) coincides with that obtained by Kalantyia (1975) for the contact problem for two elastic cylinders.

The function  $H_1(t_1)$  in Eq. (8.32) is determined by the load applied to the body  $S_1$  and has the form

$$\begin{aligned} H_1(t_1) &= \Re \left[ F_1(t_1) - t_1 F'_1(t_1) - \frac{1}{2} F_1(0) \right], \\ F_1(t_1) &= \lim_{z \rightarrow t_1} \frac{1}{2\pi i} \int_{L'_1} \frac{\sigma_r(t) dt}{t - z}, \end{aligned} \quad (8.34)$$

where  $L'_1$  is the part of the contour  $L_1$  where the load is applied.

If the load  $P$  is applied to the body  $S_1$  at the point  $F_1$  with coordinate  $t_1 = i(\rho - \delta_0)$ , the function  $F_1(t_1)$  has the form

$$F_1(t_1) = -\frac{P}{2\pi R_2 i [(\rho - \delta_0) - t_1]}. \quad (8.35)$$

Eq. (8.32) and the equilibrium condition (8.30), which can be written in the form

$$\int_{\gamma'} \sigma_r(t_1) dt_1 = -\frac{P}{R_2}, \quad (8.36)$$

are the complete system of equations to determine the normal pressure  $\sigma_r(t_1)$  within  $\gamma'$  and the contact angle  $\theta_0$ .

We map the circumference  $|z| = \rho - \delta_0$  onto the real axis using the following function

$$\begin{aligned} i(\rho - \delta_0) \frac{\xi - i\beta}{\xi + i\beta} &= t_1, \\ \beta &= \frac{\cos \theta_0}{1 + \sin \theta_0}. \end{aligned} \quad (8.37)$$

Then the contact arc transforms into the segment  $[-1, 1]$ , and the function  $H_1(t_1)$  becomes ( $F_1(t_1)$  is determined by Eq. (8.35))

$$H_1(t_1) = H(\xi) = \frac{P}{8\pi R_2 (\rho - \delta_0)} \cdot \frac{\xi^2 + \beta^2}{\beta^2}.$$

Eqs. (8.32) and (8.36) take the following forms, respectively

$$\begin{aligned} \frac{\eta\beta}{\xi^2 + \beta^2} \sigma_r(\xi) - \frac{1}{2\pi} \int_{-1}^1 \frac{\sigma'_r(\zeta) d\zeta}{\zeta - \xi} - \frac{\lambda\beta^2}{\pi(\xi^2 + \beta^2)} \int_{-1}^1 \frac{\sigma_r(\zeta) d\zeta}{\zeta^2 + \beta^2} - \\ \frac{u\xi}{2\beta} \sigma'_r(\xi) - \frac{u(\xi^2 + \beta^2)}{4\beta} \sigma''_r(\xi) = -\frac{m\beta}{\xi^2 + \beta^2} (1 - \rho) + \end{aligned} \quad (8.38)$$

$$\frac{P}{\pi R_2} \cdot \frac{\beta}{\xi^2 + \beta^2} \left[ q \frac{\xi^2 - \beta^2}{\xi^2 + \beta^2} + p \frac{\xi^2 - \beta^2}{8(\rho - \delta_0)\beta^2} \right],$$

$$\int_{-1}^1 \frac{\xi^2 - \beta^2}{(\xi^2 + \beta^2)^2} \sigma_r(\xi) d\xi = \frac{P}{2\beta R_2 (\rho - \delta_0)}. \quad (8.39)$$

### 8.2.3 Method of solution

The system of equations (8.38) and (8.39) was solved approximately by Multhopp. His method was used by Kalantyia (1975) to solve Eq. (8.38) when  $\delta_0 = 0$ . We describe here the main idea of the method.

Introducing the new variable  $\vartheta$  by equation  $\xi = \cos \vartheta$ , we rewrite Eqs. (8.38) and (8.39) in the form

$$\begin{aligned} & \frac{\eta\beta}{\cos^2 \vartheta + \beta^2} \sigma_r(\vartheta) + u \frac{\cos \vartheta}{2\beta \sin \vartheta} \left( 1 + \frac{\cos^2 \vartheta + \beta^2}{2 \sin^2 \vartheta} \right) \sigma'_r(\vartheta) - \\ & u \frac{\cos^2 \vartheta + \beta^2}{4\beta \sin^2 \vartheta} \sigma''_r(\vartheta) + \frac{1}{2\pi} \int_0^\pi \frac{\sigma'_r(\vartheta') d\vartheta'}{\cos \vartheta' - \cos \vartheta} - \\ & \frac{\lambda\beta^2}{\pi (\cos^2 \vartheta + \beta^2)} \int_0^\pi \frac{\sigma_r(\vartheta') \sin \vartheta' d\vartheta'}{\cos^2 \vartheta' + \beta^2} = \\ & \frac{P\beta}{\pi R_2 (\cos^2 \vartheta + \beta^2)} \left[ q \frac{\cos^2 \vartheta - \beta^2}{\cos^2 \vartheta + \beta^2} + p \frac{\cos^2 \vartheta + \beta^2}{8(\rho - \delta_0)\beta^2} \right] - \\ & \frac{m\beta}{\cos^2 \vartheta + \beta^2} (1 - \rho), \end{aligned} \quad (8.40)$$

$$\int_0^\pi \frac{(\cos^2 \vartheta - \beta^2) \sin \vartheta}{(\cos^2 \vartheta + \beta^2)^2} \sigma_r(\vartheta) d\vartheta = \frac{P}{2\beta R_2(\rho - \delta_0)}. \quad (8.41)$$

We construct the Lagrange interpolation polynomial for an unknown function  $\sigma_r(\vartheta)$  choosing interpolation nodes within the segment  $[-1, 1]$  as the roots of the Chebyshev polynomial of the second kind of degree  $n$ , i.e. the points

$$x_k = \cos \vartheta_k, \quad \vartheta_k = \frac{k\pi}{n+1}, \quad k = 1, 2, \dots, n.$$

Then the Lagrange polynomial which coincides with the function  $\sigma_r(\vartheta)$  in the points  $\vartheta = \vartheta_k$ , i.e.  $\sigma_k = \sigma_r(\vartheta_k)$  has the form

$$L[\sigma_k, x] = \frac{2}{n+1} \sum_{k=1}^n \sigma_k \sum_{m=1}^n \sin m\vartheta_k \sin m\vartheta. \quad (8.42)$$

Replacing integrals on the left-sides of Eqs. (8.40) and (8.41) by finite sums, and giving  $\vartheta$  the values  $\vartheta_k$  ( $k = 1, 2, \dots, n$ ), we obtain the system of equations for the unknown function at the nodes of interpolation:

$$A_k \sigma_k + \sum_{j=1}^n a_{kj} \sigma_j + b_{1k} \sigma'_k + b_{2k} \sigma''_k = B_k, \quad k = 1, 2, \dots, n, \quad (8.43)$$

where

$$\begin{aligned} A_k &= \frac{\eta\beta}{\cos^2 \vartheta_k + \beta^2}, \quad B_k = -\frac{m\beta}{\cos^2 \vartheta_k + \beta^2} (1 - \rho), \\ b_{1k} &= \frac{u \cos \vartheta_k}{2\beta \sin \vartheta_k} \left( 1 + \frac{\cos^2 \vartheta_k + \beta^2}{2 \sin^2 \vartheta_k} \right), \quad b_{2k} = -u \frac{\cos^2 \vartheta_k + \beta^2}{4\beta \sin^2 \vartheta_k}, \end{aligned}$$

$$\begin{aligned}
 a_{kj} = & \frac{1}{(n+1) \sin \vartheta_k} \sum_{m=1}^n m \sin m\vartheta_j \sin m\vartheta_k - \\
 & \frac{\lambda \beta^2}{(n+1)(\cos^2 \vartheta_k + \beta^2)} \cdot \frac{\sin \vartheta_j}{(\cos^2 \vartheta_j + \beta^2)} - \\
 & \frac{2\beta^2(\rho - \delta_0)}{(n+1)(\cos^2 \vartheta_k + \beta^2)} \left[ q \frac{\cos^2 \vartheta_k - \beta^2}{\cos^2 \vartheta_k + \beta^2} + \right. \\
 & \left. p \frac{\cos^2 \vartheta_k + \beta^2}{8(\rho - \delta_0)\beta^2} \right] \frac{\sin \vartheta_j (\cos^2 \vartheta_j - \beta^2)}{(\cos^2 \vartheta_j + \beta^2)^2}.
 \end{aligned}$$

It should be noted that the system (8.43) includes not only the values of  $\sigma_k$  but also the first and the second derivatives of the normal pressure. The polynomial (8.42) does not provide the Hermitian interpolation of the function  $\sigma_r(\vartheta)$ , i.e. the values of the first and the second derivatives of the interpolation polynomial (8.42) calculated at the points  $x_i$ , do not coincide with the values of the corresponding derivatives of the function  $\sigma_k(x)$  at the same points. Because of this, we calculated the values  $\sigma'_k$  and  $\sigma''_k$  following the standard procedure by using the values of the function (8.42) at the  $k$ -th and at the nearby nodes. Then the system (8.43) is reduced to the system of  $n$  linear algebraic equations to determine the values  $\sigma_k$ .

To evaluate the influence of the number  $n$  of nodes on the solution of the system (8.43), we solved this system for  $n = 7$ ,  $n = 15$  and  $n = 31$  (the first, second and the third approach by Multhopp, respectively). The results showed that for all values of  $\beta$  the second approach differs from the first one by less than 0.1%.

After the calculation of the values  $\sigma_k$  at the points  $\vartheta_k$  we find the load  $P$  from the following equation

$$P = R_2 \frac{2\pi\beta(\rho - \delta_0)}{n+1} \sum_{k=1}^n \frac{\sin \vartheta_k (\cos^2 \vartheta_k - \beta^2)}{(\cos^2 \vartheta_k + \beta^2)^2} \sigma_k. \quad (8.44)$$

### 8.2.4 Contact characteristics analysis

In calculations we assume that we are given the geometric characteristics ( $R_2, \rho, \delta_0$ ), the elastic characteristics of the contacting bodies ( $\mu_1, \kappa_1, \mu_2, \kappa_2, k$ ), and the parameter  $\beta$  which is determined by the angle  $\theta_0$  from Eq. (8.37).

The results of numerical calculations are shown in Fig. 8.5 where the dependence of the contact angle  $\phi_0 = \theta_0 - \frac{3}{2}\pi$  on the load  $P$  is presented. The curves 1–3 are plotted for the following parameters:  $E_1 = E_2 = 2 \cdot 10^5$  MPa,  $\nu_1 = \nu_2 = 0.3$ ;  $R_2 = 10^{-2}$  m,  $\rho = 0.995$ ,  $k = 0.5 \cdot 10^{-3}$  MPa $^{-1}$ . Curve 1 corresponds to  $\delta = 0$  (disk without coating), curve 2 – to  $\delta = 2 \cdot 10^{-3}$ , curve 3 – to  $\delta = 5 \cdot 10^{-3}$ . Curve 4 is plotted for the rigid bodies  $S_1$  and  $S_2$  and the elastic ring  $S_0$  ( $\delta = 2 \cdot 10^{-3}$ ). With this combination of properties of contacting bodies there is some limitation in increasing of the contact arc due to increasing of the load. This process is stopped when a displacement at any point of contact will reach the value  $\delta$ . Such

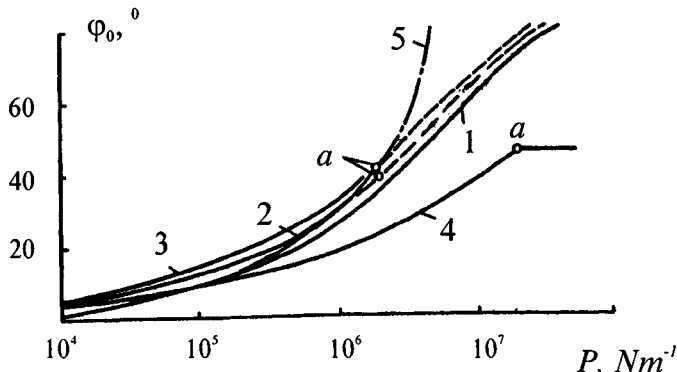


Figure 8.5: Dependence of the contact angle upon the load for a plain bearing (ISP) at different coating thickness:  $\delta = 0$  (curve 1),  $\delta = 2 \cdot 10^{-3}$  (curve 2) and  $\delta = 5 \cdot 10^{-3}$  (curve 3), at  $E_1 = E_2 = 2 \cdot 10^5$  MPa. Curve 4 is calculated neglecting the elasticity of bodies  $S_1$  and  $S_2$ ; curve 5 is calculated from the Hertz theory of contact of elastic bodies  $S_1$  and  $S_2$ .

a situation is marked on the curves by the point  $a$  and the load corresponding to this point is  $P_a$ . The parts of the curves for  $P > P_a$  can be considered as unrealistic.

Curve 5 corresponds to the Hertz theory of contact of the bodies  $S_1$  and  $S_2$ , neglecting of the coating existence.

The principal conclusions of this study are the following:

1. It is expedient to distinguish three regions for the value of the parameter  $\delta/\phi_0$ .

If  $\delta/\phi_0 > 5 \cdot 10^{-2}$  it is possible to consider the bodies  $S_1$  and  $S_2$  as rigid, and  $S_0$  as elastic. In this case the relation between the load and the size of contact arc obeys a simple analytical expression

$$P = R_2 \frac{1 - \rho}{k\delta_0} \left( \frac{\phi_0}{\cos \phi_0} - \sin \phi_0 \right), \quad (8.45)$$

which follows from the solution of the differential equation

$$\sigma_r'' + \sigma_r = \frac{1 - \rho}{k\delta_0}$$

taking the form

$$\sigma_r = \frac{1 - \rho}{k\delta_0} \left( 1 - \frac{\cos \phi}{\cos \phi_0} \right).$$

The results calculated from Eq. (8.45) and from Eq. (8.43) for  $\delta/\phi_0 > 5 \cdot 10^{-2}$  are in a good agreement.

If  $\delta/\varphi_0 < 5 \cdot 10^{-3}$  it is possible to ignore the coating  $S_0$  in calculations.

If  $5 \cdot 10^{-3} \leq \delta/\varphi_0 \leq 5 \cdot 10^{-2}$  we must take into consideration the elastic properties of the three bodies  $S_0$ ,  $S_1$  and  $S_2$ .

2. The soft coating decreases the contact pressure and increases the size of contact arc compared to the characteristics of the journal bearing without coating.
3. Hertz theory gives a good approximation to the contact characteristics of the plain journal bearing with a small contact angle (low loading), but does not agree with experiment for the bearing with coating.

### 8.2.5 Wear analysis

The results were used to study the wear kinetics of the plain journal bearing with a journal coated by a thin solid lubricant.

In calculations we used the wear law in the form of Eq. (8.1). The operating time was measured by the number  $N$  of journal revolutions. During the wear of the junction such characteristics as the contact pressure  $p(\varphi, N) = -\sigma_r(\varphi, N)$ , the contact angle  $\varphi_0(N)$ , the thickness of coating  $\delta_0(N)$ , and the journal radius  $R_0(N)$  depend on  $N$ .

Modelling the wear process, we calculate the contact characteristics after each revolution assuming that they are constant during each revolution and are changed step-wise at the instant that a new revolution begins. The wear at any fixed revolution is determined by the contact characteristics at the previous revolution.

We introduce the wear at the  $(N + 1)$ -th revolution as

$$\Delta w(N + 1) = K_w R_0(N) \int_{-\varphi_0(N)}^{\varphi_0(N)} p^\alpha(\varphi, N) d\varphi, \quad (8.46)$$

where  $\varphi = \theta - \frac{3}{2}\pi$ .

We used the following procedure for calculating the wear kinetics of the junction. From the contact problem analysis (see §§8.2.1–8.2.3) we determine the initial values of  $\varphi_0(0)$  and  $p(\varphi_0(0))$ . Then, using the relation (8.46) for  $N = 0$  we estimate the wear throughout the first revolution ( $N = 0$ ) of a journal, and then we calculate the radius  $R_0(1) = R_0(0) - \Delta w(1)$  and the new coating dimensionless thickness  $\delta(1) = \frac{h(1)}{R_2}$  where  $h(1) = h_0 - \Delta w(1)$ . This completes one sequence of steps. In order to study the wear kinetics we have to repeat such a sequence as many times as necessary.

Fig. 8.6 illustrates the dependence of the coating wear  $\bar{w}(N) = 1 - \frac{h(N)}{h_0}$  (curves 1 and 2) and the contact angle  $\varphi_0$  (curves 1' and 2') on the parameter

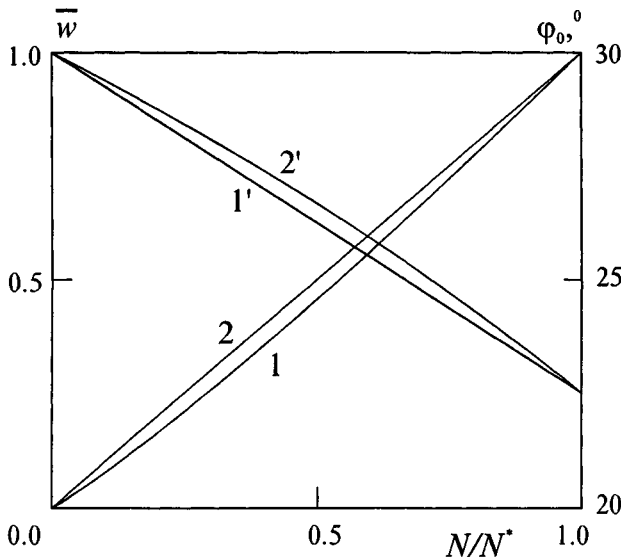


Figure 8.6: Variation of the coating wear  $\bar{w}$  (curves 1 and 2) and contact angle  $\varphi_0$  (curves 1' and 2') in wear process of the plain bearing with ISP for  $K_w = 10^{-14} \text{ Pa}^{-1}$  and  $\alpha = 1$  (curves 1, 1') and  $K_w = 10^{-19} \text{ Pa}^{-2}$  and  $\alpha = 2$  (curves 2, 2').

$N/N^*$  which is the ratio of the current number of revolution to the number of revolutions  $N^*$  corresponding to the complete wear of the coating ( $h(N^*) = 0$ ).

The results were calculated for

$$\begin{aligned} R_2 &= 10^{-2} \text{ m}, \quad \rho(0) = 0.995, \quad \delta_0 = 2 \cdot 10^{-3}, \\ \mu_1 &= \mu_2 = 8.46 \cdot 10^4 \text{ MPa}, \quad \kappa_1 = \kappa_2 = 1.8, \\ k &= 0.5 \cdot 10^{-3} \text{ MPa}^{-1}, \quad P = 1.08 \cdot 10^6 \text{ N/m}. \end{aligned}$$

For this case  $\theta_0(0) = \frac{5\pi}{3}$ . Curves 1 and 1' are calculated for  $K_w = 10^{-14} \text{ Pa}^{-1}$  and  $\alpha = 1$ ; curves 2 and 2' correspond to  $K_w = 10^{-19} \text{ Pa}^{-2}$  and  $\alpha = 2$ .

From the results we conclude that if the coating wear rate is a power function of the pressure, the wear of the coating is proportional to the number of revolutions. The contact angle decreases nearly linearly in the wear process. To understand this we may use the following simple argument. Since the journal radius (and consequently the contact angle) decreases during wear, the sliding distance per revolution also decreases. Simultaneously the contact pressure increases, resulting in increase of the wear intensity in accordance with the wear equation (8.1). Considering that the wear per revolution is the product of the wear intensity by sliding distance, it is clear that by virtue of the competing influences of the operating time

on these quantities the wear per revolution will change very little. We can consider that this is a characteristic feature of the wear of such sliding bearings.

This result can be used to calculate the lifetime of a junction within a range of operation conditions. These conditions are usually specified by the limiting value of some parameter. We often take this to be the bearing radial clearance, with the magnitude of which the secondary dynamic loads in the machine assemblies and the accuracy are associated. We shall consider that the magnitude of this clearance  $\Delta^*$  is specified in advance. Since junction wear takes place only at the expense of the journal coating, then  $\Delta^* = R_2 - R_0(N^*)$ , where  $R_0(N^*)$  is the critical value of the journal radius achieved for  $N^*$  revolutions. Because of Eq. (8.46) and the initial value of the radial clearance  $\Delta_0 = R_2 - R_0(0)$  the limiting wear can be written in the form

$$\begin{aligned} \Delta^* - \Delta_0 &= \sum_{N=1}^{N^*} \Delta w(N) = \\ K_w \sum_{N=0}^{N^*-1} R_0(N) &\int_{-\varphi_0(N)}^{\varphi_0(N)} p^\alpha(\varphi, N) d\varphi, \end{aligned} \quad (8.47)$$

$$\Delta^* - \Delta_0 \leq h_0.$$

Thus, determination of the junction service life reduces to determining  $N^*$ , satisfying the conditions (8.47).

Considering that the journal bearing wear is nearly proportional to the number of revolutions, we can find a more effective and highly accurate calculation technique by partitioning the limiting wear magnitude  $\Delta^* - \Delta_0$  into  $M$  uniform intervals  $\Delta h = (\Delta^* - \Delta_0)/M$  and calculating the average wear per revolution on each interval. In fact, determining the junction geometry at the end of the  $m$ -th interval ( $m = 1, 2, \dots, M$ ) and finding from Eqs. (8.38) and (8.39) the corresponding contact characteristics  $p(\varphi, N_m)$ ,  $\varphi_0(N_m)$ , we can use Eq. (8.46) to calculate the average wear  $\Delta \tilde{w}_m$  per revolution

$$\Delta \tilde{w}_m = \frac{1}{2} (\Delta w_{(m-1)} + \Delta w_m),$$

where

$$\Delta w_m = K_w (R_2(0) - m\Delta h) \int_{-\varphi_0(N_m)}^{\varphi_0(N_m)} p^\alpha(\varphi, N_m) d\varphi.$$

Then the approximate value of  $N^*$  is determined as follows:

$$N^* = \Delta h \sum_{m=1}^M \Delta \tilde{w}_m^{-1}.$$

Note that a very good approximation to this result can be obtained if we determine the average wear per revolution at the beginning and at the end of assembly operation, i.e.  $\Delta \tilde{w}_* = (\Delta w_*(0) + \Delta w_*(N^*))/2$ . This is explained by a characteristic

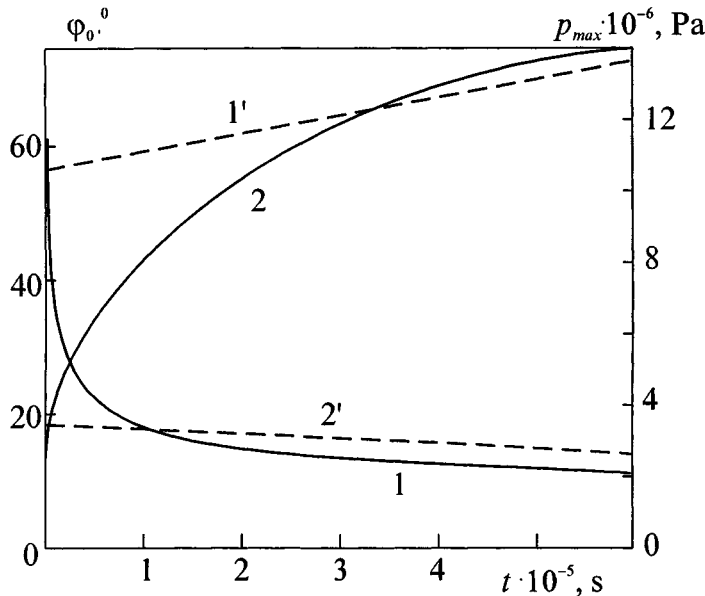


Figure 8.7: Changes of the maximum contact pressure  $p_{\max}$  (curves 1 and 1') and the contact angle  $\phi_0$  (curves 2 and 2') in time for the plain journal bearings with DSP (solid lines) and ISP (dashed lines).

of sliding bearing wear kinetics, noted previously and amounting to the fact that the wear per revolution remains practically constant during operation. Thus, we can calculate the approximate value  $\tilde{N}^*$  of  $N^*$  as

$$\tilde{N}^* = \frac{\Delta^* - \Delta_0}{\Delta \bar{w}_*}.$$

This method makes it possible to simplify the calculations considerably and at the same time ensure high accuracy.

The results show also that failure to account for coating properties in calculating the journal bearing service life leads to underestimation of the junction service life, which is due to the errors in evaluating the contact zone dimensions and the pressure distribution.

### 8.3 Comparison of two types of bearings

The results for the previous problems make it possible to compare kinetics of changes of contact and tribotechnical characteristics for two types of plain bearings, which are DSP and ISP described in § 8.1 and in § 8.2, respectively.

Fig. 8.7 illustrates the dependence of contact angle and maximum contact

pressure on operating time for the plain journal bearings with DSP (solid lines) and ISP (dashed lines). Calculations were performed for the following initial data:

$$P = 10^5 \text{ N/m}, \quad R_2 = 2.505 \cdot 10^{-2} \text{ m}, \quad R_1 = 2.5 \cdot 10^{-2} \text{ m},$$

$$k = 8.35 \cdot 10^{-4} \text{ MPa}^{-1}, \quad \alpha = 1.4,$$

$$K_w = 1.2 \cdot 10^{-19} \cdot \text{Pa}^{-1.4}, \quad \omega = 10 \text{ s}^{-1}, \quad h_0 = 3 \cdot 10^{-4} \text{ m},$$

$$\mu_1 = \mu_2 = 7.7 \cdot 10^4 \text{ MPa}, \quad \nu_1 = \nu_2 = 0.3.$$

The kinetics of changes of parameters for DSP and ISP differ in principle: for the DSP the contact angle increases and maximal pressure diminishes in the process of wear; for the ISP the contact angle diminishes and maximal pressure increases. The evolution of contact characteristics for DSP looks more favorable than for ISP. The difference in the initial values for  $p_m$  and  $\theta$  for these types of junctions can be explained by the fact that for DSP the bodies  $S_0$  and  $S_1$  are considered as rigid, and for ISP as being elastic.

There is a second significant discrepancy between the two kinds of wear processes. For DSP the shape of a bush changes during the wear process. This feature leads to a difference between the running-in stage of wear process and its steady-state stage. The first stage is characterized by intense changing of parameters and non-linear dependence of the contact pressure, contact angle and the wear rate on the operating time; over the second stage these relations are very close to the linear ones.

For ISP, there is no shape variation. Consequently for this junction the steady-state conditions are valid over the whole operating time, the dependences of  $p_{\max}(t)$ ,  $\varphi_0(t)$  and  $h_{\min}(t)$  are always slightly different from linear ones. This considerably simplifies calculations of contact and tribotechnical characteristics of such joints.

In the special case ( $\alpha = 1$ ) it can be strictly proved that the ISP lifetime is higher than DSP, all other things being equal. Let us examine the case  $\alpha = 1$  and a small contact angle  $\varphi_0$ . The wear for the  $N$ -th revolution for ISP is calculated from Eq. (8.46) as

$$\Delta w^{(2)}(N+1) = K_w \int_{-\varphi_0(N)}^{\varphi_0(N)} p(\varphi, N) R_0(N) d\varphi \approx K_w P.$$

The lifetime of DSP is determined by the wear at the point where the maximum contact pressure occurs. The friction distance during one revolution for this point is  $2\pi R_1$ . The wear for the  $N$ -th revolution for this scheme is determined by the formula

$$\Delta w^{(1)}(N+1) = 2\pi R_1 K_w p(0, N).$$

By virtue of the fact that  $2\pi R_1 p(0, N) > P$ , we obtain  $\Delta w^{(1)}(N+1) > \Delta w^{(2)}(N+1)$ . From this relationship, it follows that for the equal limiting wear ( $\Delta^* - \Delta_0$ ) the lifetime of ISP is always higher than DSP.

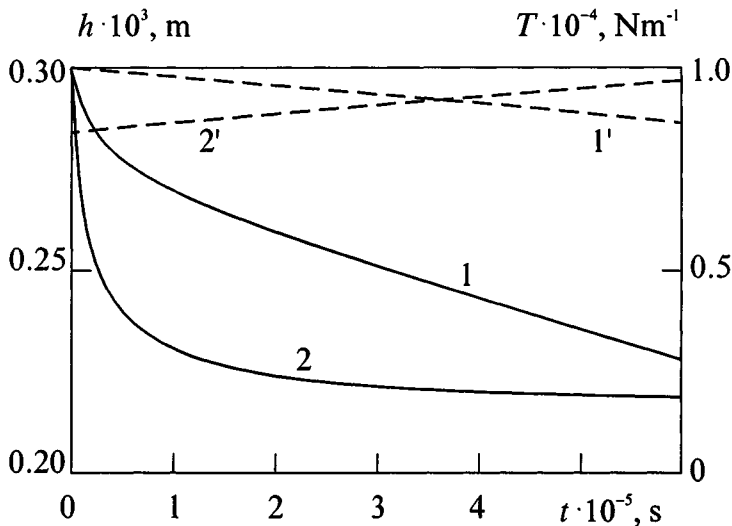


Figure 8.8: Changes of the coating thickness  $h$  (curves 1 and 1') and the friction force  $T$  (curves 2 and 2') in time for the plain bearing with DSP (solid lines) and ISP (dashed lines).

The another important tribological characteristic of the journal bearing is the friction force. It must be noted that the character of the dependence of the friction force on time for both types of bearings depends on the friction law. Particularly, if the tangential stress  $\tau$  is a power function of contact pressure

$$\tau = \mu^* p^m,$$

with a power  $m > 1$ , then DSP is more favorable than ISP in respect to the friction force. Fig. 8.8 illustrates the dependence of the friction force on time for DSP (solid lines) and ISP (dashed lines) for  $\mu^* = 10^{-8} \text{ Pa}^{-1}$  and  $m = 2$ . In this case the friction force decreases in the wear process for DSP and it increases for ISP. It should be noted that the results depend essentially on the parameter  $m$ .

From these results it is evident that the kinetics of changes of contact and friction characteristics of plain bearings with direct and inverse pairs differ considerably. So one should pay attention to their functional properties when choosing the type of configuration for a plain bearing.

## 8.4 Wheel/rail interaction

In general, rail and wheel profiles are chosen to satisfy simultaneously the following conditions:

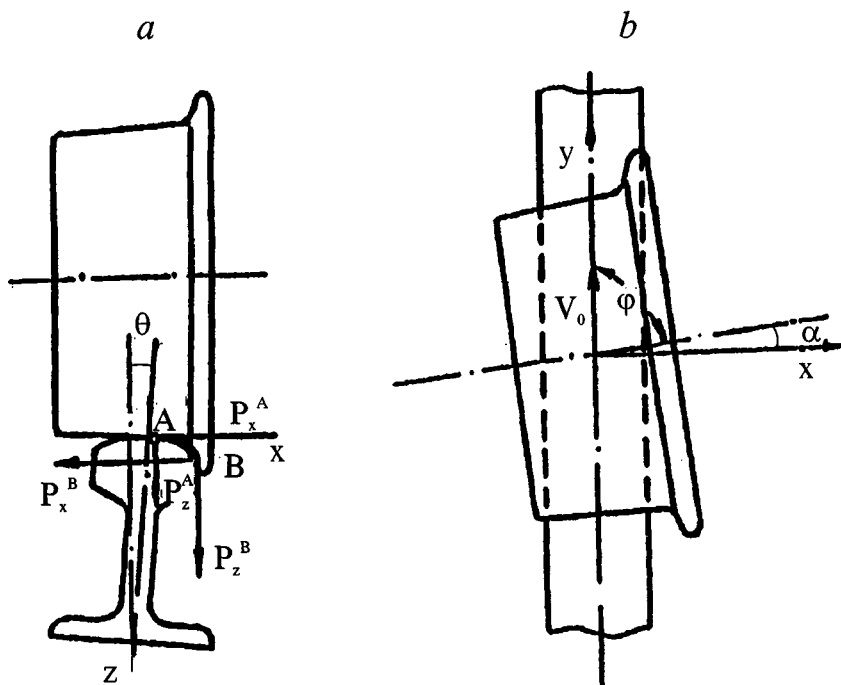


Figure 8.9: Relative position of a rail and a wheel at the planes  $y = 0$  (a) and  $z = 0$  (b).

- provision of wheel stability in contact with rail;
- reduction of contact fatigue defects;
- reduction of wear of rails and wheels.

Excessive wear and damage of rails and wheels are great problems for heavy haul railways. It should be noted that the most wear occurs at the side of the rail and at the crest of the wheel travelling on curved track.

In what follows we present the model for evaluating the tribological aspects of wheel/rail curve interaction developed in Bogdanov et al. (1996). The results could be used for selection of the rail and wheel profiles, which provide decreasing wear rate and rate of fatigue damage accumulation in rails.

#### 8.4.1 Parameters and the structure of the model

We consider a contact of a rail and a wheel travelling on a curved track. Fig. 8.9 illustrates the relative position of rail and wheel in contact. The geometry of contact is described by the angle  $\theta$  of the rail inclination about the vertical axis

$Oz$  (rail inclination angle), the attack angle  $\alpha = 90^\circ - \varphi$ , where  $\varphi$  is the angle between the axis of rotation of the wheel and the longitudinal axis  $Oy$  of the rail. We assume that the angles  $\theta$  and  $\alpha$  are random variables.

The profiles of the rail and the wheel are given and can be changed in the wear process.

Actually there is two-point contact between the wheel and the rail (the first is on the running part of the rail head and the second is on the side of the rail). At the contact spots on the top and on the side of the rail characterized by the points A and B of initial contact, the vertical  $P_z^A$  and  $P_z^B$  and lateral  $P_x^A$  and  $P_x^B$  forces of interaction between the rail and wheel are applied. These forces are also considered as random variables. They are obtained from the dynamic model of track and rolling stock interaction described by Verigo and Kogan (1986).

We consider the cyclic interaction of wheels with the fixed part of the rail on a curved track. As the result of this process the rail and the wheels are worn and damage accumulates inside the contacting bodies.

The problem may be split into several stages which are shown schematically in Fig. 8.10.

At first we solve the contact problem for rail and wheel to find the shape, size and the position of the contact zones and the contact stresses.

Then, using the contact stress distribution, we calculate the internal stresses in the rail and wheel, and the damage accumulation function. With this we determine the areas where the fatigue damage is concentrated. These problems are indicated in the left column of Fig. 8.10.

The results of the contact problem analyses are also used to calculate the wear rate of the rail and wheel surfaces and to determine the worn shapes of the rail and wheel. These problems are indicated in the right column of Fig. 8.10.

We now discuss each problem in detail.

#### 8.4.2 Contact characteristics analysis

Due to the deformation of the bodies, the contact of the rail and wheel occurs within the contact zones, including the points of initial contact. Determination of the initial points of contact is geometric problem which is described in detail by Bogdanov et al. (1996).

The initial data are rail and wheel profiles (both bodies are cylindrical) and the angles  $\theta$  and  $\alpha$ . The wheel and rail profiles are given pointwise, and then third order spline-approximations are used to produce twice continuously differentiable functions describing the profiles. After that these functions are rewritten for a common system of coordinates.

The system of equations for determination of the initial contact points A and B contains the conditions that the shape functions coincide and the normals are collinear at these points. We used an iterative method to solve the equations.

The analysis of the contact problem for the rail and wheel is based on various assumptions. The deformations of the bodies in contact are considered to be elastic. Determination of the stresses within the contact zone of elastic bodies

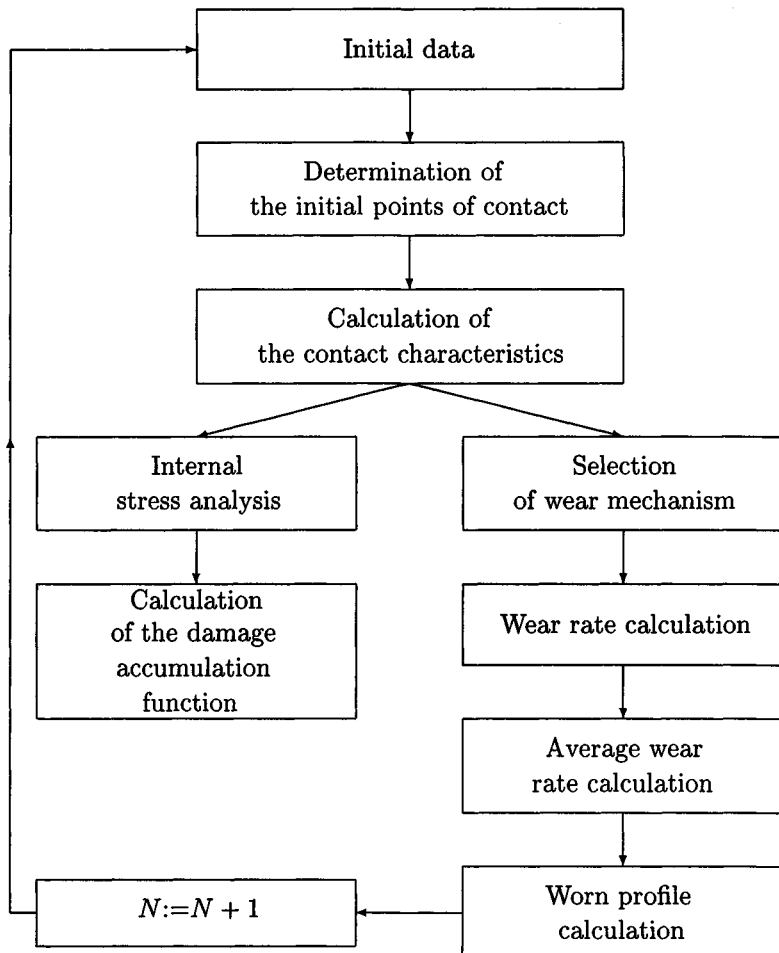


Figure 8.10: The stages of calculation of the wear and damage accumulation processes in a wheel and in a rail ( $N$  is the cycle number).

with profiles which cannot be represented adequately by their curvature radii at the initial contact point is a severe problem. In order to avoid some difficulties we model the contacting bodies by a simple Winkler elastic foundation.

The second simplification of the contact problem is connected with neglecting the tangential stress in the contact region when we calculate the contact pressure. It is well known that the tangential contact stress does not influence the normal contact stress in the contact of bodies characterized by the same elastic moduli. If the elastic properties of contacting bodies are different, there is some influence, but it is still small.

We consider some initial point  $(x_0, y_0, z_0)$  of contact of rail and wheel and place the origin  $O$  of the system of coordinates  $O\xi\eta\zeta$  there. The axis  $O\zeta$  coincides with the common normal to the contacting surfaces at the point  $(x_0, y_0, z_0)$ , the axis  $O\eta$  is aligned with a rail generatrix, and the axis  $O\xi$ , which is in the tangential plane, is determined by the condition that the axes  $O\xi$ ,  $O\eta$  and  $O\zeta$  form a right handed triple.

Undeformed surfaces of the rail and the wheel in this system of coordinates are described by equations  $\zeta_1 = f_1(\xi)$  and  $\zeta_2 = f_2(\xi, \eta)$ , respectively. The separation between the two surfaces near the initial point of contact is given by

$$h = |\zeta_1 - \zeta_2| = f(\xi, \eta) = |f_1(\xi) - f_2(\xi, \eta)|.$$

Under the normal load  $P$  the surfaces of the rail and wheel have the displacements  $w_1(\xi, \eta)$  and  $w_2(\xi, \eta)$ , respectively. The boundary condition for displacements within the contact region  $\Omega$  can be written

$$w_1(\xi, \eta) + w_2(\xi, \eta) + h = D, \quad (8.48)$$

where  $D$  is the approach of the bodies under the load.

According to the Winkler model, the contact pressure  $p(\xi, \eta)$  at any point depends only on the displacement at that point, thus

$$w_1(\xi, \eta) = K_1 p(\xi, \eta), \quad w_2(\xi, \eta) = K_2 p(\xi, \eta), \quad (8.49)$$

where  $K_1$  and  $K_2$  are the coefficients which characterize the elastic compliances of the rail and wheel, respectively. Assuming  $K = K_1 = K_2$ , from Eqs. (8.48) and (8.49) we obtain the following relationship within the contact region  $\Omega$

$$2Kp(\xi, \eta) = D - f(\xi, \eta). \quad (8.50)$$

Outside the contact region for the model under consideration the normal displacements satisfy the conditions

$$w_1(\xi, \eta) = 0, \quad w_2(\xi, \eta) = 0, \quad D \leq h. \quad (8.51)$$

Adding to Eqs. (8.50) and (8.51) the equilibrium condition

$$\iint_{\Omega} p(\xi, \eta) d\xi d\eta = P, \quad (8.52)$$

we obtain the complete system of equations for determination of the contact pressure  $p(\xi, \eta)$ , approach  $D$  and the contact region  $\Omega$ .

The normal load  $P = P^A$  (or  $P = P^B$ ) acting on each contact region  $\Omega = \Omega^A$  (or  $\Omega = \Omega^B$ ) is equal to the sum of the projections of the forces  $P_z^A$  and  $P_x^A$  ( $P_z^B$  and  $P_x^B$ ) on the axis  $O\zeta$ .

### 8.4.3 Wear analysis

We consider a cyclic interaction of the wheel moving along the fixed part of a curved track, as a result of which the wheel and the rail wear.

To calculate the wear rate of the rail and the wheel at the  $N$ -th cycle characterized by the given shape of the rail and wheel and the given probability density function  $\rho(\theta, \alpha, \vec{P}^A, \vec{P}^B)$  ( $\vec{P}^A$  and  $\vec{P}^B$  are the vectors of forces acted at the contact regions  $\Omega^A$  and  $\Omega^B$ , respectively), we represent the process of contact interaction as a number of elementary interactions. We can treat the elementary interaction as a single passage of the wheel along the fixed part of the rail. For each elementary interaction the external contact parameters ( $\theta, \alpha, \vec{P}^A, \vec{P}^B$ , etc.) are assumed to be given and fixed. Using the wear rates calculated for each elementary interactions and averaging them over the ensemble of external parameters, we obtain the desired rail and wheel wear rates.

Let us consider this procedure in more detail. The wheel moves along the rail with a constant speed  $V_0$ . The mutual position of the rail and wheel is described by the angle of inclination  $\theta$  and the attack angle  $\alpha$ . From the solution of the contact problem we know the contact pressure distribution at the contact zones  $\Omega^A$  and  $\Omega^B$ :

$$\begin{aligned} p^A(\xi, \eta) &= \Pi^A(\xi, \eta, \theta, \alpha, P^A), \\ p^B(\xi, \eta) &= \Pi^B(\xi, \eta, \theta, \alpha, P^B), \end{aligned} \quad (8.53)$$

where  $\xi$  and  $\eta$  are the local coordinates in the vicinity of the initial contact points  $A$  and  $B$ , and  $\Pi^A$  and  $\Pi^B$  are the functions obtained from the contact problem analysis.

The contact pressure in the presence of the relative sliding produces the wear of the contacting surfaces. We assume that the wear rates of the rail  $\partial W_r^i / \partial t$  and the wheel  $\partial W_w^i / \partial t$  are described by the equations

$$\begin{aligned} \frac{\partial W_r^i}{\partial t} &= F_r(p^i, V^i), \\ \frac{\partial W_w^i}{\partial t} &= F_w(p^i, V^i), \end{aligned} \quad (8.54)$$

where  $W_r^i$  and  $W_w^i$  are the wear of the rail and the wheel at the fixed point  $(\xi, \eta)$ ,  $V^i$  is the sliding speed,  $F_r$  and  $F_w$  are the known functions,  $i = A, B$  depending on the contact point under consideration.

The sliding speed  $V^A$  for the wheels mounted on a common axle while traveling on curved track is determined by the difference of lengths of their trajectories

$$V^A = \frac{D_r V_0}{2R_c}, \quad (8.55)$$

where  $R_c$  is the radius of the track curvature,  $D_r$  is the distance between the wheels at a common axle.

The sliding speed  $V^B(\xi, \eta)$  at the contact zone  $\Omega^B$  located at the lateral edges of the rail head and the wheel depends on the distance of  $\Omega^B$  from the instantaneous center of rotation of the wheel of the radius  $R$ . The function  $V^B(\xi, \eta)$  can be determined from the following relationship

$$V^B(\xi, \eta) = \frac{V_0}{R} \left[ (z_{rc}^B - \Delta + \xi \cos \beta)^2 + (y_{rc}^B + \eta)^2 \right]^{1/2}, \quad (8.56)$$

where  $(x_{rc}^B, y_{rc}^B, z_{rc}^B)$  are the coordinates of the initial contact point  $B$  at the system of coordinates  $(Ox_r y_r z_r)$  coupled to the rail (the axis  $Oz_r$  coincides with the axis of symmetry of the rail and the axis  $Oy_r$  is collinear to the rail generatrix; the origin  $O$  is at the top of the rail);  $\Delta$  is the displacement of the instantaneous axis of rotation from the point  $O$ ,  $\beta$  is the angle between the axis  $Oz_r$  and the tangential plane to the rail surface at the point  $B$ .

Note that we neglect the real speed distribution within the contact zone  $\Omega^A$  assuming it to be constant, because the characteristic size of the contact region is significantly less than the distance  $D_r$ .

In contrast, we take into account the speed distribution  $V^B(\xi, \eta)$  because the values of  $z_{rc}^B$  and  $y_{rc}^B$  on the one hand, and  $\xi$  and  $\eta$  on the other, can be commensurable.

From Eq. (8.54) we can find the wear of the rail  $\delta W_r^i(\lambda_r)$  and of the wheel  $\delta W_w^i(\lambda_w)$  in the elementary interaction ( $\lambda_r$  and  $\lambda_w$  are curvilinear coordinates at the rail and wheel profiles, respectively)

$$\begin{aligned} \delta W_r^i(\lambda_r) &= \frac{1}{V_0} \int_{a^i(\lambda_r)}^{b^i(\lambda_r)} F_r^i [p^i(\lambda_r - \lambda_r^i, \eta), V^i] d\eta, \\ \delta W_w^i(\lambda_w) &= \frac{1}{V_0} \int_{a^i(\lambda_w)}^{b^i(\lambda_w)} F_w^i [p^i(\lambda_w - \lambda_w^i, \eta), V^i] d\eta. \end{aligned} \quad (8.57)$$

where  $\lambda_r^i$  and  $\lambda_w^i$  are the curvilinear coordinates of the initial contact points at the rail and wheel, respectively,  $a^i(\lambda_r)$  ( $a^i(\lambda_w)$ ) and  $b^i(\lambda_r)$  ( $b^i(\lambda_w)$ ) are the functions describing the boundaries of the contact zones at the rail (wheel) surface. The contact pressure  $p^i(\xi, \eta)$  and the sliding speed  $V^i(\xi, \eta)$  are determined by Eqs. (8.53), (8.55) and (8.56).

The elementary wear  $\delta W_r^i$  ( $\delta W_w^i$ ) can be represented as a function of the external parameters  $\theta$ ,  $\alpha$  and  $\vec{P}^A$  and  $\vec{P}^B$ , i.e.

$$\begin{aligned} \delta W_r^i(\lambda_r) &= \Phi_r^i (\lambda_r, \theta, \alpha, \vec{P}^i), \\ \delta W_w^i(\lambda_w) &= \Phi_w^i (\lambda_w, \theta, \alpha, \vec{P}^i). \end{aligned} \quad (8.58)$$

We recall that the external contact parameters are constant during one elementary interaction and are random variables described by the probability density function  $\rho(\theta, \alpha, \vec{P}^A, \vec{P}^B)$  for the full process of the contact interaction.

Averaging Eq. (8.58) over the set of the external parameters, we obtain the average wear  $\delta\bar{W}_r(\lambda_r)$  at the point  $\lambda_r$  ( $\delta\bar{W}_w(\lambda_w)$  at the point  $\lambda_w$ ) at the  $N$ -th cycle as

$$\begin{aligned}\delta\bar{W}_r(\lambda_r) &\equiv \bar{W}_r^A(\lambda_r) + \delta\bar{W}_r^B(\lambda_r) = \\ \int_{\Sigma} [\Phi_r^A(\lambda_r, \theta, \alpha, \vec{P}^A) + \Phi_r^B(\lambda_r, \theta, \alpha, \vec{P}^B)] \rho(\theta, \alpha, \vec{P}^A, \vec{P}^B) d\Omega, \\ \delta\bar{W}_w(\lambda_w) &\equiv \bar{W}_w^A(\lambda_w) + \delta\bar{W}_w^B(\lambda_w) = \\ \int_{\Sigma} [\Phi_w^A(\lambda_w, \theta, \alpha, \vec{P}^A) + \Phi_w^B(\lambda_w, \theta, \alpha, \vec{P}^B)] \rho(\theta, \alpha, \vec{P}^A, \vec{P}^B) d\Omega,\end{aligned}\tag{8.59}$$

where  $\Sigma$  is the range of admissible values of the external parameters.

The values  $\delta\bar{W}_r(\lambda_r)$  and  $\delta\bar{W}_w(\lambda_w)$  determined from Eq. (8.59) make it possible to analyze the wear kinetics of the rail and wheel. For this aim we change the rail and wheel profile in accordance with the wear functions  $\delta\bar{W}_r(\lambda_r)$  and  $\delta\bar{W}_w(\lambda_w)$  and the given step in time of the  $N$ -th cycle, and repeat the procedure of calculations described above with the new rail and wheel profiles. Using the necessary number of cycles  $N$ , we can study the profile evolution.

#### 8.4.4 Fatigue damage accumulation process

The solution of the contact problem described in § 8.4.2 makes it possible to find the internal stresses in the rail and wheel and to study the fatigue damage accumulation process.

In this study we will use the phenomenological approach which was described in details in Chapter 5 to analyse the fatigue damage accumulation process. It is based on the linear summation theory of damage. The model can be used to determine the possible places of the fatigue crack initiation.

For definiteness we describe the process of damage accumulation inside the rail.

We suppose that the damage  $\Delta d$  accumulated at a fixed point of the rail cross-section for each elementary interaction with the moving wheel is determined by the maximum value  $\tau_{\max}^*$  of the principal shear stress  $\tau_{\max}$  at this point, and is calculated by the formula

$$\Delta d = k_d (\tau_{\max}^*)^n, \tag{8.60}$$

where  $k_d$  and  $n$  are coefficients characterizing the material properties ( $n > 1$ ). We assume that the internal stresses do not depend on the level of the damage of the contacting bodies. Since the minimum value of the function  $\tau_{\max}$  for one interaction is equal to zero, the value  $\tau_{\max}^*$  coincides with the amplitude of the function  $\tau_{\max}$ .

Averaging the value  $\Delta d$  over the set of the external parameters according to the probability density function in the  $m$ -th cycle, we calculate the average damage  $\Delta d_m$  accumulated at the fixed point for the  $m$ -th cycle.

The damage  $D$  accumulated at some point for  $N$  cycles is calculated as

$$D(x, z) = D_0(x, z) + \sum_{m=1}^N \Delta d_m,$$

where  $D_0(x, z)$  is the initial damage at the point  $(x, z)$ .

The most probable region of a fracture is identified with the region having the maximum value of the function  $D(x, z)$ .

### 8.4.5 Analysis of the results

#### Contact characteristics

We studied the influence of the inclination angle  $\theta$  and the attack angle  $\alpha$  on the characteristics of the contact interaction of the rail and wheel (the size and location of contact zones, the pressure distribution within each contact zone, etc.).

Three kinds of rail profiles (new, moderately worn and severely worn profiles) were considered in contact interaction with a new wheel. These profiles are shown in Fig. 8.11.

Fig. 8.12 illustrates the location of the contact regions on the rail surface for the contact of the new rail (Fig. 8.11 (a)) and the new wheel (Fig. 8.11 (d)). The results of calculations show that the shapes of the contact regions of the low worn rails and wheels on the running part of the rail and on its lateral edge are close to elliptical. The eccentricity of the elliptic region on the running part is nearly zero, i.e. the region is nearly a circle, but the ellipse at the lateral edge of the rail is stretched along the rail generatrix.

For the contact of new rails and wheels, the values of the angles  $\theta$  and  $\alpha$  have considerable influence on the contact pressure at the region located on the lateral edge of the rail. The maximum and average values of contact pressure increase as the angles  $\theta$  or  $\alpha$  increase.

In contrast, in the contact between the severely worn rail and the new wheel, the maximum and average pressure are essentially independent of the inclination and attack angles. In addition, the comparison of the contact characteristics within the region located on the running part of the rail for the new and the severely worn rails show that the contact area for the severely worn rail is 5 – 6 times less than for new one, and the contact pressure increases considerably. So for the worn rail the contact pressure at the running part of the rail can reach the yield stress. It can give rise to the specific configuration on the external edge of the worn rail shown in Fig. 8.13.

It was established by Bogdanov et al. (1996) that the attack angle  $\alpha$  has a considerable influence on the location of the contact region on the lateral edge of the rail, and the distance between this region and the instantaneous axis of rotation, and in turn affects the sliding velocity and the wear rate (see Eqs. (8.54) and

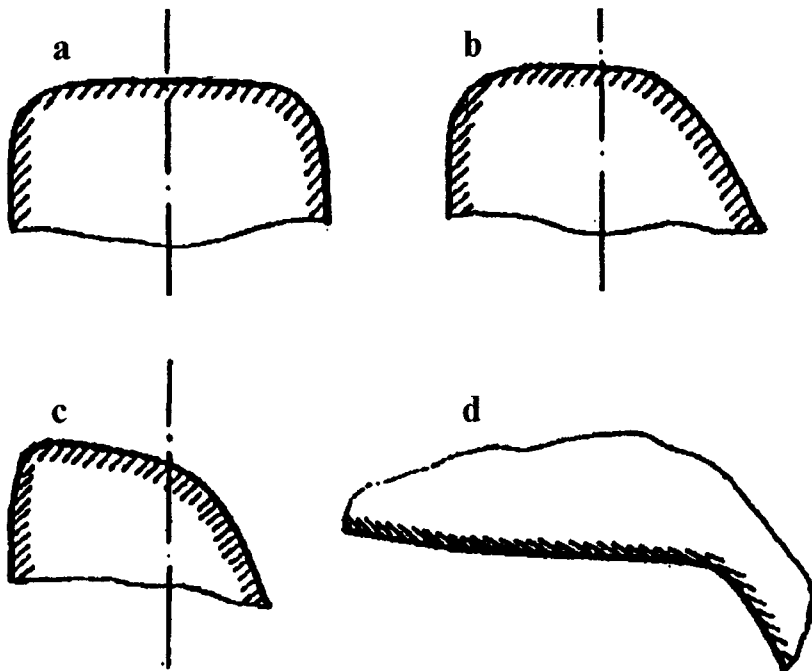


Figure 8.11: Profiles of a rail and a wheel used in the analysis of the contact characteristics: new rail (a), moderately worn rail (b), severely worn rail (c), new wheel (d).

(8.56)). The fact that the attack angle is the important characteristic determining the rail wear is supported by the experimental results discussed by Xia-Qiu Wang (1994).

### **Damage accumulation process**

The analysis of the damage accumulation process from the model described in §8.4.4 makes it possible to differentiate two main groups of parameters determining the damage accumulation rate and the points where the damage accumulation function reaches its maximum value.

The first group includes the parameters which have considerable influence on contact characteristics (size and location of the contact region, maximum contact pressure, etc.) during the elementary interaction. They are the profiles of the rail and wheel, the loads applied to the contact regions, attack and inclination angles. This group of parameters also includes the parameter  $n$  in the damage rate equation (8.60) which largely determines the depth where the damage accumulation

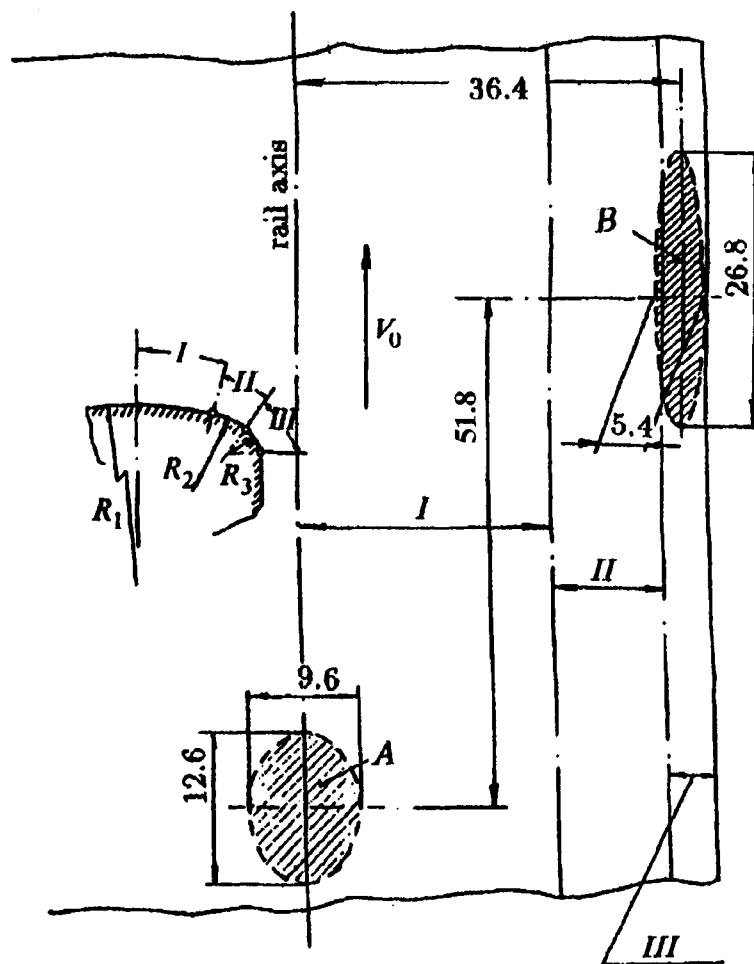


Figure 8.12: Location of the contact zones on the rail surface for the contact of a new rail and a new wheel for  $\alpha = 0.06 \text{ rad}$ ,  $\theta = 0$ ,  $P^A = 6.6 \cdot 10^4 \text{ N}$ ,  $P^B = 1.1 \cdot 10^5 \text{ N}$  (all sizes are given in millimeters).

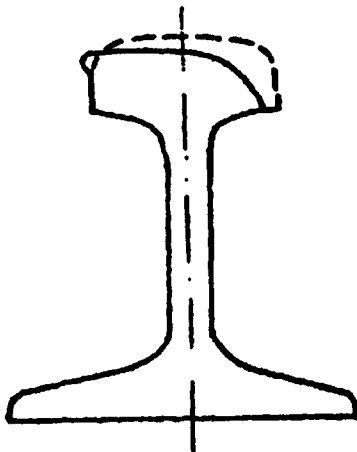


Figure 8.13: The worn rail profile in curve track ( $R_c = 303$  m) after 2 years (solid line) and the new one (dashed line).

function reaches its maximum value. Since the contact region at the lateral edge of the rail is more extended than that at the running part, the maximum value of the damage function is localized closer to the surface at the lateral edge of the rail.

The second group includes the parameters which determine the statistical characteristics of the elementary interaction ensemble. For instance, the greater the range of location of the initial contact points at the rail profile, the less is the damage concentration, and the greater is the time needed to achieve the critical value of the damage function at some point.

In calculations we found the ratio of the damage to  $k_d$ . The parameter  $n$  which influences the location of the point of maximum damage was chosen between the limits from 5.8 to 9.5 that correspond to different structures of the rail steel. Fig. 8.14 illustrates the damage accumulation function distribution within the new rail head in contact with the new wheel.

### Wear kinetics

We used Eq. (8.59) to calculate the values of  $\delta\bar{W}_r (\lambda_r)$  and  $\delta\bar{W}_w (\lambda_w)$ . The functions  $F_r(p, V)$  and  $F_w(p, V)$  in the wear equations (8.54) were taken in the form given by Specht (1987):

$$F(p, V) = \kappa \frac{\mu}{\gamma} pV, \quad (8.61)$$

where

$$\kappa = \begin{cases} \kappa_m, & \text{if } \mu pV \leq Q^*, \\ \kappa_s, & \text{if } \mu pV > Q^*, \end{cases}$$

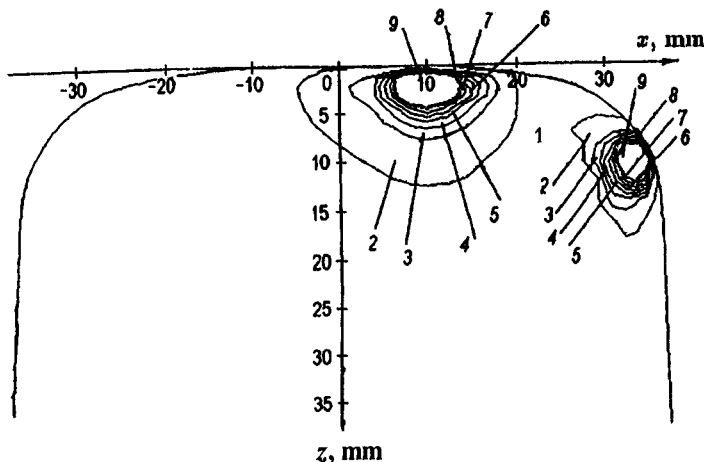


Figure 8.14: Damage distribution within the rail head for  $D$  in the intervals: (1)  $(0, 140]$ ; (2)  $(140, 1500]$ ; (3)  $(1500, 3000]$ ; (4)  $(3000, 4300]$ ; (5)  $(4300, 5800]$ ; (6)  $(5800, 7200]$ ; (7)  $(7200, 8600]$ ; (8)  $(8600, 10000]$ ; (9)  $D = 10000$  ( $D$  is measured in some conventional units).

$\mu$  is the friction coefficient,  $\gamma$  is the density of material,  $\kappa_m$  and  $\kappa_s$  are the wear coefficients,  $Q^*$  is the critical value of the specific capacity of friction. Eq. (8.61) reflects the jump in wear rate corresponding to the transition from the mild to the severe wear regime for large values of the specific capacity of friction ( $\mu pV > Q^*$ ). The values of  $\gamma$ ,  $\kappa_m$ ,  $\kappa_s$  and  $Q^*$  can be different for the rail and the wheel, but the results presented here were calculated under the assumption that these values are the same for both contacting bodies.

The function  $\rho(\theta, \alpha, \vec{P}^A, \vec{P}^B)$  was taken from Romen (1969) where the solution of the dynamic model of the contact interaction of a carriage and a railway was obtained. This function corresponds to a track with radius of curvature  $R_c = 350$ m, and the speed  $V_0 = 20\text{ms}^{-1}$ .

Fig. 8.15 illustrates the wear rate distribution along the rail (a) and wheel (b) profiles. The maximum wear rate occurs at the lateral sides of the rail and wheel.

This model makes it possible to calculate the evolution of the rail and wheel profiles in the wear process. Fig. 8.16 illustrates the rail profiles occurring after different number of cycles in contact interaction of an initially new rail with a new wheel. The results show that the worn profile calculated from the model is very close to the shape presented in Fig. 8.13. This suggests that the model can be used to predict the wear of rails and wheels in contact interaction and to evaluate the influence of different parameters on the wear and damage accumulation processes.

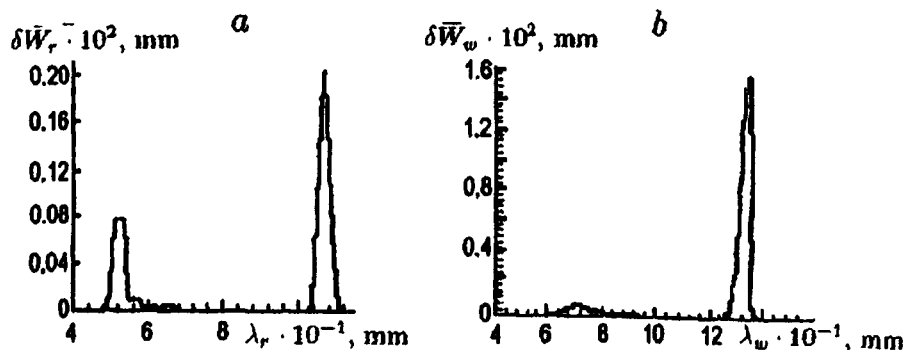


Figure 8.15: Wear rate distribution along the rail (a) and wheel (b) profiles.

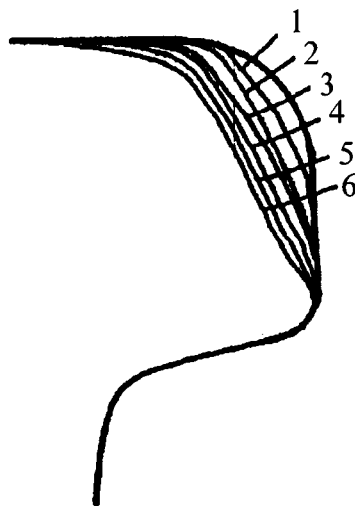


Figure 8.16: Evolution of the rail profile in wear process for  $N = 1.34 \cdot 10^6$  cycles (curve 1),  $N = 2.68 \cdot 10^6$  cycles (curve 2),  $N = 4.02 \cdot 10^6$  cycles (curve 3),  $N = 5.37 \cdot 10^6$  cycles (curve 4),  $N = 6.71 \cdot 10^6$  cycles (curve 5),  $N = 8.05 \cdot 10^6$  cycles (curve 6).

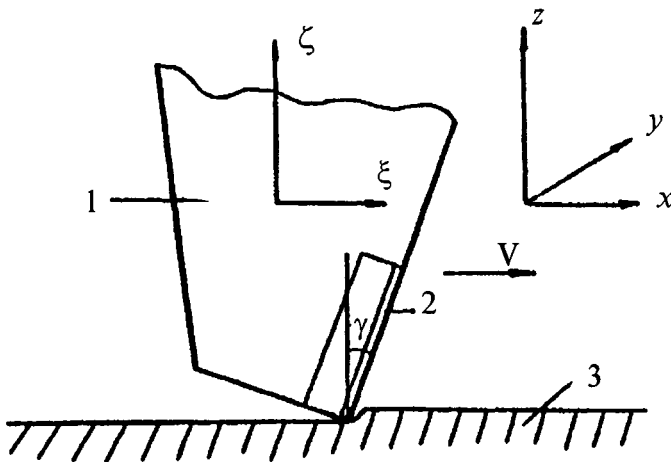


Figure 8.17: Scheme of the tool/rock contact.

## 8.5 A model for tool wear in rock cutting

A specific feature of the cutting tool – worked material (rock) pair is the variation of shape of both elements caused by fracture or wear. Thus, the problem of cutting tool operation modelling is significantly different from the traditional wear contact problems described in Chapter 6, where shape variation of only one body is taken into account. The shape variation leads to pressure redistribution in the contact zone; this in turn influences the rock fracture and tool wear. The interconnected non-stationary contact problem including wear and fracture must be studied.

To solve this problem it is necessary to develop a model of worked material fracture in cutting. Rock fracture has been studied deeply by Cherepanov (1987) and Atkinson (1987). However, a general model of rock cutting has not yet been developed. This can be considered as an obstacle for modelling of cutting tool wear. However, since the processes of rock fracture and tool wear are interconnected, information on tool wear process (shape variation, size and position of wear land) can be used for modelling the process in the contact zone.

The experimental data obtained for a tool with a diamond-hard alloy insert have been used as the basis of the model. Fig. 8.17 illustrates a schematic of the cutter (1) with the insert (2) in contact with rock (3). The \$(x, y, z)\$ coordinate system is fixed on the rock. The cutter is moving along the \$x\$-axis with the speed \$V\$; \$\gamma\$ is the rake angle.

Experiments have shown the following:

1. The wear area is inclined relative to the horizontal axis. Fig. 8.18 illustrates worn tool profiles presented by Checkina, Goryacheva and Krasnik (1996). The profiles of the worn tool were obtained for cutting sand-cement blocks; the cutting depth was 10 mm, velocity of the tool displacement (cutting speed) \$V=1.25 \text{ ms}^{-1}\$, \$\gamma = 15^\circ\$.

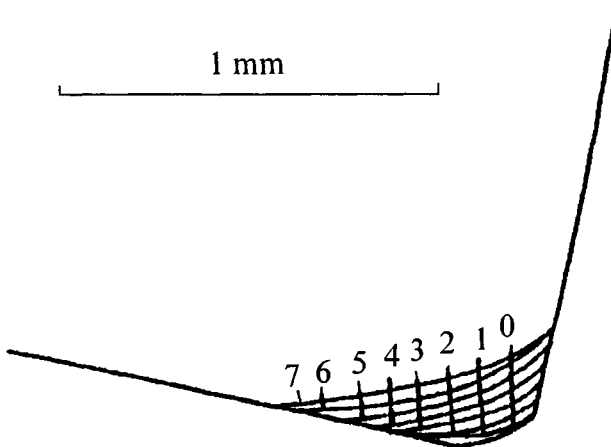


Figure 8.18: Experimental worn tool profiles. Curve number corresponds to the path of the tool in contact with rock; measurements are in kilometers.

2. When the cutting depth is equal to several millimeters, the size of the face wear area is fraction of 1 mm (see Fig. 8.18).
3. The cutting force components oscillate during the process of cutting.

In what follows we describe a model of the tool wear in cutting which was developed by Checkina, Goryacheva and Krasnik (1996). This model reproduces the features revealed in the experiments, and investigates the influence of the model parameters on tool wear and also the influence of the tool shape variation on the characteristics of the cutting process.

### 8.5.1 The model description

We treat the problem as two-dimensional, considering the tool width along the  $y$ -axis to be much greater than the size of contact zone in the  $x$ -direction. We introduce the  $(\xi, \zeta)$  coordinate system moving with the tool. The tool shape in this coordinate system is described by the function  $f(\xi, t)$ . Shape variation with time is caused by the tool wear; its initial shape is  $f(\xi, 0) = f_0(\xi)$ .

The following relationships hold between the coordinate systems  $(x, z)$  and  $(\xi, \zeta)$ :

$$x = \xi + Vt, \quad z = \zeta - c(t), \quad (8.62)$$

where  $c(t)$  is the cutting depth.

### The model of rock deformation

We consider two types of rock boundary displacement taking place in the contact zone simultaneously. They are elastic displacement  $u_z(x, t)$  along the  $z$ -axis described by the equation

$$u_z(x, t) = k\tilde{p}(x, t) \quad (8.63)$$

( $\tilde{p}(x, t) \geq 0$  is the contact pressure at the point  $x$  of the rock surface,  $k$  is a coefficient) and irreversible displacement  $w(x, t)$  along the  $z$ -axis governed by the relationship

$$\frac{dw(x, t)}{dt} = F(V)\tilde{p}(x, t). \quad (8.64)$$

Irreversible displacement is caused by the rock fracture (crushing) under the tool.

It should be mentioned that Eq. (8.64) can describe different types of process, depending on the function  $F(V)$ . For  $F(V) \sim V^\beta$  this equation is equivalent to the one used for the calculation of wear. In each case the type of the function  $F(V)$  should be chosen in accordance with the mechanical characteristics of the fractured rock. As it will be shown below, simultaneous consideration of the two mechanisms for the rock boundary displacement in the contact zone allows us to obtain a wear area shape similar to that obtained experimentally (Fig. 8.18).

### Contact conditions

The following relationship between the shape of rock boundary  $z_0(x)$ , the shape of the tool, the cutting depth and rock displacement due to elastic deformation and crushing is satisfied in the contact zone

$$z_0(x) - w(x, t) - u_z(x, t) = f(x - Vt, t) - c(t). \quad (8.65)$$

This equation can be written in differential form by taking into account Eqs. (8.63) and (8.64)

$$F(V)\tilde{p}(x, t) + k \frac{d\tilde{p}(x, t)}{dt} = \frac{dc(t)}{dt} - \frac{df(x - Vt, t)}{dt}. \quad (8.66)$$

In  $(\xi, \zeta)$  coordinate system, Eq. (8.66) has the form

$$F(V)p(\xi, t) + k \left( \frac{\partial p(\xi, t)}{\partial t} - \frac{\partial p(\xi, t)}{\partial \xi}V \right) = \frac{dc(t)}{dt} + \frac{\partial f(\xi, t)}{\partial \xi}V - \frac{\partial f(\xi, t)}{\partial t}, \quad (8.67)$$

where  $p(\xi, t) = \tilde{p}(\xi + Vt, t)$  and the following relationship obtained from Eq. (8.62) is taken into account

$$\frac{dp(\xi, t)}{dt} = \frac{\partial p(\xi, t)}{\partial t} - \frac{\partial p(\xi, t)}{\partial \xi}V. \quad (8.68)$$

A similar relationship for the tool shape is

$$\frac{df(\xi, t)}{dt} = \frac{\partial f(\xi, t)}{\partial t} - \frac{\partial f(\xi, t)}{\partial \xi}V. \quad (8.69)$$

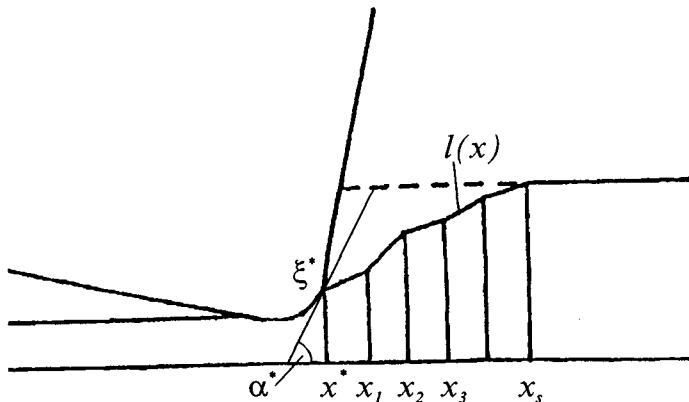


Figure 8.19: Scheme of the crack propagation.

Here  $\frac{\partial f(\xi, t)}{\partial t}$  is the tool shape variation caused by wear.

The pressure at the ends  $a(t)$  and  $b(t)$  of the contact zone is equal to zero, that is

$$p(a(t), t) = p(b(t), t) = 0. \quad (8.70)$$

The coordinate  $a(t)$  of the leading point of contact zone is obtained from the formula

$$z_0(a + Vt) = -c(t) + f(a, t) \quad (8.71)$$

which is based on Eqs. (8.63)-(8.65) and Eq. (8.70). Initial conditions for the differential equation (8.67) depend on the type of the tool motion. Eq. (8.67) in combination with Eqs. (8.70) and (8.71) can be used for the contact pressure calculation.

### Chip formation

Rock brittle fracture leading to chip formation occurs in parallel with rock elastic deformation and crushing when the tool penetration depth is considerable. Chip formation is one of the causes of cutting force oscillation in tool operation. The fragment separation is caused by propagation of the crack which originates near the cutter nose. This statement can be verified by noting that the front face of the tool is worn only near the nose (see Fig. 8.18).

We assume that separation of rock fragment occurs at the instant  $t^*$  when pressure at the point  $\xi^*$  is equal to a critical value  $p^*$ . Thus

$$p(\xi^*, t^*) = p^* \quad (8.72)$$

then crack propagation originates from the point  $x^* = \xi^* + Vt^*$ . The crack is supposed to be a polygonal line  $l(x)$  shown in Fig. 8.19. Its inclination angle  $\delta_i$  at

each segment  $[x_i, x_{i+1}]$  of the length  $\Delta x = |x_{i+1} - x_i|$  is a random value, uniformly distributed at  $[0; \alpha^*]$ ,  $\alpha^*$  is the inclination angle of the tool profile to the  $x$ -axis at the point  $x^*$ .

The crack propagates up to a point  $x_s$  of the rock boundary. The shape of the rock boundary ahead of the tool is changed as the result of chip fragment separation.

$$z_0(x)|_{t=t^*+0} = \begin{cases} l(x) & \text{if } x^* \leq x \leq x_s, \\ z_0(x)|_{t=t^*-0} & \text{if } x > x_s. \end{cases} \quad (8.73)$$

### Tool wear model

The following relationship is used to model the tool shape variation due to wear

$$\frac{\partial f_n(\xi, t)}{\partial t} = K_w p_n(\xi, t) v \quad (8.74)$$

Here  $\partial f_n(\xi, t)/\partial t$ ,  $p_n(\xi, t)$  are the wear rate and contact stress in the direction normal to the friction surface,  $v$  is the relative velocity of the worn body and the abrasive medium (rock surface) in the tangential direction,  $K_w$  is the wear coefficient.

From geometrical consideration we have the following relations:

$$v = V/\cos \alpha,$$

$$\frac{\partial f_n(\xi, t)}{\partial t} = \cos \alpha \frac{\partial f(\xi, t)}{\partial t},$$

$$\cos^{-2} \alpha = 1 + \left( \frac{\partial f(\xi, t)}{\partial \xi} \right)^2,$$

where  $\alpha$  is the inclination angle of the tool profile to the  $x$ -axis at each point  $\xi$ .

Tool shape variation caused by wear can be described by the formula following from Eq. (8.74)

$$\frac{\partial f(\xi, t)}{\partial t} = K_w p_n(\xi, t) \left[ 1 + \left( \frac{\partial f(\xi, t)}{\partial \xi} \right)^2 \right] V. \quad (8.75)$$

Thus, we propose a mathematical description for the following main processes taken into account in this model:

- elastic deformation of rock, Eq. (8.63);
- rock crushing, Eq. (8.64);
- chip formation, Eqs. (8.72) and (8.73);
- tool wear, Eq. (8.75).

The contact condition written in differential form (8.67), together with the boundary condition (8.71), gives the possibility of calculating contact characteristics (the value of the pressure  $\tilde{p}(\xi, t)$  and coordinates of the ends of contact zone  $a(t)$  and  $b(t)$ ), and hence of modelling the development of the entire process. Numerical procedure and results of the modelling are described below.

To reveal the role of separate mechanisms in the process of tool operation, we first consider the simplified situation when only some of them occur.

### 8.5.2 Stationary process without chip formation and tool wear

We analyse the pressure distribution in the contact zone when only elastic deformation and crushing described by Eqs. (8.63) and (8.64) are taken into account. The tool shape is assumed to be a wedge with angle  $90^\circ$ , rake angle  $\gamma = 15^\circ$ , and cutting edge roundness is equal to zero, that is the *absolutely sharp* cutter is considered. The shape of the cutter does not change:  $f(\xi, t) = f_0(\xi)$ , where

$$f_0(\xi) = \begin{cases} A\xi & \text{if } \xi \geq 0, \\ -\xi/A & \text{if } \xi < 0, \end{cases}$$

where  $A = \cot \gamma$ .

We study the stationary motion of the tool with constant cutting depth, assuming  $z_0(x) = 0$ , that is the rock surface is originally flat:

$$\frac{\partial p(\xi, t)}{\partial t} = 0; \quad \frac{dc(t)}{dt} = 0.$$

In this case Eq. (8.67) turns into

$$F(V)p(\xi, t) - k \frac{\partial p(\xi, t)}{\partial \xi} V = \begin{cases} AV & \text{if } \xi \geq 0, \\ -V/A & \text{if } \xi < 0. \end{cases} \quad (8.76)$$

Eq. (8.76) has the stationary solution

$$p(\xi) = \begin{cases} \frac{AV}{F(V)} \left( 1 - \exp \frac{F(V)(\xi - a)}{kV} \right) & \text{if } \xi \geq 0, \\ \frac{V}{AF(V)} \left( -1 + \exp \frac{F(V)(\xi - b)}{kV} \right) & \text{if } \xi < 0. \end{cases} \quad (8.77)$$

Coordinate  $a$  of the leading point of contact is given, the coordinate  $b$  is obtained from the condition

$$b = -\frac{kV}{F(V)} \ln \left[ A^2 \left( 1 - \exp \frac{-F(V)a}{kV} \right) + 1 \right].$$

Eq. (8.70) and the condition of pressure continuity at the point  $\xi = 0$  have been used to construct these relationships.

Fig. 8.20 illustrates the functions  $p(\xi)/p(0)$  for different values of the param-

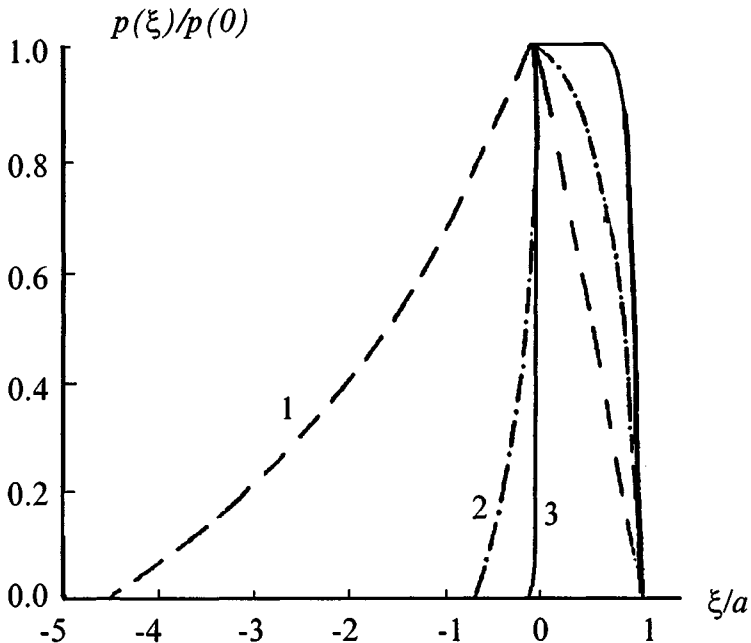


Figure 8.20: Contact pressure distribution for various values of  $\beta$ :  $\beta = 0.3$  (curve 1),  $\beta = 3$  (curve 2),  $\beta = 30$  (curve 3) (tool operation without chip formation).

eter  $\beta = \frac{F(V)a}{kV}$ . The results show that the contact zone size  $b/a$  decreases as  $\beta$  increases (that is when the role of crushing increases), the pressure distribution on the front face tending to a constant (curve 3). Increasing the effect of elastic deformation causes an increase of the contact zone size on the rear face.

We can conclude from Eq. (8.77) that the pressure  $p(\xi)$  is independent of the velocity  $V$  in the stationary stage, if  $F(V)$  is a linear function. As is shown in a set of experimental investigations by Vorozhtsov et al. (1989), the components of the cutting force depend only slightly on the velocity  $V$ ; in future we shall suppose  $F(V) = \lambda V$ .

### 8.5.3 Analysis of the cutting process

To analyse the model behaviour, we developed a numerical procedure. It includes a step-by-step in time solution of the differential equation (8.67) in the process of the cutter displacement in the  $x$ - and  $z$ -direction; instant changes of the rock shape occur ahead of the tool in accordance with Eq. (8.73) when condition (8.72) holds. Permanent wear of the tool is calculated on the basis of Eq. (8.76). Since

the variation of cutting forces due to rock fragment separation, and the tool wear are processes with different time scales, the time-averaged value of the contact pressure was used for calculation of wear. This procedure significantly reduced the calculation time.

The system of Eqs. (8.67), (8.71)–(8.73) was solved in dimensionless form. The system depends on the dimensionless parameter  $\lambda p^* = \bar{p}^*$ .

The calculation has been carried out for a tool, which has a wedge shape with angle  $90^\circ$ ,  $\gamma = 15^\circ$ , and cutting edge roundness is 0.2 mm. It is supposed that the tool and rock are out of contact originally, initial conditions being  $p(\xi, 0) = 0$ ,  $a(t) - b(t) = 0$ . At first tool penetration is  $c(t) = c_0 t$  with constant rate  $c_0$  ( $c_0/V = 0.2$ ), then cutting with constant depth takes place. The dependence of cutting depth on time is illustrated by Fig. 8.21(a).

The vertical ( $P_v$ ) and horizontal ( $P_h$ ) components of cutting force are calculated from

$$P_v = \int_b^a p(\xi, t) d\xi,$$

$$P_h = \int_b^a p(\xi, t) \frac{\partial f(\xi, t)}{d\xi} d\xi.$$

Note that the force  $P_h$  is caused by the rock crushing under the tool. It is only a part of the cutting force horizontal component. The other part of the force which is caused by the chip formation is not considered here.

### Cutting process without tool wear

First we analysed the cutting process without tool wear, and assumed that the cutter shape is independent of time  $f(\xi, t) = f_0(\xi)$ . Fig. 8.21 (b)–(d) illustrates the variations of  $a(t)$  and  $b(t)$ ,  $P_v(t)$  and  $P_h(t)$ , respectively. The calculation has been carried out for  $\Delta x = 0.4$  mm. It should be mentioned that the cutting depth and the size of contact zone are shown in dimensional units (mm) to make the comparison with experimental results easier.

Fig. 8.21 demonstrates that initially rock crushing without chip formation occurs, and cutting force components and size of contact zone increase monotonously. Then after the beginning of chip formation, essential oscillations of cutting force components occur, and the size of contact zone does not increase appreciably, in spite of the growth of the cutting depth. After transition to operation with constant cutting depth, the process quickly becomes quasistationary.

It should be mentioned that the characteristics of the cutting process turn out to be sensitive to change of penetration speed  $dc/dt$ . When the speed is changed abruptly from 0.2 V to zero (constant cutting depth) the value of vertical force  $P_v$  (Fig. 8.21 (c)), as well as the frequency of contact parameter oscillation (Fig. 8.21 (b)–(d)) and size of contact zone  $a(t) - b(t)$  (Fig. 8.21 (b)), diminish.

Fig. 8.22 gives a typical view of cracks arising successively in penetration and horizontal displacement of the cutter. This figure shows that fragments of different

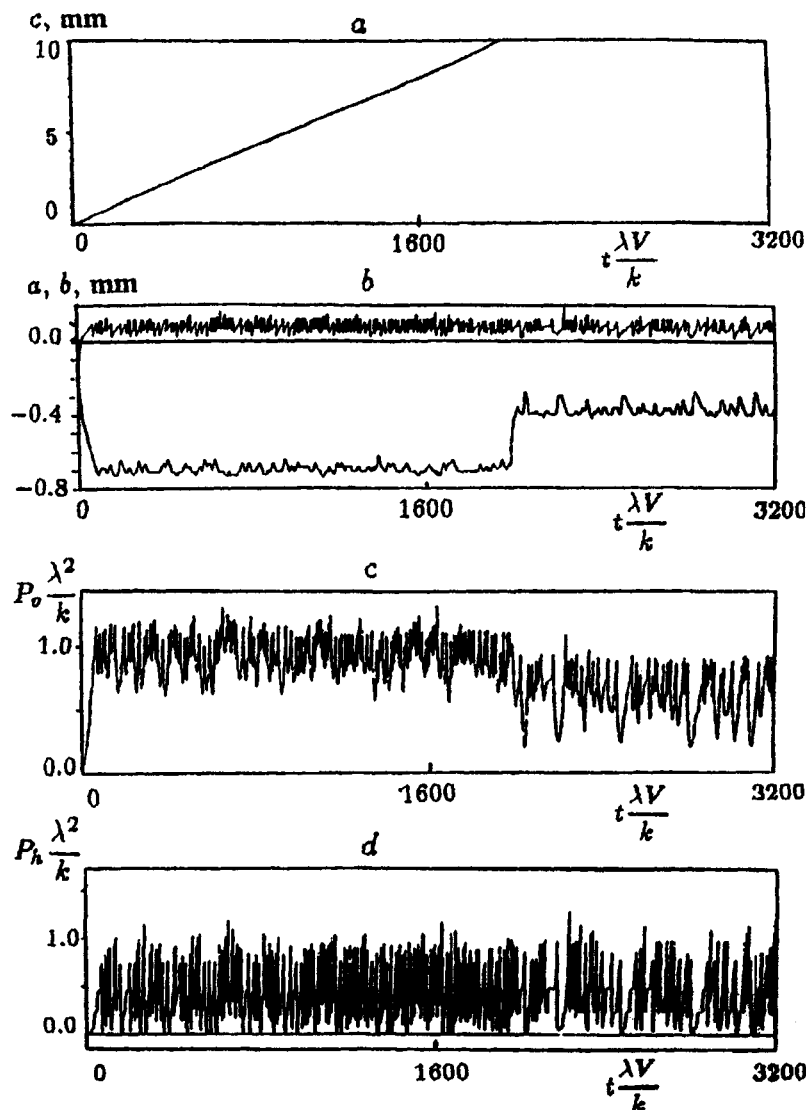


Figure 8.21: Characteristics of the tool operation as a function of time (cutting process without tool wear): (a) the tool penetration  $c(t)$ ; (b) the coordinates of the edge points  $a(t)$  and  $b(t)$  of contact zone; vertical  $P_v$  (c) and horizontal  $P_h$  (d) components of cutting force at  $\bar{p}^* = 0.84$ ,  $\lambda/k = 40 \text{ mm}^{-1}$ .



Figure 8.22: Typical view of cracks arising successively in cutter penetration and horizontal displacement obtained from calculations.

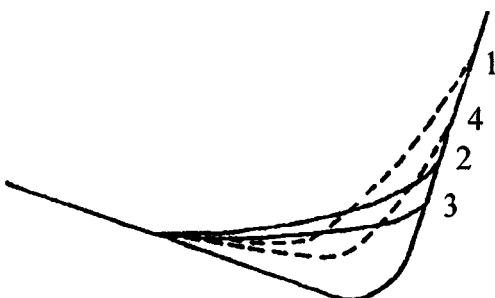


Figure 8.23: Profiles of worn cutter calculated at  $\bar{p}^* = 0.84$ ,  $\lambda/k = 40 \text{ mm}^{-1}$  (curve 1);  $\bar{p}^* = 0.28$ ,  $\lambda/k = 40 \text{ mm}^{-1}$  (curve 2),  $\bar{p}^* = 0.14$ ,  $\lambda/k = 20 \text{ mm}^{-1}$  (curve 3);  $\bar{p}^* = 0.28$ ,  $\lambda/k = 10 \text{ mm}^{-1}$  (curve 4).

sizes are separated in cutting.

#### 8.5.4 Influence of tool wear on the cutting process

Tool shape variation in the wear process leads to gradual variation of contact characteristics, unlike the case analysed above when, in the absence of wear, the cutting process becomes quasistationary.

Fig. 8.23 illustrates typical profiles of the worn cutter calculated for different sets of model parameters. The results show that the worn cutter profile depends essentially on the rock mechanical characteristics that describe elastic deformation, crushing, and brittle fracture of rock.

The parameters that correspond to curve 2 in Fig. 8.23 give a shape for the wear area extremely close to that obtained experimentally (Fig. 8.18). In this case the calculations accurately reproduce the details of the wear process for a real tool.

Fig. 8.24 illustrates the function  $P_v(t)$  at different stages of the tool wear. The calculation has been carried out for the parameters that correspond to curve 1 in Fig. 8.23. The sizes of wear area  $S$  in Fig. 8.24 are determined as

$$S(t) = \max_{\tau < t} a(\tau) - \min_{\tau < t} b(\tau).$$

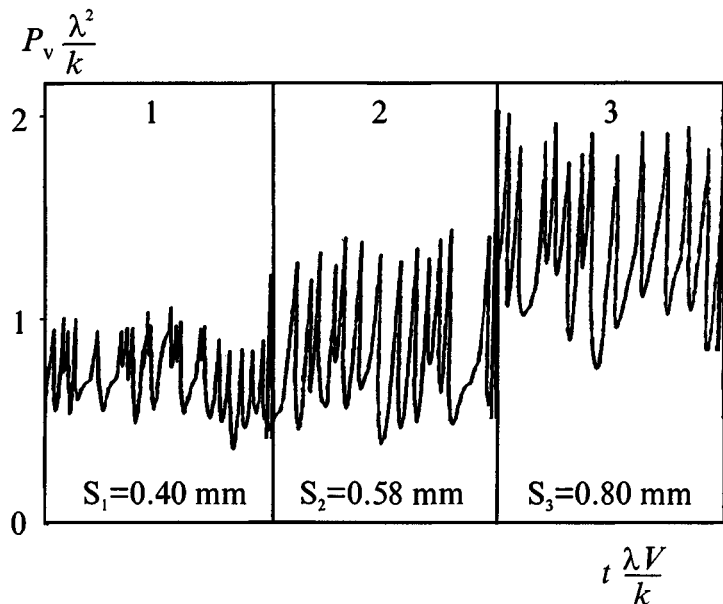


Figure 8.24: Dependence of the vertical component of the cutting force on time at different stages of the tool wear for  $\bar{p}^* = 0.84$  and  $\lambda/k = 40 \text{ mm}^{-1}$ .

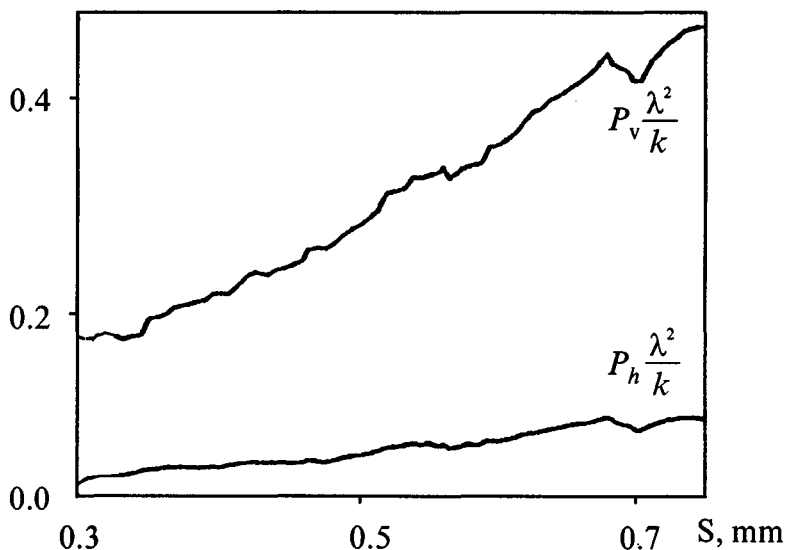


Figure 8.25: Dependence of the averaged cutting force components  $P_v$  and  $P_h$  on the wear area size.

The time interval  $\Delta t = 400k/(\lambda V)$  is the same for regions 1, 2, 3. The mean values of the vertical force  $\bar{P}_v$  are  $0.69k/\lambda^2$ ;  $0.77k/\lambda^2$ ;  $1.31k/\lambda^2$  for the regions 1, 2, and 3, respectively. As follows from Fig. 8.24, wear causes growth of the oscillation amplitudes and the value of  $\bar{P}_v$ ; it causes the oscillation frequency to diminish. The behaviour of the  $P_h$  component is similar. In practice, growth of the oscillation amplitude and the mean value of the forces can cause the tool to break-down.

Cutting force components  $P_v$  and  $P_h$  averaged over a large number of time steps are shown in Fig. 8.25 as a function of the wear area size  $S$ . The calculation parameters here are the same as for the curve 2 in Fig. 8.23. It is interesting to mention that variations of the vertical and horizontal components of cutting force with the size of wear area obtained in the experiment on cutting of cement-sand blocks described above are also close to linear ones; they coincide qualitatively with the results of calculation. This is one more confirmation of the idea that the tool profile variation in wear can be an indicator of the processes occurring in rock fracture.

The investigation of the proposed model allows us to conclude that the analysis of tool shape variation caused by wear provides important information that can be used for modelling of the processes in the contact zone.

The model is based on simultaneous consideration of tool wear, rock elastic deformation, crushing, and brittle fracture leading to rock fragment separation. Numerous phenomena observed in tests confirm the adequacy of the theory.

The investigation revealed the influence of the tool wear on various characteristics of the cutting process, and also the influence of the rock mechanical characteristics on tool shape variation caused by wear.

This model allows us to predict the cutting process characteristics for tools with different initial geometrical parameters (cutter shape, rake angle, etc.) and could be used for the optimal choice of these parameters.